Title
Organic Chemistry Methods Towards the Development of Molecular Imaging Tracers

Author
Gamache, Raymond

Publication Date
2018

Peer reviewed|Thesis/dissertation

UNIVERSITY OF CALIFORNIA

Los Angeles

Organic Chemistry Methods Towards the Development of Molecular Imaging Tracers

A dissertation submitted in partial satisfaction of the

requirements for the degree Doctor of Philosophy

in Chemistry

by

Raymond Francis Gamache

2018

ABSTRACT OF THE DISSERTATION

Organic Chemistry Methods Towards the Development of Molecular Imaging Tracers

by

Raymond Francis Gamache

Doctor of Philosophy in Chemistry

University of California, Los Angeles, 2018

Professor Michael E. Jung, Chair

This dissertation describes how modern organic chemistry can be used to improve and advance the field of molecular imaging, particularly in the realm of positron emission tomography (PET) imaging. Organic chemistry is an interdisciplinary art that is featured in many scientific disciplines to advance problem-solving capabilities. Herein, I report how chemical methods developed in our laboratory have expanded the scope of available labeling technologies for molecular imaging applications. Additionally, we designed a bifunctional chemical linker to produce a dual-modality (optical/PET) imaging tracer and investigated its physicochemical properties *in vivo*.

Chapter One reviews the procedures developed in organic chemistry that have been of particular importance to PET and fluorescence imaging. The topics covered in detail are fluorine-18 chemical methodologies, bioorthogonal chemistry, and multi-functional chemical linkers used in antibody imaging systems.

Chapter Two describes the development of a regiospecific copper-mediated oxidative fluorination methodology that is compatible with aryl stannanes. This methodology tolerates nucleophilic functionalities, uses a recyclable fluorine source and proceeds under mild conditions (60 ^{o}C, 3.2h). In addition to nucleophilic groups, the procedure allows for the fluorination of heteroaryl rings and bioactive molecules, such as estrone.

Chapter Three demonstrates the creation of an ambiphilic cyclopentadiene that can be used as a bioorthogonal reagent. The diene undergoes fast reaction rates with multiple dienophiles already being used in bioorthogonal applications. Practical applications of this new bioorthogonal ligation are highlighted via fluorescence labeling of a commercial neuropeptide.

Chapter Four discloses the synthesis of a series of multi-modal imaging linkers used in the molecular imaging of prostate specific cell antigen (PSCA) expressing tumors. These linkers were conjugated to engineered antibody fragments that target PSCA and allow for dual PET and optical imaging. The PET imaging portion allows for whole body PET scans to obtain tumor localization and metastasis information while the optical portion facilitates intra-operative removal of tumor tissue through fluorescence-guided surgery.

The dissertation of Raymond Francis Gamache is approved.

Alexander Michael Spokoyny

Jennifer M. Murphy

Michael E. Jung, Committee Chair

University of California, Los Angeles

2018

A dedication is not enough thanks to what I owe my mom and dad for getting me to this point…

Without their help and support I would not be the person I am today, I love you two.

TABLE OF CONTENTS

LIST OF FIGURES

CHAPTER THREE

CHAPTER FOUR

LIST OF SCHEMES

CHAPTER ONE

CHAPTER TWO

CHAPTER THREE

CHAPTER FOUR

LIST OF TABLES

CHAPTER TWO

LIST OF ABBREVIATIONS

[^{18}F]	fluorine-18
18-c-6	1,4,7,10,13,16-hexaoxacyclooctadecane
Ac	acetyl, acetate
AcOH	acetic acid
α	alpha
Ar	aryl
aq.	aqueous
atm	atmosphere
br	broad
BAIB	bis-acetoxy iodobenzene
Boc	*tert*-butoxycarbonyl
Bq	becquerel
Bu	butyl
t-Bu	*tert*-butyl
°C	degrees Celsius
calcd	calculated
cat.	catalytic
Ci	curie(s)
COD	cyclooctadiene
CP	cyclopropene
Cy_5	cyanine-5 dye
d	doublet
DCC	*N,N*'-dicyclohexylcarbodiimide
DCM	dichloromethane
DFO	deferoxamine
DIPEA	*N,N*-diisopropylethylamine
DMF	*N,N*-dimethylformamide

DMSO	Dimethyl sulfoxide
DOTA	1,4,7,10-Tetraazacyclododecane-1,4,7,10-tetraacetic acid
EDG	electron donating group
EWG	electron withdrawing group
equiv	equivalent
ESI	electrospray ionization
Et	ethyl
EtOH	ethanol
F^-	nucleophilic fluoride
FDG	[^{18}F]fluorodeoxyglucose
FDOPA/ ^{18}F-DOPA	6-fluoro-L-3,4-dihydroxyphenylalanine
g	gram(s) or giga
h	hour(s)
HATU	1-[Bis(dimethylamino)methylene]-1H-1,2,3-triazolo[4,5-b] pyridinium 3-oxide hexafluorophosphate
HRMS	high resolution mass spectrometry
Hz	hertz
ID	injected dose
IR	infrared (spectroscopy)
J	coupling constant
k	equilibrium constant
k2.2.2	4,7,13,16,21,24-Hexaoxa-1,10-diazabicyclo[8.8.8]hexacosane
L	liter
L-DOPA	L-3,4-dihydroxyphenylalanine
M	molarity or molecular mass
m	multiplet or milli
m	meta
m/z	mass to charge ratio
μ	micro
Me	methyl

MsCl	methanesulfonyl chloride
MeOH	methanol
MHz	megahertz
min	minute(s)
mol	mole(s)
mp	melting point
MRI	magnetic resonance imaging
MS	molecular sieves
n-Bu	*n*-butyl
NBS	*N*-bromosuccinimide
NHS	*N*-hydroxysuccinimide
NMR	nuclear magnetic resonance
o	ortho
p	para
PBS	phosphate buffered saline
PET	positron emission tomography
Ph	phenyl
pH	hydrogen ion concentration in aqueous solution
ppm	parts per million
py	pyridine
i-Pr	isopropyl
q	quartet
rt	room temperature
R_f	retention factor
s	singlet
sat.	saturated
sCy5	Sulfo-Cyanine5 dye
t	triplet
TBAF	tetrabutylammonium fluoride

TCEP	(tris(2-carboxyethyl)phosphine)
TCO	*trans*-cyclooctene
TEAB	tetraethylammonium bromide
TEAF	tetraethylammonium fluoride
TEMPO	(2,2,6,6-Tetramethylpiperidin-1-yl)oxyl
Tf	trifluoromethane sulfonyl
TFA	trifluoroacetic acid
THF	tetrahydrofuran
TLC	thin layer chromatography
Ts	*p*-toluenesulfonyl (tosyl)
TSTU	N,N,N′,N′-Tetramethyl-O-(N-succinimidyl)uronium tetrafluoroborate,O-[N-Succinimidyl)-1,1,3,3-tetramethyluronium tetrafluoroborate
Tz	tetrazine
UV	ultraviolet
λ	wavelength

ACKNOWLEDGEMENTS

I am very thankful to my advisor Professor Jennifer M. Murphy for accepting me into her lab and taking me on as her first graduate student. Jennifer, gave me a lot of independence in my work (sometimes more than I deserved) and I really appreciated this freedom. The granted autonomy helped me grow as a scientist by forcing me to troubleshoot any encountered obstacles, write papers and proposals, and strengthen my networking skills. If I was ever banging my head against the wall for too long Jennifer was always available to help give me suggestions to get my projects back moving again, as well as edit my papers and proposals in a timely manner. With every passing year our lab has grown intellectually and I'm excited to observe its continued growth.

My lab members despite being so few, deserve a great and many thanks in working to keep me motivated and providing posing scientific dialogue that has enabled much scientific growth. When I first joined the lab, I was the only graduate student and had one postdoc as a labmate, Maruthi. Maruthi has taught me many scientific skills, while being extremely patient during my many small mistakes and forgetfulness. He has also helped me feel welcomed by hosting various events and feeding me real Indian food! Chris Waldman was the next postdoc who joined the lab and was a model to follow in terms of note taking and cleanliness in the lab space. My fondness for surfing is also thanks to Chris, after lending me his board and driving up to Santa Monica and Venice. The next postdoc to join our lab was Gaoyuan, which really created a diverse melting pot of a group. Gaoyuan and I have had many informative talks on the changes needed in chemistry that have helped strengthen my ideals for what I want out of my future career. After four years our group finally obtained another graduate student in Jay McDaniels, a brilliant writer and scientifically stimulating thinker, who has been plagued by the strangeness that is simple organic

chemistry that fails to work. Despite the setbacks he has faced in research, he is more upbeat than most and I hope he will transition into a great lecturer.

Professor Carney was the undergraduate advisor who got me interested in pursuing a Ph.D. in organic chemistry. I remember talking to him just about every day my sophomore year during the second semester after being introduced to him in the Fall. It was such an interesting time, just discovering a subject that I really loved for the first time and I am lucky he was available to nourish my curiosity. He was my point man when learning what is required for admission to graduate school and offered me a position in his lab to help facilitate the process. I have no doubt his letter was instrumental in my admission to UCLA, which has led to a wealth of opportunities. Dr. Mike Roland is another professor who took a chance on me during my undergrad years. Prof. Neil Garg helped build my organic chemistry lab foundation, I was very fortunate to access his tutelage when I first arrived at UCLA. Working under Neil taught me how to work hard and efficiently along with strengthening my scientific writing foundation. Prof. Spokoyny of UCLA was kind enough as a new professor to take extra time out of his busy schedule to be one of my thesis committee members, and I'm sure there's a million other things he'd rather be doing to help his career and students. Early on in my research Prof. Spokoyny was kind enough to share advice on copper chemistry and help postulate experiments, which I am grateful for.

It is interesting that while writing this dissertation, summing up five years that now seemed so short, I can still remember times when I wanted nothing more than to quit. Because of these instances and my previous challenges with suicidal thoughts during my teenage years, I want to thank my amazing counselor Dr. Kei Takahashi. I have a tendency to blame myself for every problem I encounter, including problems that are not my fault. This thought process tends to snowball on itself leaving me in a dark and depressing place. Dr. Takahashi helped me become

happier with who I am and what I have accomplished; for that I cannot thank him enough. After graduating my current plan is to convince him to take house calls, because I have my doubts that I will ever meet another person as understanding and caring as him. I'm hoping that this paragraph can serve as a platform to help bring attention to suicide awareness and mental health. These disorders can affect anyone and providing an afflicted person with help is a big step in potentially saving someone's life or helping their career.

Continuing my thanks to people working at CAPS, Dr. Kalsi has been great as a psychiatrist. Because of my history with suicidal thoughts while on ADHD medicine I was hesitant to begin taking stimulants again after high school, however, I realized that I would not be able to be successful in graduate school as my inattentiveness was causing a narcoleptic state even with more-than-substantial sleep and caffeine pills. Dr. Kalsi helped me find a proper dosage and therapeutic (after more trials than I care to discuss) while always concerning herself with my symptoms and side-effects. She is truly a wonderful person and I will miss her and all of her kitten paraphernalia.

There are several more doctors I want to acknowledge for helping me at UCLA. To begin my general physician, Dr. Mukherjee, has helped me through strange stomach issues. She trusted took my pain symptoms seriously and had me seen by specialists in a timely manner. Next, Dr. Hame was the first surgeon, out of five, I've seen in the past nine years to put in a little elbow grease to diagnose my chronic hip pain. Despite having little MRI evidence for any problems with my hip, she cut me open and was able to repair a badly torn labrum and shave down my femur to fix a femoral impingement. Before meeting her I believed that I'd have to endure that chronic pain for the remainder of my life. The last medical official I'd like to thank is my physical therapist Kirstin who had to deal with me for a combined total of 8 months of 1-3x a week! We had a lot of

good jokes together and can't think of any other person, whom I'd rather have drive their elbow into my butt.

The colleagues and friends I've made since joining this program have been numerous and quite important in helping to keep my sanity. Emma Baker is the sister I wish I had. I'm 95% positive she hated me at first, but who would've guessed that me puking in her car and apologizing with two Toblerone bars would lead to such a fun and exciting relationship. Our restaurant and dessert expeditions have been relaxing trips to break up the week. Not only has she been there for emotional support, but as a scientific peer as well. Emma made herself available to edit my NIH NRSA Fellowship and talk me through all the necessary steps. I am in awe of her efficiency, maturity, and sense of humor, and think she is someone to look out for in the future. Next, I want to thank my original posse of Elias, Andy, and Rocky. Never would I have guessed that studying for cumes could be so fun! I am so pumped for Elias on finding the woman of his dreams and acceptance into his dream school for a postdoc. Andy is a brilliant scientist, and even better friend. When he left graduate school, I was so sad for the field, because he has such an amazing blend of creativity, brains, and drive. Andy is just able to accomplish whatever he desires, and I am so happy that he is returning to chemistry as a data scientist! Rocky is an extremely caring guy, who was always fun to be around, and hope is doing well in Philly.

Early on in my first year, the organic chemistry class broke out into little study groups; the group I stayed with included: Elias, Rocky, Andy, Juno, Emma P. I still keep in contact with this group four years later and am happy everyone is doing well. Juno has been a good friend, who I've discussed a few existential crises with in the early hours of the day. I'm happy that I was able to provide the information that led her to find a lab she enjoyed and allowed us to keep in touch during our co-advisor's group meetings. Me and Emma P. bonded over the fact that both of us

took part in NCAA athletics at DIII liberal arts schools. The only thing that matches Emma's determination is her happy and enthusiastic attitude.

I've had the pleasure of meeting many other people who I have no doubt will have an impact in the scientific community. Tyler Allred is a brilliant organic chemist, who can spout off and design some of the most interesting chemical reactions you could think of. I'm quite proud of myself for convincing him to attend the University of California-Chemical Symposium Conference that I helped put together, which essentially allowed him to network his way into a postdoc with Prof. Larry Overman. Francesco Manoni is another member of the Harran lab that helped make grad school more bearable. He is one of the most social and empathetic individuals I have ever met, just a person that would give the shirt off his back if you needed it. I am hoping to come across another opportunity that enables us to work together.

JK (Jeong Hoon) and Brett Cory are two other graduate students at UCLA that have helped me feel at home and happy in Los Angeles, while also giving me great insight on tackling chemical problems. JK is incredibly kind and the type of person that if when you pass by and says "how are you doing?" really means it. I've had a few simple greetings with him turn into 20min conversations in Young hall or the Mol. Sci. stair case talking about our future plans and graduate school problems. I'm super happy he has secured a postdoc with Grubbs! Brett may love chemistry more than anyone else I have met, and he can draw better than most people too. He has had an interesting path leading to graduate school and it has been fun talking to him about motorcycles, surfing, and teaching. I have no doubt he will win some great teaching awards in the future.

Prof. Mike Jung and his group have acted as my adoptive lab in graduate school and accepted me with open arms despite my plentiful quirks. Courtney Roberts was a graduate student in the lab and I first really got to meet her while teaching Chem 144. While teaching with Courtney

I was pleasantly surprised to learn we had similar senses of humor and it made the long hours go by remarkably more quickly. She was also great for talking about personal issues and is pretty good person to come to for advice. Ironically, she is now working at the Naval Research Laboratory, which is where I interned in undergrad during the summers and winters. The power couple of Xiaohong and Xiaoguang have been extremely supportive, reminding that I'm intelligent, whenever I finished a conversation with them I felt like I could go out and accomplish an important problem in the sciences. They also have fed me numerous times and that on its own is worth a shout out, the hospitality they provide during their hot pots is legendary. I have also been most fortunate to meet with Prof. Jung as much as I did. He is an incredibly brilliant scientist with a memory that would make an elephant envious… at one point I confronted him about his memory capabilities just to confirm he has an eidetic memory, which he did. Attending his group meetings kept me engaged in the principles of organic chemistry and without them I would most likely have forgotten to write mechanisms. Outside of science Prof. Jung was a go to person when I needed advice on health issues or personal matters. The most important thing he has done for me though is make xtandi, which is helping to keep my grandpa alive and I am so grateful.

In CNSI I have made numerous friends, which is due to the truly wonderful collaborative atmosphere on our floor. The joint labs of Prof. Sam Sadeghi and Prof. Mike van Dam kept a smile on my face through enjoyable conversation and random trips throughout the city. Philip entered graduate school in the same year as me and has been super helpful in discussions on radiochemistry and beer picks. Jia, Jason, Noel, Ksenia, Adrian and Alejandra have been really inviting and kind enough to let me tag along to their lab events and outings.

At UCLA I've had the opportunity to collaborate with well-known and impactful professors, who have helped broaden my breadth of knowledge in the sciences and need to thank

them for such successful projects. Near the end of 2016, I was randomly contacted by Brian Levandowski who was in the Houk lab and a member of my cohort, asking if I'd be interested in helping him with a bioorthogonal project. At the time all I could think was Houk equals big publications and immediately agreed. The project ended up being much more fun and exciting than I thought and am happy to see it get into JACS with a spotlight on the work soon to be published and have a potential full patent on the way. Prof. Houk's knowledge on what additional experiments are needed to push the project into what journal was incredibly helpful and will be quite prudent if I become an academic in the future. The other collaboration I was fortunate to take part in was with Prof. Wu's group where I had the privilege to work with Kirstin, Wenting, and Felix. They have taught me a lot about immunology and what one should consider in the design of good ImmuoPET tracers. Kirstin was kind enough to let me watch the injections and mice imaging, while answering my million questions! Wenting, a fellow fifth year, has been one of my go-to people for biology and cancer questions and quite good in replying in a manner that a chemist can understand. Felix has been slowly turning into a Kings fan and know it's one of the better life choices he's made. From the Clark lab, Alicia, Jessica, and Bao have been there to answer biology questions. Alicia and Bao provided some great feedback on the biology portion of my NIH fellowship and have been provided a quality forum for discussions on good anime series.

Fortunately, for me I have made some great friends that kept me motivated in grad school by offering to talk about difficult issues or keep me occupied on some other activity. My college roommate Scott was kind enough to come visit me and accompany me to sports games and teach me how to "pwn" in call of duty. Throughout my time in Los Angeles he's made time to visit me with his awesome wife, Shelby, and feel so fortunate to have been a groomsman in their wedding. He has been there for me through the best and worst of times and I am lucky to have him as a

friend. Three other college teammates ‘Sporty’, Michael, Emily, and Tony have been helping me keep my cool in graduate school through simple, fun conversation about their lives in the military/accounting world. Sporty was my first friend I got to see in California, since he was able to make the cross-country trip with me! Little did we know that destiny would have him stationed at Vandenberg for training and enable some weekend getaways to hang out and go running a few more times together. Tony can be one of the most mature and immature guys you’ll meet! A perfect characteristic in a friend as you can discuss real life issues one day and be lounging on a floaty in a lake with bud light the next. Michael Hoy is a super charismatic and driven guy, happy to help his friends out in any way that he can. Like my friendship with Emma Baker, me and Emily didn’t always get along, but for some odd reason after college we have remained close. I think it’s attributed to our more lewd and silly shared sense of humor. Her and my other college friends have been there for each other during the rough patches after college and they mean so much to me.

I also want to acknowledge a few more people that have been there for me in graduate school. My oldest friends, Gil and Lonnie, are a staple group of people I have to see when I go home. Gil is one of the more resilient people after still pursuing his dreams of being a playwright in Chicago after suffering through a tragic family event. Lonnie and I were in a rock band way back when and is extremely stubborn and driven, as well as dorky. I am not in the least bit surprised he is in a much better and more successful band, Wylder (shameless plug), and am so lucky he will be in Los Angeles during my hooding ceremony! His band deserves recognition and am stoked to hear what Lord Huron’s producer can do for them. The next person I’d like to thank is my friend Cassie left me with a year of fond memories, from camping to meme sharing. I am super proud of her for graduating from Columbia with a M.P.H. and have no idea why she is now going to Berkeley to get another M.S. in environment engineering but wish her the best of luck. Tina is my

good friend in the medical school and is brilliant, I don't know how someone can be as disciplined as her in terms of working out, cooking, going on fun vacations, while preparing and then crushing the step exams, but she's managed it. I'm hoping she decides to join me in Philly with our mutual friend Matt. At any point during graduate school I could call up Matt and usually goad him into joining me. He was my running buddy, surfing buddy, hiking buddy, foodie buddy, and hockey buddy. The only frustrating thing with Matt is how good he is at everything from chess to surfing, I swear his abstaining from ever having an alcoholic drink has blessed him with super powers. My girlfriend Ariel has had a huge role in my graduate school journey. During the fourth and fifth years of graduate school, I experienced a multitude of health problems that caused me to be in quite a large amount of daily pain to the point that narcotics were necessary for me to function ok at work and home. I can't imagine I was very fun to be around at this point, but she stuck by me and helped in any way she could from keeping me company and providing a distraction, to making me meals for the week to help save me money, to driving over at midnight because I was having an emotional breakdown. She is so selfless and willing to do so much for her friends, that listening to her talk about other reminds me that I chose a good one :). I'm excited to continue learning and growing as a couple with her in Philadelphia as we tackle our next adventure.

Lastly, I want to thank my mom and dad for their selfless support of me. They are far from perfect but have always been there for me when I needed them most no matter what was going on in their own lives. I have been fortunate to grow up in a family that paid for my college and honestly let me choose my own life path. Growing up around such educated and community-oriented people allowed me to not put limits on myself, try out as many as activities as possible, and helped foster the importance of helping others.

BIOGRAPHICAL SKETCH

Education

University of California Los Angeles, Los Angeles, CA 2013 - present
- **Ph.D. Candidate** in Organic Chemistry

Christopher Newport University, Newport News, VA 2009 - 2013
- **B.S.** in Chemistry

Research Experience

University of California Los Angeles, Los Angeles, CA 2014 - present
Ph.D. Candidate, Advisor: Professor Jennifer Murphy
- Developed a copper-mediated fluorination of aryl stannanes
- Designed and developed a general platform for a multifunctional chemical linker to produce a dual modality (PET/optical) antibody-based imaging agent for PSCA-expressing prostate cancer
- Synthesized and reformulated [^{18}F]*trans*-cyclooctene ([^{18}F]TCO) for *in vivo* molecular imaging studies
- Evaluation of a novel bioorthogonal ligation involving cyclopentadienes
- Synthesis of cyclopentadiene derivatives and calculation of their reaction rates via *pseudo*-first order kinetics

University of California Los Angeles, Los Angeles, CA July – November 2013
Graduate Research Assistant, Mentor: Professor Neil Garg
- Synthesized imidazopyridyne precursors
- Performed scale up reactions for the synthesis of the natural product picrinine

Christopher Newport University 2011 - 2013
Undergraduate Research Assistant, Advisor: Professor Jeffrey Carney
- Utilization of the Hosami-Sakurai reaction as a route to synthesize new natural products

Naval Research Laboratory summers 2011, 2012
Summer Intern, Mentor: Dr. Michael Roland
- Researched new applications of polymers to be implemented as armor

Awards

UCLA Research Showcase Fellowship Spring 2017

Publications

1. **Gamache, R. F.**; Zettlitz, K.; Waldmann, C.; Tsai, W.; Murphy, J. M.; Wu, A. Synthesis of a Renal Clearing Tri-Modal Linker that Enables Dual PET and Fluorescence Imaging of PSCA^{+} Prostate Cancer. (In Preparation)
2. Levandowski, B. J.†; **Gamache, R. F.**†; Murphy, J. M.; Houk, K. N. Readily Accessible Ambiphilic Cyclopentadienes for Bioorthogonal Labeling. *J. Am. Chem. Soc.,* **2018***, 140*, 6426–6431. †**Authors contributed equally *JACS Spotlight**

3. **Gamache, R. F.**; Waldmann, C.; Murphy, J. M. Copper-Mediated Oxidative Fluorination of Aryl Stannanes with Fluoride. *Org. Lett.* **2016**, *18*, 4522-4525. **Highlighted in Synfacts* Highlighted in Synform***

4. Casalini, R.; **Gamache, R. F.**; Roland, C.M. Density-Scaling and the Prigogine-Defay ratio in liquids. *J. Chem. Phys.* **2011**, *135*, 224501-224505.

Presentations

1. **Raymond F. Gamache**, Brian Levandowski, Jennifer M. Murphy, Kendall Houk. Readily Accessible Ambiphilic Cyclopentadienes for Bioorthogonal Labeling. University of California Chemical Symposium, UCLA Lake Arrowhead Conference Center, Lake Arrowhead, CA, Spring 2018

2. **Raymond F. Gamache**, Christopher Waldmann, Kirstin Zettlitz, Wenting Tsai, Anna Wu, Jennifer M. Murphy. Evaluation of chemical linkers for ^{18}F-labeling of antibody-fragments to image PSCA-expressing prostate cancer. Poster Abstract. UCLA Pharmacology Retreat 2016, University of California-Los Angeles, Los Angeles, CA, Fall 2017

3. **Raymond F. Gamache**, Christopher Waldmann, Jennifer M. Murphy. Copper-Mediated Oxidative Fluorination of Aryl Stannanes with Fluoride. Poster Abstract. American Chemical Society National Meeting Spring 2017, San Francisco, CA, Spring 2017

4. **Raymond F. Gamache**, Christopher Waldmann, Jennifer M. Murphy. Copper-Mediated Oxidative Fluorination of Aryl Stannanes with Fluoride. Poster Abstract. University of California Chemical Symposium, UCLA Lake Arrowhead Conference Center, Lake Arrowhead, CA, Spring 2017

5. **Raymond F. Gamache**, Christopher Waldmann, Kirstin Zettlitz, Wenting Tsai, Anna Wu, Jennifer M. Murphy. Evaluation of chemical linkers for ^{18}F-labeling of antibody-fragments to image PSCA-expressing prostate cancer. Poster Abstract. UCLA Pharmacology Retreat 2016, University of California-Los Angeles, Los Angeles, CA, Fall 2016

6. **Raymond F. Gamache**, Christopher Waldmann, Jennifer M. Murphy. Copper-Mediated Oxidative Fluorination of Aryl Stannanes with Fluoride. Poster Abstract. UCLA Pharmacology Retreat 2016, University of California-Los Angeles, Los Angeles, CA, Fall 2015

7. **Raymond F. Gamache**, The Application of Chiral Thiourea Catalysts in Natural Product Total Synthesis. Oral Presentation. Chemistry 248 Organic Student Seminar, University of California-Los Angeles, Los Angeles, CA, Fall 2014

8. **Raymond Gamache**. The Synthesis of a new Diarylheptanoid using Organometallic Coupling Methods. Oral Presentation. Pogia Research Presentation, Christopher Newport University, Newport News, VA, Spring 2013

CHAPTER ONE

Synthetic Chemistry Strategies towards ^{18}F-labeling of Arenes and Biomolecules for Molecular Imaging Applications

1.1 Abstract

PET imaging is a useful diagnostic tool capable of detecting and quantifying a variety of diseases, disorders, and physiological ailments. Through the administration of a tracer containing a positron-emitting isotope, a PET scanner is able to generate three dimensional images of the uptake and metabolism of the radiopharmaceutical. Fluorine-18 represents one of the more popular isotopes used in this technology due to its half-life of 109 minutes and ease to create in a cyclotron facility. With PET becoming a more widely used technique, practical methods to incorporate fluorine-18 and other radioisotopes into small molecules and biomolecules are being rapidly developed. The field of organic chemistry specializes in making new molecules and methods and is pioneering reactions and syntheses to advance this field by producing PET tracers more efficiently and quickly. In particular this chapter will focus on nucleophilic fluorine-18 incorporation into aryl rings and prosthetic groups.

1.2 Introduction

PET imaging presents a viable option in the diagnosis of many ailments including cancer, Alzheimer's Disease, and autoimmune diseases.[1–3] This technique is reliant on the uptake of a tracer into target tissues of interest, which also provides a means to monitor treatment response. One of the more popular isotopes, when working with small molecule PET tracers, is fluorine-18.

This particular isotope of fluorine is perfectly suited for imaging as it decays ~97% through positron emission with a half-life of 109 minutes. These attributes are advantages over alternative positron-emitting isotopes such as carbon-11, which possesses a half-life of 20 minutes. Copper-64 is another commonly used isotope and has a half-life of 12 hours but suffers from the requirement of chelating ligands as it cannot form very stable bonds to carbon. In addition, only 18% of copper-64 decays through positron emission; the other decay methods include both harmful beta particle emission and gamma radiation.

The carbon-fluorine-18 bond formation represents a challenge in the synthesis of PET tracers. When working with an element that contains a very short half-life, careful consideration in the timing of its incorporation needs to be a concern. Early integration of a positron emitting isotope may lead to a final compound that has too little activity to be useful for imaging. However, some compounds will not withstand traditional radiofluorination methods and require earlier incorporation of the isotope. One of the original fluorination methods is the S_N2 substitution of a fluorine anion to displace a leaving group. This simple reaction has been used to make the most commonly used PET tracer, FDG, which is useful in the diagnosis of a variety of diseases including: cancer, dementia, and autoimmune encephalitis.[3–5] The biggest obstacle associated with S_N2 substitution is that it is most useful when applied to a substrate bearing a leaving group on a primary carbon. Although this reaction has been used many times on substrates containing a leaving group on a methylene carbon, typically higher temperature is needed for the reaction to occur in a useful timeframe with good radiochemical yield.

Another obstacle of organic chemistry reactions utilizing fluoride as a nucleophile is its high oxidative potential, electronegativity, and basicity. S_N2 reactions are simpler in terms of conditions, but there is still a high potential to get many side products due to these characteristics.

The basic nature of fluoride excludes a variety of protic solvents from being used as they form hydration shells around the fluoride anion, which lowers its nucleophilicity. Water must be thoroughly removed from the reaction otherwise the fluoride can form bifluoride (HF_2^-), which has very strong hydrogen bond interactions,[6] thus killing the nucleophilicty of the reagent.

The traditional approaches leading to aryl fluorination usually require harsh conditions to yield the desired product. In addition, many aromatic substrates will still not deliver the desired product depending on the electronics of the system. Organic chemists have teamed up with radiochemists to help solve these problems and make many radiopharmaceuticals readily available. Through the use of more reactive groups such as iodonium salts, phenols, and transmetalating groups, many substrates can now be radiolabeled under mild conditions.

1.3 Iodoinum Salts

A functional group that is used often in the synthesis of radiopharmaceuticals is an iodonium salt. Diaryliodonium salts are highly reactive and when subjected to a nucleophile, such as fluoride, will result in the insertion of the nucleophile into one of the aromatic rings. Controlling the regioselectivity of the fluorine group posed a difficult problem upon the initial findings of this reaction but have since been optimized. Various substitutions on the unwanted aryl ring to increase its steric bulk and/or modify its electronic nature have proven to be viable methods to create more selectivity in this reaction. A general mechanism of this fluorination technique is shown below in Scheme 1.1.[7] The initial step of this reaction proceeds through a ligand exchange on the iodonium salt where a salt such as a triflate is replaced with a fluoride ion. This T-shape molecular conformation can exist as two isomers: one has the electron rich aryl ring perpendicular to the fluoride group (above), while the other prefers the electron poor aryl ring perpendicular (below).

From this position the fluoride can only insert into the aryl ring separated by ninety degrees. Preference in which T-shape conformation reacts more readily is due to the ability to form a more stable intermediate from the iodonium substitution. The new bond formed as fluoride enters the ring creates a partial negative charge in the ring; this partial negative charge is stabilized more with an electron withdrawing group than with an electron donating group. Better stabilization of the reactive intermediate allows for the electron deficient ring to be more readily reactive to fluoride than the electron rich ring.

Scheme 1.1. Radiofluorination mechanism of diaryliodonium.

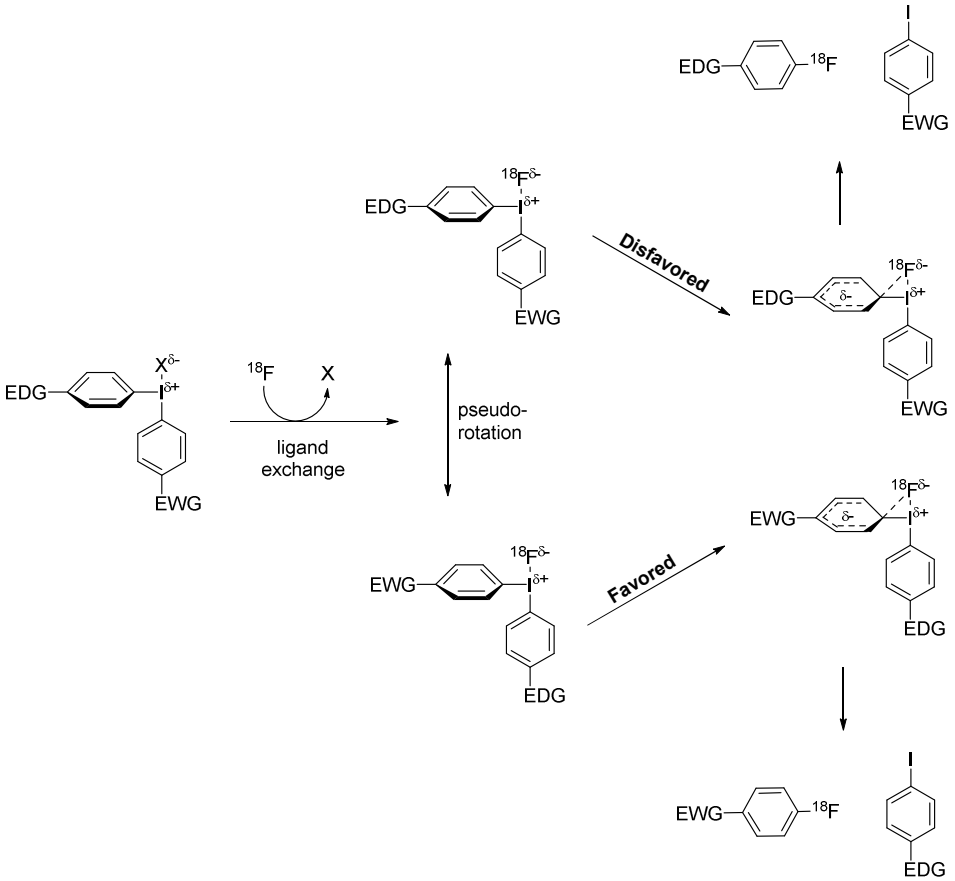

Use of diaryliodonium salts in the synthesis of a PET tracer is showcased by Elsinga and coworkers in their synthesis of ^{18}F-DOPA (Scheme 1.2).[8] ^{18}F-DOPA is an analog of L-DOPA a

compound synthesized readily in humans. The reason why an L-DOPA analog is an important tracer is due to the parent compound being a precursor to many of the catecholamine neurotransmitters, including: Dopamine, 3-Methoxytyramine, Norepinephrine, and Epinephrine.[9,10] By taking advantage of these innate properties, ^{18}F-DOPA has been utilized in the study of disorders of depression and schizophrenia,[11–13] which have a correlation to neurotransmitters.[10] Additionally, FDOPA has shown higher accuracy in the detection of low grade and recurrent brain tumors when compared to FDG.[14,15] In their report, the synthesis of ^{18}F-DOPA is compared between the conventional electrophilic method[16] to starting from an iodonium precursor. Higher radiochemical yields were obtained from the electrophilic method, 33% versus 14%, but the product was obtained with much lower specific activity, 11 GBq/mmol versus 35,050 GBq/mmol. Elsinga's synthesis began from the triflate salt of the anisole iodonium salt, which could be fluorinated with kryptand fluorine-18. The kryptand ligand chelates with the potassium ion of potassium fluoride, thus increasing fluoride's nucleophilicity. then treated with sulfuric acid to remove the EOM, Boc, and methyl ester protecting groups to furnish ^{18}F-DOPA in a decay corrected 14% yield. Further optimization of the radiofluorination of diaryliodonium salts was pioneered by the Sanford and Scott groups at Michigan.[17,18] Using these groups' newly developed methodology, fluorination of electron rich rings proceeded well by the use of a sterically bulky counter aryl ring and a copper catalyst.

Scheme 1.2. Elsinga's synthesis of ^{18}F-DOPA.

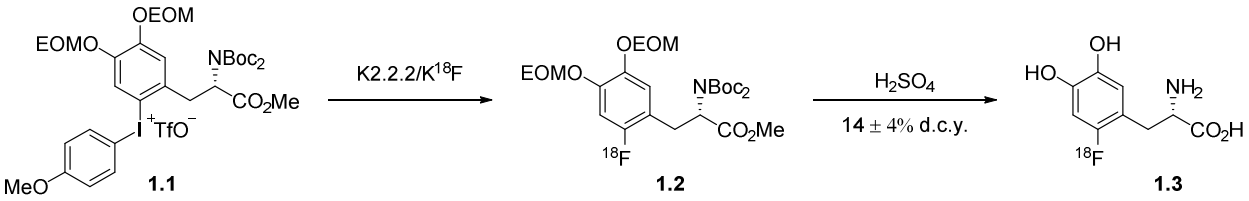

As the versatility of the iodonium salts expanded, higher selectivity and yields were sought after. The next advancement came from patented work by Barrio and Satyamurthy[19] along with the joint effort of Liang and Vasdev through the fluorination of an iodonium ylide.[20] The mechanism of this reaction and the computed energy barrier to give the two regioisomers is shown in Scheme 1.3.[21] Nucleophilic attack of fluorine-18 onto the iodine creates a stabilized anion alpha to the diester, which greatly hinders the ability of any nucleophile to displace the iodonium at that position. The buildup of electronegativity on the diester allows the fluoride to preferentially displace iodine on the aryl ring that has less electron density alpha to the iodonium.

Scheme 1.3. Radiofluorination mechanism of iodonium ylide **1.4**.

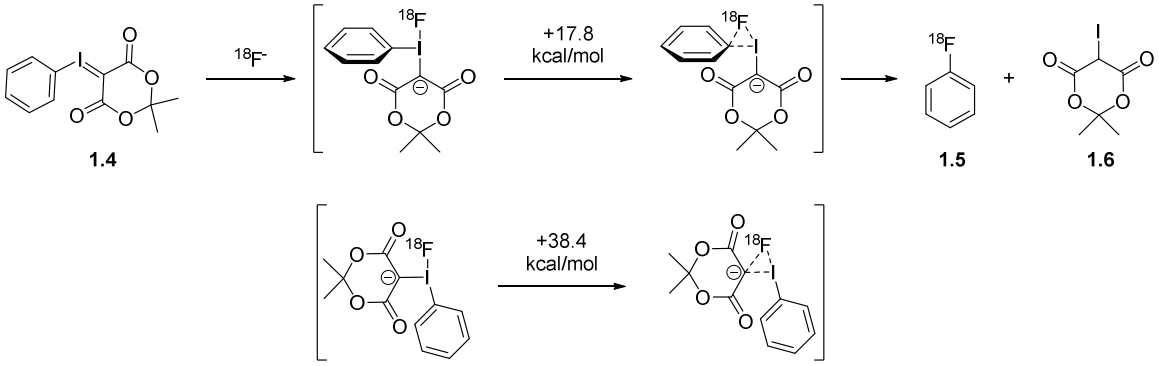

Liang and Vasdev continued to work on this methodology leading to the syntheses of 5-[^{18}F]fluorouracil[20] (Scheme 1.4) and [^{18}F]FPEB (Scheme 1.5).[22] Highlights of Liang's synthesis of fluorouracil include a final non-decay corrected radiochemical yield of 11%, despite the introduction of the radioisotope occurring in an earlier step. The high specific activity of this compound along with the yield make this route suitable for clinical production, which is useful for monitoring the therapy of patients being treated with 5-fluorouracil.[23] A synthesis established by Vasdev also enables a clinically viable route to the radiopharmaceutical [^{18}F]FPEB, a metabotropic

glutamate receptor subtype 5 (mGlu5) antagonist used in brain imaging.[24,25] In this synthesis fluorine-18 substitution is performed in the last step leading to a higher non-decay corrected yield of 20% along with high specific activity.

Scheme 1.4. Liang's synthesis of 5-[^{18}F]fluorouracil.

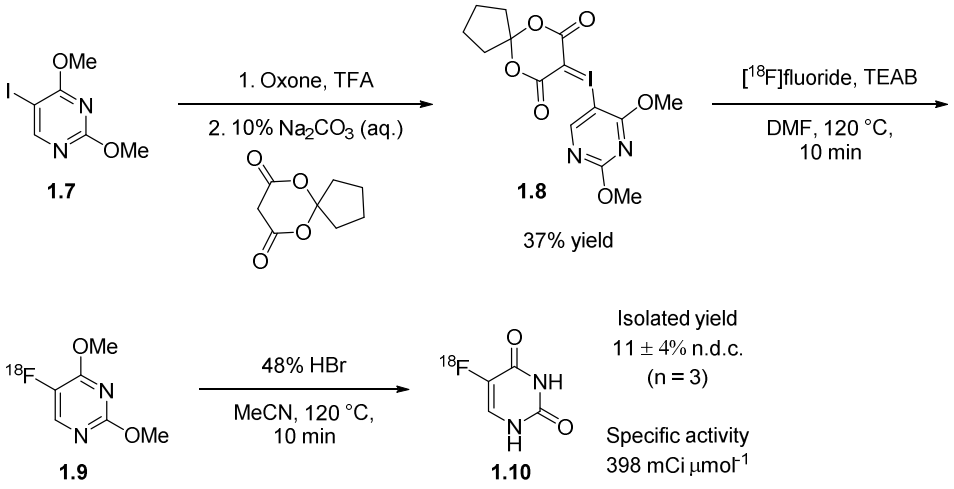

Scheme 1.5. Vasdev's synthesis of [^{18}F]FPEB.

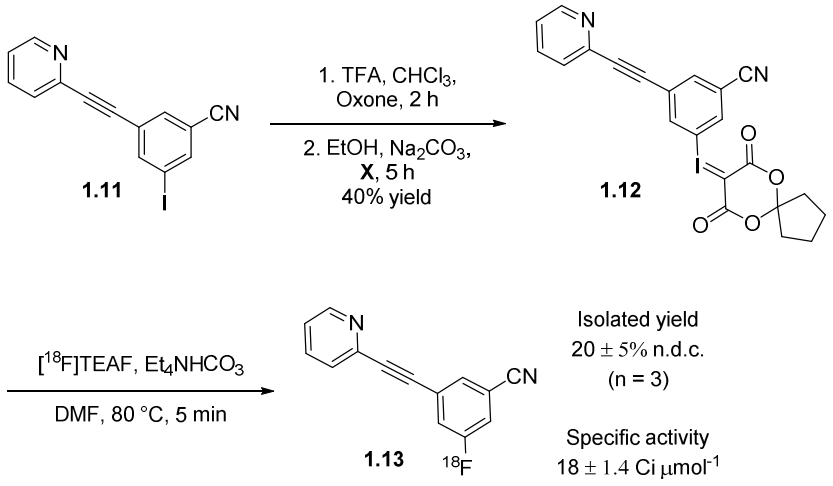

1.4 Phenol Fluorination

Further advancements in the field of fluorination and radiofluorination came from work in the Ritter lab. Ritter's group were able to determine a method to effect fluorination at the site of a readily available functionalities available in many starting materials, a phenol.[26–28] In this methodology the phenol is treated with the deoxyfluorinating reagent phenofluor **1.15** or phenofluor mix to cause the transformation shown in Scheme 1.6. Nucleophilic substitution of the phenol onto the reagent generates the diaryl imidalzolium salt. A nucleophilic fluoride salt can then insert onto the electron poor carbon of the imidazolium, which allows a concerted displacement of the aryl ether to produce the fluorinated product and the imidazolinone.

Scheme 1.6. Proposed mechanism of the fluorination of phenols using phenofluor.

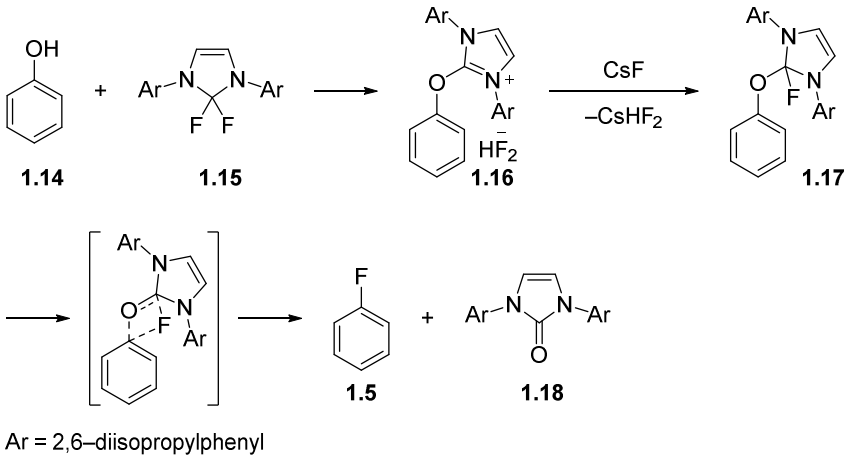

In Ritter's inaugural work, many complex, biologically active derivatives were fluorinated and radiofluorinated in high yields. One such compound was [^{18}F]4-fluoro-thieno[2,3-d] pyrimidine (Scheme 1.7), a member of the thienopyrimidine family, which have a broad range of activity including: cGMP phosphodiesterase inhibitors, anti-viral agents, anti-inflammatory agents,[29] anti-microbial agents,[30] as well as kinase inhibitors and anti-cancer agents.[31,32] Use of the

phenofluor mix **1.20** enabled isolation of intermediate **1.21** that was readily fluorinated in the presence of no-carrier added fluorine-18, delivering a novel radiotracer in 81% radiochemical conversion.

Scheme 1.7. Ritter's synthesis of [^{18}F]4-fluoro-thieno[2,3-d]pyrimidine.

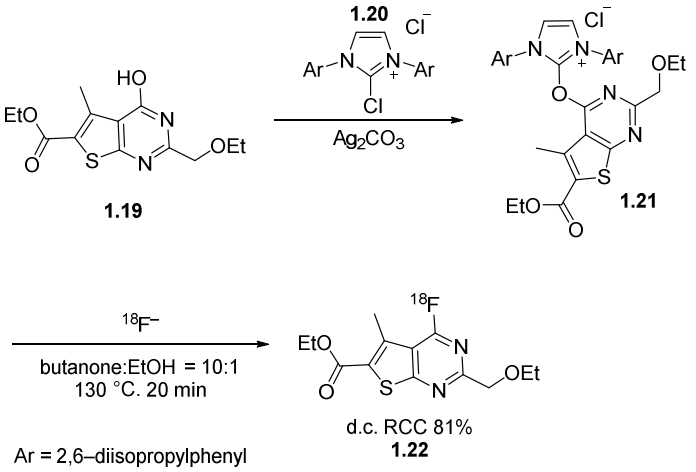

The fluorination of these phenols worked quite well when performed on electron deficient aromatic rings but could not tolerate electron rich substrates. Addition of fluorine into the aromatic ring had too high of an energy barrier. A solution to this problem came in the form of a Ru π-complex to the aryl ring, which reduces electron density in the arene (Scheme 1.8).[27] Enabling the π-complex to form is essential in lowering the barrier associated with fluoride addition into the imidazolium favoring the product formation in equilibrium K_2. In contrast, when the Ru π-complex is not formed the equilibrium K_1 is much lower resulting in the reactant being preferred. Use of a high valent Ruthenium allows this methodology to be tolerant of a wide variety of nucleophilic functionalities. The reaction only suffers from the difficulty in decomplexation of the arene from ruthenium, which is the rate-limiting step and typically requires high temperature.

Scheme 1.8. Proposed mechanism of the radiofluorination of electron-rich phenols.

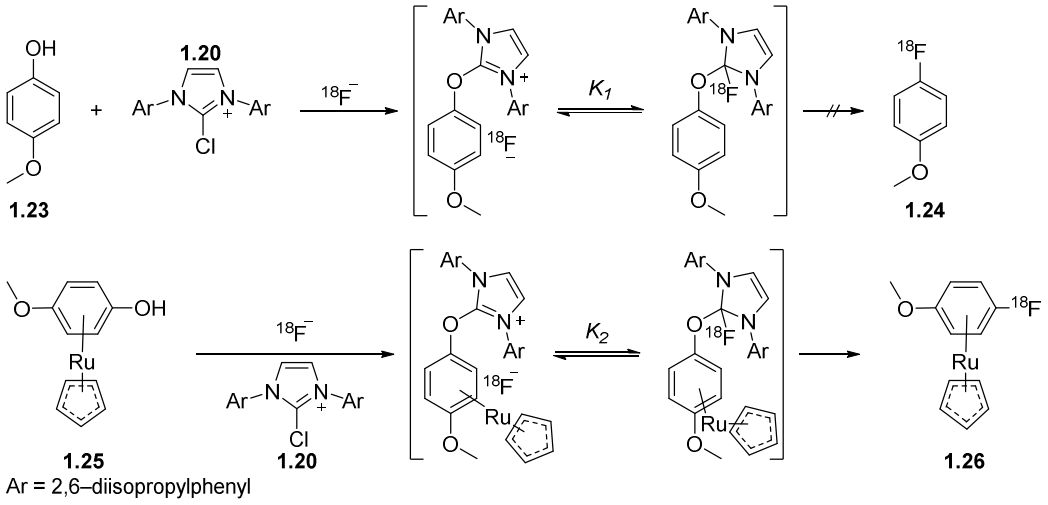

Radiofluorination of phenols utilizing the phenofluor mix was used in the clinical production of the novel HDAC6 inhibitor, Bavarostat, in the Hooker lab (Scheme 1.9).[28] This tracer allows for the imaging of epigenetic proteins that have been implicated in the cause of many neurological disorders. Use of this methodology allowed production of the tracer in high enough radiochemical yields and specific activity to be used in both rat and non-human primate imaging.

Scheme 1.9. Hooker's synthesis of the HDAC6 inhibitor Bavarostat.

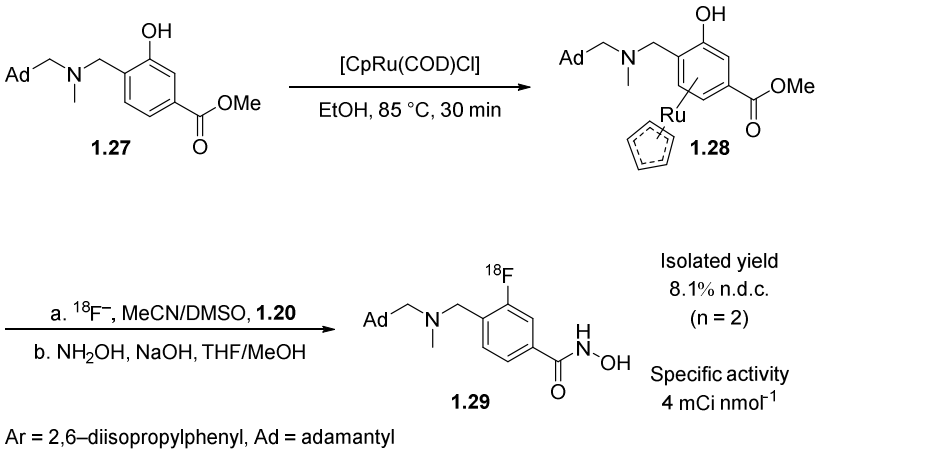

1.5 Transition Metal Fluorination

Radiofluorinations of aryl rings with nucleophilic fluorine-18 has also been facilitated through transition metals including: copper, nickel, and palladium.[33,34] These metals exhibit a wide range of reactivity and operate through different mechanisms. Copper represents an important metal for use in organometallic chemistry; it is in higher natural abundance and less expensive than many precious metals used in this class of reactions. Fluorination methodology of aryl rings utilizing a nucleophilic source and copper have been demonstrated before in the literature giving rise to the possible idea of conversion to radiochemistry.[35,36] Mechanisms for forming the fluorinated product are not well known, but a postulated disproportionation of copper triflate is believed to be the driving force of the reaction (Scheme 1.10). Initially copper triflate is proposed to undergo a ligand exchange with the fluoride to deliver complex **A**, which can undergo a transmetallation with a boron or metal species to deliver aryl copper compound **B**. Disproportionation of copper triflate is then theorized to oxidize the aryl copper (II) to the more reactive copper (III), which is known to readily reductive eliminate generating the fluorinated product.

Scheme 1.10. Proposed copper(II) triflate fluorination mechanism.

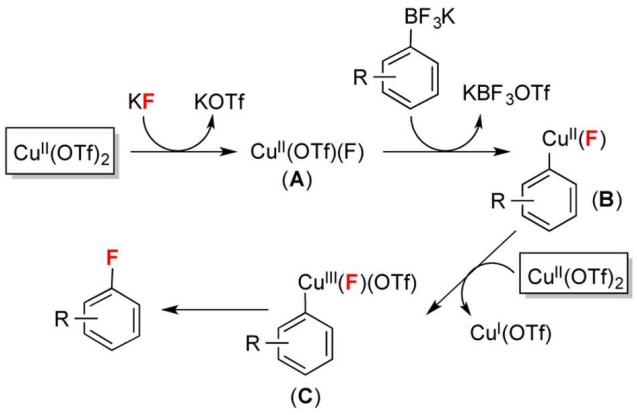

Sanford and Scott along with Gouverneur were able to make use of this methodology and modified the conditions to allow radiofluorinations of aryl rings bearing organoboranes[37–41] and organotin[42] functionalities. The radiolabeling of an organostannane precursor to the radiopharmaceutical, [^{18}F]MPPF, was performed in clinical quantities using this copper approach (Scheme 1.11). In contrast, creating this pharmaceutical from the aryl nitro precursor resulted in a lower radio chemical yield of 7%, verifying the potential of the copper methodology. Furthermore, the final product passed all cGMP quality control testing.

Scheme 1.11. Synthesis of [^{18}F]MPPF.

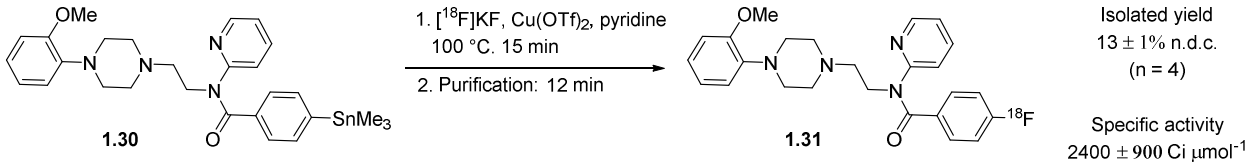

Other metals utilized for the synthesis of PET tracers have been pioneered by the Ritter lab, where palladium[43,44] and also nickel[45] have led to extremely fast reactions with nucleophilic fluoride. The original palladium methods acted as an efficient means to quickly fluorinate a broad substrate scope, but suffered from issues of the electrophilic palladium (IV) complex's instability and an additional fluorine-18 capture step. To overcome this challenge a similar ligand design with nickel was developed and allowed one step radiofluorination (Scheme 1.12).

Scheme 1.12. Proposed mechanism on the radiofluorination of Nickel complexes.

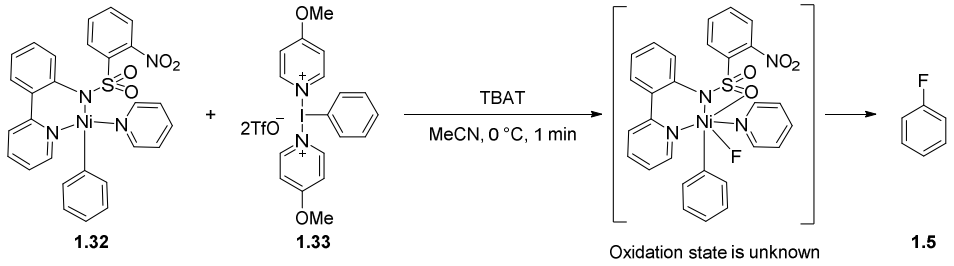

Proof-of-concept of this reaction's usefulness in clinical production of PET tracers was shown in the synthesis of [^{18}F]uracil.[46] Protection of uracil as a tert-butyl precursor enabled the precursor to be engaged as an appropriate ligand to be labeled. The fluorination required only one minute to reach completion and led to a 15% manual radiochemical yield of the precursor. When the procedure was optimized for automated production, the automated synthesis of uracil delivered 13.5-18.8 mCi of product in an isolated non-decay corrected yield of 0.92%, values suitable for human imaging.

Scheme 1.13. Ritter's synthesis of uracil.

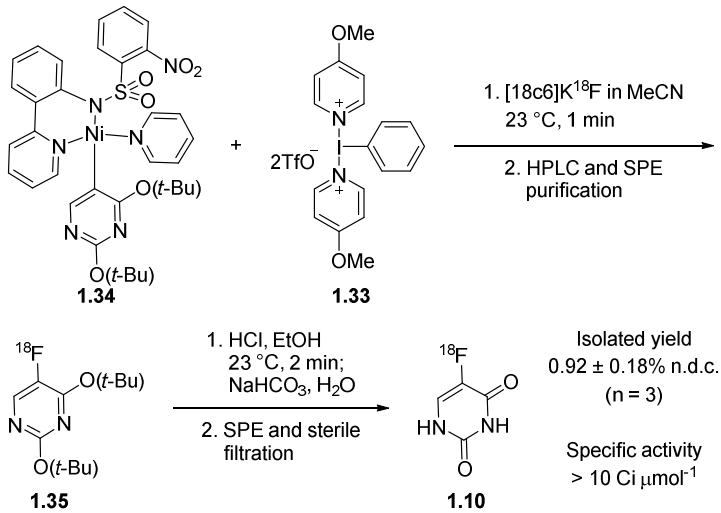

1.6 ImmunoPET and Peptide Labeling

Radiolabeling of antibodies, antibody fragments, other proteins, and peptides represent an important class of imaging agents to garner biological information. However, there are many challenges to accomplishing the development of proteins and peptides as tracers. Many of these compounds cannot withstand harsh conditions that facilitate fluorination and become denatured at elevated temperature. Furthermore, the solvents used in organic chemistry can also denature proteins and usually result in solubility issues. Chemists and biologists have circumvented this barrier by developing fluorine-18 prosthetic groups that can label these classes in more amenable conditions.

One of the most common prosthetic groups that is used, via random labeling, is *N*-succinimidyl 4-[^{18}F]-fluorobenzoate ([^{18}F]SFB). This prosthetic group is typically synthesized from the ester precursor **1.36**. An S_NAr reaction on the phenyl ring enables fluorine-18 displacement of the ammonium salt followed by hydrolysis and activation of the acid delivers [^{18}F]SFB **1.37**. The activated ester is quite reactive with free amines and is commonly used to label primary and secondary amines present on proteins or peptides. For example, Anna Wu and co-workers used this prosthetic to label an anti-HER2 cys-diabody that was able to target HER2 expressing breast cancer tumors in mice (Scheme 1.16).[47]

Scheme 1.14. Non-site specific labeling of anti-HER2 cys-diabody.

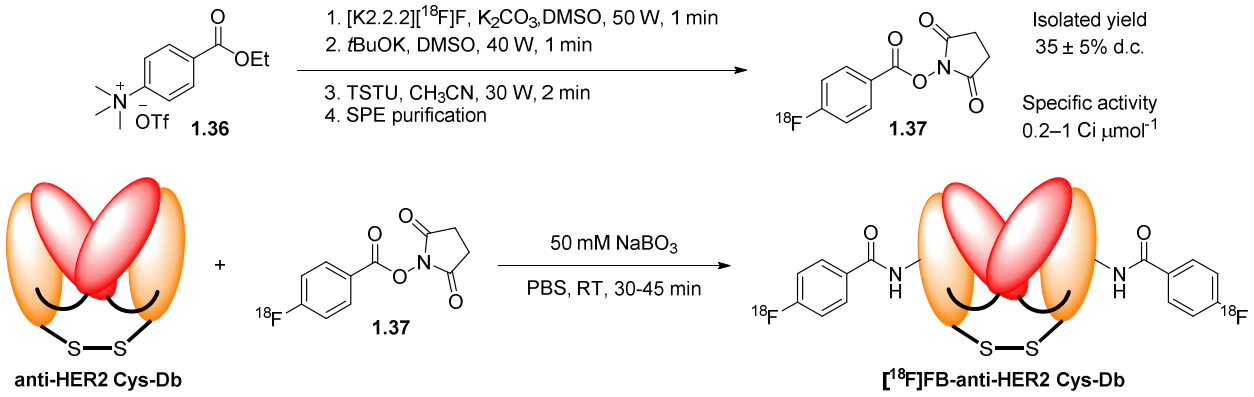

.

Random labeling may interfere with a tracer's ability to bind to its target with high affinity. As such, an alternative to random labeling is a site-specific labeling approach which targets specific amino acids of the protein or peptide. The prosthetic group [^{18}F]FBEM is able to label only cysteine residues in proteins and peptides through a maleimide functionality. [^{18}F]FBEM is synthesized from the previous prosthetic group [^{18}F]SFB through an activated ester coupling with an amino maleimide. Despite the long step count [^{18}F]FBEM is able to be isolated in decent non-decay corrected yields, which has led to its conjugation to a derivatized RGD peptide that was used in the imaging of integrin $\alpha_v\beta_3$ (Scheme 1.17).[48]

Scheme 1.15. Site specific labeling of SRGD peptide with [^{18}F]FBEM.

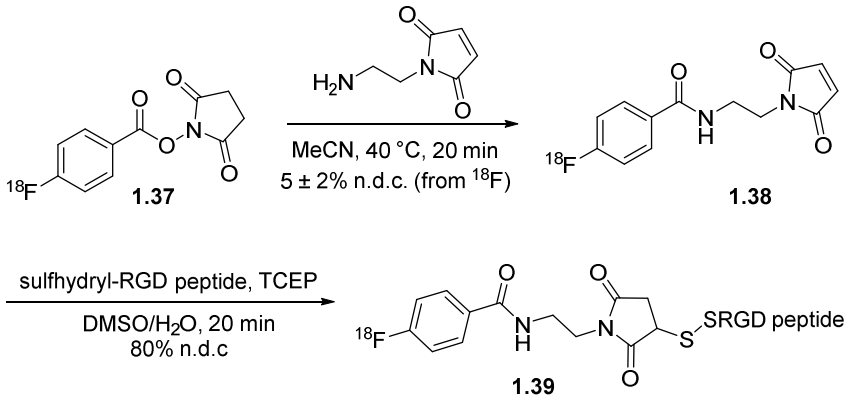

Another means to create a radiolabeled prosthetic group is through the use of isotope exchange methodology, where an isotope of an element of an isotope is exchanged with a different isotope of the same element. This effect is typically used for radiochemistry purposes by exchanging fluorine-19 with fluorine-18 on silicon fluoride bonds as well as boron fluoride bonds. Schirrmacher and co-workers utilized this approach in the synthesis of the prosthetic group [^{18}F]SiFB, which contains the activated ester component of SFB, but utilizes fluorine-18 incorporation in the final step giving higher radiochemical yields. The high radiochemical yields allowed them to use [^{18}F]SiFB to label rabbit serum albumin (RSA) and image its biodistribution in rats (Scheme 1.18).[49]

Scheme 1.16. Labeling of RSA protein using the isotope exchange prosthetic [^{18}F]SiFB.

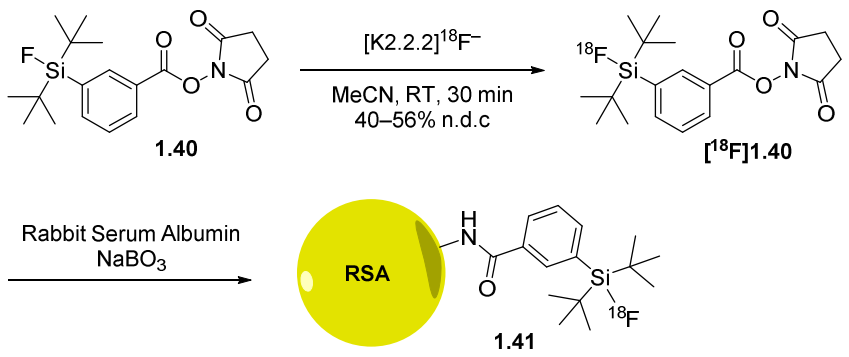

Bioorthogonal chemistry has also proven to be a feasible means to label compounds beginning from nucleophilic fluorine-18 through "click" type reactions. Click reactions are quick reactions that can take place in a variety of different mediums and only react with orthogonal partners. The orthogonal reactivity prevents side-reactions from taking place in the body that may lead to off-target labeling. Imaging of biomolecules using click chemistry for *in vivo* applications requires reactions with second order rate constants of at least 10 M^{-1} s^{-1}; the reaction between tetrazine and *trans*-cyclooctene has a rate constant of 10^4 M^{-1} s^{-1},[50] and has been used many times in PET imaging applications.[51] The fast reaction rates have led researchers to develop methods to fluorinate both of these groups, so that they may be used interchangeably.[50,52–54] The tetrazine has poor stability in physiological conditions due to cross reactivity with water and cysteine, so it is more advisable for long term imaging studies to have the TCO incubated longer in the body. Sarparanta and his group used this bioorthogonal labeling to study the biodistribution and internalization of the antibody therapies trastuzumab and cetuximab using a TCO pre-targeting approach (Scheme 1.19).[53]

Scheme 1.17. *In vivo* labeling of antibody using a radiofluorinated tetrazine.

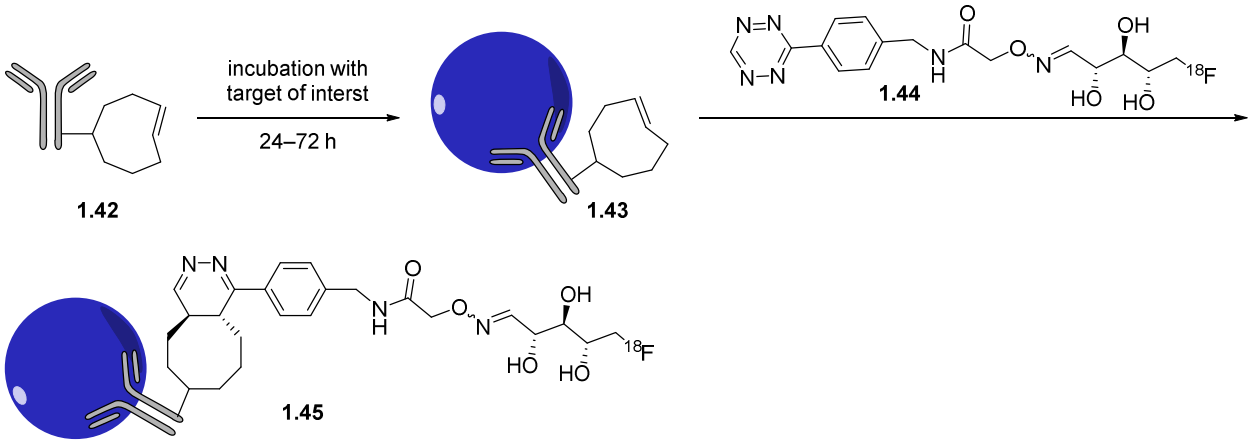

In combination with developing a bioorthogonal technique and new methods to fluorinate aryl rings, the Murphy group discovered that the sydnone functionality, which is well known for undergoing 3+2 cycloadditions,[55] could also act as a leaving group during S_NAr reactions (Scheme 1.20).[56] Using this technique the bis-sydnone **1.46** was radiolabeled with fluorine-18 to give mono-sydnone **1.47**. The [^{18}F]mono-sydnone can then act as a prosthetic group for imaging by cyclizing onto strained alkenes and alkynes on biological relevant compounds. Proof-of-concept was shown through the conjugation of **1.47** with a derivatized neuropeptide, DBCO-[D-Ala2, D-Leu5]-Enkephalin, to afford the PET tracer **1.48**. This methodology was also used to facilitate the radiofluorination of a wide variety of aryl and heteroaryl rings bearing electron-withdrawing groups.

Scheme 1.18. Labeling of a neuropeptide using a radiofluorinated sydnone prosthetic.

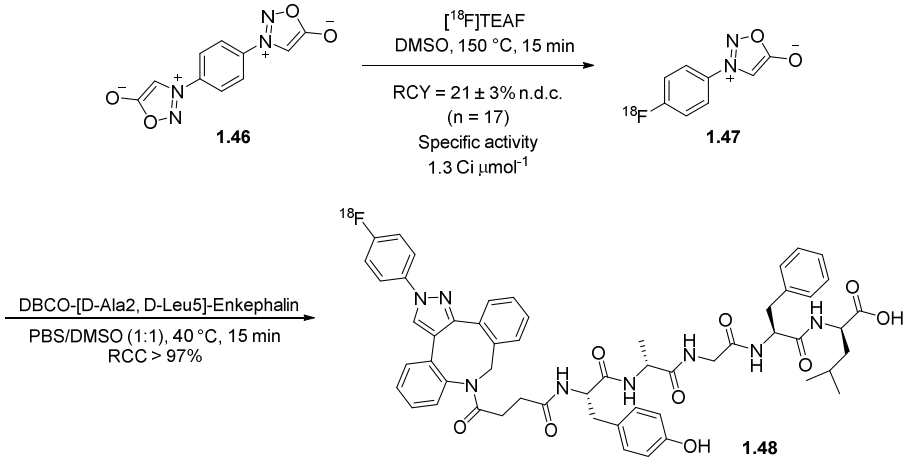

1.7 Conclusion

Nucleophilic sources of fluorine-18 represent efficient starting reagents to access a wide variety of aryl fluorides as well as alkyl fluorides for production of radiolabeled tracers used in

PET imaging applications. This nucleophilic source typically leads to reactions with higher specific activities than electrophilic sources. Many researchers have discovered methods to incorporate fluorine-18 into a small molecule late-stage in the synthesis through iodonium reagents, phenol groups, transition metal catalysis, and prosthetic groups. These reactions have been demonstrated to make clinical-grade PET tracers that were validated for human doses. New techniques are still needed to increase the availability of valuable tracers for use in clinical settings.

1.8 Notes and References

(1) Brugarolas, P.; Sánchez-Rodríguez, J. E.; Tsai, H.-M.; Basuli, F.; Cheng, S.-H.; Zhang, X.; Caprariello, A. V.; Lacroix, J. J.; Freifelder, R.; Murali, D.; DeJesus, O.; Miller, R. H.; Swenson, R. E.; Chen, C.-T.; Herscovitch, P.; Reich, D. S.; Bezanilla, F.; Popko, B. *Sci. Rep.* **2018**, *8*, 607.

(2) Bao, W.; Jia, H.; Finnema, S.; Cai, Z.; Carson, R. E.; Huang, Y. H. *PET Clin.* **2017**, *12*, 329–350.

(3) Zhu, A.; Lee, D.; Shim, H. *Semin. Oncol.* **2011**, *38*, 55–69.

(4) Brown, R. K. J.; Bohnen, N. I.; Wong, K. K.; Minoshima, S.; Frey, K. A. *RadioGraphics* **2014**, *34*, 684–701.

(5) Morbelli, S.; Djekidel, M.; Hesse, S.; Pagani, M.; Barthel, H. *Lancet Neurol.* **2016**, *15*, 1009–1010.

(6) Grabowski, S. *Crystals* **2015**, *6*, 3.

(7) Yusubov, M. S.; Svitich, D. Y.; Larkina, M. S.; Zhdankin, V. V. *Arkivoc* **2013**, *2013*, 364.

(8) Kuik, W.-J.; Kema, I. P.; Brouwers, A. H.; Zijlma, R.; Neumann, K. D.; Dierckx, R. A. J. O.; DiMagno, S. G.; Elsinga, P. H. *J. Nucl. Med.* **2015**, *56*, 106–112.

(9) Broadley, K. J. *Pharmacol. Ther.* **2010**, *125*, 363–375.

(10) Lindemann, L.; Hoener, M. C. *Trends Pharmacol. Sci.* **2005**, *26*, 274–281.

(11) Conway, C. R.; Chibnall, J. T.; Cumming, P.; Mintun, M. A.; Gebara, M. A. I.; Perantie, D. C.; Price, J. L.; Cornell, M. E.; McConathy, J. E.; Gangwani, S.; Sheline, Y. *Psychiatry Res. Neuroimaging* **2014**, *221*, 231–239.

(12) Koerts, J.; Leenders, K. L.; Koning, M.; Portman, A. T.; Van Beilen, M. *Eur. J. Neurosci.* **2007**, *25*, 3132–3136.

(13) Kumakura, Y.; Cumming, P.; Vernaleken, I.; Buchholz, H.-G.; Siessmeier, T.; Heinz, A.;

Kienast, T.; Bartenstein, P.; Gründer, G. *J. Neurosci.* **2007**, *27*, 8080–8087.

(14) Chen, W.; Silverman, D. H. S.; Delaloye, S.; Czernin, J.; Kamdar, N.; Pope, W.; Satyamurthy, N.; Schiepers, C.; Cloughesy, T. *J. Nucl. Med.* **2006**, *47*, 904–911.

(15) Dadone-Montaudié, B.; Ambrosetti, D.; Dufour, M.; Darcourt, J.; Almairac, F.; Coyne, J.; Virolle, T.; Humbert, O.; Burel-Vandenbos, F. *PLoS One* **2017**, *12*, e0184625.

(16) de Vries, E. F. .; Luurtsema, G.; Brüssermann, M.; Elsinga, P. H.; Vaalburg, W. *Appl. Radiat. Isot.* **1999**, *51*, 389–394.

(17) Ichiishi, N.; Brooks, A. F.; Topczewski, J. J.; Rodnick, M. E.; Sanford, M. S.; Scott, P. J. H. *Org. Lett.* **2014**, *16*, 3224–3227.

(18) McCammant, M. S.; Thompson, S.; Brooks, A. F.; Krska, S. W.; Scott, P. J. H.; Sanford, M. S. *Org. Lett.* **2017**, *19*, 3939–3942.

(19) Barrio, J.; Satyamurthy, N. WO 2010117435 A2, 2010.

(20) Rotstein, B. H.; Stephenson, N. A.; Vasdev, N.; Liang, S. H. *Nat. Commun.* **2014**, *5*, 4365.

(21) Rotstein, B. H.; Wang, L.; Liu, R. Y.; Patteson, J.; Kwan, E. E.; Vasdev, N.; Liang, S. H. *Chem. Sci.* **2016**, *7*, 4407–4417.

(22) Stephenson, N. A.; Holland, J. P.; Kassenbrock, A.; Yokell, D. L.; Livni, E.; Liang, S. H.; Vasdev, N. *J. Nucl. Med.* **2015**, *56*, 489–492.

(23) Brix, G.; Bellemann, M. E.; Haberkorn, U.; Gerlach, L.; Lorenz, W. J. *Nucl. Med. Biol.* **1996**, *23*, 897–906.

(24) Majo, V. J.; Prabhakaran, J.; Mann, J. J.; Kumar, J. S. D. *Drug Discov. Today* **2013**, *18*, 173–184.

(25) Sullivan, J. M.; Lim, K.; Labaree, D.; Lin, S.-F.; McCarthy, T. J.; Seibyl, J. P.; Tamagnan, G.; Huang, Y.; Carson, R. E.; Ding, Y.-S.; Morris, E. D. *J. Cereb. Blood Flow Metab.* **2013**,

33, 532–541.

(26) Neumann, C. N.; Hooker, J. M.; Ritter, T. *Nature* **2016**, *534*, 369–373.

(27) Beyzavi, M. H.; Mandal, D.; Strebl, M. G.; Neumann, C. N.; D'Amato, E. M.; Chen, J.; Hooker, J. M.; Ritter, T. *ACS Cent. Sci.* **2017**, *3*, 944–948.

(28) Strebl, M. G.; Campbell, A. J.; Zhao, W.-N.; Schroeder, F. A.; Riley, M. M.; Chindavong, P. S.; Morin, T. M.; Haggarty, S. J.; Wagner, F. F.; Ritter, T.; Hooker, J. M. *ACS Cent. Sci.* **2017**, *3*, 1006–1014.

(29) Rizk, O. H.; Shaaban, O. G.; El-Ashmawy, I. M. *Eur. J. Med. Chem.* **2012**, *55*, 85–93.

(30) Aly, H. M.; Saleh, N. M.; Elhady, H. A. *Eur. J. Med. Chem.* **2011**, *46*, 4566–4572.

(31) Turner, N.; Grose, R. *Nat. Rev. Cancer* **2010**, *10*, 116–129.

(32) Kottakis, F.; Polytarchou, C.; Foltopoulou, P.; Sanidas, I.; Kampranis, S. C.; Tsichlis, P. N. *Mol. Cell* **2011**, *43*, 285–298.

(33) van der Born, D.; Pees, A.; Poot, A. J.; Orru, R. V. A.; Windhorst, A. D.; Vugts, D. J. *Chem. Soc. Rev.* **2017**, *46*, 4709–4773.

(34) Brooks, A. F.; Topczewski, J. J.; Ichiishi, N.; Sanford, M. S.; Scott, P. J. H. *Chem. Sci.* **2014**, *5*, 4545–4553.

(35) Gamache, R. F.; Waldmann, C.; Murphy, J. M. *Org. Lett.* **2016**, *18*, 4522–4525.

(36) Ye, Y.; Schimler, S. D.; Hanley, P. S.; Sanford, M. S. *J. Am. Chem. Soc.* **2013**, *135*, 16292–16295.

(37) Mossine, A. V.; Brooks, A. F.; Makaravage, K. J.; Miller, J. M.; Ichiishi, N.; Sanford, M. S.; Scott, P. J. H. *Org. Lett.* **2015**, *17*, 5780–5783.

(38) Mossine, A. V.; Brooks, A. F.; Ichiishi, N.; Makaravage, K. J.; Sanford, M. S.; Scott, P. J. H. *Sci. Rep.* **2017**, *7*, 233.

(39) Tredwell, M.; Preshlock, S. M.; Taylor, N. J.; Gruber, S.; Huiban, M.; Passchier, J.; Mercier, J.; Génicot, C.; Gouverneur, V. *Angew. Chem. Int. Ed.* **2014**, *53*, 7751–7755.

(40) Preshlock, S.; Calderwood, S.; Verhoog, S.; Tredwell, M.; Huiban, M.; Hienzsch, A.; Gruber, S.; Wilson, T. C.; Taylor, N. J.; Cailly, T.; Schedler, M.; Collier, T. L.; Passchier, J.; Smits, R.; Mollitor, J.; Hoepping, A.; Mueller, M.; Genicot, C.; Mercier, J.; Gouverneur, V. *Chem. Commun.* **2016**, *52*, 8361–8364.

(41) Taylor, N. J.; Emer, E.; Preshlock, S.; Schedler, M.; Tredwell, M.; Verhoog, S.; Mercier, J.; Genicot, C.; Gouverneur, V. *J. Am. Chem. Soc.* **2017**, *139*, 8267–8276.

(42) Makaravage, K. J.; Brooks, A. F.; Mossine, A. V.; Sanford, M. S.; Scott, P. J. H. *Org. Lett.* **2016**, *18*, 5440–5443.

(43) Kamlet, A. S.; Neumann, C. N.; Lee, E.; Carlin, S. M.; Moseley, C. K.; Stephenson, N.; Hooker, J. M.; Ritter, T. *PLoS One* **2013**, *8*, e59187.

(44) Lee, E.; Kamlet, A. S.; Powers, D. C.; Neumann, C. N.; Boursalian, G. B.; Furuya, T.; Choi, D. C.; Hooker, J. M.; Ritter, T. *Science* **2011**, *334*, 639–642.

(45) Lee, E.; Hooker, J. M.; Ritter, T. *J. Am. Chem. Soc.* **2012**, *134*, 17456–17458.

(46) Hoover, A. J.; Lazari, M.; Ren, H.; Narayanam, M. K.; Murphy, J. M.; van Dam, R. M.; Hooker, J. M.; Ritter, T. *Organometallics* **2016**, *35*, 1008–1014.

(47) Olafsen, T.; Sirk, S. J.; Olma, S.; Shen, C. K.-F.; Wu, A. M. *Tumor Biol.* **2012**, *33*, 669–677.

(48) Cai, W.; Zhang, X.; Wu, Y.; Chen, X. *J. Nucl. Med.* **2006**, *47*, 1172–1180.

(49) Kostikov, A. P.; Chin, J.; Orchowski, K.; Schirrmacher, E.; Niedermoser, S.; Jurkschat, K.; Iovkova-Berends, L.; Wängler, C.; Wängler, B.; Schirrmacher, R. *Nat. Protoc.* **2012**, *7*, 1956–1963.

(50) Li, Z.; Cai, H.; Hassink, M.; Blackman, M. L.; Brown, R. C. D.; Conti, P. S.; Fox, J. M. *Chem. Commun.* **2010**, *46*, 8043.

(51) Sečkutė, J.; Devaraj, N. K. *Curr. Opin. Chem. Biol.* **2013**, *17*, 761–767.

(52) Denk, C.; Svatunek, D.; Filip, T.; Wanek, T.; Lumpi, D.; Fröhlich, J.; Kuntner, C.; Mikula, H. *Angew. Chem. Int. Ed.* **2014**, *53*, 9655–9659.

(53) Keinänen, O.; Fung, K.; Pourat, J.; Jallinoja, V.; Vivier, D.; Pillarsetty, N. K.; Airaksinen, A. J.; Lewis, J. S.; Zeglis, B. M.; Sarparanta, M. *EJNMMI Res.* **2017**, *7*, 95.

(54) Keinänen, O.; Li, X.-G.; Chenna, N. K.; Lumen, D.; Ott, J.; Molthoff, C. F. M.; Sarparanta, M.; Helariutta, K.; Vuorinen, T.; Windhorst, A. D.; Airaksinen, A. J. *ACS Med. Chem. Lett.* **2016**, *7*, 62–66.

(55) Narayanam, M. K.; Liang, Y.; Houk, K. N.; Murphy, J. M. *Chem. Sci.* **2016**, *7*, 1257–1261.

CHAPTER TWO

Copper-Mediated Oxidative Fluorination of Aryl Stannanes with Nucleophilic Fluoride

Raymond F. Gamache, Christopher Waldmann, Jennifer M. Murphy

Org. Lett., **2016**, *18*, 4522–4525.

2.1 Abstract

A regiospecific method for the oxidative fluorination of aryl stannanes using tetrabutylammonium triphenyldifluorosilicate (TBAT) and copper(II) triflate is described. This reaction is robust, uses readily available reagents, and proceeds via a stepwise protocol under mild conditions (60 °C, 3.2 h). Broad functional group tolerance, including arenes containing protic and nucleophilic groups, is demonstrated.

2.2 Introduction

Numerous and valuable applications of fluorinated aromatic small molecules have stirred powerful interest within the chemistry community. As such, a remarkable increase in synthetic methodologies for C-F bond construction has been reported in the past decade.[1-3] Notable improvements in aryl fluoride bond formation have utilized transition metals to facilitate this transformation.[4-6] While early examples were focused on palladium[7-14] and silver[15-19] catalytic methods, lower cost metals such as copper[20-27] and nickel[28] have recently emerged as alternative mediators of C-F bond formation. Despite attention from many research groups, most modern fluorination methods use electrophilic fluorinating sources (e.g., Selectfluor, *N*-fluoropyridinium salts) or specialized precursors. These methods have considerably improved accessibility of

fluorinated arenes yet they are not useful for applications in positron emission tomography (PET) due to the fact that ^{18}F is generated as nucleophilic [^{18}F]fluoride. While [^{18}F]F_2 and other electrophilic ^{18}F-fluorination reagents exist, their use in the synthesis of PET radiotracers results in low specific activity, namely a low $^{18}F/^{19}F$ ratio and, consequently, are not broadly useful for molecular imaging applications.[29]

The development of an electrophilic fluorination reaction that utilizes a readily available nucleophilic fluoride source in combination with an external oxidant is a highly attractive approach that would be particularly valuable for translation into radiofluorination for PET imaging applications. Such oxidative fluorination transformations are conceptually challenging due to fluorine's inherent nature as the most oxidizing element present. In spite of this challenge, a few groups have reported oxidative fluorination transformations. Meng and Li reported a hypervalent iodine mediated method to provide *para*-fluorinated anilides in moderate to good yields[30] using similar conditions reported earlier for the synthesis of 4-fluorophenols via oxidative fluorination of 4-*tert*-butylphenols.[31] Studies by the Daugulis group utilized an 8-aminoquinoline directing group to demonstrate an oxidative C-H fluorination of benzoic acid derivatives via copper catalysis using super stoichiometric amounts of AgF and *N*-methylmorpholine (NMO).[32] While these methods demonstrate good yields, the substrate scopes are limited and directing groups are required.

The first example of oxidative fluorination with a first row transition metal, reported by the Ritter group in 2012, proceeds via an arylnickel (II) complex in the presence of a hypervalent iodine oxidant and tetrabutylammonium triphenyldifluorosilicate (TBAT) (Scheme 1, eq 1).[28] Subsequently, the Sanford group disclosed a copper mediated fluorination of aryl trifluoroborates with potassium fluoride using copper (II) triflate (4 equiv) (Scheme 1, eq 2).[26] In the context of

^{18}F-radiofluorination, synthesis of the PET probe [^{18}F]5-fluorouracil was reported for human doses via the nickel-mediated methodology.[33]

Scheme 2.1. Oxidative fluorination of aryl metal complexes with fluoride.

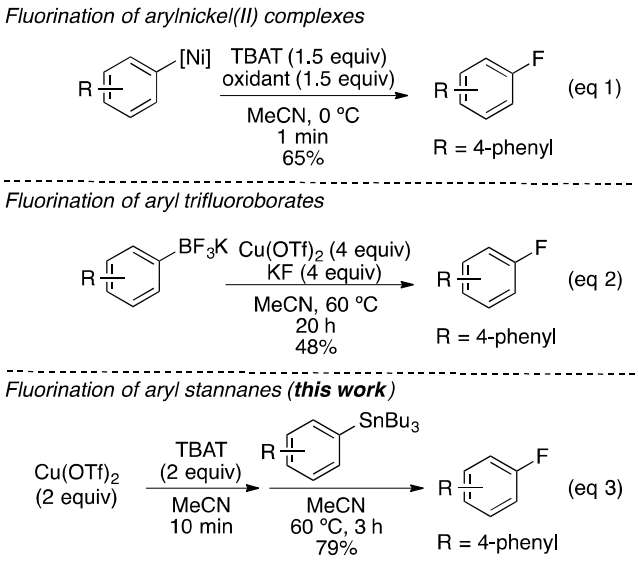

Trifluoroborate substrates for ^{18}F-radiofluorination are likely to undergo isotopic dilution via ^{18}F/^{19}F exchange between the starting material and [^{18}F]KF; therefore, alternative aryl boron reagents have recently been investigated for applications in radiofluorination.[34] While these methods demonstrate broad substrate scope and high yields, they require synthesis of complex starting materials or long reaction times and a large excess of transition metal. Thus, improvement upon the current methods for oxidative fluorination is warranted.

We sought to develop a mild, relatively quick fluorination reaction using nucleophilic fluoride and synthetically accessible starting materials. Reports confirming reductive elimination of high valent Cu(III) species[20-22, 24, 25] initiated our interest in utilizing this transition metal to enable aryl C-F bond formation with nucleophilic fluoride. Aryl stannanes have been reported

from a wide scope of complex functionality[17] and can be accessed in one step from the halide or triflate. This synthetic accessibility in addition to stability and robustness attracted our attention to their use over other starting materials such as aryl iodonium precursors, which can be challenging to prepare and functionalize. Here, we report the oxidative fluorination of aryl stannanes, using nucleophilic fluoride and copper (II) triflate, under mild conditions (Scheme 1, eq 3).

2.3 Objective and Initial Finding

Copper-based methods for arene C-F bond formation and mechanistic studies have seen a dramatic increase since Ribas' initial report of a Cu(III) isolated complex.[20, 35] In particular, mechanistic studies from the Sanford group suggest that copper plays the dual role of transition metal mediator for aryl-F coupling as well as the oxidant to access the Cu(III) intermediate, requiring excess copper (II) triflate (4 equiv).[26] The proposed mechanism involves transmetalation of a Cu(II)(OTf)(F) complex and subsequent oxidation by another equivalent of copper (II) triflate to generate the highly reactive Cu(III) species. In agreement with this proposed dual role of copper, our initial experiments exploring the fluorination of aryl stannanes required upwards of 4 equiv of copper to obtain moderate yields that dramatically dropped off when less than 2 equiv were used. However, we hypothesized that initial formation of the Cu(II)(OTf)(F) complex might be capable of facilitating the transmetalation more efficiently. We tested this hypothesis by pre-stirring the fluoride source and copper (II) triflate briefly to potentially form the Cu(II)(OTf)(F) complex followed by addition of the aryl stannane. Remarkably, this step-wise protocol resulted in a significant increase in yield of the aryl fluoride, 70% yield compared to the 46% obtained from single addition (Scheme 2). Of note, the effects of the pre-stir were more apparent with CsF,

which enabled the reaction to proceed with only 2 equiv of copper (II) triflate. Various oxidants were screened in an attempt to replace the second equiv of copper but little to no detectable fluorination was observed (see SI).

Scheme 2.2. Effects of pre-stir towards oxidative fluorination of aryl stannanes.

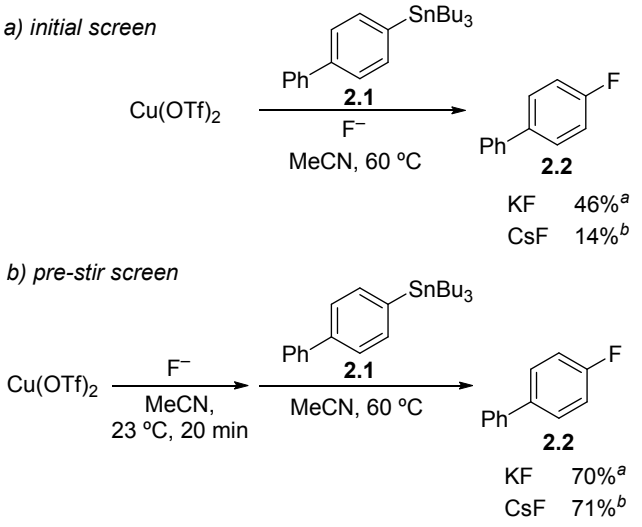

Yields determined by ^{19}F NMR spectroscopy with 1-fluoro-3-nitrobenzene as an internal standard. [a]$Cu(OTf)_2$ (4 equiv), KF (4 equiv), 1 h. [b]$Cu(OTf)_2$ (2 equiv), CsF (2 equiv), 3 h.

2.4 Solvent Screen

We next evaluated the effects of solvent on the reaction. Consistent with Sanford's findings, our initial solvent screen revealed that the fluorination failed in all solvents other than acetonitrile (Table 1). A report from the Wang group demonstrating copper-mediated C-H fluorination of azacalix[1]arene[3]pyridines suggests that acetonitrile may play a key role in facilitating a facile reductive elimination via stabilization of the Cu(I) ion that is ejected during this step.[21] We hypothesized that MeCN-ligation may be required to stabilize the copper intermediates for the fluorination reaction to proceed. To test this hypothesis, we screened the reaction in various solvents spiked with acetonitrile (Table 1). As predicted, the reaction proceeds in all solvents

screened except DMF, with as little as 10% acetonitrile in the solvent mixture. Non-coordinating solvents such as dichloromethane gave higher yields whereas coordinating solvents such as DMF gave no product, presumably due to interference with MeCN-ligation to the copper center. Other nitriles such as propionitrile and isobutyronitrile were also able to facilitate fluorination albeit in lower yields (see SI). Attempts to isolate an acetonitrile-coordinated copper-fluoride intermediate were unsuccessful.

Table 2.1. Dependence of fluorination on MeCN.

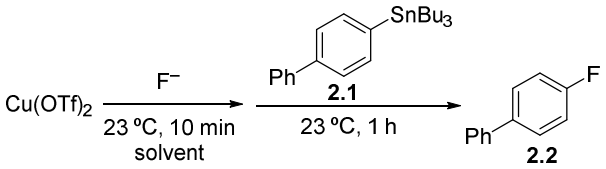

Entry	Solvent	Yield
1	MeCN	58%
2	Et_2O	0% (33%)[b]
3	THF	0% (28%)[b]
4	DCM	0% (53%)[b]
5	Toluene	0% (18%)[b]
6	DMF	0% (0%)[b]
7	EtOAc	0% (42%)[b]
8	1,4-Dioxane[d]	0% (47%)[c]
9	Toluene[d]	0% (47%)[c]

[a]Conditions: $Cu(OTf)_2$ (2 equiv) and KF (2 equiv), solvent (300 μL). Yields were determined by ^{19}F NMR spectroscopy with 1-fluoro-3-nitrobenzene as an internal standard added after the reaction. [b]30 μL MeCN added. [c]200 μL MeCN added. [d]200 μL of solvent used.

2.5 Substrate Scope

In our evaluation of fluoride sources, TBAT gave the highest yields; therefore, optimized conditions using this reagent via the step-wise protocol were applied to a series of aryl stannanes to examine the substrate scope for this reaction (Scheme 3). Both electron-deficient and electron-rich aryl stannanes underwent oxidative fluorination in good to excellent yields. This reaction demonstrates broad compatibility as fluorination can proceed in the presence of common

functionality including esters, nitriles, aldehydes, ketones, ethers, sulfones and alcohols. Substrates containing pyridine derivatives or substituted amines were amenable to fluorination, albeit in modest yield. Notably, arenes bearing protic groups as well as nucleophilic thioethers participated in fluorination, which has been consistently challenging for fluorination methodologies using nucleophilic fluoride sources.

Scheme 2.3. Oxidative fluorination of aryl stannanes with $Cu(OTf)_2$ and TBAT.

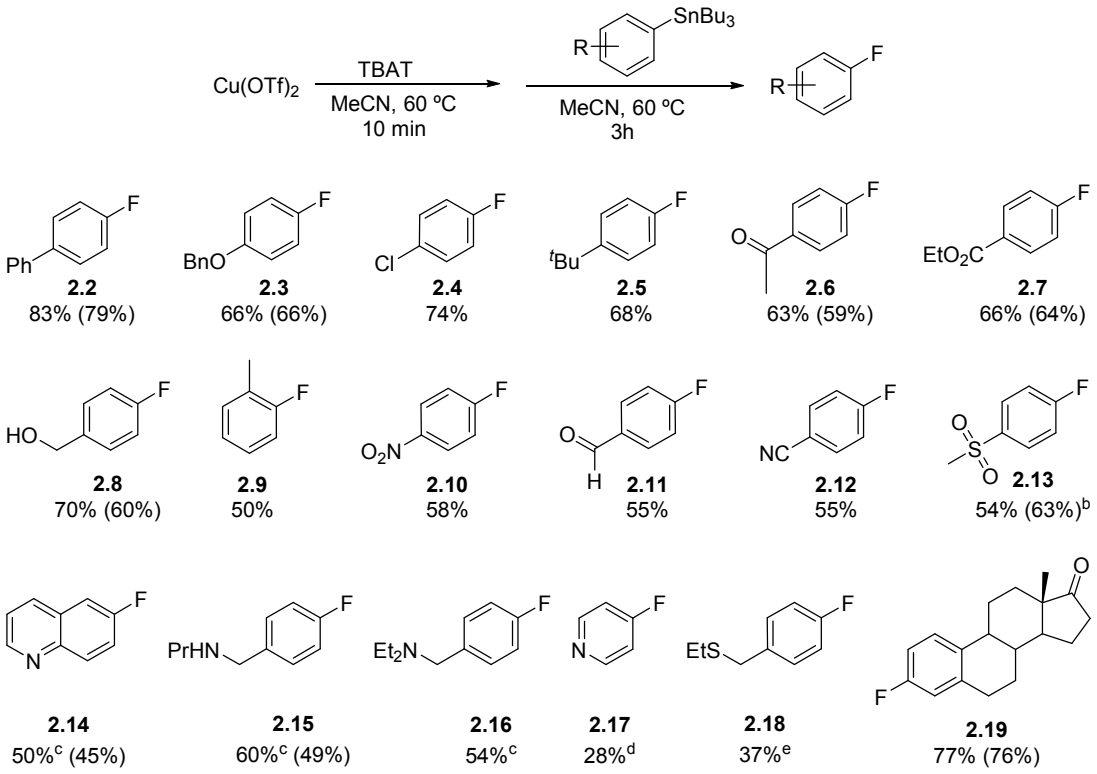

[a] Reaction Conditions: $Cu(OTf)_2$ (2 equiv), TBAT (2 equiv), MeCN (0.083M), 60 °C, 3 h. Copper salt and TBAT were prestirred in MeCN for 10 min followed by addition of the stannane. Yields were determined by ^{19}F NMR spectroscopy with 1-fluoro-3-nitrobenzene as an internal standard added after the reaction. Yields of isolated and purified compounds are reported in parenthesis. [b]Stirredfor 5 h. [c]$Cu(OTf)_2$ (4 equiv). [d]80 °C, 3 h. [e]$Cu(OTf)_2$ (3 equiv), TBAT (3 equiv).

2.6 TBAT Regeneration

The use of less than 2 equiv of TBAT resulted in a decrease in yield. We hypothesized that the byproduct, fluorotriphenylsilane, could be utilized to regenerate excess reagent. With the addition of TBAF after completion of the reaction and subsequent filtration, TBAT could be regenerated in 87% yield, effectively recovering most of the excess reagent used in the transformation. The recovered TBAT was recycled and provided the aryl fluoride in comparable yield (77% vs 79%) (Scheme 4). Alternatively, CsF, which outperforms KF in the context of alkali metal fluoride sources, can be used in place of TBAT to give similar fluorination yields (Scheme 3).

Scheme 2.4. TBAT Regenration.

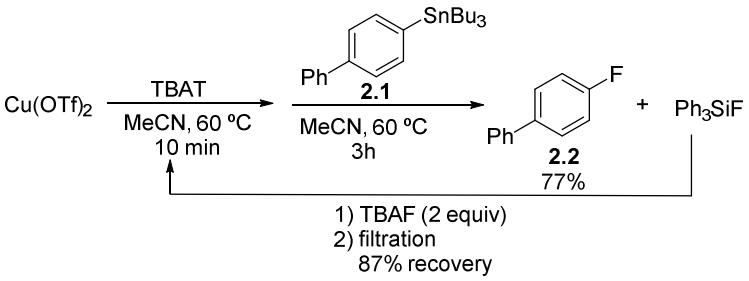

2.7 Conclusion

In summary, we report a regiospecific oxidative fluorination of aryl stannanes with copper (II) triflate and nucleophilic fluoride. This transformation proceeds under mild conditions to afford fluoro arenes with broad functional group tolerance including protic and nucleophilic groups. Use of a step-wise protocol enables a lower copper loading than previously reported for aryl trifluoroborates and recovery of nearly 1 equiv of TBAT allows for recycling of the fluoride source. Our studies support the previously suggested mechanism in which copper acts as both an

oxidant and a mediator of carbon-fluorine bond formation. Presumably, initial formation of a copper (II) fluoride complex via a step-wise protocol facilitates transmetalation to efficiently afford aryl fluorides. We propose that acetonitrile plays a key role in stabilization of the copper center, possibly to promote rapid transmetalation and to support reductive elimination of the arylcopper (III) intermediate. Investigations of this methodology for applications in ^{18}F-radiochemistry are currently underway in our laboratory.

2.8 Experimental Section

2.8.1 Materials and Methods. All fluorination reactions were conducted in an inert argon atmosphere glovebox or using standard Schlenk techniques unless otherwise stated. All chemicals and reagents were purchased from commercial sources and used without further purification unless noted otherwise. All deuterated solvents were purchased from Cambridge Isotope Laboratories. (4-chlorophenyl)tributylstannane, [4-(benzyloxy)phenyl]tributylstannane, 4-(tributylstannyl) pyridine, tetrabutyl ammonium triphenyldifluorosilicate (TBAT) and 1-fluoro-3-nitrobenzene were purchased from Sigma Aldrich. 4-Pyridyltributylstannane was purchased from Alfa Chemistry. $Cu(OTf)_2$ was purchased from Strem. Anhydrous solvents were obtained by filtration through activated alumina columns unless indicated otherwise. Solvents used for extractions and chromatography were not anhydrous. All other aryl stannanes were synthesized following known literature procedures and characterization data match that which was previously reported. Reactions and chromatography fractions were analyzed by thin-layer chromatography (TLC) using Merck precoated silica gel 60 F_{254} glass plates (250 μm) and visualized by ultraviolet irradiation, potassium permanganate stain, and phosphomolybdic acid. Flash column chromatography was performed using E. Merck silica gel 60 (230−400 mesh) with compressed air. Preparatory plate isolation was performed using Merck precoated silica gel 60 F_{254} glass plates (1,000 μm). NMR spectra were obtained on a Bruker AV300 (300 MHz for ^{1}H; 282 MHz for ^{19}F), a Bruker AV500 (500 MHz for ^{1}H; 125 MHz for ^{13}C), and a Bruker AV600 (600 MHz for ^{1}H; 150 MHz for ^{13}C). ^{1}H and ^{13}C chemical shifts are reported in parts per million (ppm) using the solvent resonance as an internal reference. ^{19}F NMR spectra are calibrated to the internal standard 1-fluoro-3-nitrobenzene, which appears at -110.5 ppm. The coupling constants, *J*, are reported in Hertz (Hz), and the multiplicities are reported as follows: singlet (s), broad single (br s) doublet (d), triplet (t),

quartet (q), and multiplet (m). High-resolution electrospray mass spectrometry data was collected with a Waters LCT Premier XE time-of-flight instrument controlled by MassLynx 4.1 software. High-resolution mass spectra were obtained on Thermo Scientific™ Exactive Mass Spectrometer with DART ID-CUBE. Samples were dissolved in methanol and infused using direct loop injection from a Waters Acquity UPLC into the Multi-Mode Ionization source.

2.8.2 Experimental Procedures.

Synthesis of aryl stannanes

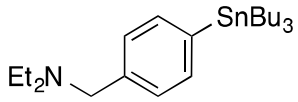

[4-(Diethylaminomethyl)phenyl]tributylstannane. To a solution of 4-(diethylaminomethyl)-bromobenzene (0.6 g, 2.48 mmol, 1.0 equiv) in THF (12 ml) at -78 °C was added dropwise *n*-butyllithium (2.5 M, 1.2 ml, 2.98 mmol, 1.2 equiv). The solution was kept at -78 °C and allowed to stir for 10 min. To the reaction mixture was added dropwise a solution of Bu_3SnCl (0.843 ml, 2.98 mmol, 1.2 equiv) in THF (3.6 ml) and the reaction was allowed to warm to 23 °C and stirred for 1 h. The solution was diluted with 48 ml of a 1:1 solution of Et_2O:hexanes and washed with water (2 x 70 ml) followed by brine (40 ml). The organic layer was dried over Na_2SO_4 and concentrated in vacuo. The desired product was purified by column chromatography 10% w/w K_2CO_3 in silica and eluted with 1:9:90 NEt_3:EtOAc:Hexane (Rf = 0.3) to afford 923 mg of the desired compound as a yellow oil (82% Yield). NMR Spectroscopy: ^{1}H NMR (600 MHz, $CDCl_3$): δ 7.39 (d, *J* = 7.75 Hz, 2H), 7.29 (d, *J* = 7.26 Hz, 2H), 3.56 (s, 2H), 2.54 (br s, 4H), 1.56-1.51 (m, 6H), 1.33 (h, *J* = 7.32 Hz, 7.32 Hz, 6H), 1.06 – 1.02 (m, 12H), 0.88 (t, *J* = 7.32 Hz, 9H). ^{13}C NMR

(150 MHz, $CDCl_3$): δ 139.66, 136.37, 136.17, 128.57, 57.38, 46.60, 29.02, 27.32, 13.61, 11.64, 9.44. HRMS-ESI (*m/z*) $[M+H]^+$ calcd for $C_{23}H_{44}NSn$, 454.2495; found 454.2468.

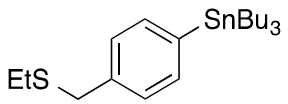

[4-(Ethyl-methylenesulfide)phenyl]tributylstannane. To a solution of ethanethiol (0.041 ml, 0.56 mmol, 1.1 equiv) in THF (2 ml) at 0 °C was added 60% NaH (0.024 g, 0.606 mmol, 1.15 equiv). The solution was stirred for 40 min at 0 °C. To the reaction mixture was added [4-(methylsulfonyl)1-methylene]phenyltributylstannane (0.24 g, 1.0 equiv, 0.51 mmol) in THF (1.0 ml) The solution was allowed to stir overnight at 23 °C. The reaction was quenched with water and extracted with ethyl acetate (2 x 6 ml). The organic layer was washed with 5 ml of 5% $NaHCO_3$, dried over Na_2SO_4 and concentrated in vacuo. The reaction was purified by column chromatography 10% w/w K_2CO_3 in silica and eluted with 1:50 EtOAc:Hexane to afford 170.5 mg of the desired compound as a clear oil (69% Yield) Rf=.3 in hexane. NMR Spectroscopy: ^1H NMR (500 MHz, $CDCl_3$): δ 7.40 (d, J = 7.85 Hz, 2H), 7.27 (d, J = 7.30 Hz, 2H), 3.70 (s, 2H), 2.45 (q, J = 7.49 Hz, 2H), 1.58-1.47 (m, 6H), 1.37-1.28 (m, 6H), 1.24 (t, J = 7.35 Hz, 3H), 1.11-0.97 (m, 6H), 0.88 (t, J = 7.30 Hz, 9H). ^{13}C NMR (150 MHz, $CDCl_3$): δ 140.18, 138.09, 136.46, 128.24, 35.83, 28.97, 27.25, 25.21, 14.27, 13.54, 9.44. HRMS-ESI (*m/z*) $[M+H]^+$ calcd for $C_{21}H_{39}SSn$, 443.1794; found 443.1765.

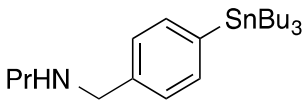

[4-(Propylaminomethyl)phenyl]tributylstannane. To a solution of propylamine (0.21 ml, 2.4 mmol, 1.1 equiv), K_2CO_3 (0.594 g, 4.3 mmol, 2.0 equiv) in DMF (9 ml) was added [4-(chloromethyl)phenyl]tributylstannane (900 mg, 2.18 mmol, 1 equiv) after 30 min of stirring. The reaction was monitored by TLC and allowed to stir until complete consumption of starting material. The mixture was diluted with Et_2O (10 mL) and water (10 mL). The organic layer was separated and washed with water (3 x 3 mL) followed by brine (3 mL). The organic layer was dried over Na_2SO_4 and concentrated in vacuo. The desired product was purified by column chromatography 10% w/w K_2CO_3 in silica and eluted with 1:19:80 NEt_3:EtOAc:Hexane (Rf = 0.25) to afford 350 mg of the desired compound as a yellow oil (37% yield). NMR Spectroscopy: ^{1}H NMR (600 MHz, $CDCl_3$): δ 7.45 (d, *J* = 7.02 Hz, 2H), 7.31 (d, *J* = 7.26 Hz, 2H), 3.79 (s, 2H), 2.63 (t, *J* = 7.47 Hz, 2H), 2.26 (s 1H), 1.58 - 1.53 (m, 8H), 1.36 (h, *J* = 7.45 Hz, 6H), 1.10 - 1.05 (m, 6H), 0.94 (t, *J* = 7.32 Hz, 3H), 0.90 (t, *J* = 7.32 Hz, 9H). ^{13}C NMR (150 MHz, $CDCl_3$): δ 140.23, 139.86, 136.57, 127.84, 53.97, 51.35, 29.10, 27.39, 23.08, 13.69, 11.79, 9.55. HRMS-ESI (*m/z*) $[M+H]^+$ calcd for $C_{22}H_{42}NSn$, 440.2339; found 440.2305.

Synthesis of aryl fluoride reference compounds

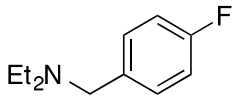

reference standard

***N,N*-Diethyl-(4-fluorobenzyl)amine.** Diethylamine (3.5 mmol, 0.36 ml, 2.2 equiv) was added to a solution containing DCM (2 ml) and 4-fluorobenzylbromide (1.6 mmol, 0.2 ml, 1 equiv) at 0 °C. The solution was allowed to warm to 23 °C and stirred overnight. The organic layer was diluted with ethyl acetate and washed with KOH (2x10 ml) and brine (10 ml). The organic layer was dried over Na_2SO_4 and concentrated *in vacuo* resulting in 203 mg of the desired product as a red-orange oil (70% yield). ^{1}H NMR (500 MHz, $CDCl_3$): δ 7.29 (dd, *J* = 8.29, 5.62 Hz, 2H), 6.98 (t, *J* = 8.73 Hz, 2H), 3.53 (s, 2H), 2.51 (q, *J*=7.14 Hz, 4H), 1.03 (t, *J*=7.12 Hz, 6H). ^{13}C NMR (125 MHz, $CDCl_3$): δ 161.83 (d, *J* = 242.78 Hz), 135.38, 130.33 (d, *J* = 7.80 Hz), 114.90 (d, *J* = 21.0 Hz), 56.69, 46.57, 11.63. ^{19}F NMR(282 MHz, $CDCl_3$): δ -116.47.

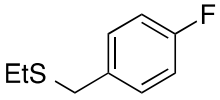

reference standard

Ethyl 4-fluorobenzyl sulfide. Under argon, THF (6 mL) was added to ethanethiol (1.32 mmol, 0.095 ml, 1.1 equiv) and the mixture was cooled to 0 °C. NaH (1.44 mmol, 58 mg, 1.2 equiv) was added, slowly, at 0 °C. The solution was stirred for an additional 20 min at 0 °C before 4-fluorobenzylbromide (1.2 mmol , 227 mg, 1 equiv) was added. The mixture was allowed to warm to 23 °C and stirred overnight. The reaction was quenched with water and extracted with ethyl acetate (2 x 10 ml). The organic layer was washed with 10 ml of 5% $NaHCO_3$, dried over Na_2SO_4

and concentrated *in vacuo*. The crude oil was purified by silica column chromatography and eluted with hexane to afford 166 mg of the desired compound as a clear oil (81% Yield) ^{1}H NMR (500 MHz, $CDCl_3$): δ 7.31-7.24 (m, 2H), 6.99 (dd, J = 8.65 Hz, 8.67 Hz, 2H), 3.69 (s, 2H), 2.43 (q, J = 7.38 Hz, 2H), 1.23 (t, J = 7.40 Hz, 3H). ^{13}C NMR (125 MHz, $CDCl_3$): δ 161.84 (d, J = 243.63 Hz), 134.31 (d, J = 3.16 Hz), 130.29 (d, J = 7.98 Hz), 115.29 (d, J = 21.28 Hz), 35.14, 25.22, 14.35. ^{19}F NMR (282 MHz, $CDCl_3$): δ -115.91.

Optimization Data:

Copper Source Screen

To a vial containing KF (0.05 mmol, 2.8 mg, 2.0 equiv) and MeCN (300 µl) was added a copper salt (0.05 mmol, 18.1 mg, 2.0 equiv). The vial was sealed with a Teflon cap and removed from the glovebox and stirred for 10 min at 60 °C. After 10 min, 4-(biphenyl)tributylstannane (0.025 mmol, 1.0 equiv) was added and the reaction was stirred at 60 °C for 3 h in a sealed vial and subsequently cooled to 23 °C. To the reaction mixture was added 1-fluoro-3-nitrobenzene (3.0 µl, 0.0282 mmol) and MeCN or DCM. The resulting solution was analyzed by ^{19}F NMR spectroscopy. Yields were determined by comparing the integration of the ^{19}F NMR resonance of 4-fluorobiphenyl (-118.1 ppm) with that of 1-fluoro-3-nitrobenzene (-112.0 ppm).

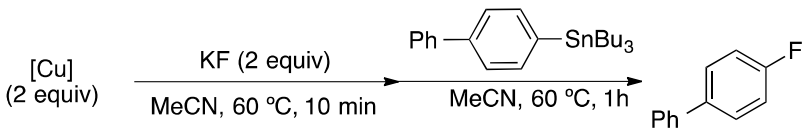

Entry	[Cu]	Yield
1	$Cu(OTf)_2$	58
2	$(MeCN)_4CuOTf$	0
3	$(py)_4Cu(OTf)_2$	0
4	CuF_2	0

Fluoride Source Screen

To a vial containing the fluoride source (0.05 mmol, 2.0 equiv) and additive in MeCN (300 µl) was added $Cu(OTf)_2$ (0.05 mmol, 18.1 mg, 2.0 equiv). The vial was sealed with a Teflon cap, removed from the glovebox and stirred for 10 min at 60 °C. After 10 min, 4-(biphenyl)tributylstannane (0.025 mmol, 1 equiv) was added and the reaction was stirred at 60 °C for 3 h in a sealed vial and subsequently cooled to 23 °C. To the reaction mixture was added 1-fluoro-3-nitrobenzene (3.0 µl, 0.0282 mmol) and MeCN or DCM (0.5 ml). The resulting solution was analyzed by ^{19}F NMR spectroscopy. Yields were determined by comparing the integration of the ^{19}F NMR resonance of 4-fluorobiphenyl (-118.1 ppm) with that of 1-fluoro-3-nitrobenzene (-112.0 ppm).

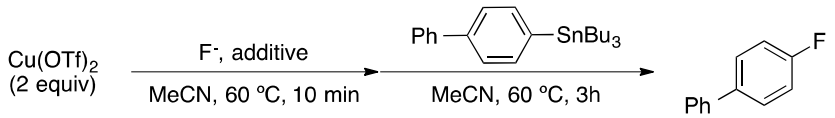

Entry	F^- (2 eq)	Additive	Yield (%)
1	KF	---	58
2	CsF	---	71
3	TBAT	---	83
4	TBAF	---	21
5	TBAT (tin)	---	69
6	NaF	18–C–6 (2 eq)	44
7	KF	18–C–6 (2 eq)	71
8	CsF	18–C–6 (2 eq)	70

Effect of pre-stirring

To a vial containing a fluoride source (0.05 mmol, 2.0 equiv) in MeCN (300 µl) was added $Cu(OTf)_2$ (0.05 mmol, 18.1 mg, 2.0 equiv). The vial was sealed with a Teflon cap, removed from the glovebox and stirred at 60 °C for the indicated time. 4-(biphenyl)tributylstannane (0.025 mmol, 1.0 equiv) was added and the reaction was stirred at 60 °C for 3 h in a sealed vial and subsequently

cooled to 23 °C. To the reaction mixture was added 1-fluoro-3-nitrobenzene (3.0 μl, 0.0282 mmol) and MeCN or DCM. The resulting solution was analyzed by ^{19}F NMR spectroscopy. Yields were determined by comparing the integration of the ^{19}F NMR resonance of 4-fluorobiphenyl (-118.1 ppm) with that of 1-fluoro-3-nitrobenzene (-112.0 ppm).

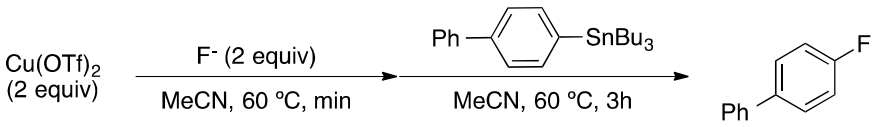

Entry	F^-	Pre-Stir (min)	Yield (%)
1	KF	0	46
2	CsF	0	14
3	TBAT	0	83
4	KF	10	58
5	KF	20	58
6	CsF	10	71
7	TBAT	10	83

Nitrile Solvent Screen

To a vial containing CsF (0.05 mmol, 27 mg, 2.0 equiv) in 300 μl of various nitrile solvents was added $Cu(OTf)_2$ (0.05 mmol, 18.1 mg, 2.0 equiv). The reaction mixture was stirred in a sealed vial at 60 °C for 10 min. After 10 min 4-(biphenyl)tributylstannane (0.025 mmol, 1.0 equiv) was added and the reaction was stirred at 60 °C for 3 h and subsequently cooled to 23 °C. To the reaction mixture was added 1-fluoro-3-nitrobenzene (3.0 μl, 0.0282 mmol) and MeCN. The resulting solution was analyzed by ^{19}F NMR spectroscopy. Yields were determined by comparing the integration of the ^{19}F NMR resonance of 4-fluorobiphenyl (-118.1 ppm) with that of 1-fluoro-3-nitrobenzene (-112.0 ppm).

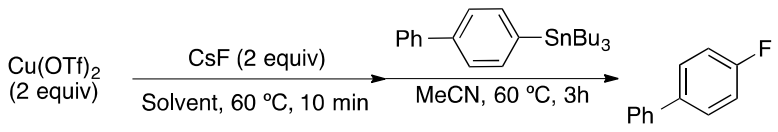

Entry	Solvent	Yield
1	MeCN	71
2	CH_3CH_2CN	50
3	$(CH_3)_2CHCN$	34
4	(CH3)3CCN	6

Additives Screen

To a vial containing CsF (0.05 mmol, 27 mg, 2.0 equiv) in MeCN (300 µl) was added $Cu(OTf)_2$ (0.05 mmol, 18.1 mg, 2.0 equiv) and an additive. The reaction mixture was stirred in a sealed vial at 60 °C for 10 min. After 10 min 4-(biphenyl)tributylstannane (0.025 mmol, 1.0 equiv) was added and the reaction was stirred at 60 °C for 3 h and subsequently cooled to 23 °C. To the reaction mixture was added 1-fluoro-3-nitrobenzene (3.0 µl, 0.0282 mmol) and MeCN or DCM. The resulting solution was analyzed by ^{19}F NMR spectroscopy. Yields were determined by comparing the integration of the ^{19}F NMR resonance of 4-fluorobiphenyl (-118.1 ppm) with that of 1-fluoro-3-nitrobenzene (-112.0 ppm).

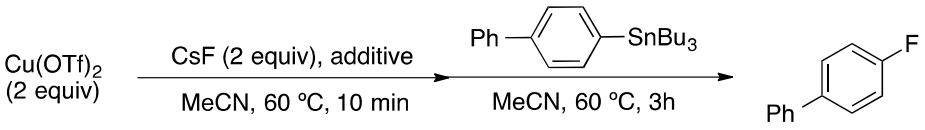

Entry	Additive	Yield (%)
1	O_2 (1 atm)	67
2[a]	DMP (1 equiv)	0
3[a]	TEMPO (2 equiv)	0
4	nBu_4NOMs (1 equiv)	28
5	nBu_4NOMs (1 equiv)	17
6	nBu_4NPF_6 (1 equiv)	70
7	H_4NPF_6 (1 equiv)	67
8	LiCl (2 equiv)	0

a) TBAT (2 equiv) was used instead of CsF

Concentration Screen

To a vial containing CsF (0.05 mmol, 7.6 mg, 2.0 equiv) in the indicated volume of MeCN was added $Cu(OTf)_2$ (0.05 mmol, 18.1 mg, 2.0 equiiv). The vial was then sealed with a Teflon cap, removed from the glovebox and stirred for 10 min at 60 °C. After 10 min, 4-(biphenyl)tributylstannane (0.025 mmol, 1.0 equiv) was added and the reaction was stirred at 60 °C for 3 h in a sealed vial and subsequently cooled to 23 °C. To the reaction mixture was added 1-fluoro-3-nitrobenzene (3.0 µl, 0.0282 mmol) and MeCN or DCM. The resulting solution was analyzed by ^{19}F NMR spectroscopy. Yields were determined by comparing the integration of the ^{19}F NMR resonance of 4-fluorobiphenyl (-118.1 ppm) with that of 1-fluoro-3-nitrobenzene (-112.0 ppm).

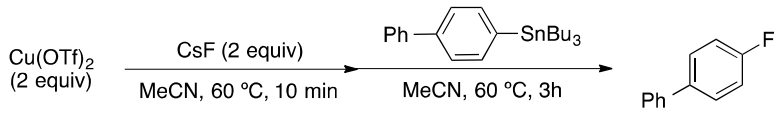

Entry	Volume (µL)	Yield (%)
1	200	73
2	300	71
3	400	75
4	500	54
5	600	26
6	700	27

Temperature Screen

To a vial containing CsF (0.05 mmol, 7.6 mg, 2.0 equiv) in MeCN (300 µl) was added $Cu(OTf)_2$ (0.05 mmol, 18.1 mg, 2.0 equiv). The vial was then sealed with a Teflon cap, removed from the glovebox and stirred at room temp. After 10 min, 4-(biphenyl)tributylstannane (0.025 mmol, 1.0 equiv) was added and the reaction was stirred at the indicated temperature for 2 h in a sealed vial and subsequently cooled to 23 °C. To the reaction mixture was added 1-fluoro-3-nitrobenzene

(3.0 µl, 0.0282 mmol) and MeCN or DCM. The resulting solution was analyzed by ^{19}F NMR spectroscopy. Yields were determined by comparing the integration of the ^{19}F NMR resonance of 4-fluorobiphenyl (-118.1 ppm) with that of 1-fluoro-3-nitrobenzene (-112.0 ppm).

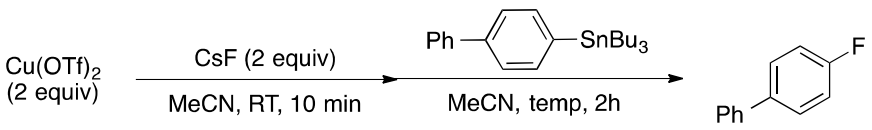

Entry	Temp (°C)	Yield (%)
1	RT	55
2	60	71
3	70	74
4	80	66

(General Procedure A): Optimized Reaction Condition

In a glovebox, to a vial containing tetrabutylammonium triphenyldifluorosilicate (TBAT) (0.05 mmol, 27 mg, 2.0 equiv) in MeCN (300 µl) was added $Cu(OTf)_2$ (0.05 mmol, 18.1 mg, 2.0 equiv). The vial was sealed with a Teflon cap, removed from the glovebox and stirred for 10 min at 60 °C. After 10 min the stannane (0.025 mmol, 1.0 equiv) was added and the reaction was stirred at 60 °C for 3 h in a sealed vial and subsequently cooled to 23 °C. To the reaction mixture was added 1-fluoro-3-nitrobenzene (3.0 µl, 0.0282 mmol) as the internal standard and DCM (0.5 ml). The resulting solution was analyzed by ^{19}F NMR spectroscopy. Yields were determined by comparing the integration of the ^{19}F NMR resonance of the product peak with that of 1-fluoro-3-nitrobenzene (-110.5 ppm).

(General Procedure B): Optimized conditions isolation

In a glovebox, to an 8 ml vial containing tetrabutylammonium triphenyldifluorosilicate (TBAT) (2 equiv) in MeCN was added $Cu(OTf)_2$ (2 equiv) to form a 0.083 M solution. The solution was

stirred for 10 min at 23 °C and the stannane was added. The vial was sealed with a Teflon cap, removed from the glovebox and stirred for 3 h at 60 °C. The resulting solution was diluted with 8 ml of Et_2O and washed with 2x8 ml of water. The organic layer was washed with 2x10ml of a 0.22 M solution of lithium sulfide. The organic layer was dried over Na_2SO_4 and concentrated *in vacuo* at 30 °C. The residue was purified by preparative TLC to afford the desired product.

Substrates

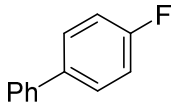

2.2

Following general procedure B, 4-fluorobiphenyl was synthesized from (4-biphenyl)tributylstannane[17] in 79% yield, 30.7 mg was isolated as a white solid using preparative TLC with 1% triethylamine in pentane as the eluent. The ^{1}H, ^{13}C and ^{19}F NMR spectroscopic data of the purified material correctly match data previously reported.[17]

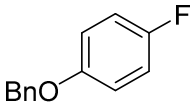

2.3

Following general procedure B, 1-(benzyloxy)-4-fluorobenzene was synthesized from [4-(benzyloxy)phenyl]tributylstannane in 66% yield, 28.2 mg was isolated as a white solid using preparative TLC with 3% EtOAc/Hexanes as the eluent. The ^{1}H, ^{13}C and ^{19}F NMR spectroscopic data of the purified material correctly match data previously reported.[36]

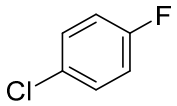

2.4

Following general procedure A, 1-chloro-4-fluorobenzene was synthesized from (4-chlorophenyl)tributylstannane in 74% yield as determined by ^{19}F NMR spectroscopic analysis. ^{19}F NMR (282 MHz, CH_3CN): δ -117.85. The ^{19}F NMR spectroscopic data match NMR data for 1-chloro-4-fluorobenzene previously reported in the literature.[25]

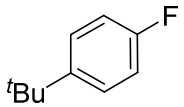

2.5

Following general procedure A, fluoro-4-*tert*-butylbenzene was synthesized from (4-*tert*-butylphenyl)tributylstannane in 68% yield as determined by ^{19}F NMR spectroscopic analysis. ^{19}F NMR (282 MHz, CH_3CN): δ -120.64. The ^{19}F NMR spectroscopic data match NMR data for fluoro-4-*tert*-butylbenzene previously reported in the literature.[26]

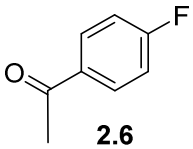

2.6

Following general procedure B, 1-acetyl-4-fluorobenzene was synthesized from (4-acetylphenyl)tributylstannane[37] in 59% yield (70% brsm), 19.9 mg was isolated as an oil using preparative TLC with 3% EtOAc/Hexanes as the eluent. The ^{1}H, ^{13}C and ^{19}F NMR spectroscopic data of the purified material correctly match data previously reported.[26]

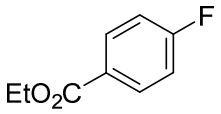

2.7

Following general procedure B, ethyl 4-fluorobenzoate was synthesized from ethyl 4-(tributylstannyl)benzoate[17] in 64% yield, 24.54 mg was isolated as an oil using preparative TLC with 3% EtOAc/Hexane as the eluent. The ^{1}H, ^{13}C and ^{19}F NMR spectroscopic data of the purified material correctly match data previously reported.[17]

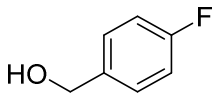

2.8

Following general procedure B, 4-fluorobenzyl-alcohol was synthesized from 4-(tributylstannyl)benzyl alcohol[17] in 60% yield, 19 mg was isolated as an oil using silica gel column chromatography with 10:1 Hexane:EtOAc as the eluent. The ^{1}H, ^{13}C and ^{19}F NMR spectroscopic data of the purified material correctly match data previously reported.[17]

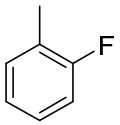

2.9

Following general procedure A, 1-fluoro-2-methylbenzene was synthesized from (2-methylphenyl)tributylstannane in 50% yield as determined by ^{19}F NMR spectroscopic analysis. ^{19}F NMR (282 MHz, CH_3CN): δ -120.07. The ^{19}F NMR spectroscopic data match NMR data for 1-fluoro-2-methylbenzene previously reported in the literature.[25]

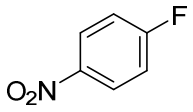

2.10

Following general procedure A, 1-nitro-4-fluorobenzene was synthesized from (4-nitrophenyl)tributylstannane[37] in 58% yield as determined by ^{19}F NMR spectroscopic analysis. ^{19}F NMR (282 MHz, CH_3CN): δ -104.87. The ^{19}F NMR spectroscopic data match NMR data for 1-nitro-4-fluorobenzene previously reported in the literature.[26]

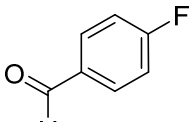

2.11

Following general procedure A, 4-fluorobenzaldehyde was synthesized from (4-formylphenyl)tributylstannane[16] in 55% yield as determined by ^{19}F NMR spectroscopic analysis. ^{19}F NMR (282 MHz, CH_3CN): δ -105.59. The ^{19}F NMR spectroscopic data match NMR data for 4-fluorobenzaldehyde previously reported in the literature.[16]

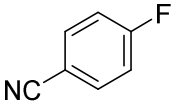

2.12

Following general procedure A, 1-cyano-4-fluorobenzene was synthesized from (4-cyanophenyl)tributylstannane[17] in 55% yield as determined by ^{19}F NMR spectroscopic analysis. ^{19}F NMR (282 MHz, CH_3CN): δ -104.87. The ^{19}F NMR spectroscopic data match NMR data for 1-cyano-4-fluorobenzene previously reported in the literature.[17]

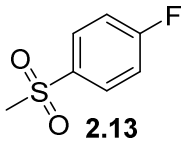

2.13

Following general procedure B, 1-fluoro-4-methylsulfonylbenzene was synthesized from [4-(methylsulfonyl)phenyl]tributylstannane,[17] except stirring was increased to 5 h. 27.1 mg of the desired product was isolated as a solid in 63% yield using preparative TLC using 50% EtOAc/Hexane. The ^{1}H, ^{13}C and ^{19}F NMR spectroscopic data of the purified material correctly match data previously reported.[17]

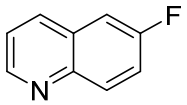

2.14

In a glovebox, $Cu(OTf)_2$ (4 equiv) was added to a 8 ml vial containing TBAT (2 equiv) and dissolved in MeCN to form a 0.083 M solution. The solution was stirred for 10 min at 23 °C after which the 6-(quinolinyl)tributylstannane[16] (0.10 g, 1 equiv) was added. The vial was sealed with a teflon cap, removed from the glovebox and stirred for an additional 3 h at 60 °C. The resulting solution was diluted with 2 ml of MeCN, after which 1 g of poly-4-vinyl pyridine was added and the mixture was stirred overnight. The solution was diluted with 10 ml of Et_2O, washed with 2x10 ml of water and extracted. The organic layer was washed aggressively with 2x10ml of a 0.22 M solution of lithium sulfide. The organic layer was dried over Na_2SO_4, concentrated *in vacuo* and purified by preparative TLC to give 17.2 mg of 6-fluoroquinoline as an oil in 50% yield. The ^{1}H, ^{13}C and ^{19}F NMR spectroscopic data of the purified material correctly match data previously reported.[16]

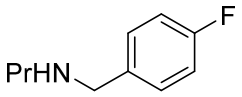

2.15

In a glovebox, $Cu(OTf)_2$ (247 mg, 0.684 mmol, 4 equiv) was added to a 8 ml vial containing TBAT (184 mg, 0.342 mmol, 2 equiv) and dissolved in MeCN to form a 0.083 M solution. The solution was stirred for 10 min at 23 °C after which [4-(propylaminomethyl)phenyl]tributylstannane (75 mg, 0.171 mmol, 1 equiv) was added. The vial was sealed with a Teflon cap, removed from the glovebox and stirred for an additional 3 h at 60 °C. The mixture was diluted with 8 ml of Et_2O and washed with 3x5 ml of 1.0 N HCl. The aqueous phase was brought to a pH of 10 and extracted with 3x10 ml of DCM. The organic layer was dried over Na_2SO_4, concentrated *in vacuo* and purified by preparative TLC using 1:19:80 NEt_3:EtOAc:Hexane to give 14 mg of the desired product as an oil in 49% yield. NMR Spectroscopy: ^{1}H NMR (600 MHz, $CDCl_3$): δ 7.28 (m, 2H), 7.01 (t, J = 8.3 Hz, 2H), 3.75 (s, 2H), 2.58 (t, J = 7.20 Hz, 2H), 1.56 – 1.49 (m, 3H), 0.92 (t, J = 7.33 Hz, 3H). ^{13}C NMR (125 MHz, $CDCl_3$): δ 161.9 (d, J = 242.99 Hz), 136.19, 129.64 (d, J = 7.87 Hz), 115.12 (d, J = 21.08 Hz), 53.23, 51.28, 23.13, 11.77. ^{19}F NMR (282 MHz, $CDCl_3$): δ -117.63. HRMS-ESI (*m/z*) $[M+H]^+$ calcd for $C_{10}H_{15}NF$, 168.1188; found 168.1173.

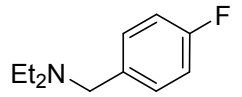

2.16

In a glovebox, $Cu(OTf)_2$ (253 mg, 0.7 mmol, 4 equiv) was added to a 8 ml vial containing TBAT (189 mg, 0.35 mmol, 2 equiv) and dissolved in MeCN to form a 0.083 M solution. The solution was stirred for 10 min at 23 °C after which [4-(diethylaminomethyl)phenyl]tributylstannane (80 mg, 0.177 mmol, 1 equiv) was added. The vial was sealed with a teflon cap, removed from the

glovebox and stirred for an additional 3 h at 60 °C. The mixture was diluted with 8 ml of Et_2O and washed with 3x5 ml of 1N HCl. The aqueous phase was brought to a pH of 10 and extracted with 3x10 ml of DCM. The organic layer was dried over Na_2SO_4, concentrated *in vacuo*. The identity of the product was confirmed by ^{19}F NMR spectroscopic analysis to the fully characterized reference, *N,N*-diethyl-(4-fluorobenzyl)amine, on 37.

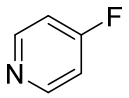

2.17

Following general procedure A, with the exception of heating the reaction to 80 °C, 4-fluoropyridine was synthesized in 28% yield from 4-tributylstannanylpyridine. The mixture was then diluted with 0.5 ml of MeCN and 0.3 g of poly-4-vinyl pyridine was added and the mixture was stirred overnight. The yield was determined by ^{19}F NMR spectroscopic analysis. NMR Spectroscopy: ^{19}F NMR (282 MHz, CD_3CN): δ -104.85. The ^{19}F NMR spectroscopic data match NMR data for 4-fluoropyridine previously reported in the literature.[26]

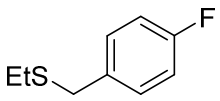

2.18

In a glovebox, $Cu(OTf)_2$ (0.075 mmol, 27 mg, 3.0 equiv) was added to a vial containing TBAT (0.075 mmol, 40.5 mg, 3.0 equiv) and MeCN (300 µl). The vial was sealed with a teflon cap, removed from the glovebox and stirred for 10 min at 60 °C. After 10 min [4-(ethyl-methylenesulfide)phenyl]tributylstannane (0.025 mmol, 1.0 equiv) was added and the reaction was stirred at 60 °C for 3 h and subsequently cooled to 23 °C. To the reaction mixture was added 1-

fluoro-3-nitrobenzene (3.0 µl, 0.0282 mmol) as the internal standard and MeCN or DCM (0.5 ml). The resulting solution was analyzed by ^{19}F NMR spectroscopy. A yield of 37% was determined by comparing the integration of the ^{19}F NMR resonance of Ethyl 4-fluorobenzyl sulfide (-118.02 ppm, previously synthesized and characterized on S7) with that of 1-fluoro-3-nitrobenzene (-112.0 ppm). Product identification was further confirmed via ^{19}F NMR spectroscopy by spiking the crude product mixture with the reference compound and by matching the analytical HPLC retention time of both the crude product mixture and the reference compound. ^{19}F NMR (282 MHz, CH_3CN): δ -118.02.

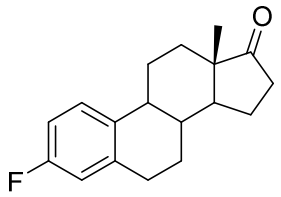

2.19

Following general procedure B, 3-deoxy-3-fluoroestrone was synthesized from 3-deoxy-3-(tributylstannyl)estrone[17] in 76% yield, 25.47 mg was isolated as a white powder using preparative TLC with 10% EtOAc/Hexane as the eluent. The ^{1}H, ^{13}C and ^{19}F NMR spectroscopic data of the purified material correctly match data previously reported.[17]

2.9 Spectra Relevant to Chapter Two

Copper-Mediated Oxidative Fluorination of Aryl Stannanes with Nucleophilic Fluoride

Raymond F. Gamache, Christopher Waldmann, Jennifer M. Murphy

Org. Lett., **2016**, *18*, 4522–4525

^{1}H NMR

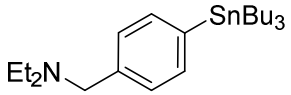
SnBu3
Et2N

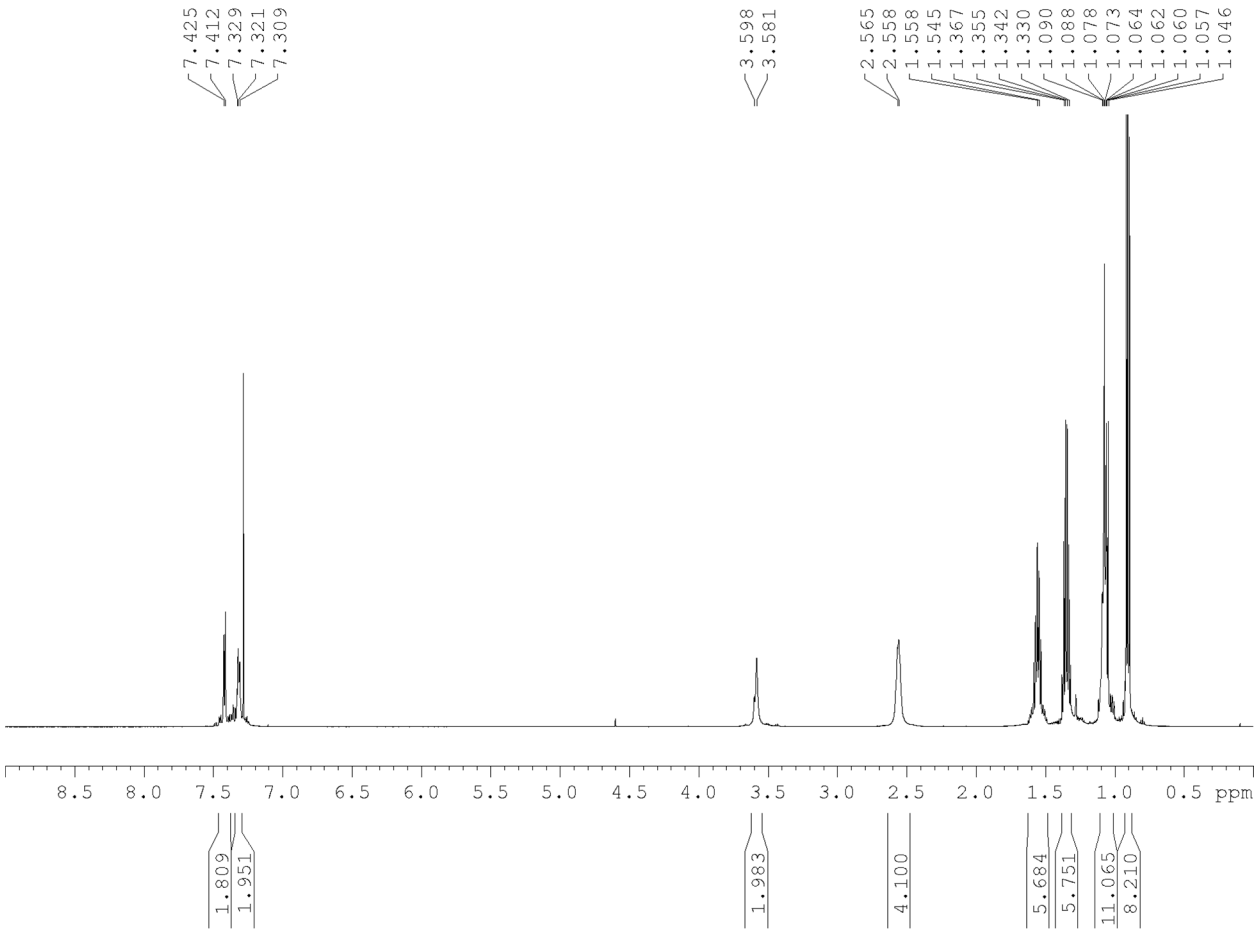
7.425
7.412
7.329
7.321
7.309
3.598
3.581
2.565
2.558
1.558
1.545
1.367
1.355
1.342
1.330
1.090
1.088
1.078
1.073
1.064
1.062
1.060
1.057
1.046
8.5
8.0
7.5
7.0
6.5
6.0
5.5
5.0
4.5
4.0
3.5
3.0
2.5
2.0
1.5
1.0
0.5
ppm
1.809
1.951
1.983
4.100
5.684
5.751
11.065
8.210

^{13}C NMR

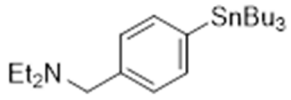
SnBu3
Et2N

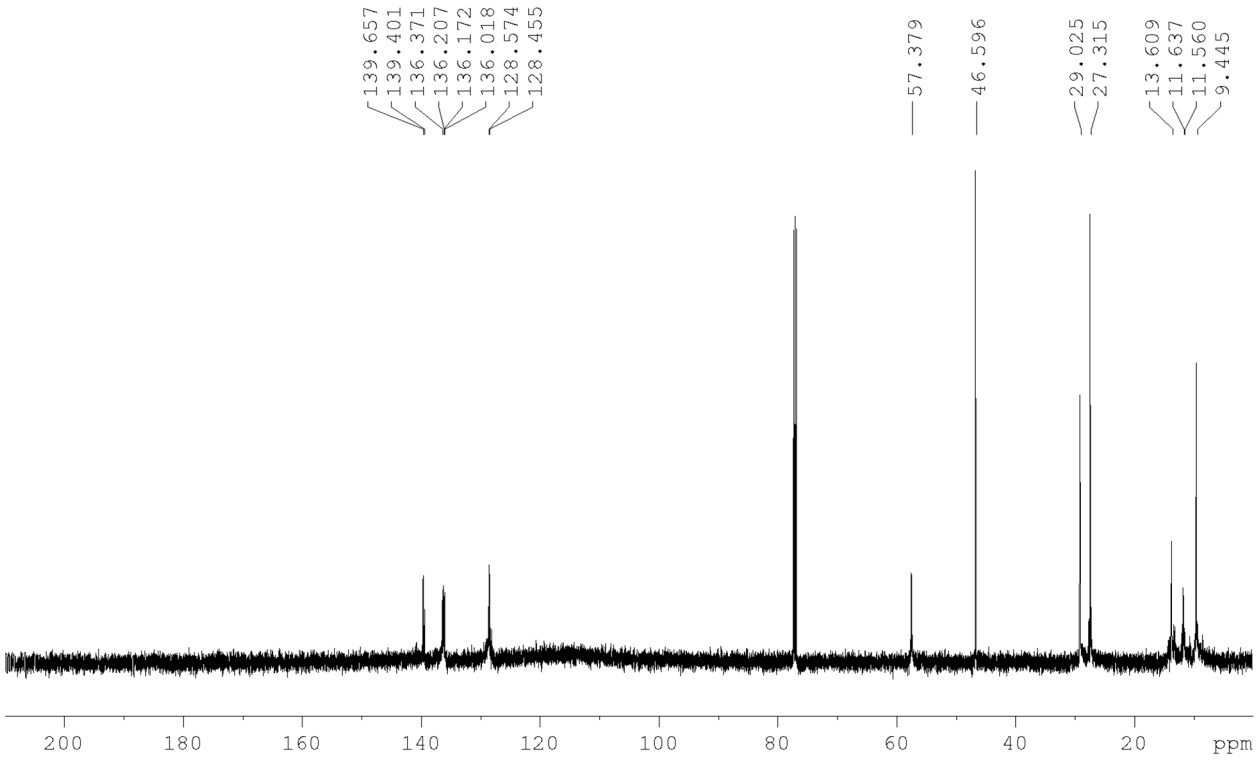
139.657
139.401
136.371
136.207
136.172
136.018
128.574
128.455
57.379
46.596
29.025
27.315
13.609
11.637
11.560
9.445
200
180
160
140
120
100
80
60
40
20
ppm

^{1}H NMR

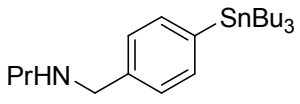
SnBu3
PrHN

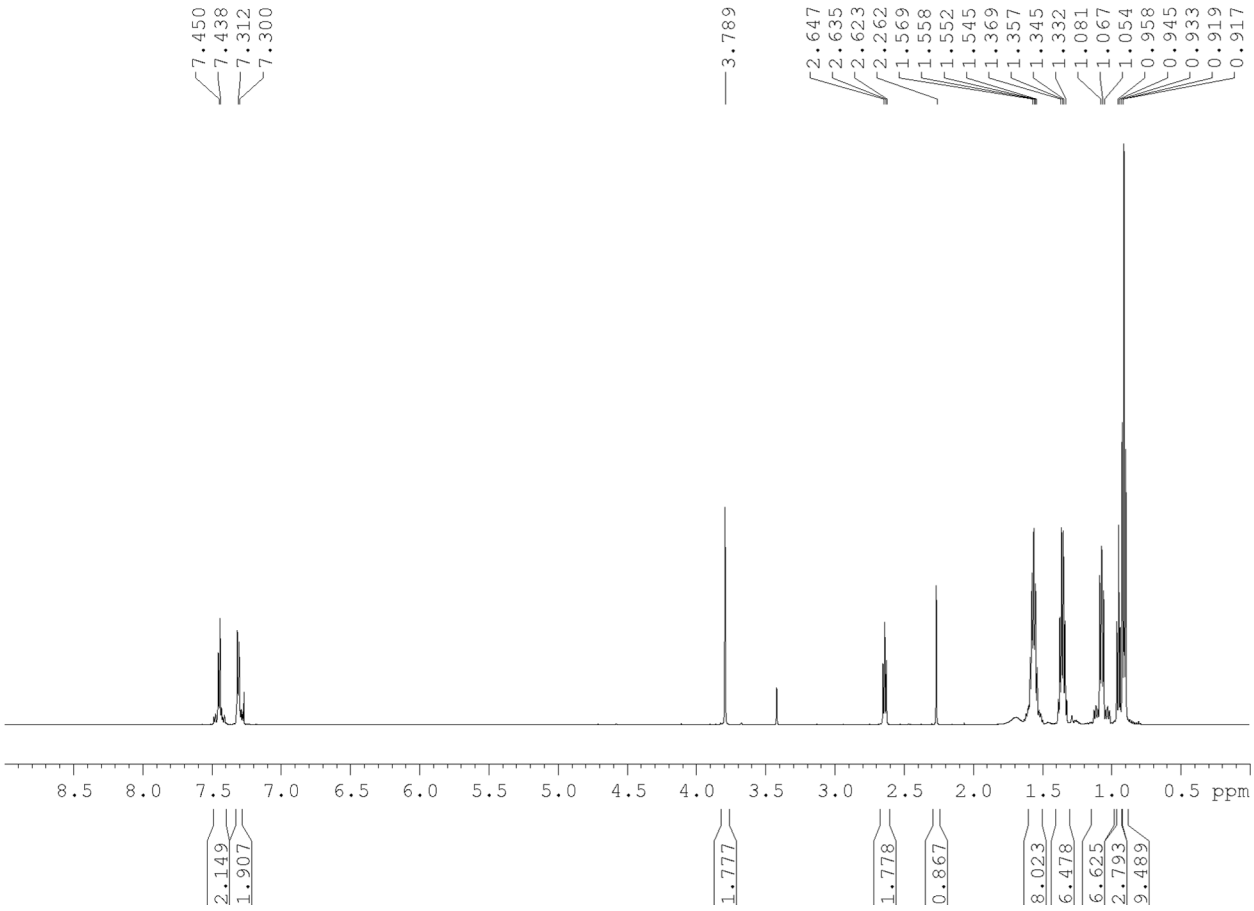
7.450
7.438
7.312
7.300
3.789
2.647
2.635
2.623
2.262
1.569
1.558
1.552
1.545
1.369
1.357
1.345
1.332
1.081
1.067
1.054
0.958
0.945
0.933
0.919
0.917
8.5 8.0 7.5 7.0 6.5 6.0 5.5 5.0 4.5 4.0 3.5 3.0 2.5 2.0 1.5 1.0 0.5 ppm
2.149
1.907
1.777
1.778
0.867
8.023
6.478
6.625
2.793
9.489

^{13}C NMR

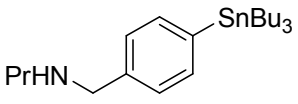
SnBu3
PrHN

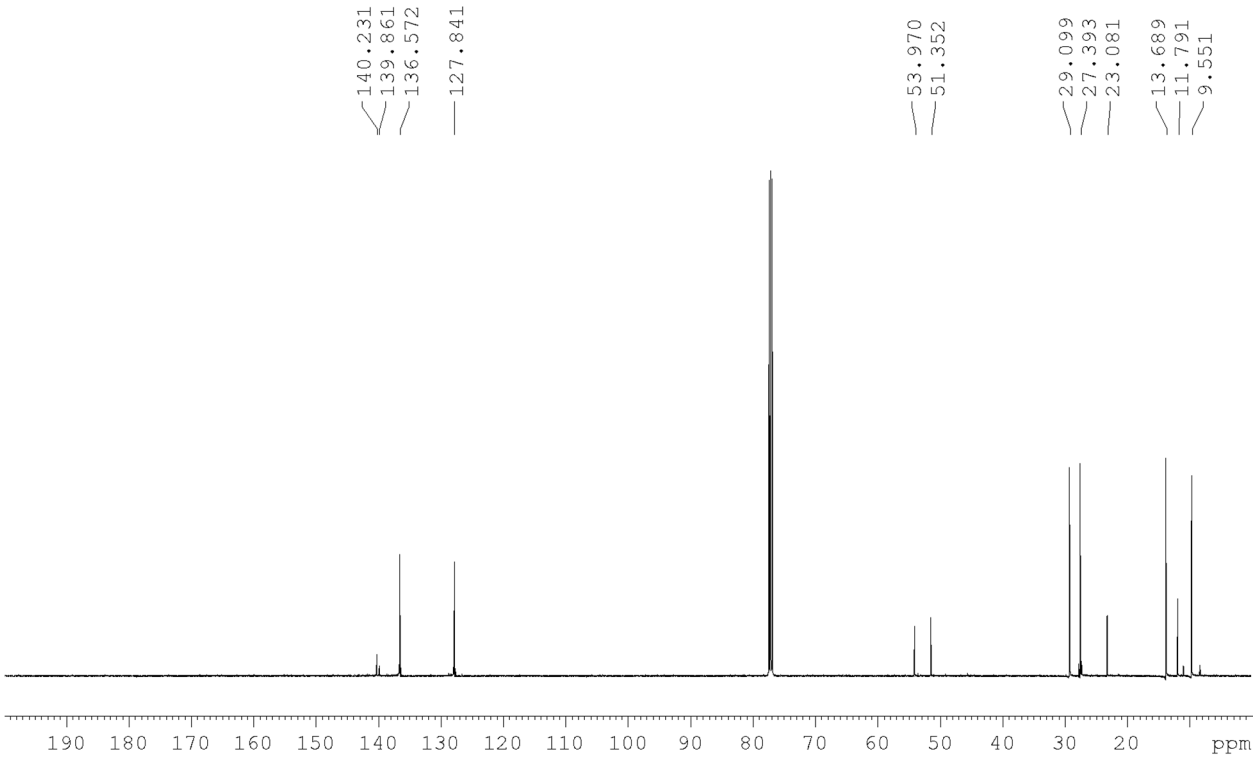
140.231
139.861
136.572
127.841
53.970
51.352
29.099
27.393
23.081
13.689
11.791
9.551
190 180 170 160 150 140 130 120 110 100 90 80 70 60 50 40 30 20 ppm

^{1}H NMR

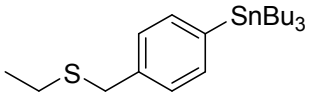
SnBu3
S

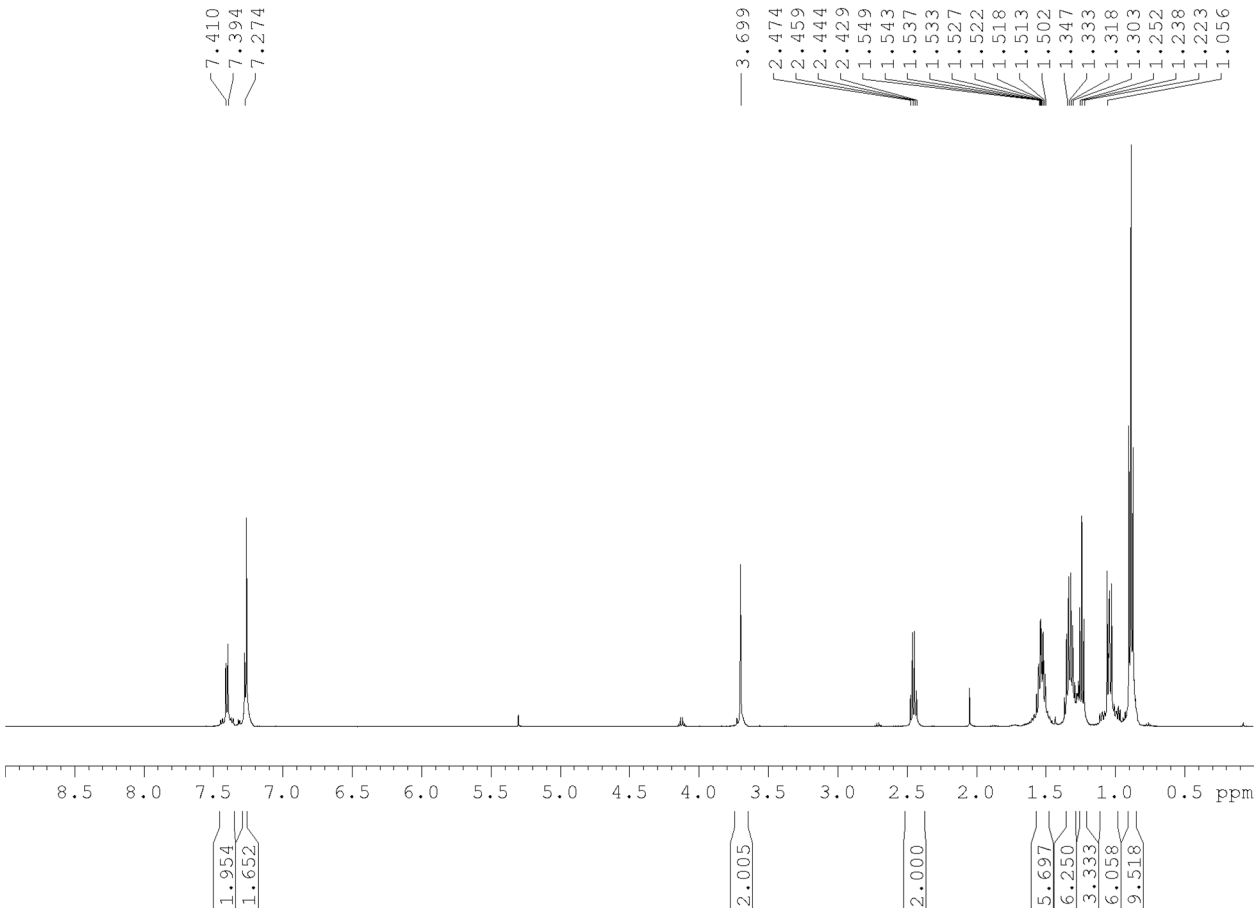
7.410
7.394
7.274
3.699
2.474
2.459
2.444
2.429
1.549
1.543
1.537
1.533
1.527
1.522
1.518
1.513
1.502
1.347
1.333
1.318
1.303
1.252
1.238
1.223
1.056
8.5 8.0 7.5 7.0 6.5 6.0 5.5 5.0 4.5 4.0 3.5 3.0 2.5 2.0 1.5 1.0 0.5 ppm
1.954
1.652
2.005
2.000
5.697
6.250
3.333
6.058
9.518

^{13}C NMR

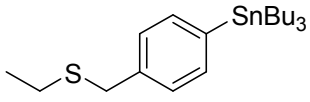
SnBu3
S

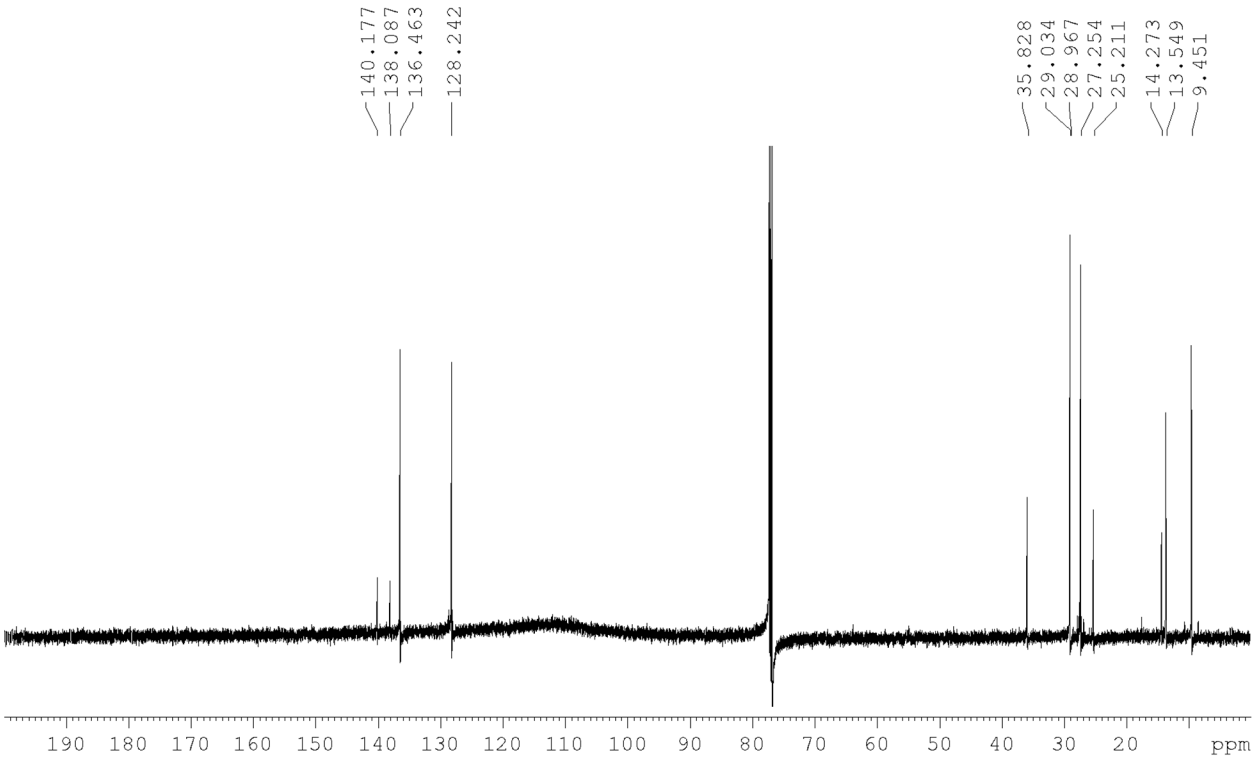
140.177
138.087
136.463
128.242
35.828
29.034
28.967
27.254
25.211
14.273
13.549
9.451
190 180 170 160 150 140 130 120 110 100 90 80 70 60 50 40 30 20 ppm

^{1}H NMR

reference

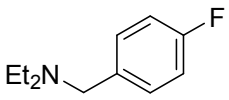

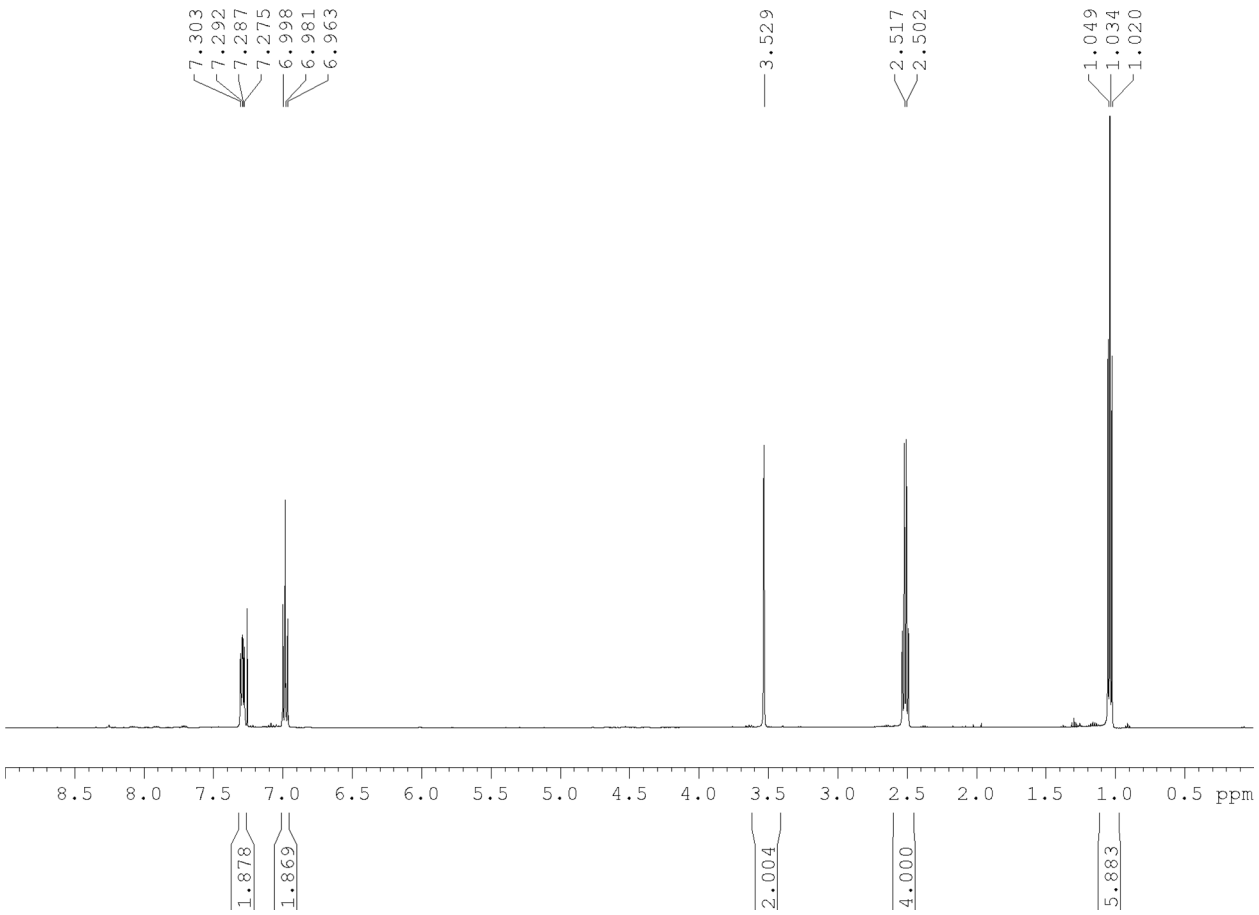

^{13}C NMR

reference

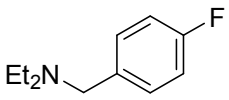

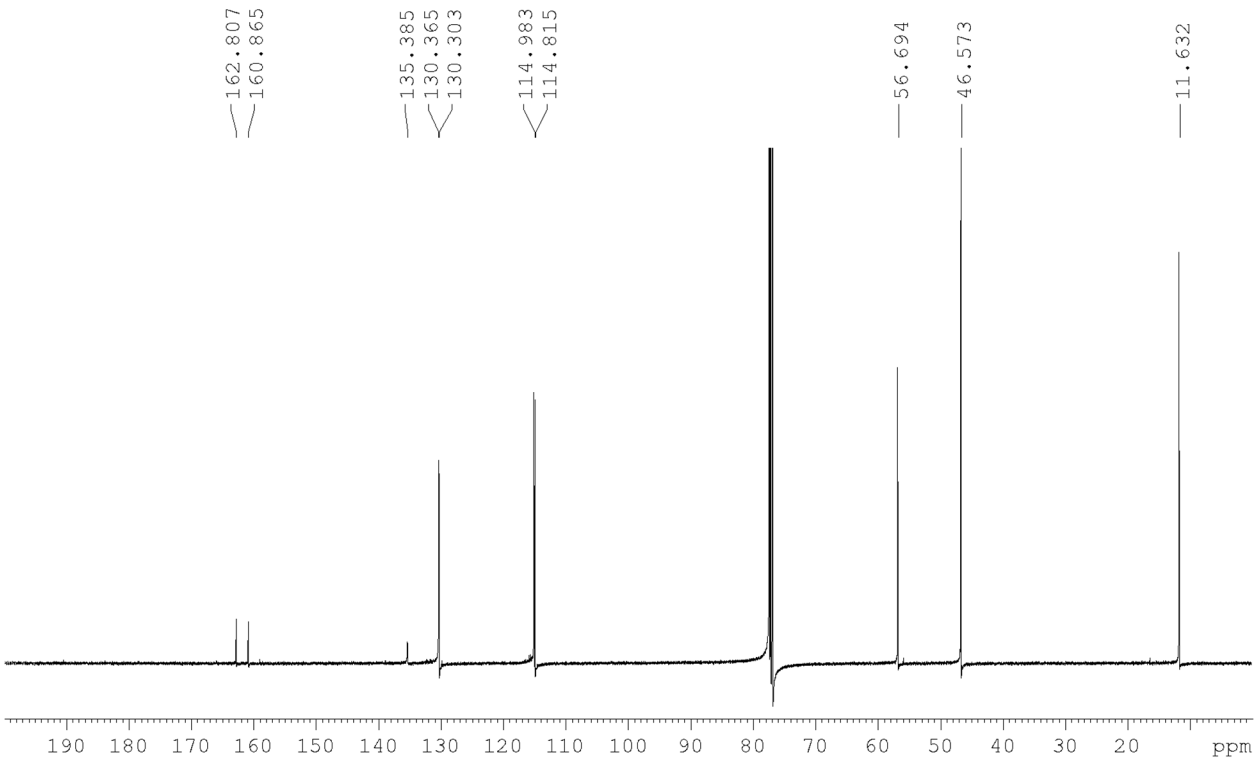

^{19}F NMR

reference

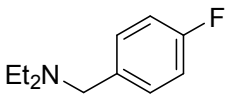

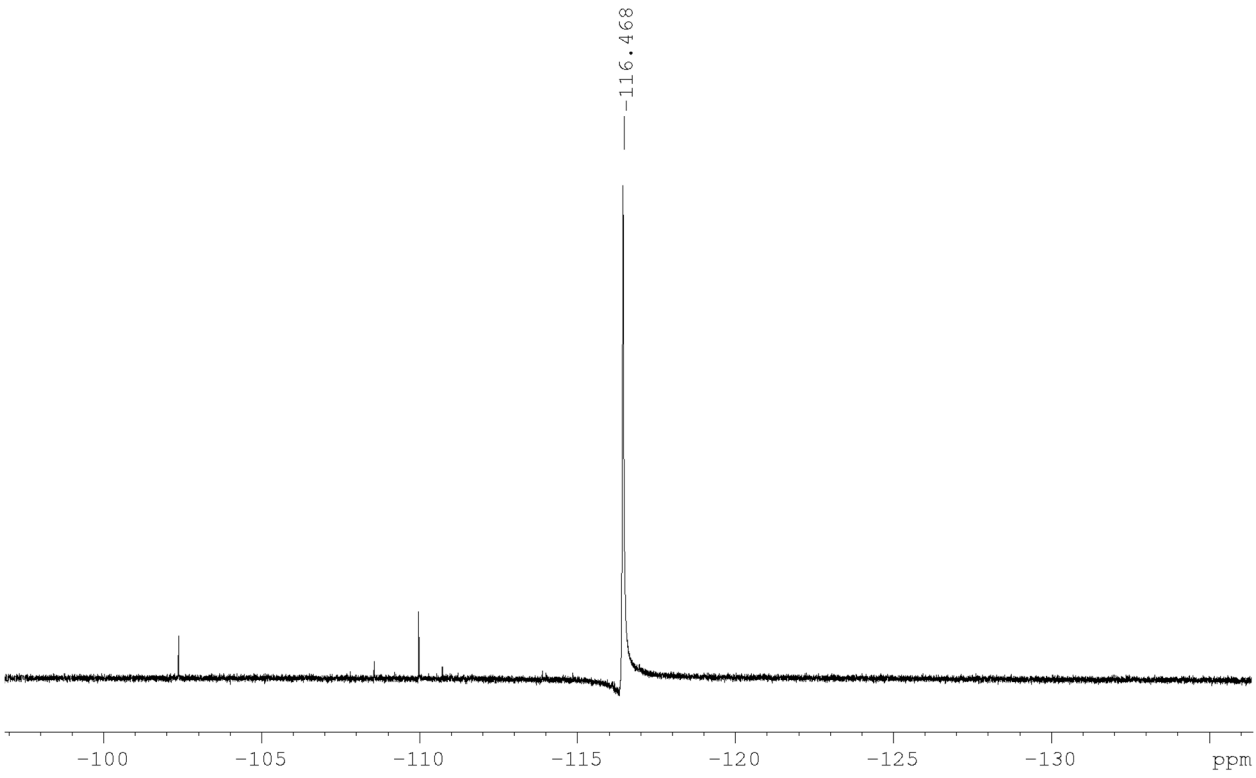

^{1}H NMR

reference

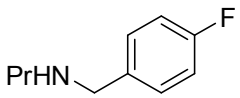

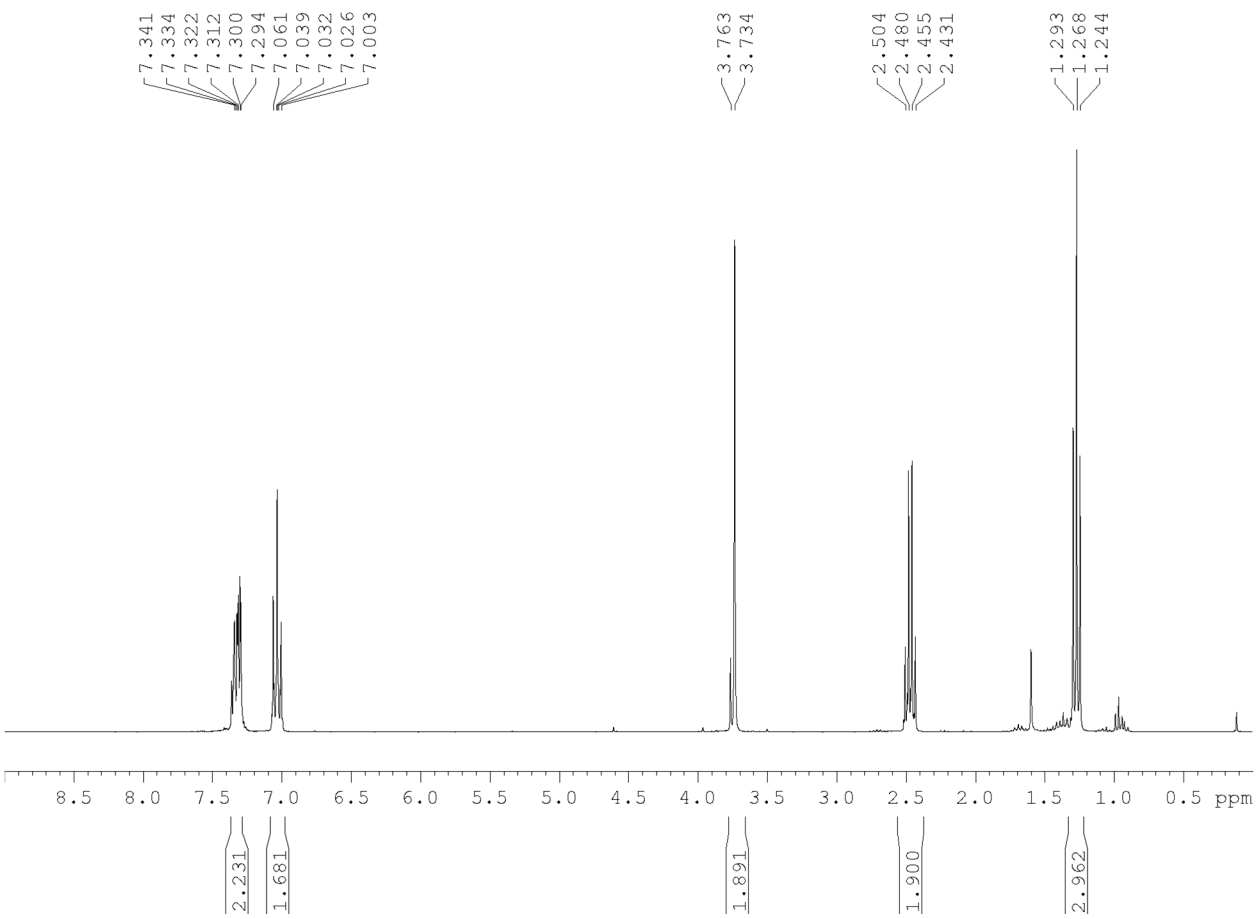

^{13}C NMR

reference

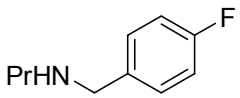

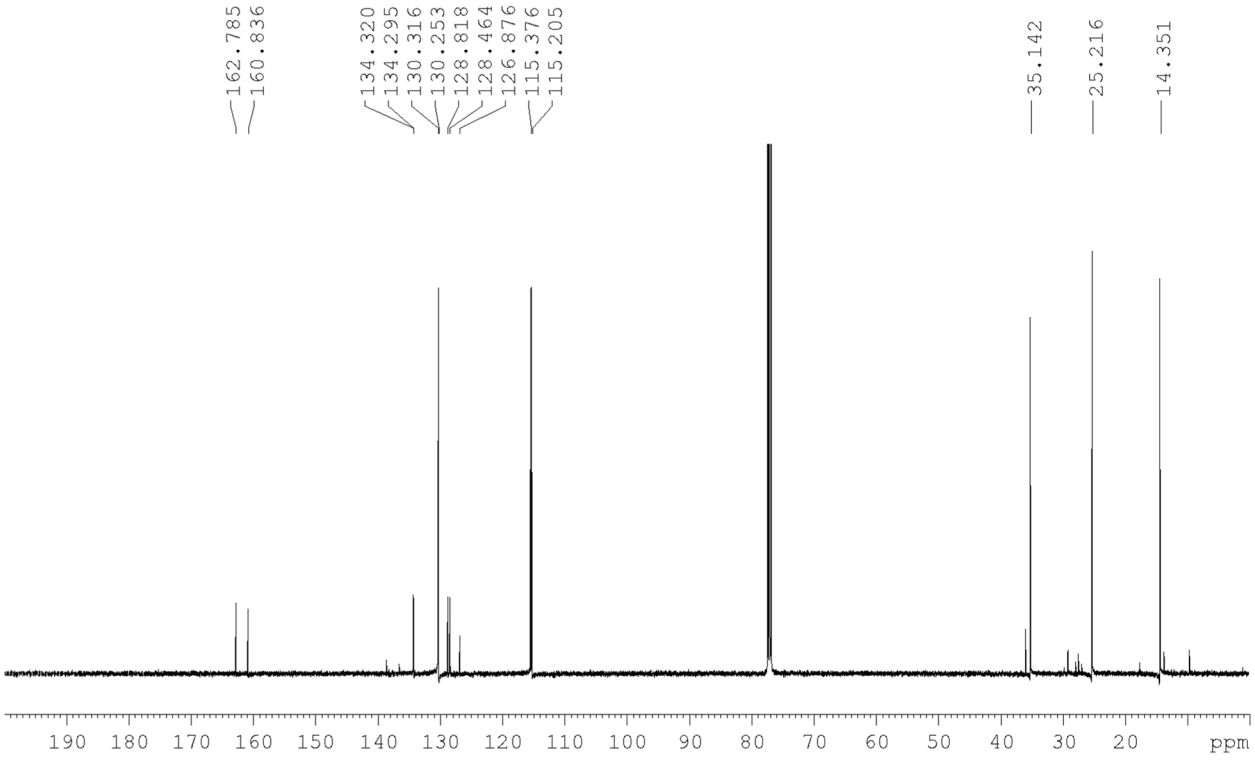

^{19}F NMR

reference

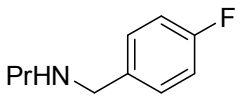

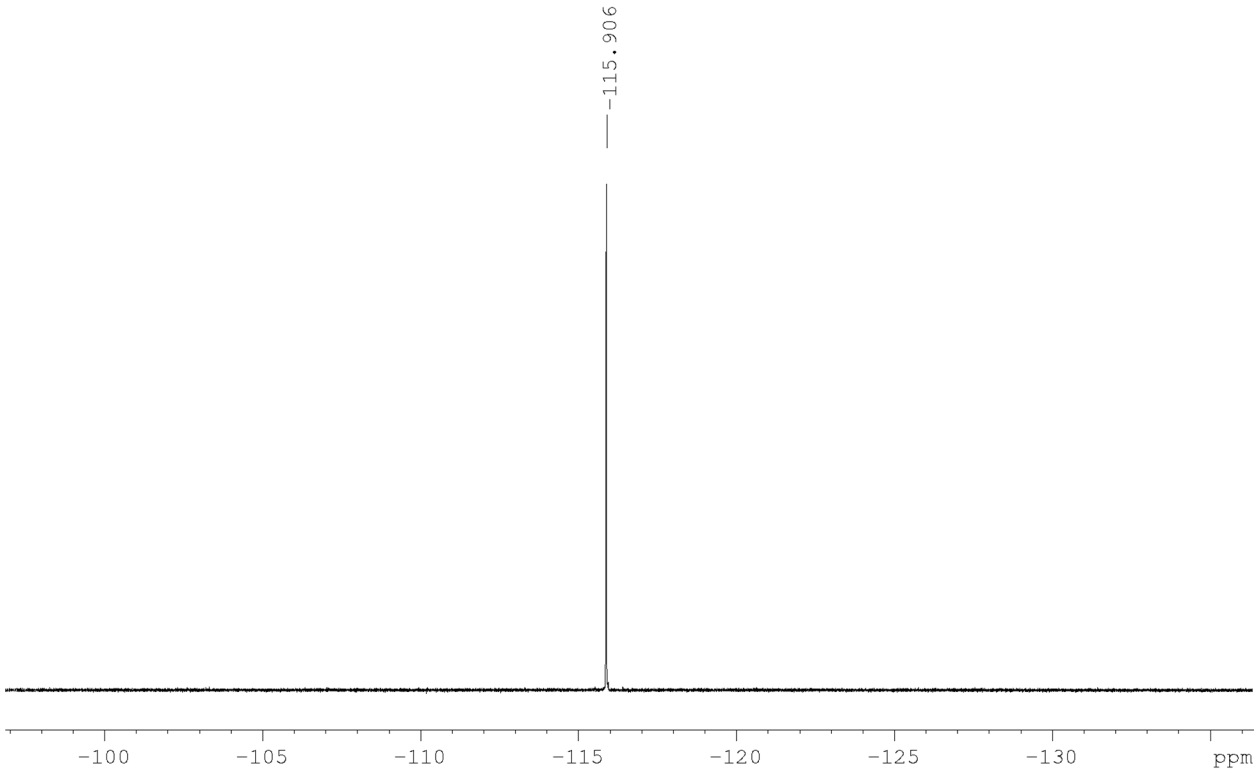

^{1}H NMR

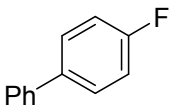
F
Ph

2.2

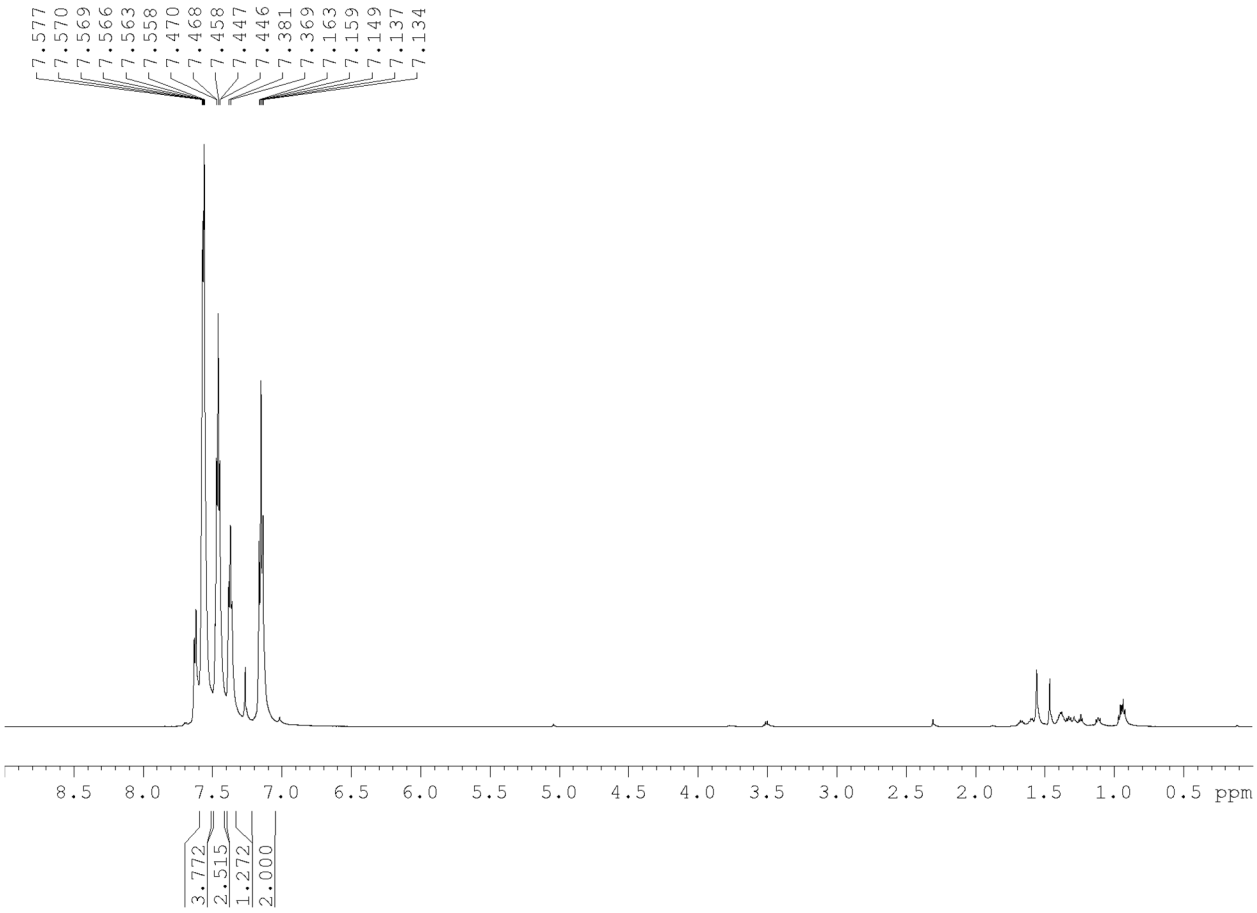
7.577
7.570
7.569
7.566
7.563
7.558
7.470
7.468
7.458
7.447
7.446
7.381
7.369
7.163
7.159
7.149
7.137
7.134
8.5 8.0 7.5 7.0 6.5 6.0 5.5 5.0 4.5 4.0 3.5 3.0 2.5 2.0 1.5 1.0 0.5 ppm
3.772
2.515
1.272
2.000

^{13}C NMR

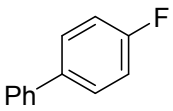
F
Ph

2.2

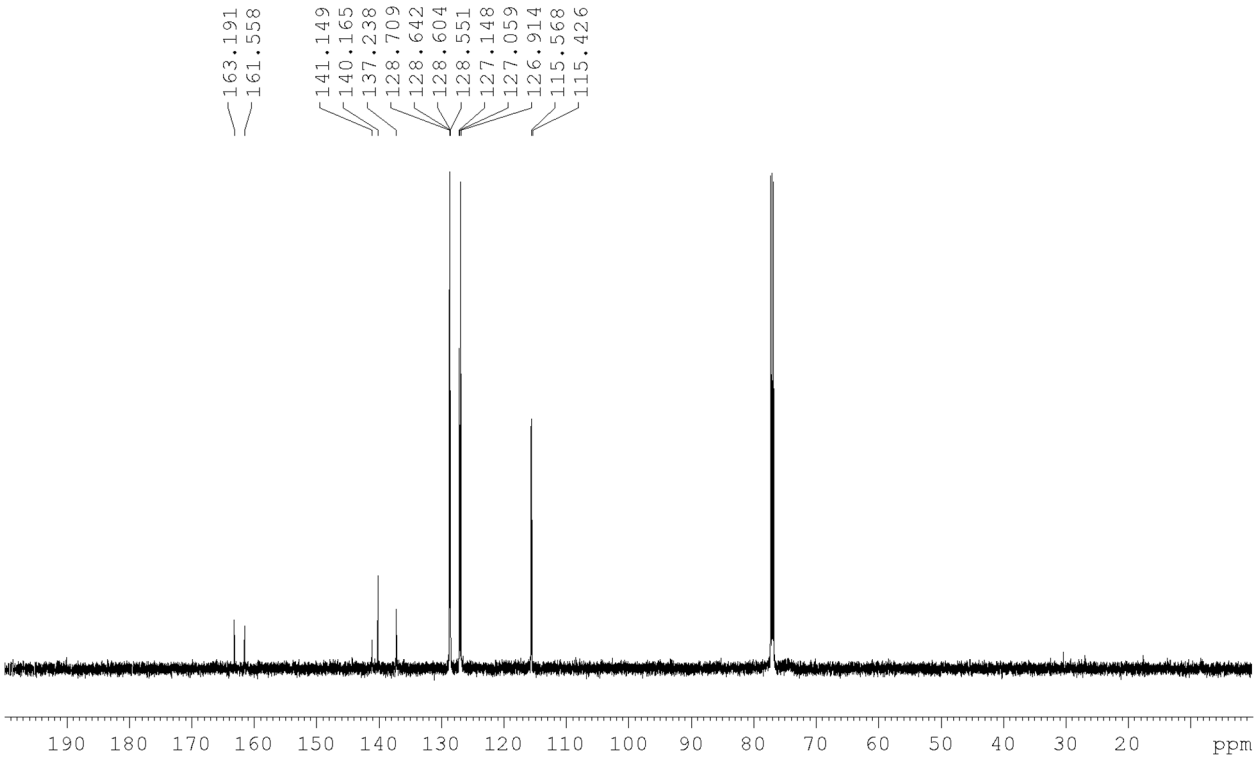
163.191
161.558
141.149
140.165
137.238
128.709
128.642
128.604
128.551
127.148
127.059
126.914
115.568
115.426
190 180 170 160 150 140 130 120 110 100 90 80 70 60 50 40 30 20 ppm

^{19}F NMR

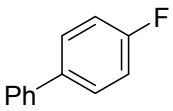

2.2

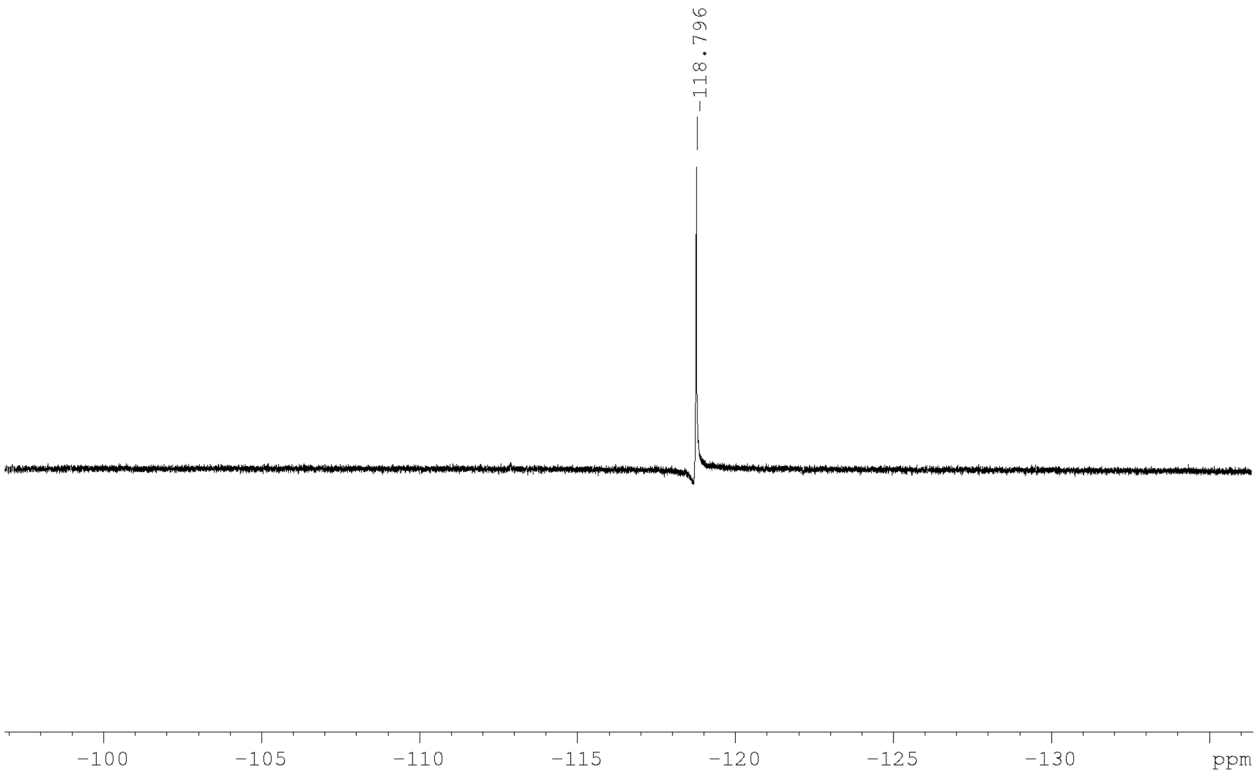

^{1}H NMR

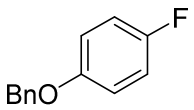
F
BnO

2.3

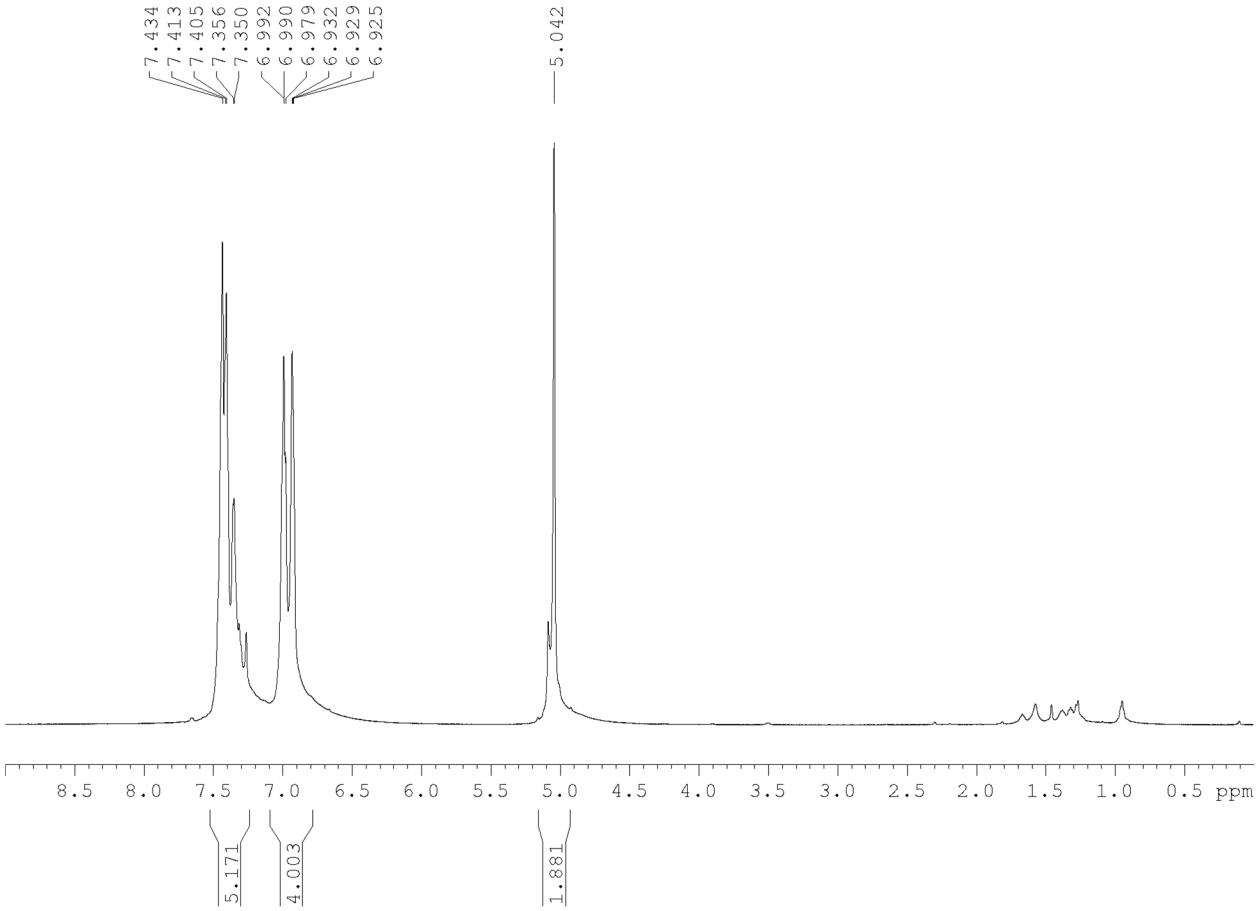
7.434
7.413
7.405
7.356
7.350
6.992
6.990
6.979
6.932
6.929
6.925
5.042
8.5 8.0 7.5 7.0 6.5 6.0 5.5 5.0 4.5 4.0 3.5 3.0 2.5 2.0 1.5 1.0 0.5 ppm
5.171
4.003
1.881

^{13}C NMR

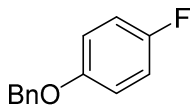
F
BnO

2.3

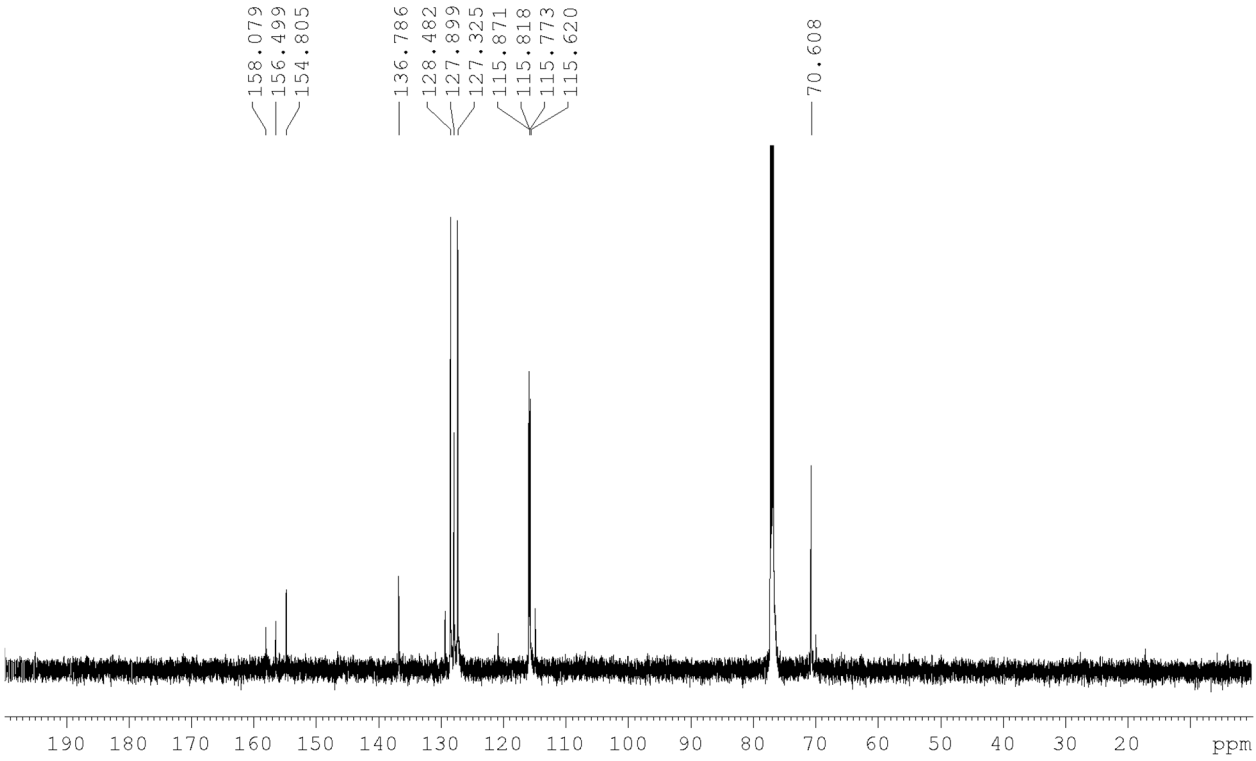
158.079
156.499
154.805
136.786
128.482
127.899
127.325
115.871
115.818
115.773
115.620
70.608
190 180 170 160 150 140 130 120 110 100 90 80 70 60 50 40 30 20 ppm

^{19}F NMR

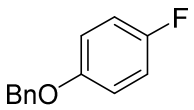

2.3

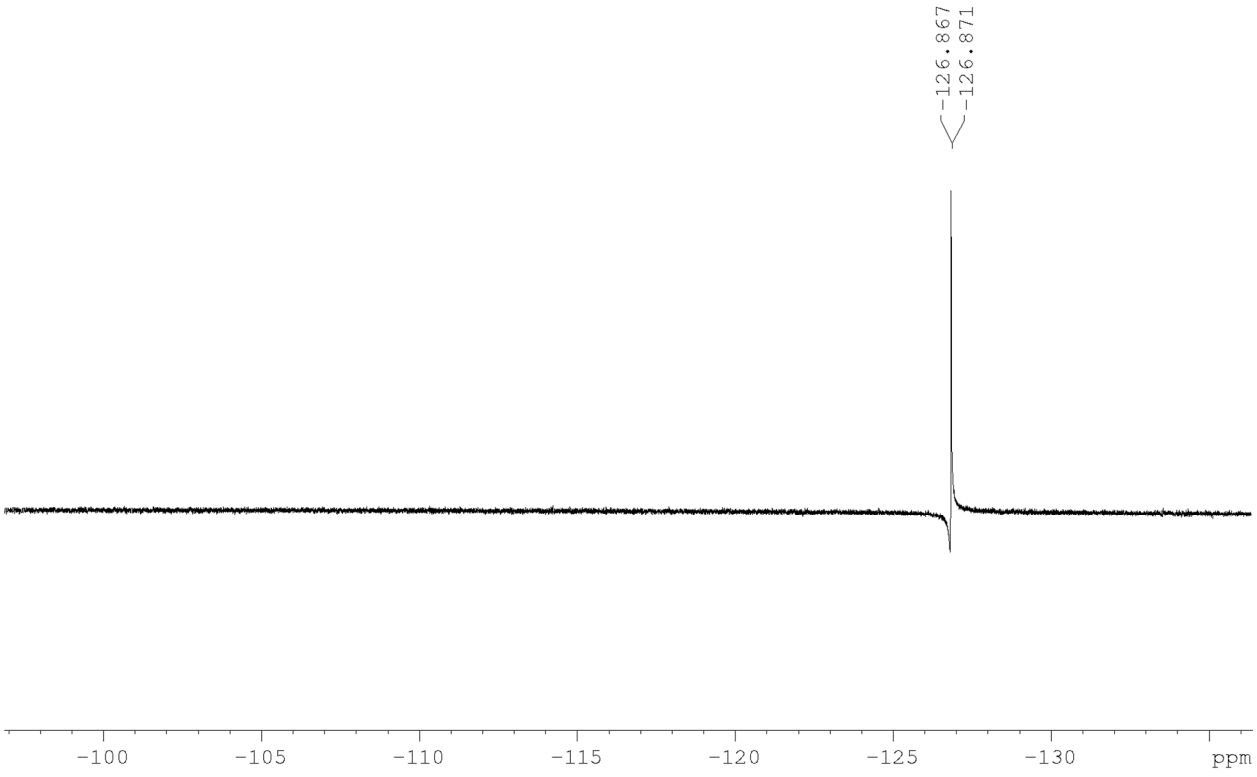

^{19}F NMR

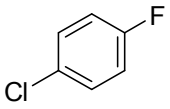

2.4

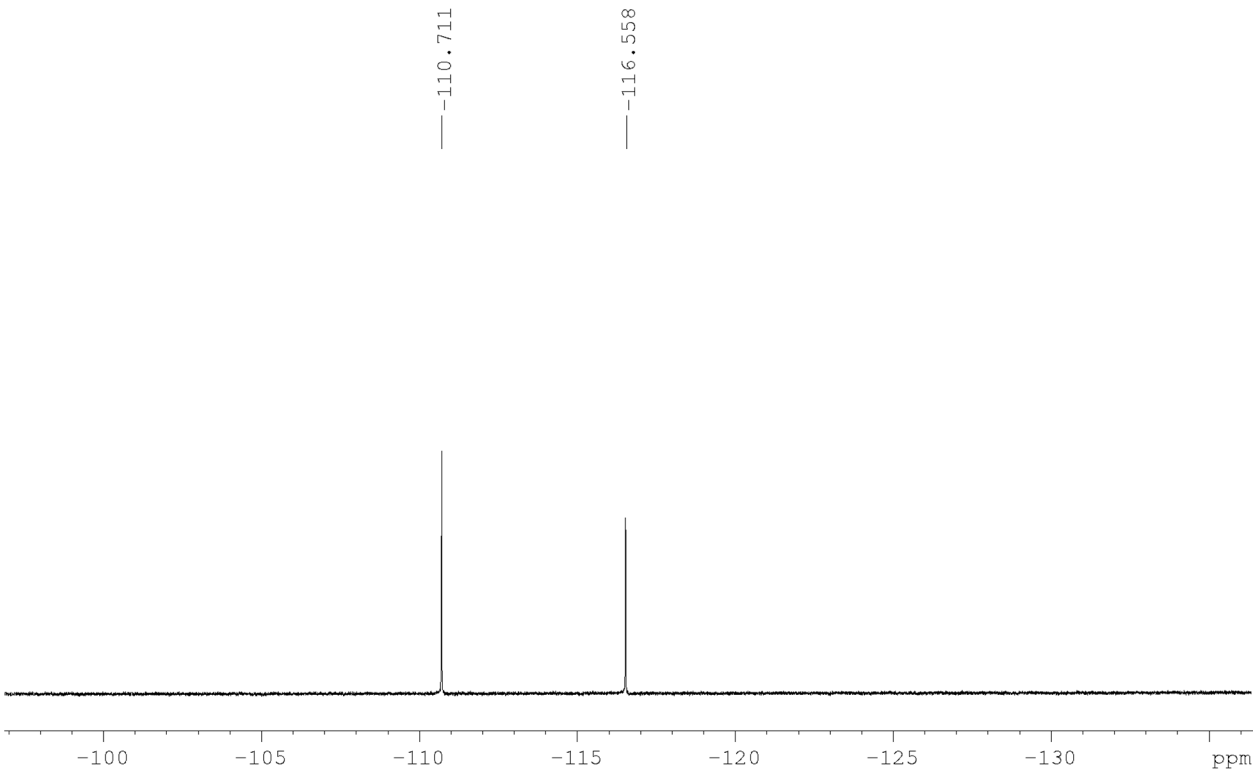

^{19}F NMR

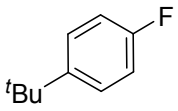

2.5

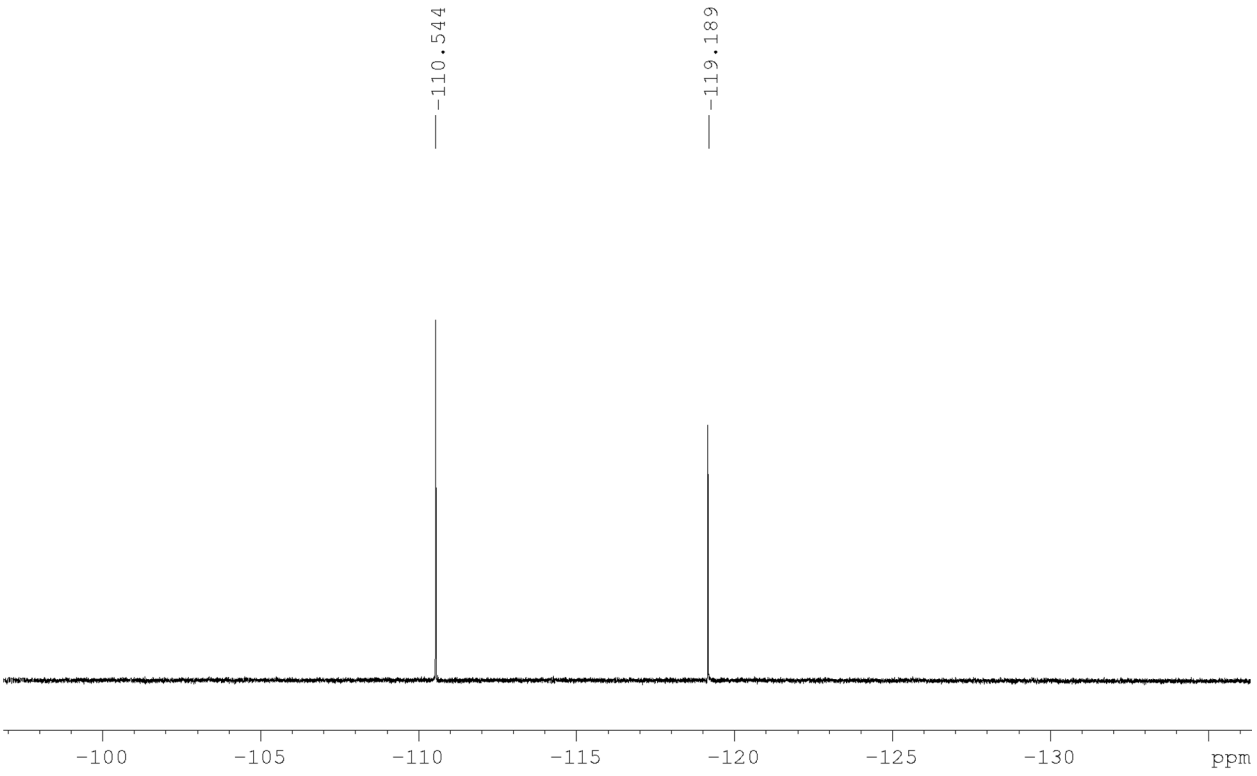

^{1}H NMR

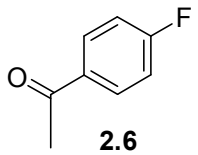
F
O

2.6

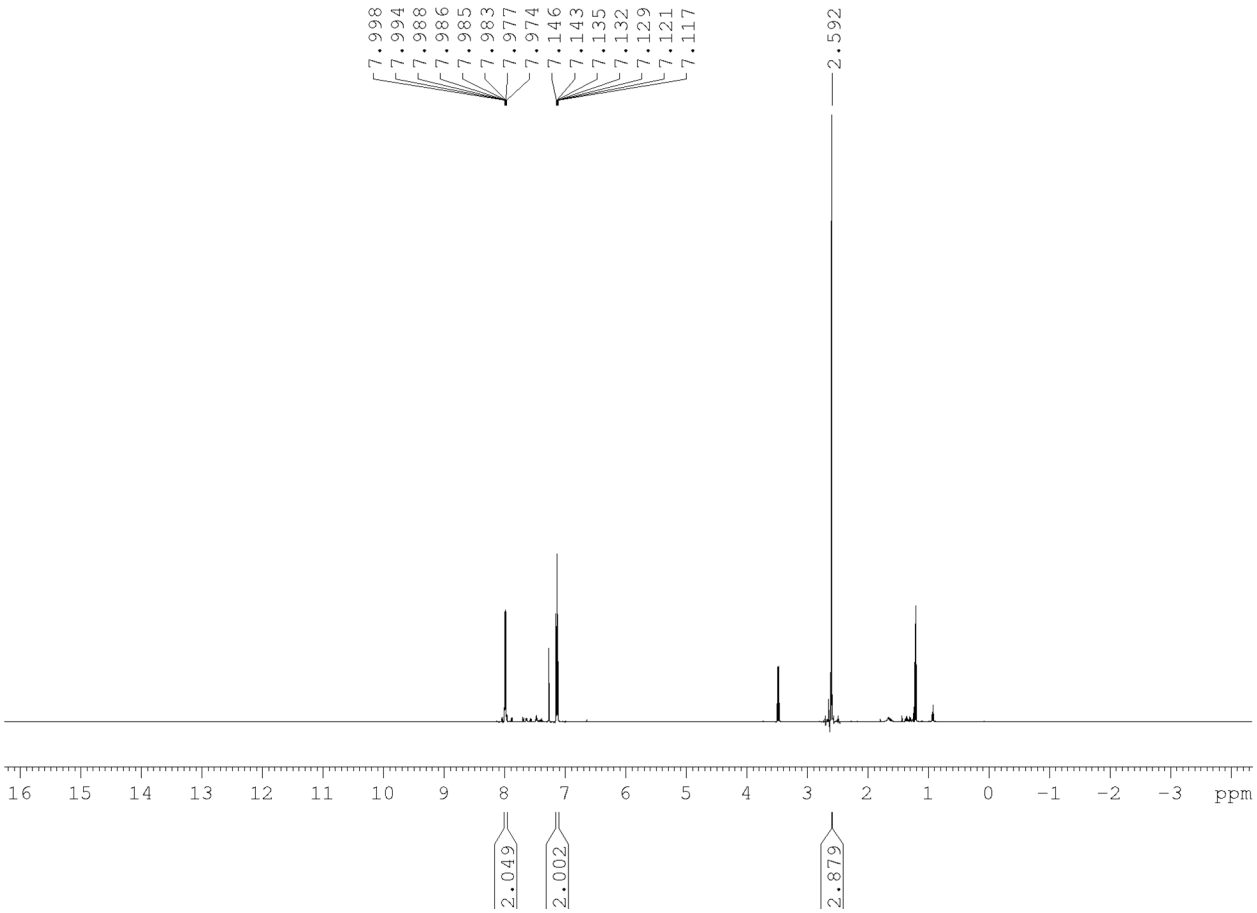
7.998
7.994
7.988
7.986
7.985
7.983
7.977
7.974
7.146
7.143
7.135
7.132
7.129
7.121
7.117
2.592
16 15 14 13 12 11 10 9 8 7 6 5 4 3 2 1 0 −1 −2 −3 ppm
2.049
2.002
2.879

^{13}C NMR

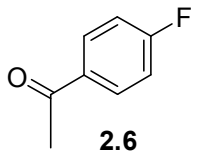
F
O

2.6

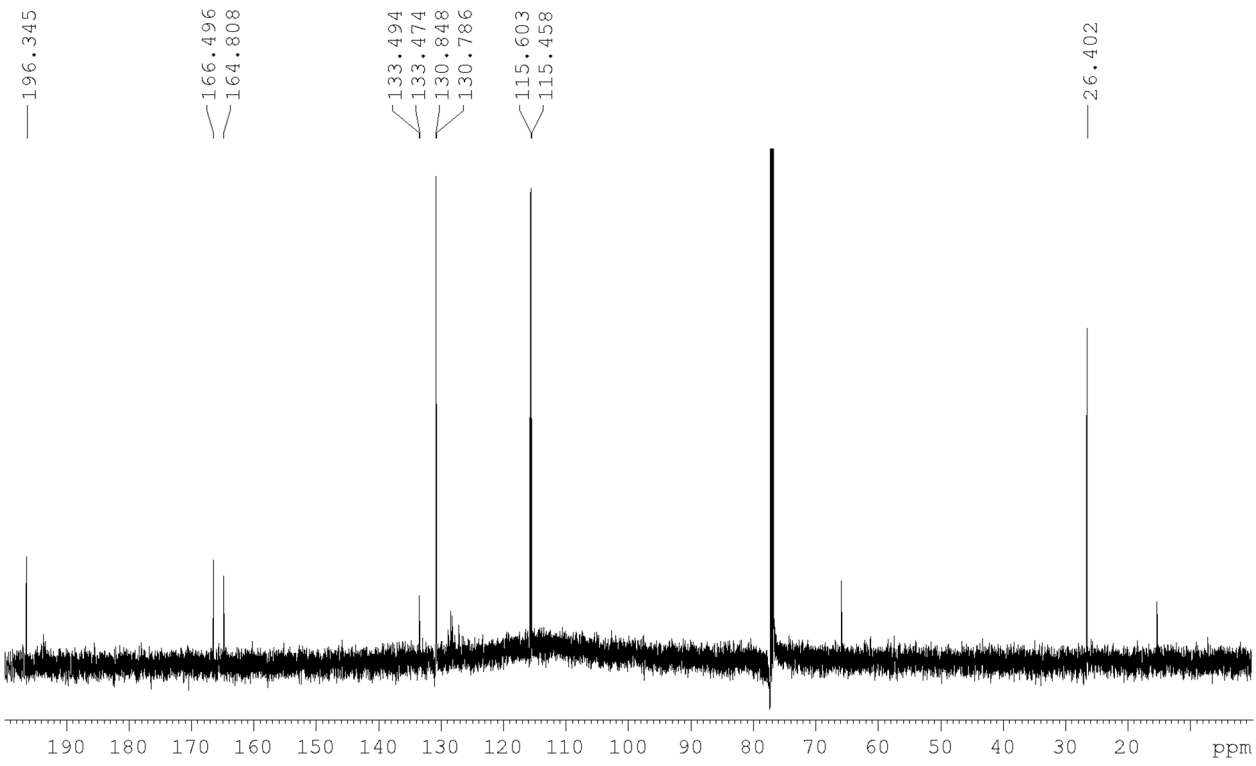
196.345
166.496
164.808
133.494
133.474
130.848
130.786
115.603
115.458
26.402
190 180 170 160 150 140 130 120 110 100 90 80 70 60 50 40 30 20 ppm

^{19}F NMR

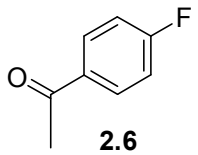

2.6

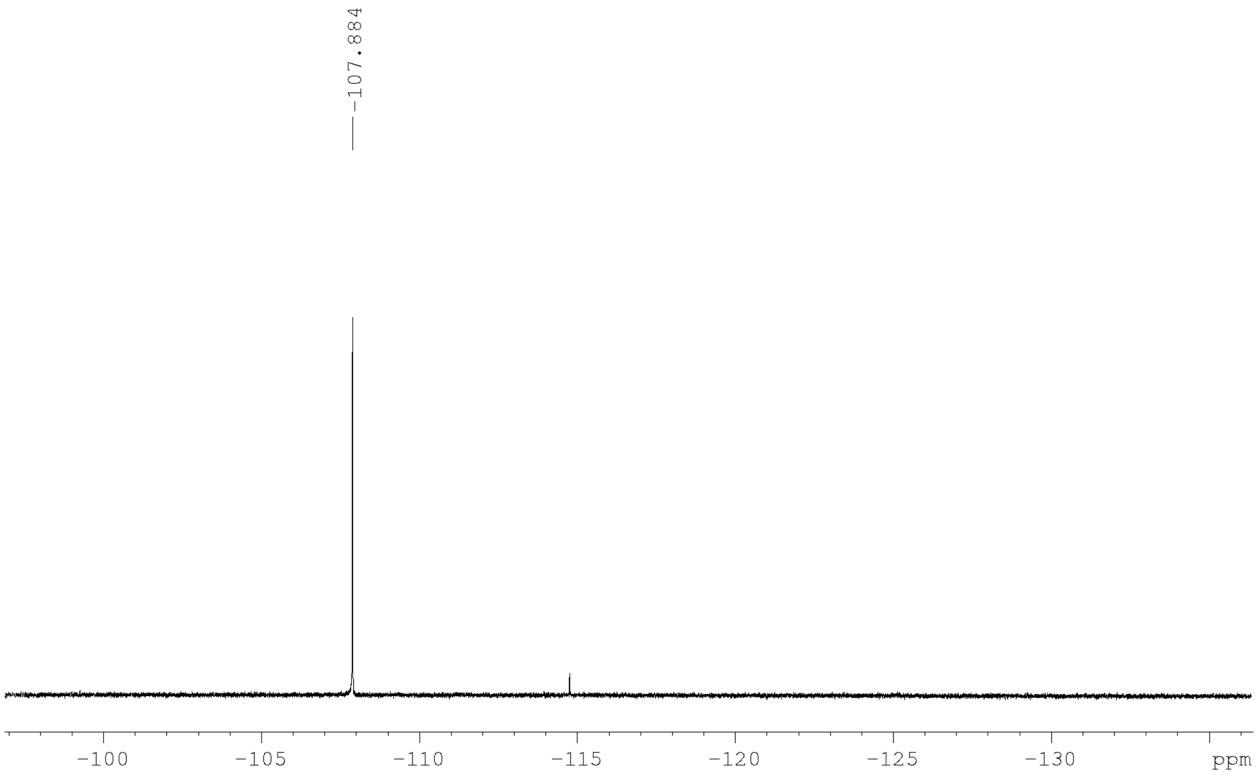

^{1}H NMR

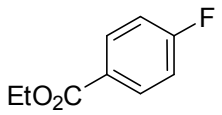
F
EtO2C

2.7

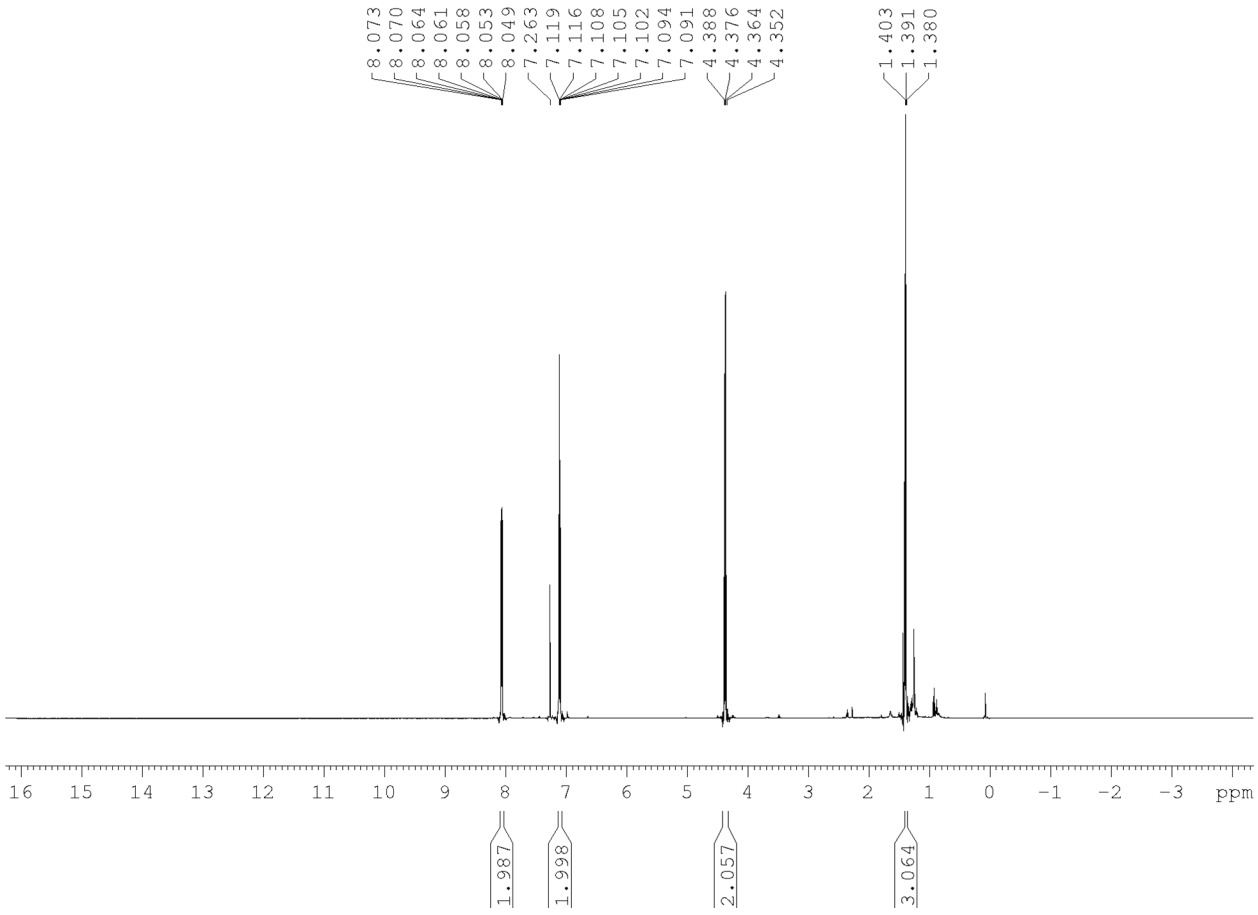
8.073
8.070
8.064
8.061
8.058
8.053
8.049
7.263
7.119
7.116
7.108
7.105
7.102
7.094
7.091
4.388
4.376
4.364
4.352
1.403
1.391
1.380
16 15 14 13 12 11 10 9 8 7 6 5 4 3 2 1 0 -1 -2 -3 ppm
1.987
1.998
2.057
3.064

^{13}C NMR

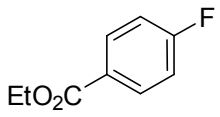
F
EtO2C

2.7

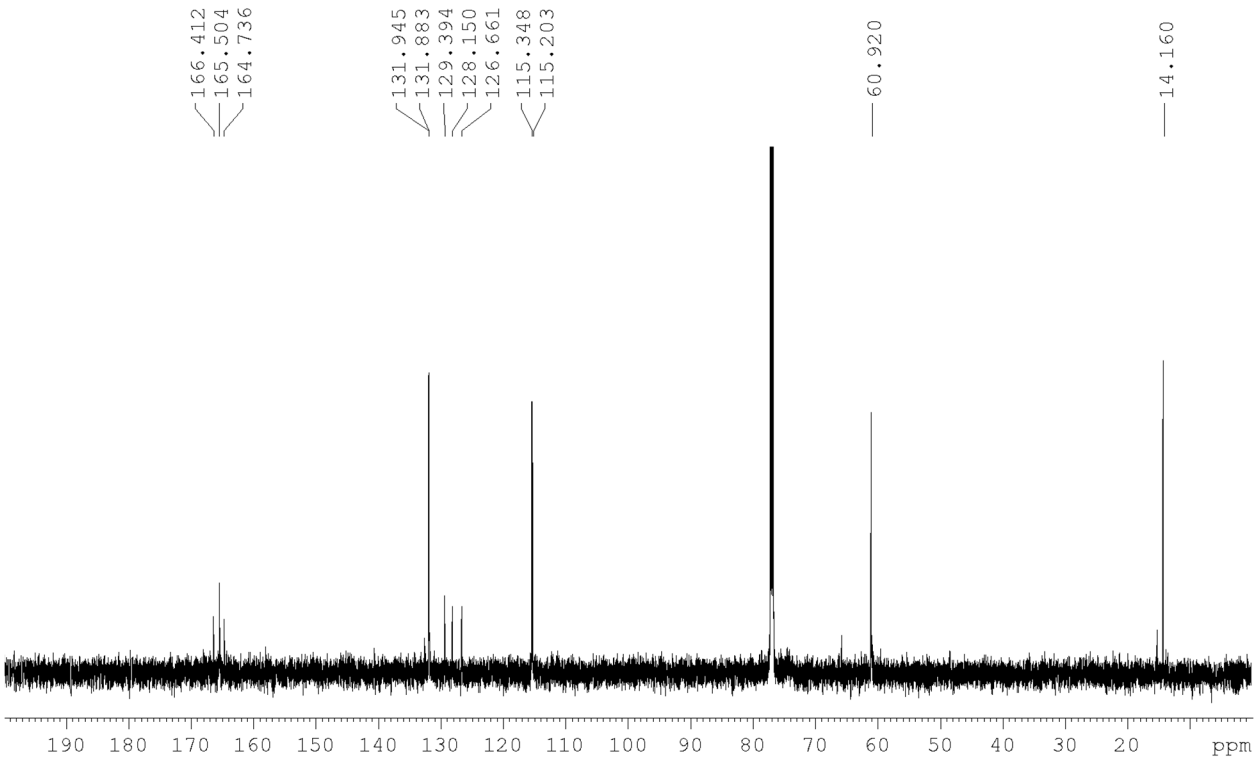
166.412
165.504
164.736
131.945
131.883
129.394
128.150
126.661
115.348
115.203
60.920
14.160
190 180 170 160 150 140 130 120 110 100 90 80 70 60 50 40 30 20 ppm

^{19}F NMR

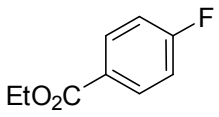

2.7

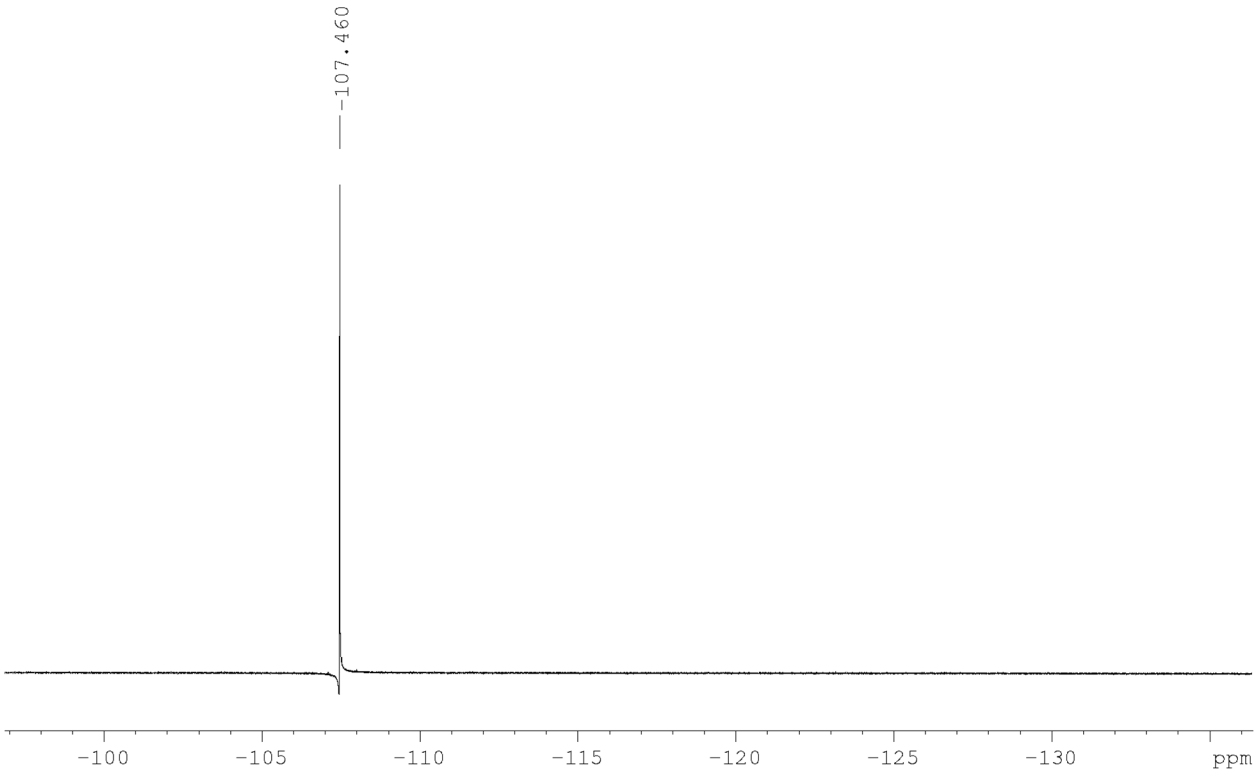

^{1}H NMR

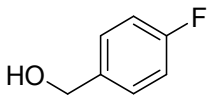
F
HO

2.8

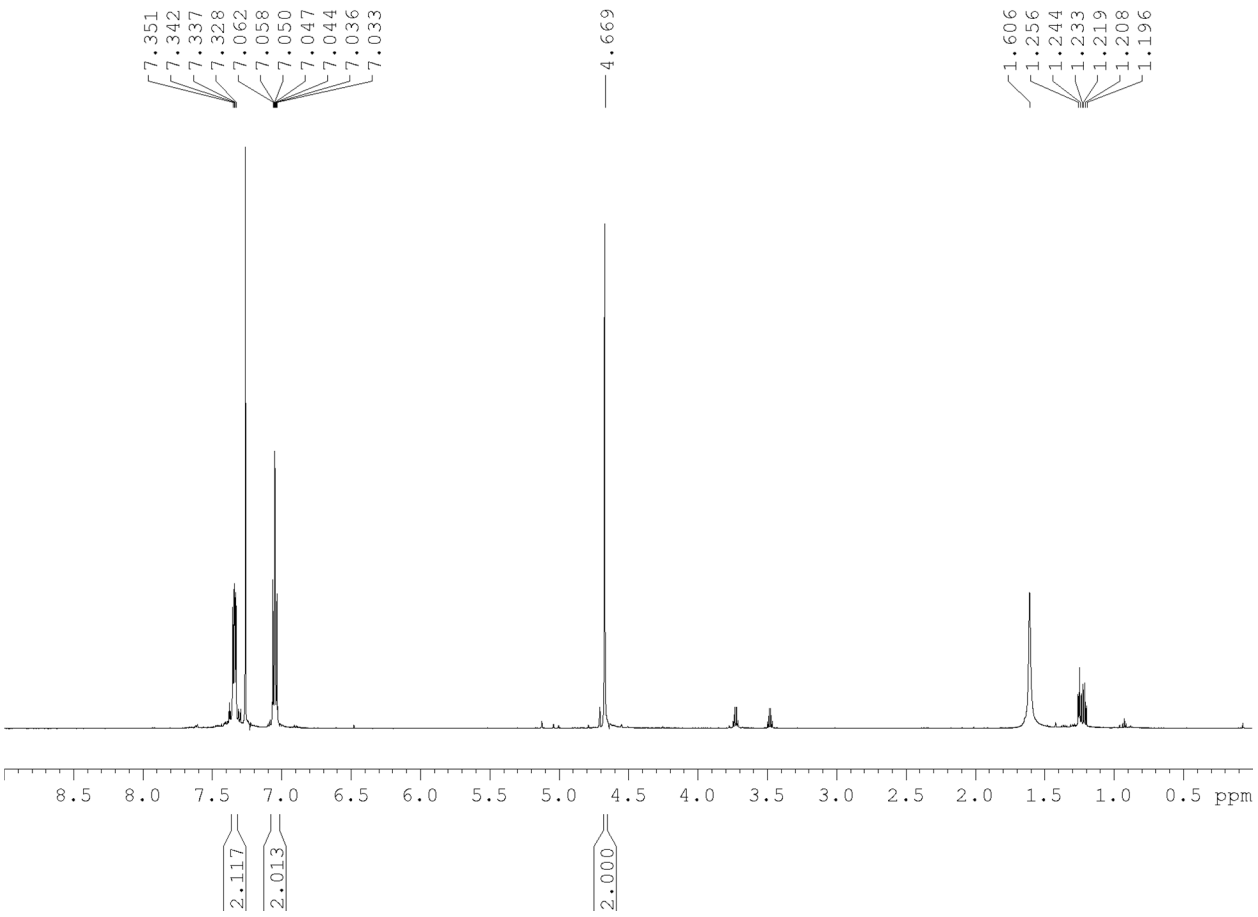
7.351
7.342
7.337
7.328
7.062
7.058
7.050
7.047
7.044
7.036
7.033
4.669
1.606
1.256
1.244
1.233
1.219
1.208
1.196
8.5 8.0 7.5 7.0 6.5 6.0 5.5 5.0 4.5 4.0 3.5 3.0 2.5 2.0 1.5 1.0 0.5 ppm
2.117
2.013
2.000

^{13}C NMR

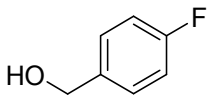
F
HO

2.8

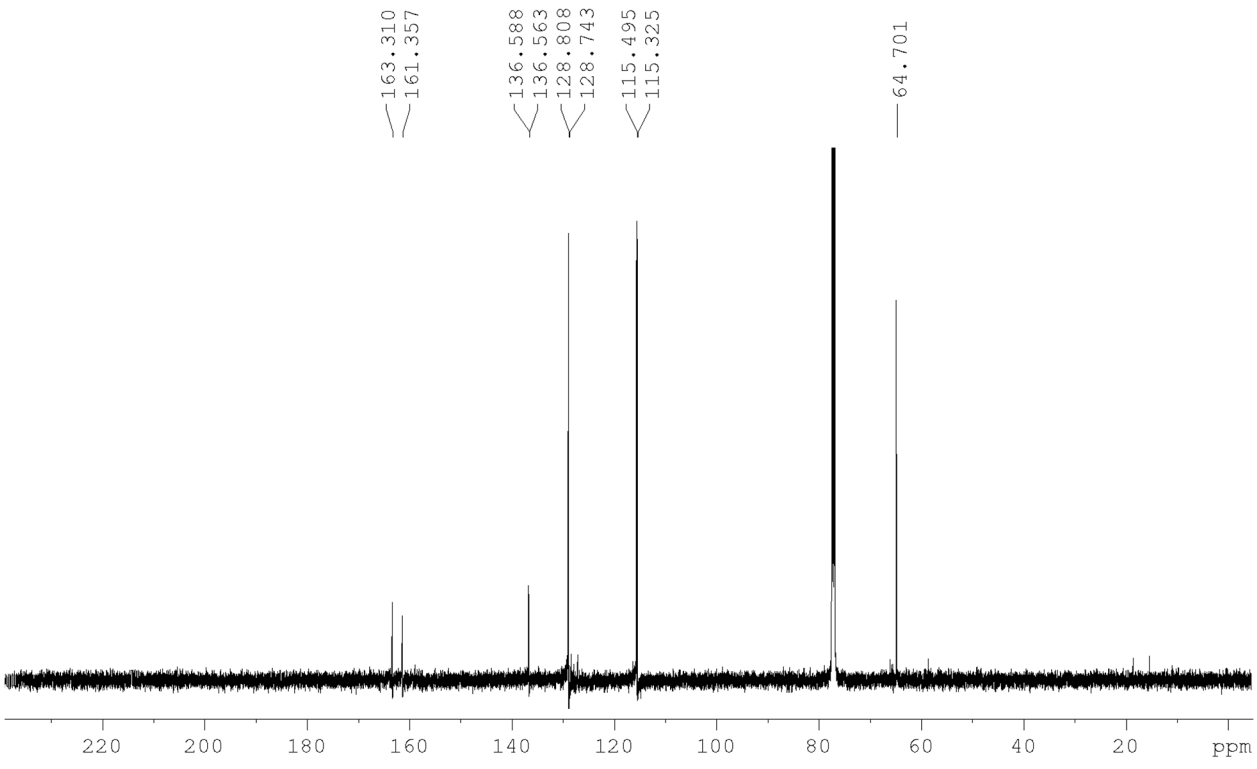
163.310
161.357
136.588
136.563
128.808
128.743
115.495
115.325
64.701
220
200
180
160
140
120
100
80
60
40
20
ppm

^{19}F NMR

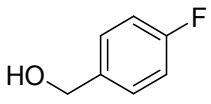

2.8

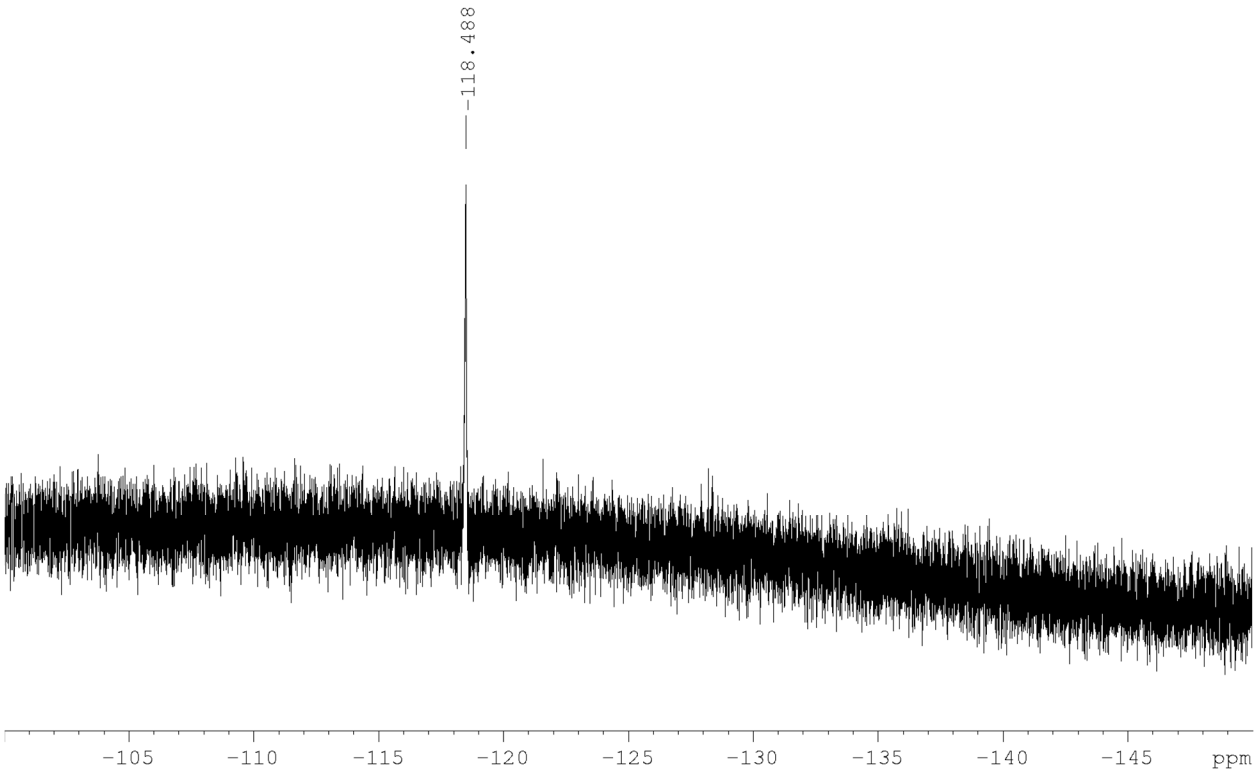

^{19}F NMR

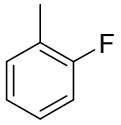

2.9

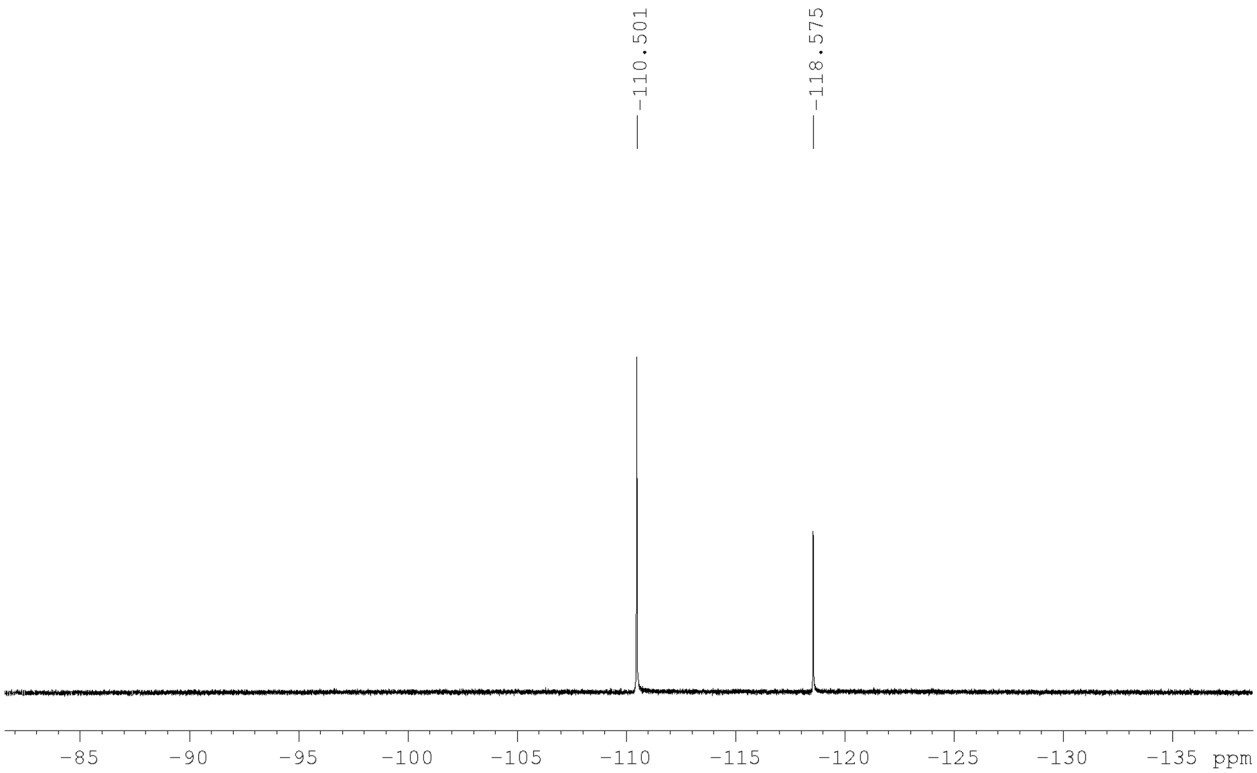

^{19}F NMR

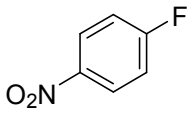

2.10

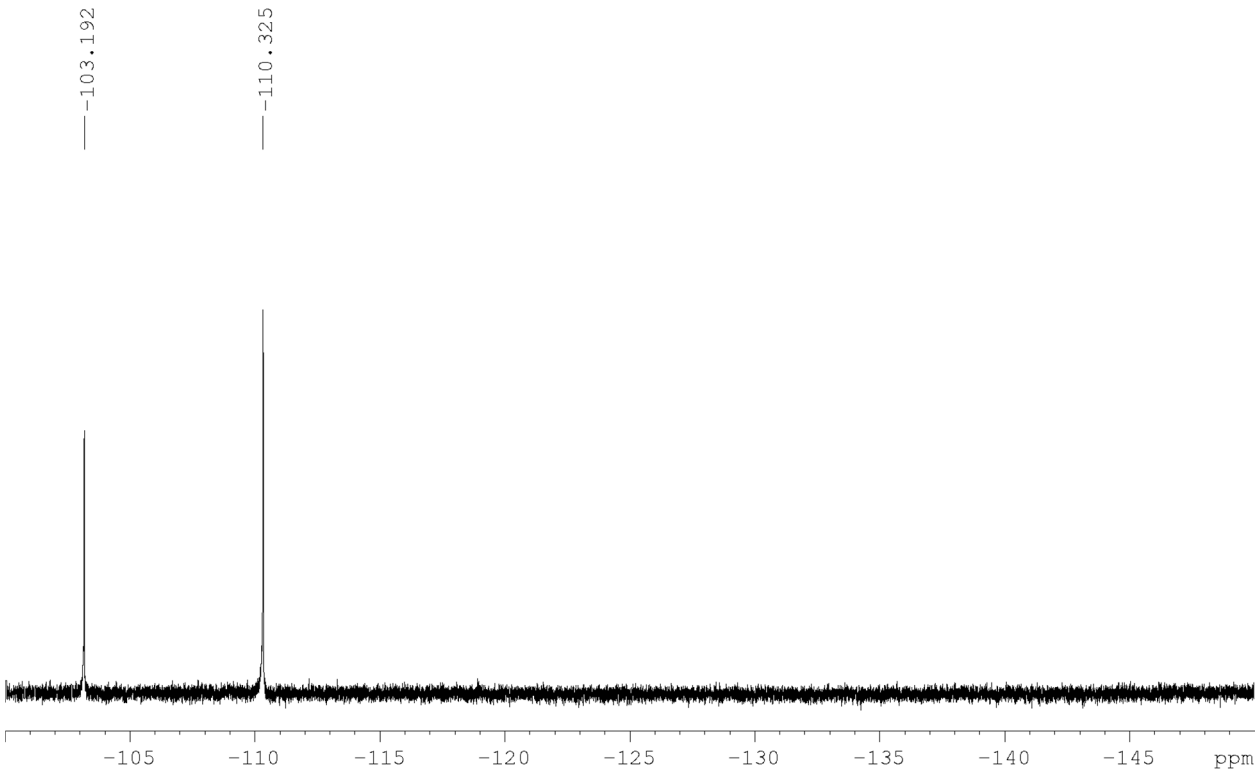

^{19}F NMR

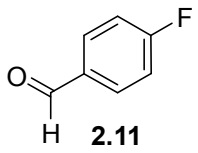

2.11

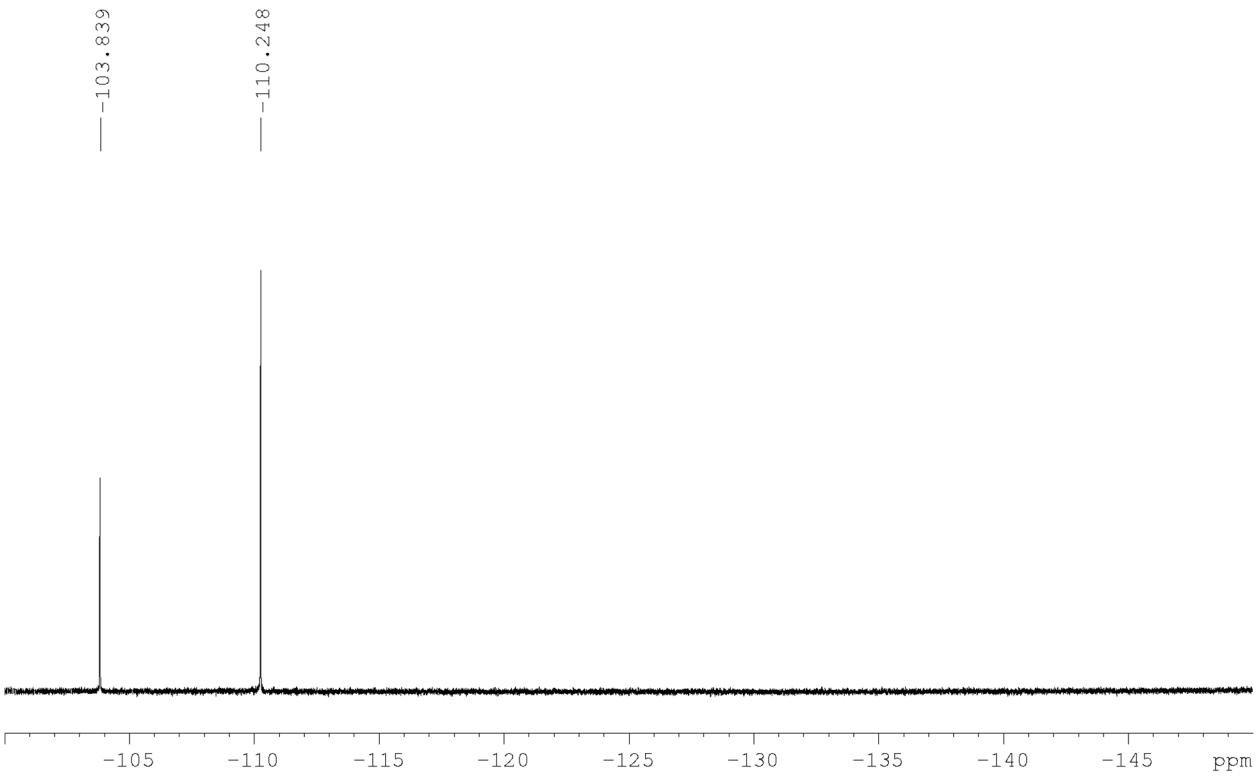

^{19}F NMR

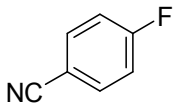

2.12

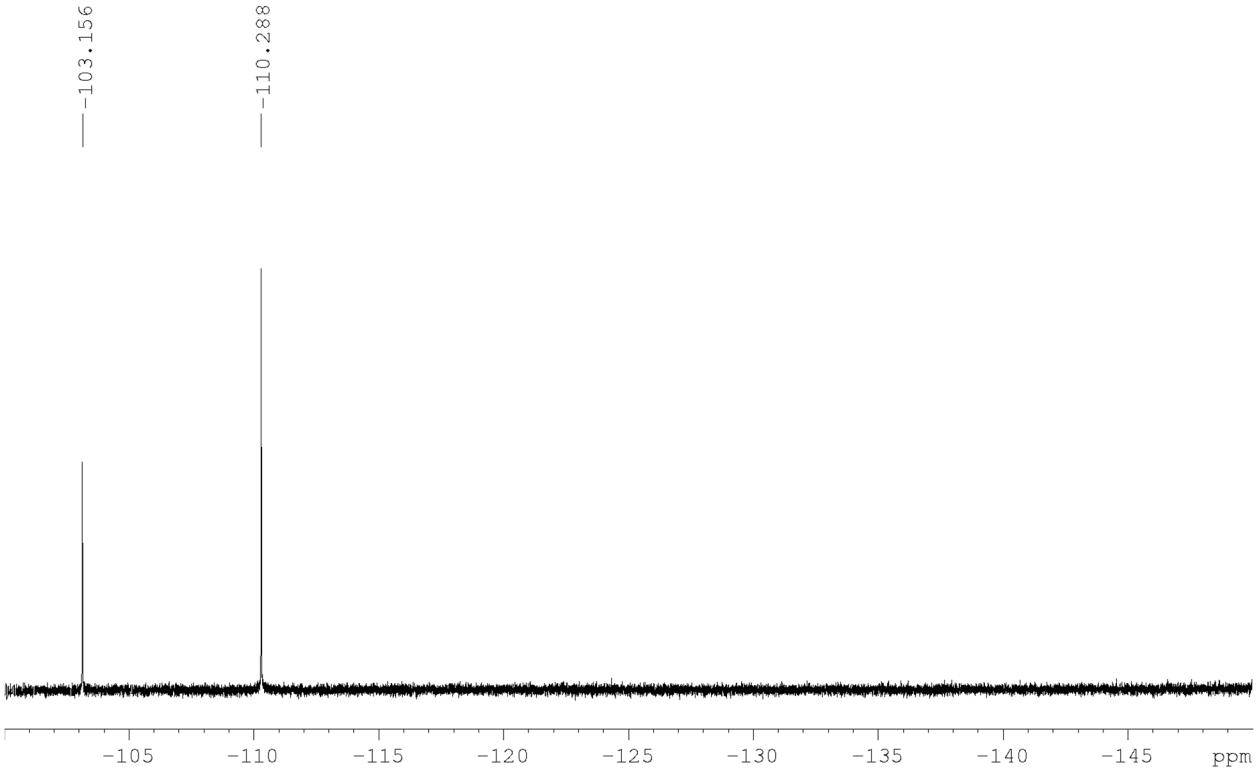

^{1}H NMR

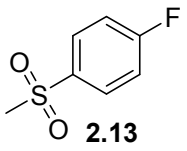
F
O
S
O
O

2.13

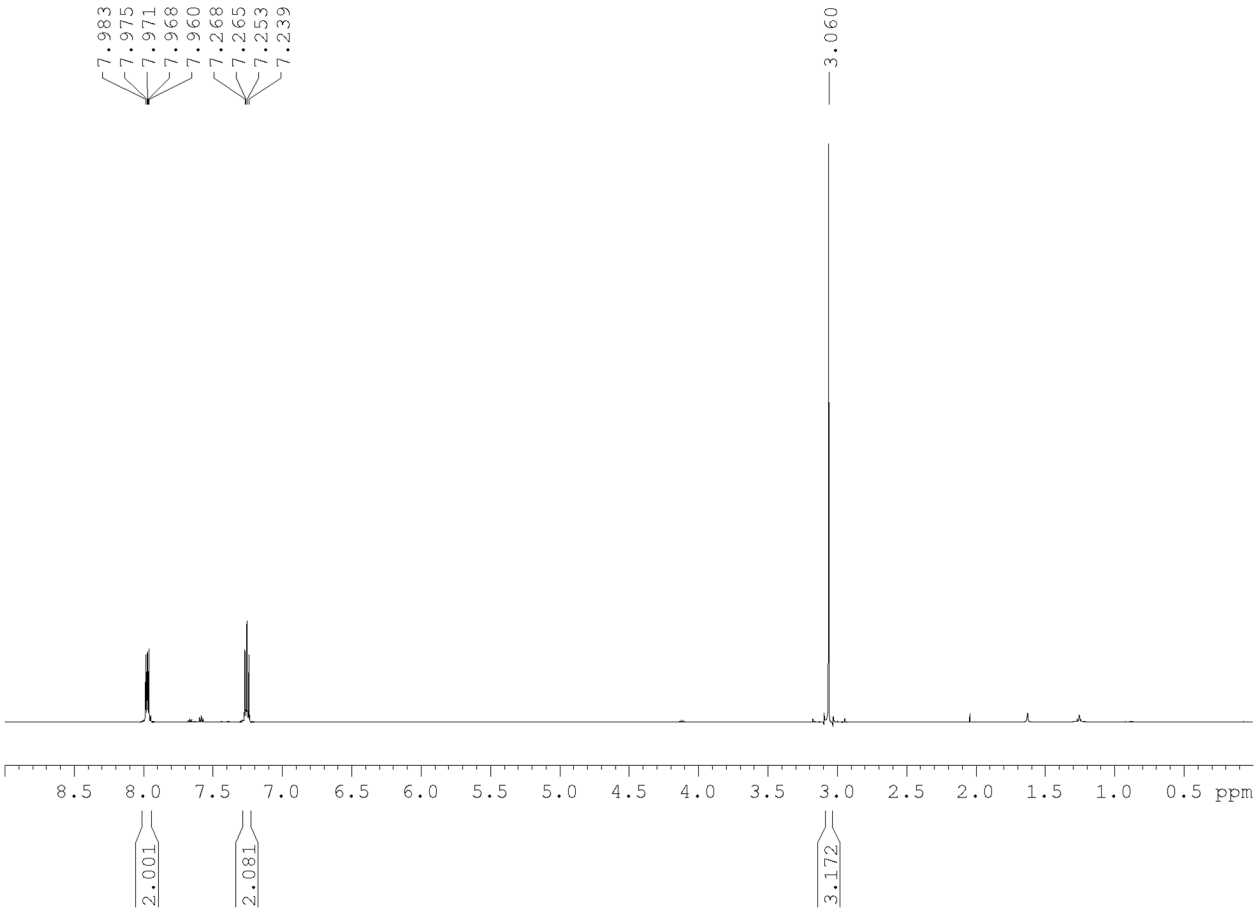
7.983
7.975
7.971
7.968
7.960
7.268
7.265
7.253
7.239
3.060
8.5
8.0
7.5
7.0
6.5
6.0
5.5
5.0
4.5
4.0
3.5
3.0
2.5
2.0
1.5
1.0
0.5 ppm
2.001
2.081
3.172

^{13}C NMR

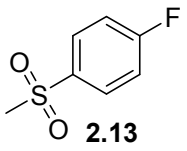
F
O
S
O
O

2.13

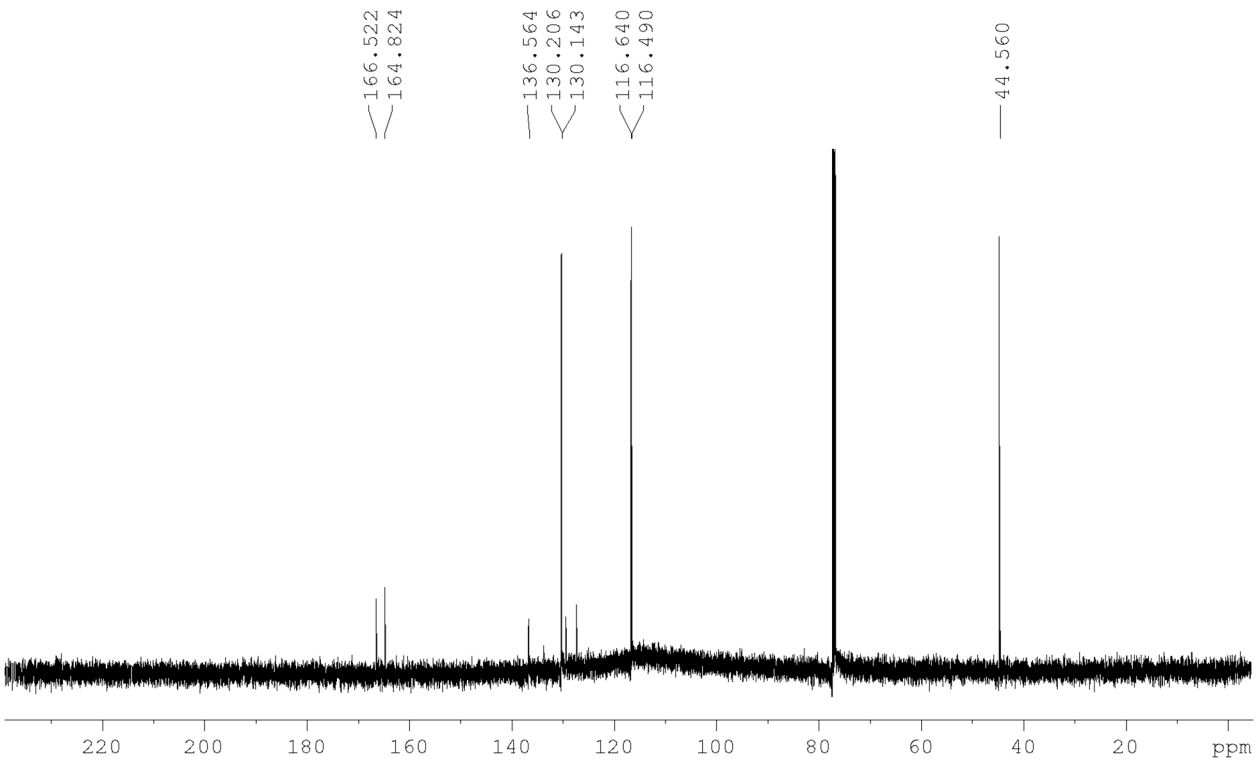
166.522
164.824
136.564
130.206
130.143
116.640
116.490
44.560
220
200
180
160
140
120
100
80
60
40
20
ppm

^{19}F NMR

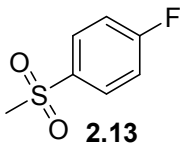

2.13

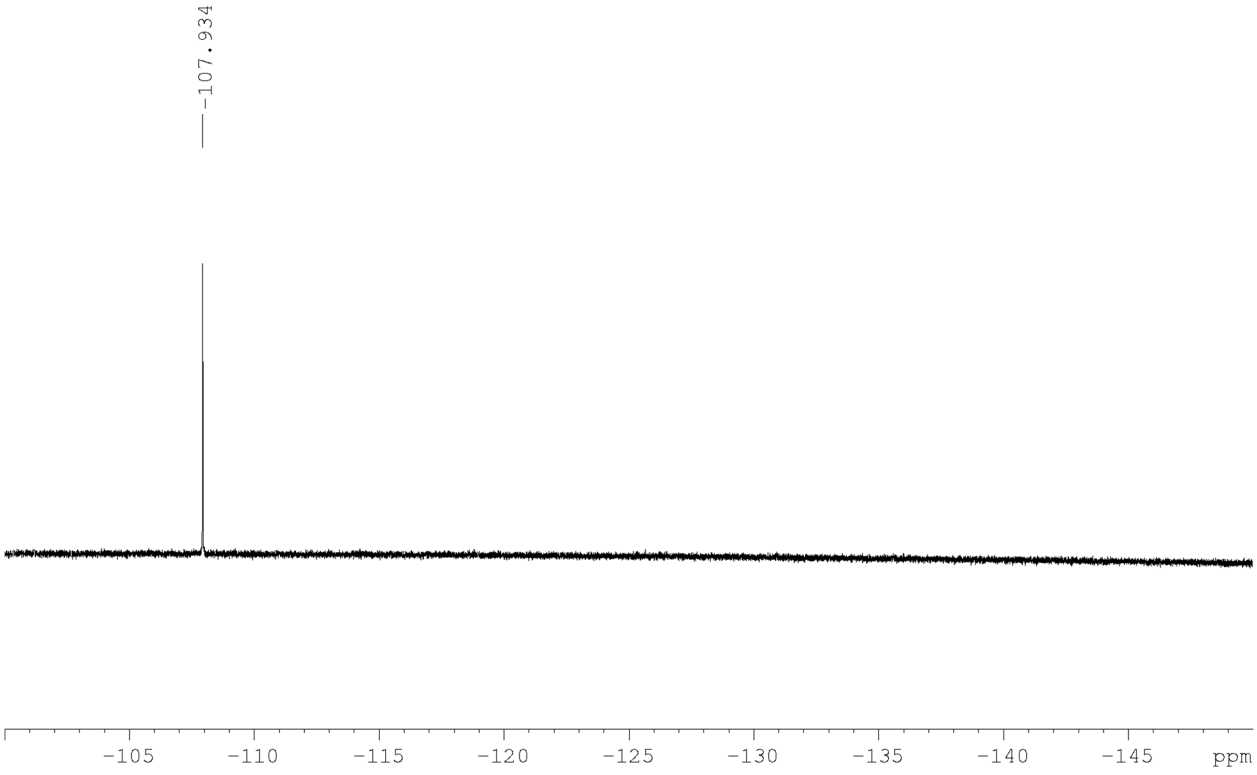

^{1}H NMR

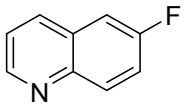
F
N

2.14

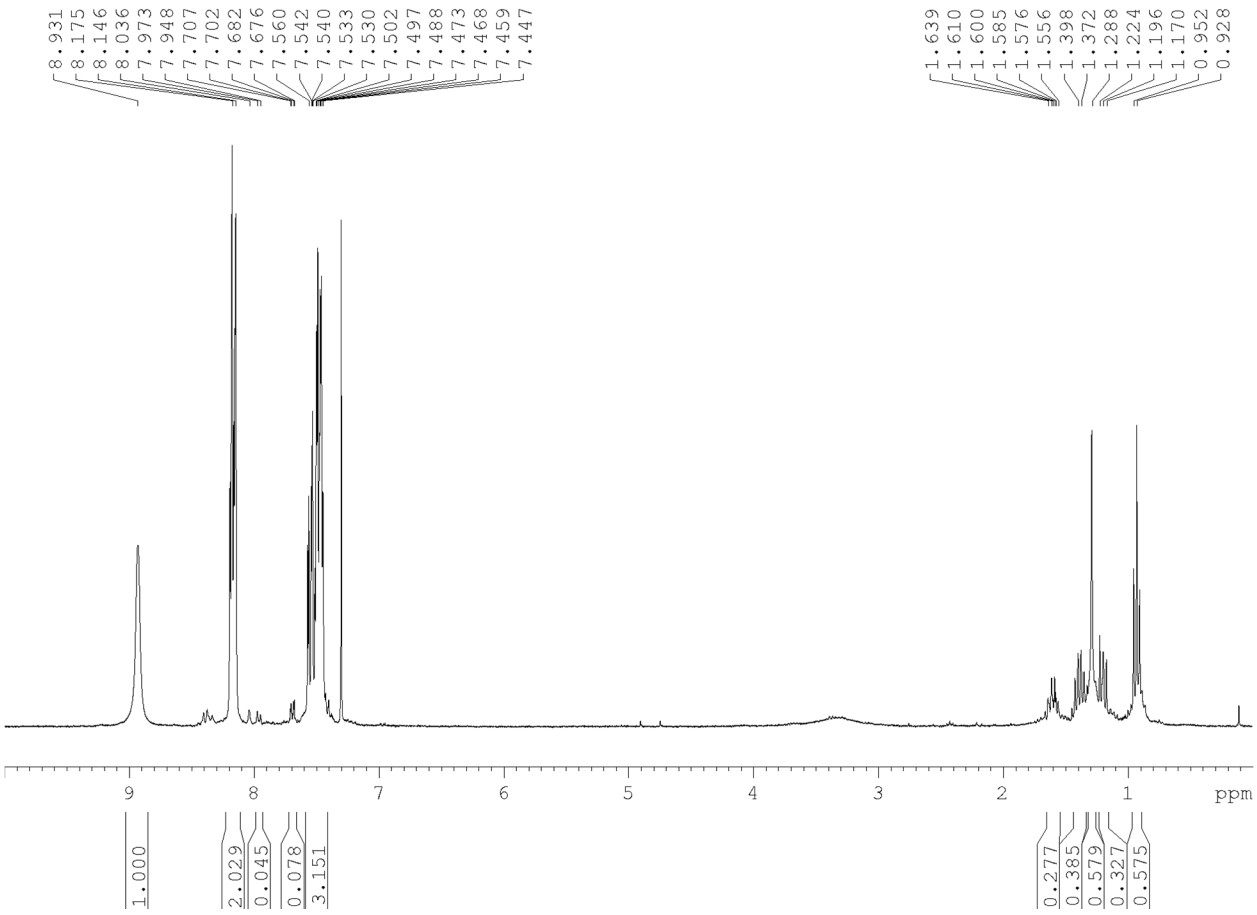
8.931
8.175
8.146
8.036
7.973
7.948
7.707
7.702
7.682
7.676
7.560
7.542
7.540
7.533
7.530
7.502
7.497
7.488
7.473
7.468
7.459
7.447
1.639
1.610
1.600
1.585
1.576
1.556
1.398
1.372
1.288
1.224
1.196
1.170
0.952
0.928
9
8
7
6
5
4
3
2
1
ppm
1.000
2.029
0.045
0.078
3.151
0.277
0.385
0.579
0.327
0.575

^{13}C NMR

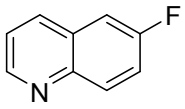
F
N

2.14

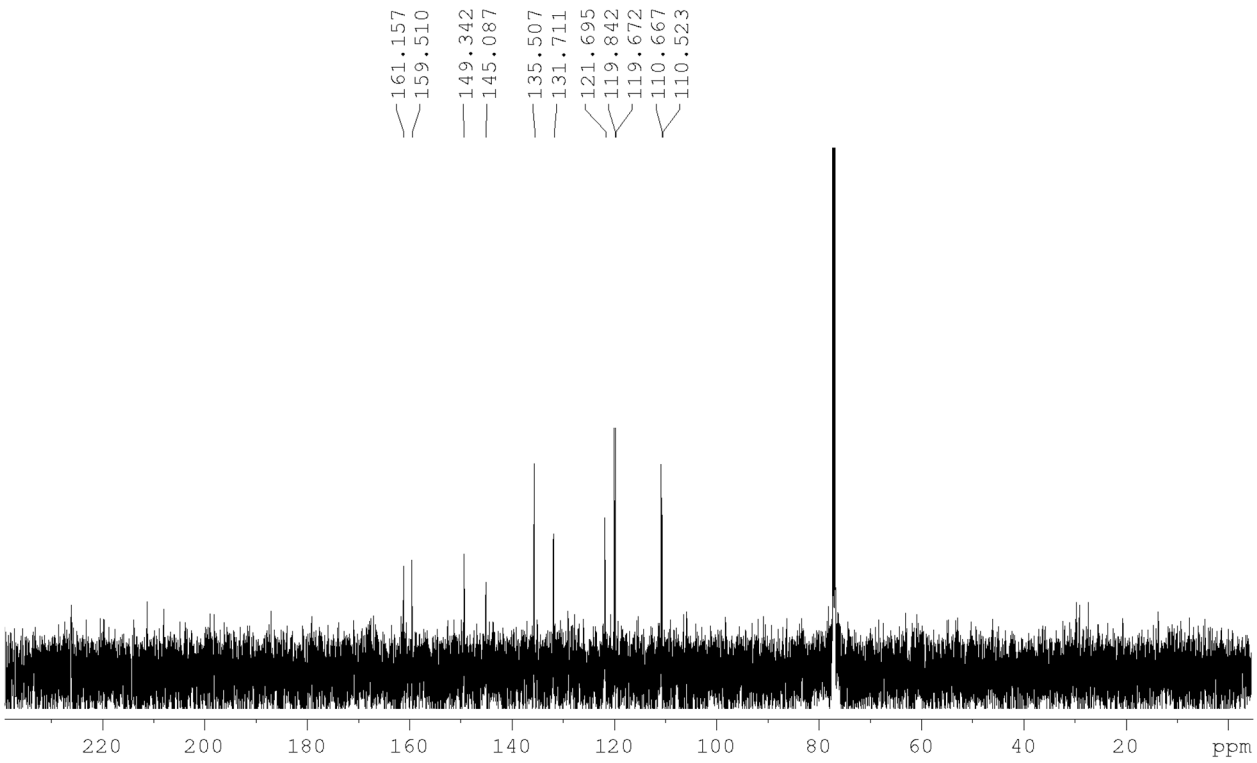
161.157
159.510
149.342
145.087
135.507
131.711
121.695
119.842
119.672
110.667
110.523
220
200
180
160
140
120
100
80
60
40
20
ppm

^{19}F NMR

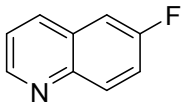

2.14

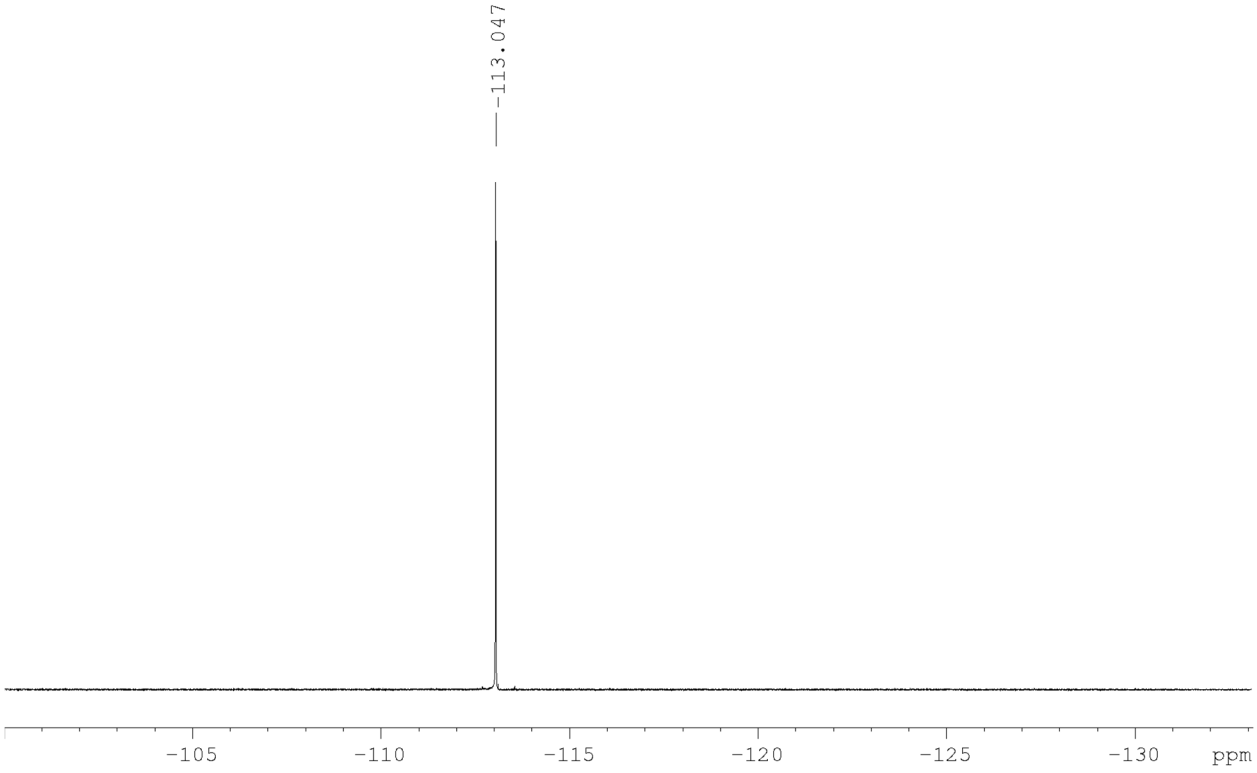

^{1}H NMR

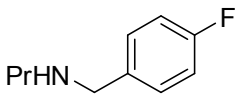
F
PrHN

2.15

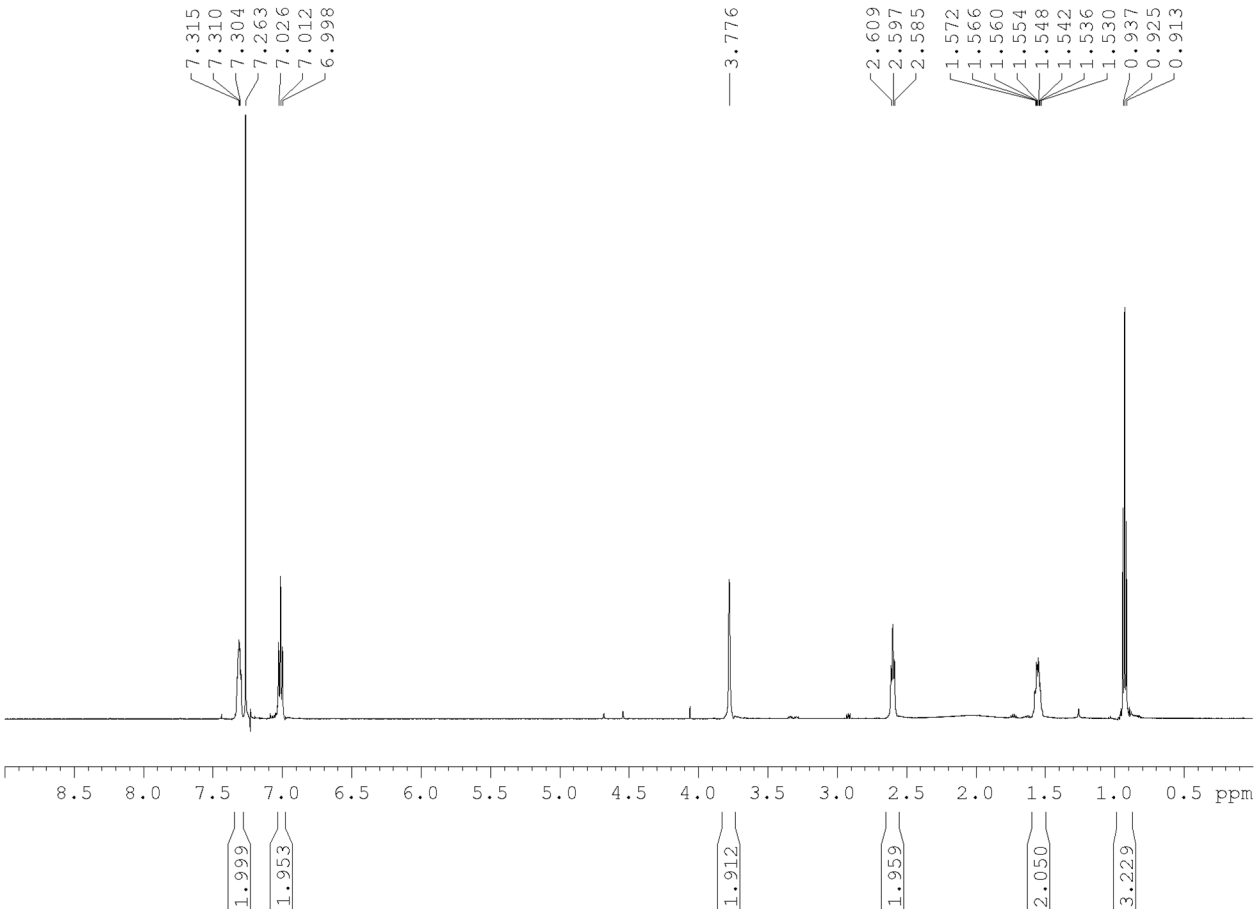
7.315
7.310
7.304
7.263
7.026
7.012
6.998
3.776
2.609
2.597
2.585
1.572
1.566
1.560
1.554
1.548
1.542
1.536
1.530
0.937
0.925
0.913
8.5 8.0 7.5 7.0 6.5 6.0 5.5 5.0 4.5 4.0 3.5 3.0 2.5 2.0 1.5 1.0 0.5 ppm
1.999
1.953
1.912
1.959
2.050
3.229

^{13}C NMR

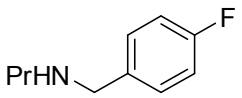
F
PrHN

2.15

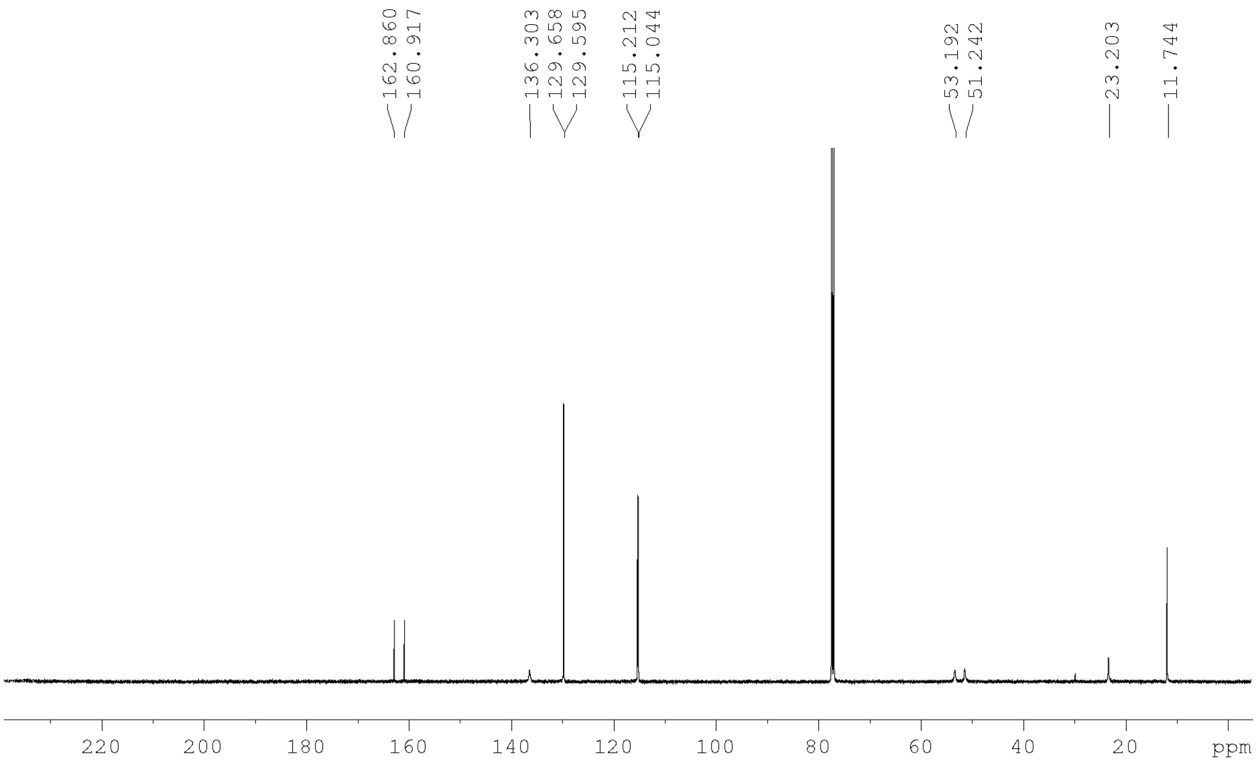
162.860
160.917
136.303
129.658
129.595
115.212
115.044
53.192
51.242
23.203
11.744
220
200
180
160
140
120
100
80
60
40
20
ppm

^{19}F NMR

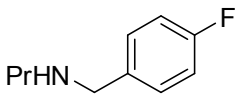

2.15

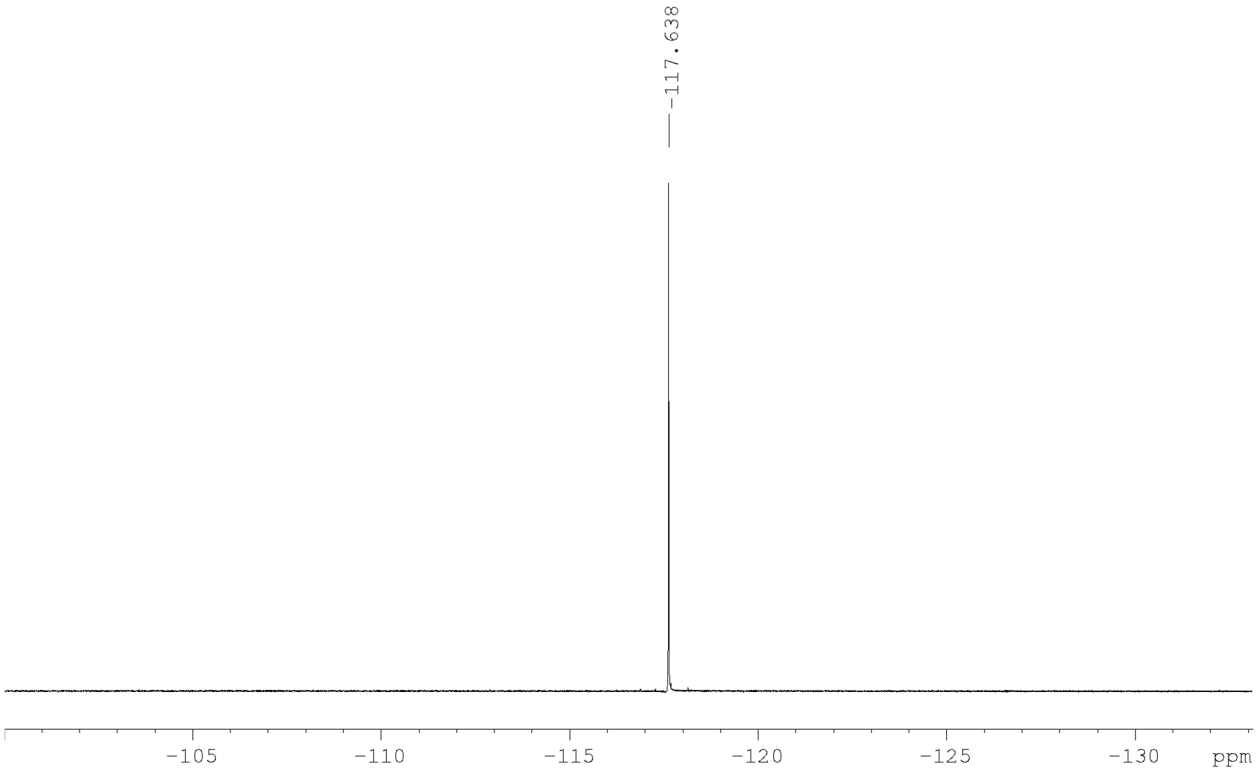

^{19}F NMR

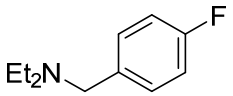

2.16

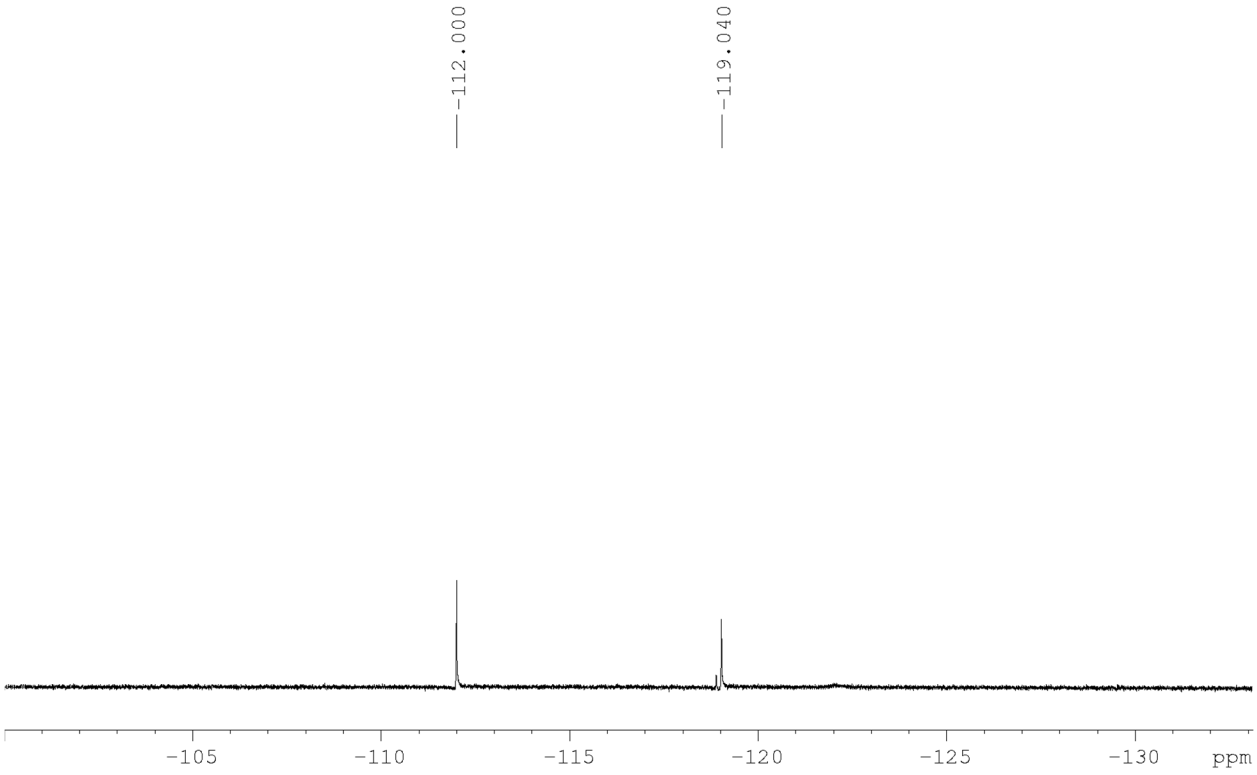

^{19}F NMR

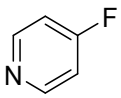

2.17

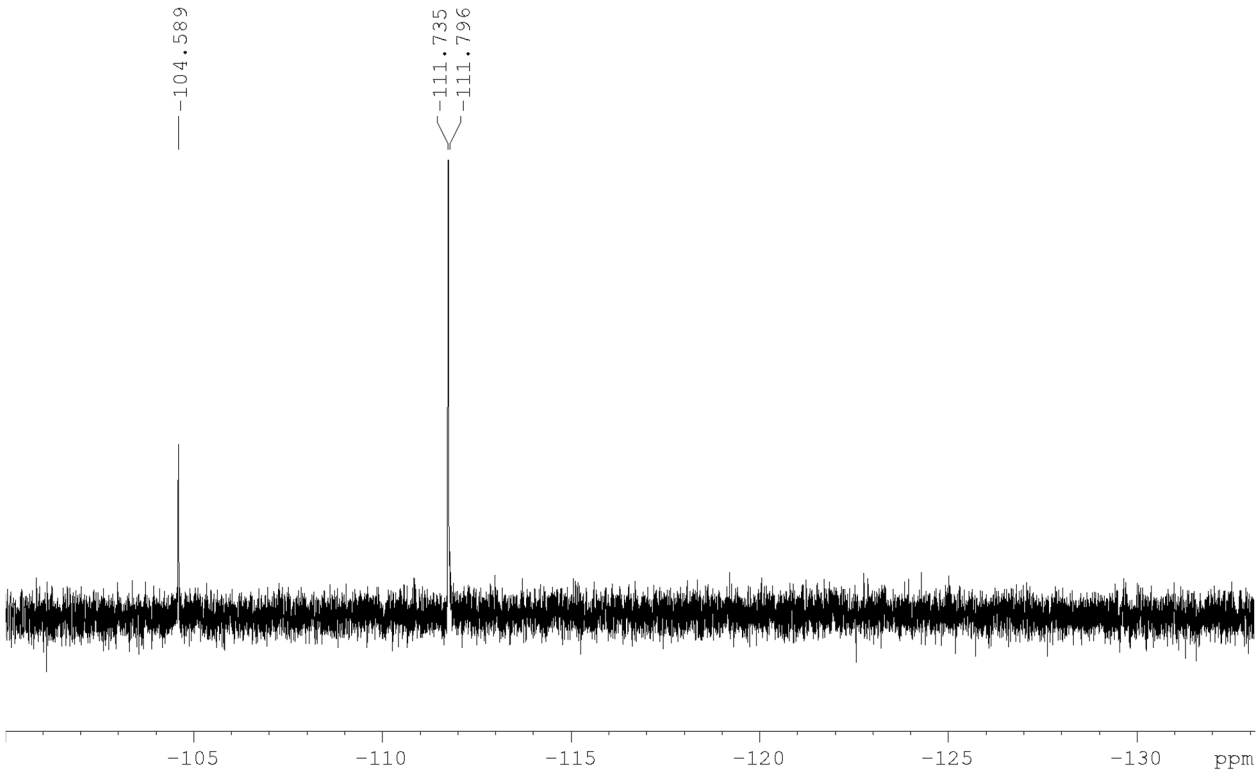

^{19}F NMR

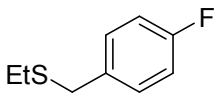

2.18

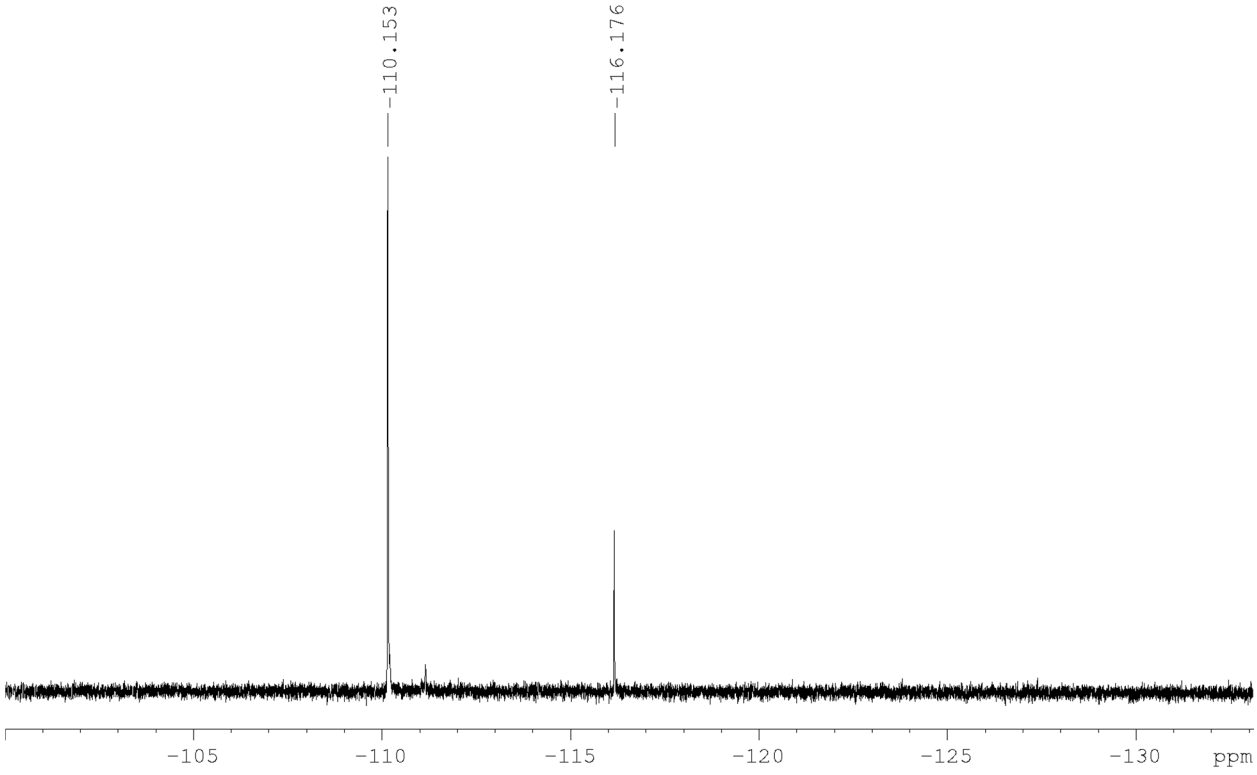

^{1}H NMR

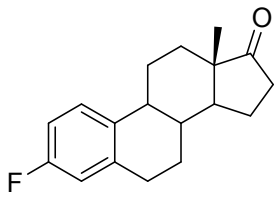
O
F

2.19

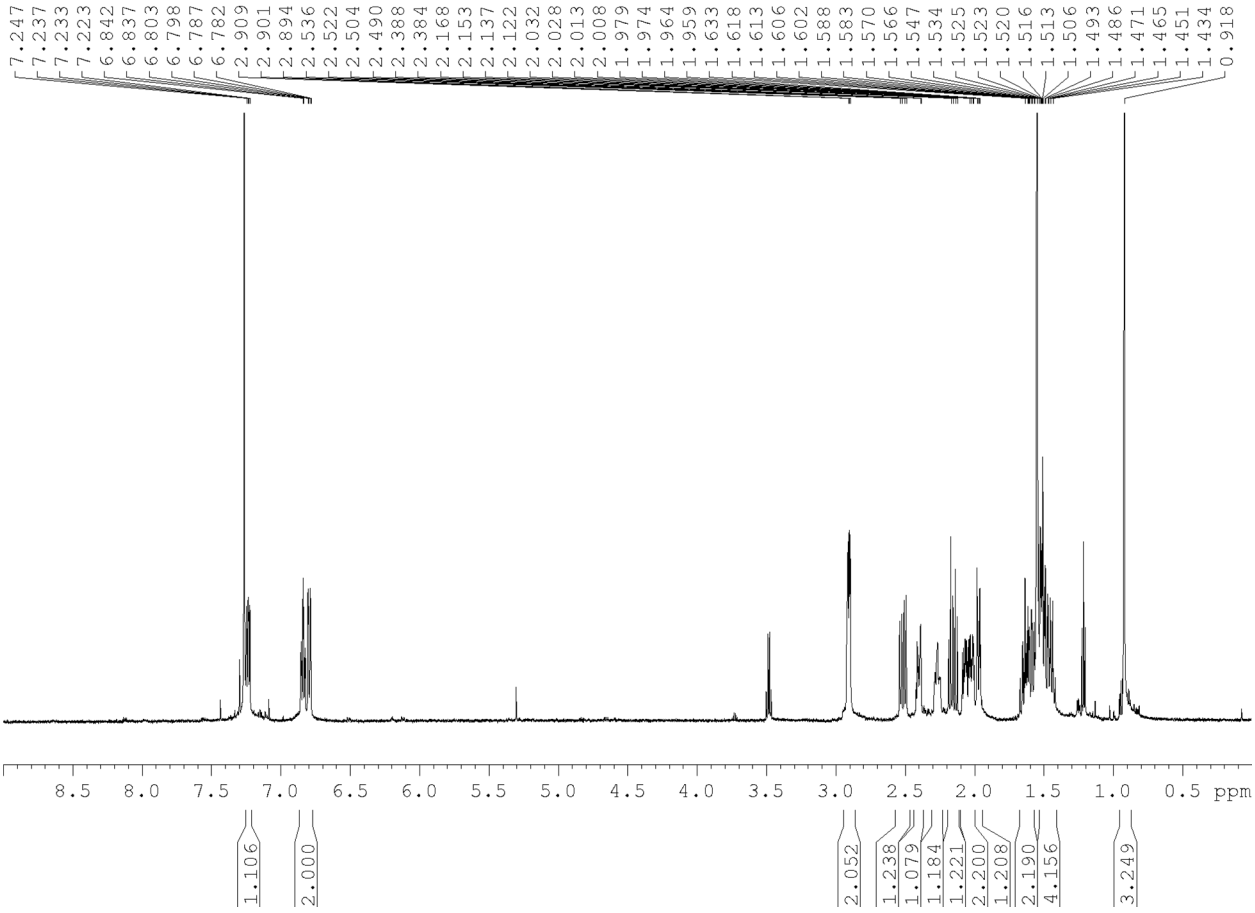
7.247
7.237
7.233
7.223
6.842
6.837
6.803
6.798
6.787
6.782
2.909
2.901
2.894
2.536
2.522
2.504
2.490
2.388
2.384
2.168
2.153
2.137
2.122
2.032
2.028
2.013
2.008
1.979
1.974
1.964
1.959
1.633
1.618
1.613
1.606
1.602
1.588
1.583
1.570
1.566
1.547
1.534
1.525
1.523
1.520
1.516
1.513
1.506
1.493
1.486
1.471
1.465
1.451
1.434
0.918
8.5 8.0 7.5 7.0 6.5 6.0 5.5 5.0 4.5 4.0 3.5 3.0 2.5 2.0 1.5 1.0 0.5 ppm
1.106
2.000
2.052
1.238
1.079
1.184
1.221
2.200
1.208
2.190
4.156
3.249

^{13}C NMR

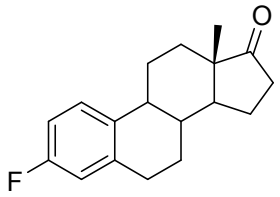
O
F

2.19

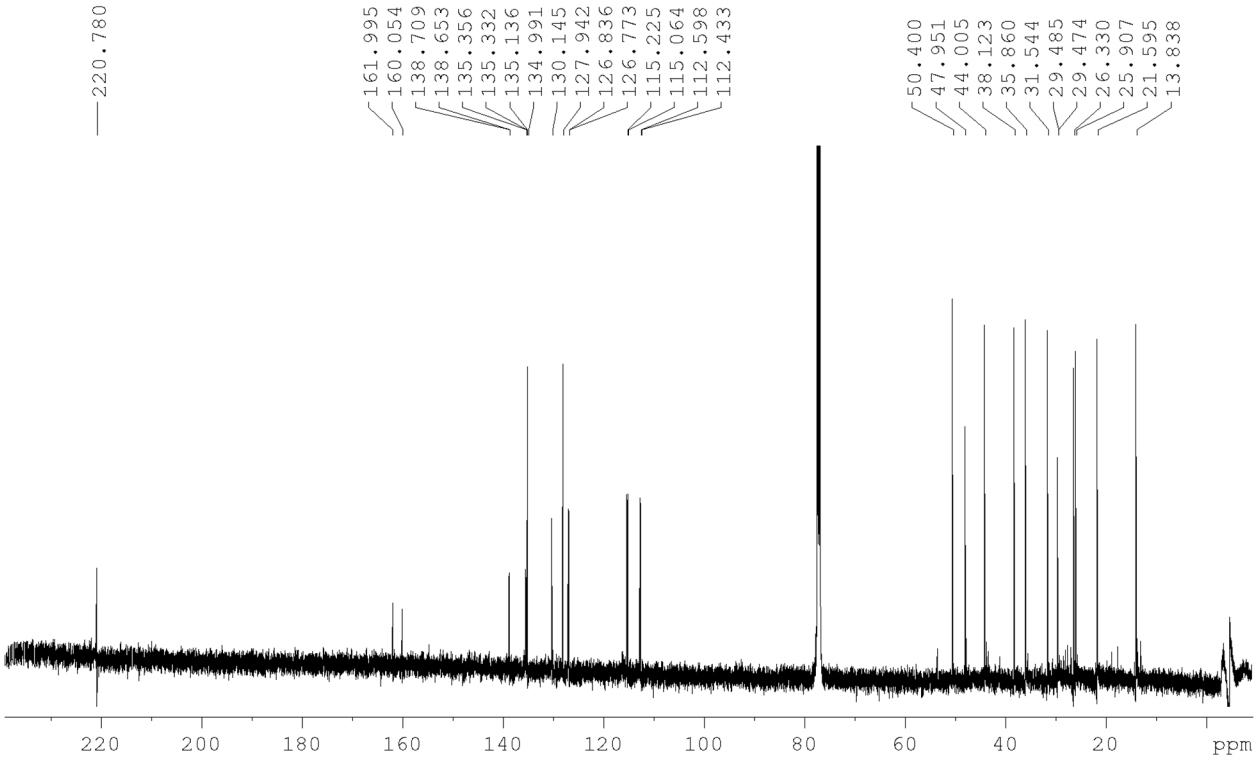
220.780
161.995
160.054
138.709
138.653
135.356
135.332
135.136
134.991
130.145
127.942
126.836
126.773
115.225
115.064
112.598
112.433
50.400
47.951
44.005
38.123
35.860
31.544
29.485
29.474
26.330
25.907
21.595
13.838
220
200
180
160
140
120
100
80
60
40
20
ppm

^{19}F NMR

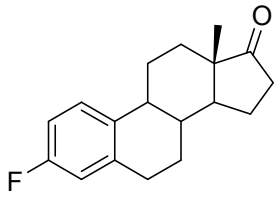

2.19

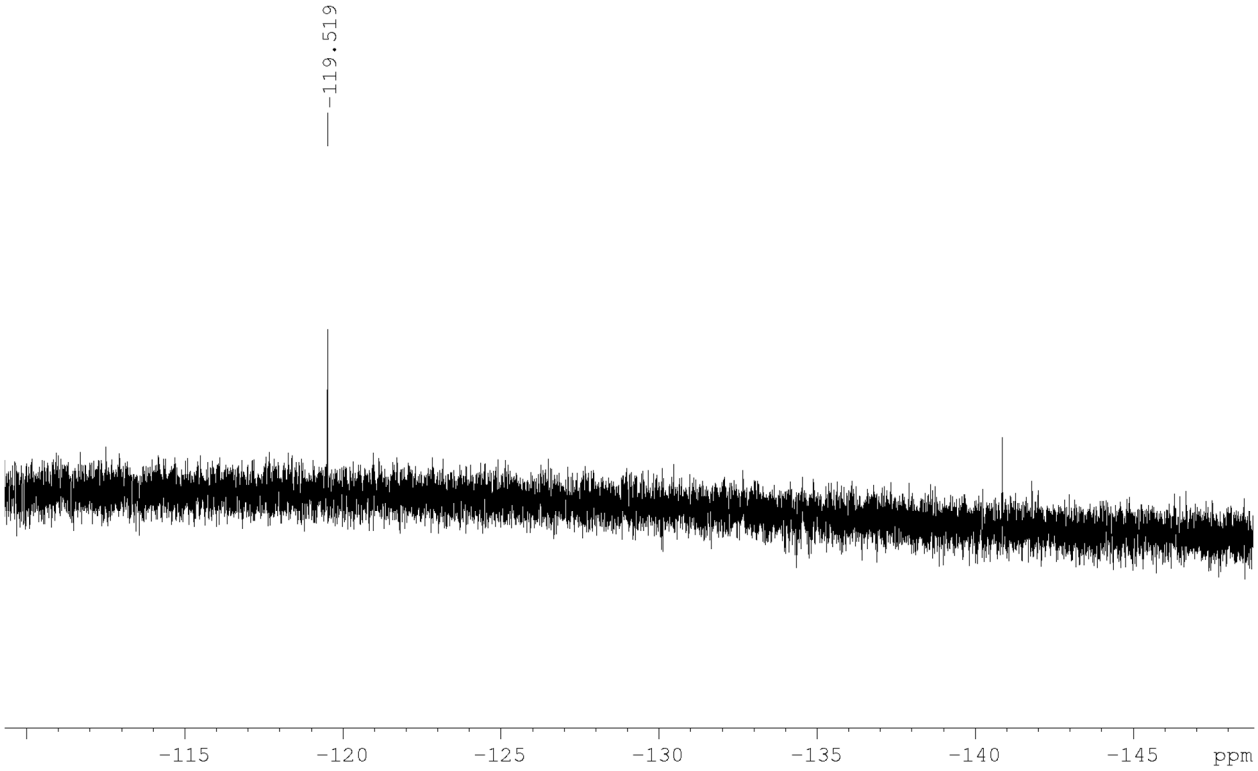

2.10 Notes and References

(1) Furuya, T.; Klein, J. E. M. N.; Ritter, T. *Synthesis* **2010,** *2010*, 1804-1821.

(2) Liang, T.; Neumann, C. N.; Ritter, T. *Angew. Chem. Int. Ed.* **2013,** *52*, 8214-8264.

(3) Campbell, M. G.; Ritter, T. *Chem Rev.* **2015,** *115*, 612-633.

(4) Brown, J. M.; Gouverneur, V. *Angew. Chem. Int. Ed.* **2009,** *48*, 8610-8614.

(5) Furuya, T.; Kamlet, A. S.; Ritter, T. *Nature* **2011,** *473*, 470-477.

(6) Hollingworth, C.; Gouverneur, V. *Chem. Commun.* **2012,** *48*, 2929-2942.

(7) Yandulov, D. V.; Tran, N. T. *J. Am. Chem. Soc.* **2007,** *129*, 1342-1358.

(8) Watson, D. A.; Su, M.; Teverovskiy, G.; Zhang, Y.; García-Fortanet, J.; Kinzel, T.; Buchwald, S. L. *Science* **2009,** *325*, 1661-1664.

(9) Hull, K. L.; Anani, W. Q.; Sanford, M. S. *J. Am. Chem. Soc.* **2006,** *128*, 7134-7135.

(10) Furuya, T.; Kaiser, H. M.; Ritter, T. *Angew. Chem. Int. Ed.* **2008,** *47*, 5993-5996.

(11) Wang, X.; Mei, T.-S.; Yu, J.-Q. *J. Am. Chem. Soc.* **2009,** *131*, 7520-7521.

(12) Mazzotti, A. R.; Campbell, M. G.; Tang, P.; Murphy, J. M.; Ritter, T. *J. Am. Chem. Soc.* **2013,** *135*, 14012-14015.

(13) Lee, H. G.; Milner, P. J.; Buchwald, S. L. *Org. Lett.* **2013,** *15*, 5602-5605.

(14) Lee, H. G.; Milner, P. J.; Buchwald, S. L. *J. Am. Chem. Soc.* **2014,** *136*, 3792-3795.

(15) Furuya, T.; Ritter, T. *Org. Lett.* **2009,** *11*, 2860-2863.

(16) Furuya, T.; Strom, A. E.; Ritter, T. *J. Am. Chem. Soc.* **2009,** *131*, 1662-1663.

(17) Tang, P.; Furuya, T.; Ritter, T. *J. Am. Chem. Soc.* **2010,** *132*, 12150-12154.

(18) Tang, P.; Ritter, T. *Tetrahedron* **2011,** *67*, 4449-4454.

(19) Fier, P. S.; Hartwig, J. F. *Science* **2013,** *342*, 956-960.

(20) Casitas, A.; Canta, M.; Solà, M.; Costas, M.; Ribas, X. *J. Am. Chem. Soc.* **2011,** *133*, 19386-19392.

(21) Yao, B.; Wang, Z.-L.; Zhang, H.; Wang, D.-X.; Zhao, L.; Wang, M.-X. *J. Org. Chem.* **2012,** *77*, 3336-3340.

(22) Fier, P. S.; Hartwig, J. F. *J. Am. Chem. Soc.* **2012,** *134*, 10795-10798.

(23) Ichiishi, N.; Canty, A. J.; Yates, B. F.; Sanford, M. S. *Org. Lett.* **2013,** *15*, 5134-5137.

(24) Fier, P. S.; Luo, J.; Hartwig, J. F. *J. Am. Chem. Soc.* **2013,** *135*, 2552-2559.

(25) Ye, Y.; Sanford, M. S. *J. Am. Chem. Soc.* **2013,** *135*, 4648-4651.

(26) Ye, Y.; Schimler, S. D.; Hanley, P. S.; Sanford, M. S. *J. Am. Chem. Soc.* **2013,** *135*, 16292-16295.

(27) Mu, X.; Zhang, H.; Chen, P.; Liu, G. *Chem. Sci.* **2014,** *5*, 275-280.

(28) Lee, E.; Hooker, J. M.; Ritter, T. *J. Am. Chem. Soc.* **2012,** *134*, 17456-17458.

(29) Tredwell, M.; Gouverneur, V. *Angew. Chem. Int. Ed.* **2012,** *51*, 11426-11437.

(30) Tian, T.; Zhong, W.-H.; Meng, S.; Meng, X.-B.; Li, Z.-J. *J. Org. Chem.* **2013,** *78*, 728-732.

(31) Bienvenu, A.; Barthelemy, A.; Boichut, S.; Marquet, B.; Billard, T.; Langlois, B. R. *Collect. Czech. Chem. Commun.* **2002,** *67*, 1467-1478.

(32) Truong, T.; Klimovica, K.; Daugulis, O. *J. Am. Chem. Soc.* **2013,** *135*, 9342-9345.

(33) Hoover, A. J.; Lazari, M.; Ren, H.; Narayanam, M. K.; Murphy, J. M.; van Dam, R. M.; Hooker, J. M.; Ritter, T. *J. Am. Chem. Soc.* **2015**.

(34) During our studies of this chemistry two methods involving copper-mediated C-^{18}F bonds from aryl boron reagents were reported. See: (a) Tredwell, M.; Preshlock, S.M.; Taylor, N.J.; Gruber, S.; Huiban, M.; Passchier, J.; Mercier, J.; Genicot, C.; Gourverneur, V. *Angew. Chem. Int.*

Ed. **2014**, *53*, 7751. (b) Mossine, A.V.; Brooks, A.F.; Makaravage, K.J.; Miller J.M.; Ichiishi, N.; Sanford, M.S.; Scott, P. J. H. *Org. Lett.* **2015**, *17*, 5780.

(35) Mu, X.; Liu, G. *Org. Chem. Front.* **2014,** *1*, 430-433.

(36) Kim, A.; Powers, J. D.; Toczko, J. F. *J. Org. Chem.* **2006,** *71*, 2170-2172.

(37) Kosugi, M.; Shimizu, K.; Ohtani, A.; Migita, T. *Chem. Lett.* **1981,** *10*, 829-830.

CHAPTER THREE

Readily Accessible Ambiphilic Cyclopentadienes for Bioorthogonal Labeling

Brian J. Levandowski[†], Raymond F. Gamache[†], Jennifer M. Murphy*, and K. N. Houk*

J. Am. Chem. Soc. **2018***, 140,* 6426 – 6431.

3.1 Abstract

A new class of bioorthogonal reagents based on the cyclopentadiene scaffold is described. The diene 6,7,8,9-tetrachloro-1,4-dioxospiro[4,4]nona-6,8-diene (TCK) is ambiphilic and self-orthogonal with remarkable stability in physiological environments. The diene reacts rapidly with a *trans*-cyclooctene and an *endo*-bicyclononyne, but slowly with dibenzoazacyclooctyne (DIBAC), allowing for tandem labeling studies with a mutually orthogonal azide, which reacts rapidly with DIBAC. TCK analogs are synthesized in three steps from inexpensive, commercially available starting materials.

3.2 Introduction

Bioorthogonal reactions enable the study of biomolecules in living systems for the elucidation of biological processes.[1] The strain-promoted 3+2 azide-alkyne cycloaddition (SPAAC) developed by Bertozzi,[2] and the inverse-electron demand tetrazine *trans*-cyclooctene Diels-Alder reaction introduced by Fox[3] are bioorthogonal cycloadditions that have been utilized to study complex interactions within biological settings. These reactions take place rapidly and selectively under physiological conditions while avoiding reactions with nucleophiles present in cellular systems.

Research focused on improving the reactivity of the SPAAC and the inverse-electron demand Diels-Alder (IED-DA) reactions has mostly centered around modifications of the two-π-electron (dienophile or dipolarophile) component. Scheme 3.1 shows the reactivity of benzyl azide (**3.1**) with some of the cyclooctynes developed for bioorthogonal applications. The introduction of a propargylic fluoride (MOFO)[4] on the cyclooctyne scaffold doubles the reactivity of the cyclooctyne, while incorporation of a second electron deficient fluorine atom at the propargylic position (DIFO)[5] results in a 30-fold increase in reactivity. Negative hyperconjugation involving the $\sigma^*_{C\text{-}F}$ stabilizes the transition state.[6,7]

Theoretical work by the Alabugin group guided the design of SNO-OCTs (sulfur, nitrogen, and oxygen containing heterocyclic cyclooctynes) where the propargylic heteroatom is endocyclic and antiperiplanar to the alkyne π-bond to maximize the stabilizing effect of the π-σ* hyperconjugative interaction.[8,9] Tomooka and coworkers synthesized several SNO-OCTs and confirmed that the rate enhancement associated with an endocyclic propargyl heteroatom exceeds that of exocyclic propargyl substitution.[8] The hyperconjugative interaction involving the endocyclic heteroatom in SNO-OCTS is stronger because it is antiperiplanar to the reactive π-bond, while the heteroatoms in MOFO and DIFO are gauche.[8] While modulating the electronic properties of the cycloalkyne has improved reactivity, the most reactive cyclooctynes are highly strained multi-cyclic cyclooctynes such as dibenzocyclooctyne (DIBO),[10] biarylazacyclooctynone (BARAC)[11], dibenzoazacyclooctyne (DIBAC)[12] and *endo* 9-hydroxymethylbicyclo[6.1.0]nonyne (BCN).[13] Optimization of the azide cyclooctyne cycloaddition has led to rate constants that have leveled off near 1 M^{-1} s^{-1}. For more rapid rate constants, the tetrazine ligation can be used.[3]

Scheme 3.1. Cyclooctynes and second order-rate constants (M^{-1} s^{-1}) for reactions with benzyl azide (**3.1**). Reaction rates were measured in acetonitrile (CD_3CN)[a], methanol (CD_3OD)[b], or 3:1 CD_3CN/D_2O[c] at ambient temperature.

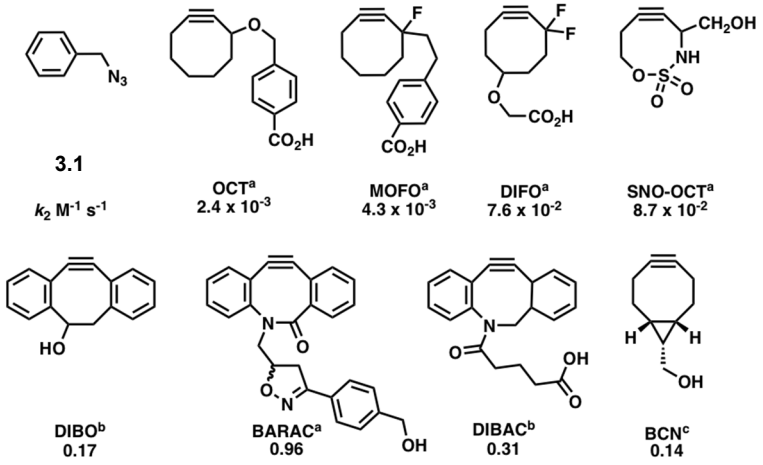

Tetrazines are electron-deficient, highly reactive dienes that undergo IED-DA reactions with strained dienophiles to label biomolecules of interest.[14,15] The rate constants for IED-DA reactions of 3,6-di-2-pyridyl-1,2,4,5-tetrazine (**3.2**) with a series of dienophiles are shown in Scheme 3.2. In the IED-DA reaction, the low-lying LUMO of the highly electrophilic tetrazine interacts with the HOMO of the nucleophilic and strained dienophile. Dienophiles with higher lying HOMOs are more reactive towards tetrazines. For example, *trans*-cyclooctene has a higher HOMO energy than cyclooctyne and is more reactive.[16] An interesting exception is in the series of cycloalkenes. From cyclopropene to cyclohexene the reactivity diminishes despite the increasing HOMO energies in the series.[14,15,17] Recent analyses by our group and the Bickelhaupt group showed that differences in the strength of the secondary orbital interactions, which are especially strong with cyclopropene and weaken with increasing cycloalkene ring size, overcome the differences in primary orbital interactions.[18,19]

The tetrazine-*trans*-cyclooctene reactions are among the fastest bioorthogonal cycloadditions, with rates exceeding 10^4 M^{-1} s^{-1}.[3] Cyclooctynes,[16] norbornenes,[20] and cyclopropenes[21,22] have been paired with tetrazines when a more stable dienophile is required, but these reactions are considerably slower (Scheme 3.2). Bulky dienophiles, such as 3,3-disubstituted cyclopropenes[23] and 3,3,6,6-tetramethylthiacycloheptynes (TMTH),[24] react poorly with tetrazines. These bulky dienophiles react with azides and allow for tandem labeling studies with tetrazine-*trans*-cyclooctene reactions for multi-target imaging.[25] The use of tetrazines in bioorthogonal chemistry is hampered by their bulkiness and vulnerability to nucleophilic attack from biological nucleophiles.[26] To address these issues the Prescher group has developed bioorthogonal reactions with the less reactive 1,2,4-triazine scaffold.[27]

Scheme 3.2. Dienophiles and their second-order rate constants for reactions with 3,6-di-2-pyridyl-1,2,4,5-tetrazine (**3.2**). Reactions rates are measures in 9:1 MeOH/H_2O[a] or MeOH[b] at ambient temperature. N/R indicates no reaction.

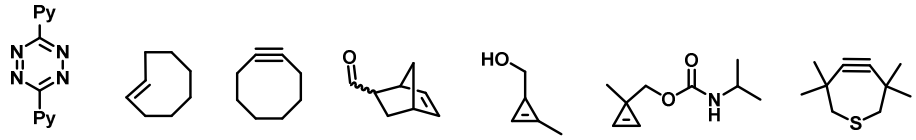

3.2	TCO[a]	CO[a]	NB[b]	1,3-CP[b]	3,3-CP	TMTH
k_2 M^{-1} s^{-1}	2.0×10^4	2.0	2.0	1.9×10^{-2}	N/R	N/R

New reactions are continually being developed that enable rapid, selective ligations to study molecules in a chemically complex environment.[28,29] Cyclopentadiene is a classic diene that was used by Diels and Alder in their seminal 1928 publication on the Diels-Alder reaction.[30] Substituted cyclopentadienes have since enjoyed much success in synthesis,[31,32] material functionalization,[33,34] bioconjugation,[35] and chemical trapping,[36,37] yet their potential in

bioorthogonal chemistry remains unexplored. We have used computational screening to probe the reactivity of cyclopentadienes with bioorthogonal 2π cycloaddends to design a cyclopentadiene-based bioorthogonal reaction. This method of screening reduces the toil of tedious large-scale reactivity screenings in the laboratory and vastly accelerates the discovery of new bioorthogonal reactions by providing a short list of promising cyclopentadiene-based bioorthogonal reactions to study experimentally.

Cyclopentadiene reacts as both a diene and a dienophile in the Diels-Alder reaction and readily dimerizes at room temperature.[38] Highly substituted cyclopentadienes, such as hexachlorocyclopentadiene, are reactive as dienes, but do not readily dimerize at room temperature.[39,40] This lack of self-reactivity is referred to as "self-orthogonal". Substituents at the 1,2 and 3,4 positions of cyclopentadiene sterically impede dimerization by clashing with the substituents at the 5-position of the cyclopentadiene. Extensive experimental and computational studies by the Schleyer group on the stability of 5-substituted cyclopentadienes demonstrate that electronegative substituents destabilize the cyclopentadiene by inducing 4π antiaromatic electron delocalization, whereas electropositive substituents stabilize the cyclopentadiene by creating 6π aromatic character.[41,42,43] Our group expanded upon Schleyer's work with a computational study that predicts that the Diels-Alder reactivity of the cyclopentadiene is tunable through substitution at the 5-position, and that electronegative substituents accelerate the reactivity.[44,45]

3.3 Identification of a Diene to be used in Bioorthogonal Diels-Alder Reactions

Sauer's pioneering studies on the synthesis and reactivity of 1,2,4,5-tetrazines with many dienophiles have been a variety of inspiration for the design of reactions in bioorthogonal chemistry.[14,15] Sauer's detailed reports on the synthesis and reactivities of substituted

cyclopentadienes, however, have gone relatively unrecognized.[39,40] The highly reactive, self-orthogonal, and ambiphilic properties of the tetrachlorocyclopentadiene ketal (TCK) shown in Figure 3.1 and described by Sauer, attracted our attention as a potential bioorthogonal diene.[39,40] TCK is stable at room temperature and requires heating to 80 °C in toluene for 11 days to form 71% yield of the TCK Diels-Alder dimer.[37] TCK is ambiphilic and reacts with both electron-deficient dienophiles such as maleic anhydride and electron-rich dienophiles such as (1*Z*,5*Z*)-cycloocta-1,5-diene.[46]

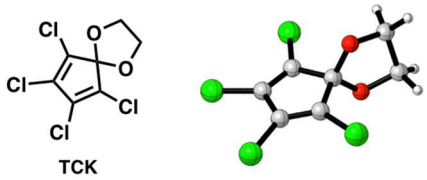

Figure 3.1. Tetrachlorocyclopentadiene ketal (TCK)

3.4 Computational Modeling of TCK with Dienophiles

We have probed computationally the bioorthogonal potential of the TCK with bioorthogonal 2π scaffolds. The M06-2X[47] functional with the 6-31G(d) basis set was used for geometry optimizations. Single point energies were calculated with the 6-311++G(d,p) basis set and solvation effects of water were included through use of the conductor-like polarizable continuum model (CPCM).[48,49] Figure 3.2 shows the computed transition state structures and activation free energies for the Diels-Alder reactions of TCK with the bioorthogonal cycloaddends of *trans*-cyclooctene (**TS-TCO**), bicyclononyne (**TS-BCN**), cyclooctyne (**TS-CO**), norbornene (**TS-NB**), 3,3-dimethylcyclopropene (**TS-3,3-CP**), and dibenzocyclooctyne (**TS-DIBO**). For the reactions of TCK with *trans*-cyclooctene, dibenzocyclooctyne, and cyclooctyne, the

computational screening reveals activation free energies of 18.1 – 20.6 kcal/mol, indicating potential as viable partners with TCK in bioorthogonal cycloadditions. By contrast, the activation free energies for the Diels-Alder reactions of TCK with norbornene, 3,3-dimethylcyclopropene, and dibenzocyclooctyne range from 23.1 – 27.7 kcal/mol, and are too high for bioorthogonal applications. These latter scaffolds are highly reactive with some 1,3-dipoles, providing an opportunity to develop mutually orthogonal cycloadditions.

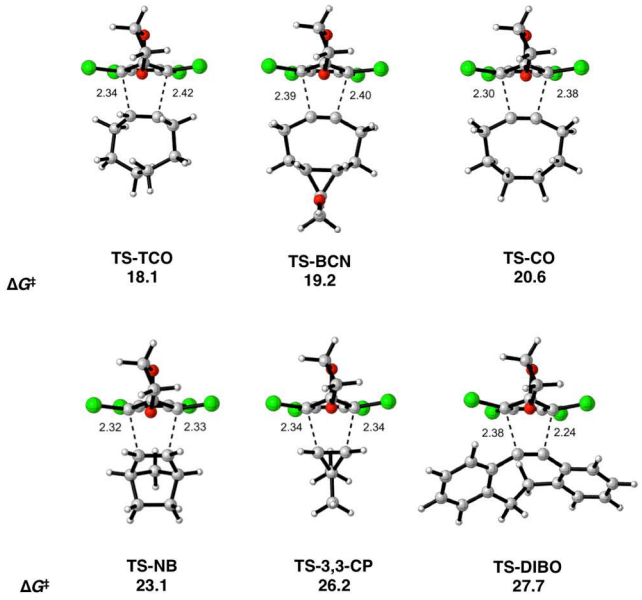

Figure 3.2. Transition state structures and activation free energies in kcal/mol for the Diels-Alder reactions of TCK with bioorthogonal cycloaddends.

3.5 Synthesis of TCK and measurement of its Second-Order Rate Constant

To test our *in-silico* predictions and evaluate the potential of TCK as a bioorthogonal reaction partner, the second-order rate constants of TCK with BCN and TCO cycloaddends were measured experimentally. We chose BCN and TCO as the cycloaddends because they were predicted to be the most reactive bioorthogonal dienophiles towards TCK from the computational

screening (Figure 3.2). TCK was prepared from commercially available hexachlorocyclopentadiene according to Chang's protocol shown in Scheme 3.3.[46] Hexachlorocyclopentadiene **3.3** was treated with potassium hydroxide (KOH) and ethylene glycol to yield TCK. TCK undergoes a rapid 4+2 cycloaddition with BCN and the axial 5-hydroxy *trans*-cyclooctene (TCO-OH) stereoisomer to give cycloadducts **3.4** and **3.5**, respectively. The reactions of TCK with BCN and TCO-OH give a mixture of two and stereoisomers, respectively.

Scheme 3.3. Synthesis of TCK and cycloaddition rates with TCO-OH and BCN.

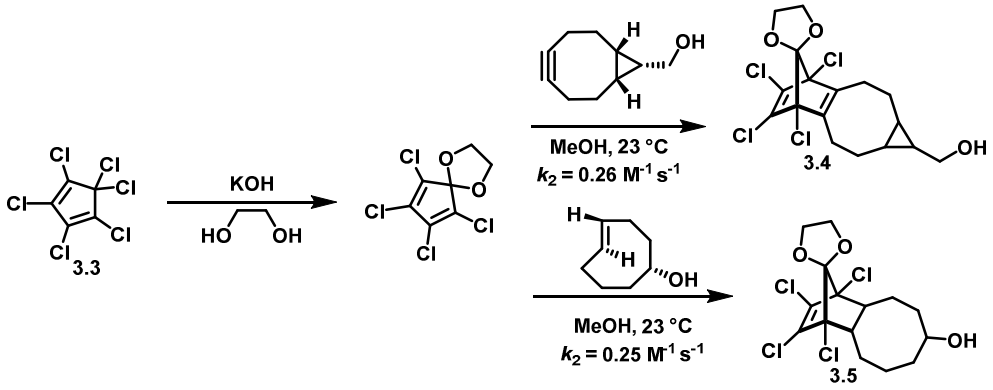

Rate constants were measured with ultraviolet visible (UV/Vis) spectroscopy by monitoring the disappearance of the TCK absorption peak under *pseudo*-first order conditions. The experimentally observed second-order rate constants for the Diels-Alder reactions of TCK with BCN and TCO-OH in methanol are 0.26 M^{-1} s^{-1} and 0.25 M^{-1} s^{-1}, respectively (Figure 3.3). These rate constants are comparable to previously reported SPAAC bioorthogonal labeling approaches shown in Scheme 3.1.

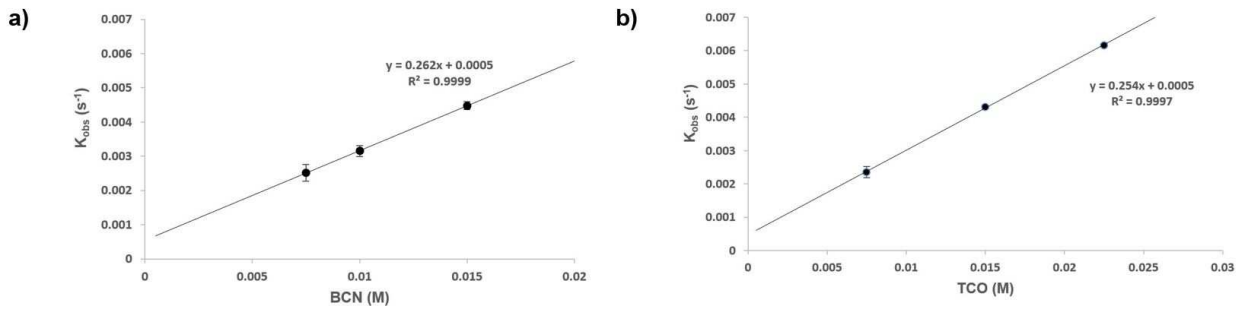

Figure 3.3. a) Plot of rate observed vs. concentration of BCN with the slope taken as the second-order rate constant. b) Plot of rate observed vs. concentration of TCO-OH with the slope taken as the second-order rate constant.

3.6 Evaluation of Potential Mutual Orthogonality

Mutually orthogonal bioorthogonal reactions allow for dual labeling studies that monitor multi-component biological processes by targeting multiple biomolecules.[22] Computational screening predicts that DIBO derivatives will react poorly with TCK. To test this prediction, TCK and DIBAC were stirred together for 20 hours at room temperature, and no cycloaddition products were observed. 1,3-dipoles such as azides react quickly with DIBAC, and poorly with TCO derivatives as shown in Scheme 3.4.[12,50] Scheme 3.4 outlines these findings and demonstrates how tandem labeling is possible with the mutually orthogonal TCK-TCO and benzyl azide-DIBAC reactions.

Scheme 3.4. Mutual orthogonality between the TCK TCO-OH and benzyl azide-DIBAC reactions.

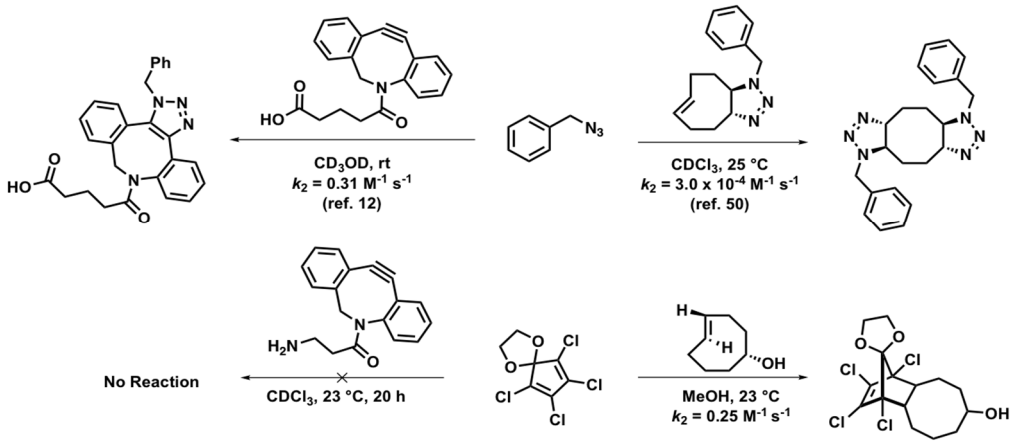

3.7 Synthesis of TCK reagent for peptide bioconjugation and fluorescence labeling

Scheme 3.5 illustrates a three-step protocol for the synthesis of a *N*-hydroxysuccinimide functionalized TCK to enable bioconjugation to primary amines. Ketalization of hexachlorocyclopentadiene **3.3** was carried out with (±)-1,2,4-butanetriol to yield the intermediate alcohol **3.6**. Oxidation to the corresponding carboxylic acid **3.7** and subsequent coupling to *N*-hydroxysuccinimide under standard conditions afforded the desired activated ester **3.8**.

Scheme 3.5. Synthesis of TCK succinimidyl ester **3.8** for bioconjugation to primary amines.

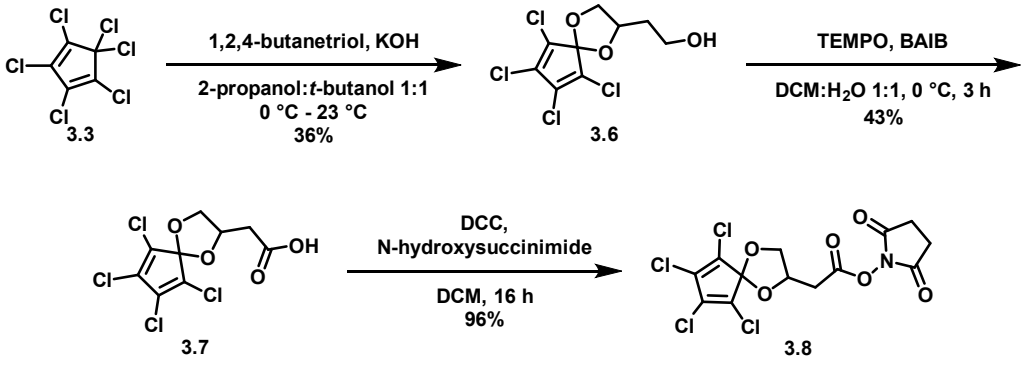

To validate the biocompatibility of the reaction, the commercial neuropeptide used to prevent neuronal damage against hypoxic or ischemic induced brain injury, [D-Ala^2, D-Leu^5]-Enkephalin, was chosen for initial labeling experiments.[51] Activated diene **3.8** was readily conjugated to [D-Ala^2, D-Leu^5]-Enkephalin via the succinimidyl ester to afford cyclopentadiene-peptide conjugate **3.9**. Peptide-conjugate **3.9** efficiently underwent the Diels-Alder cycloaddition with Cy5-TCO in ambient temperature to afford the fluorescent peptide **3.10**, as shown in Scheme 3.6.

Scheme 3.6. Bioconjugation and fluorescence labeling of [D-Ala^2, D-Leu^5]-Enkephalin.

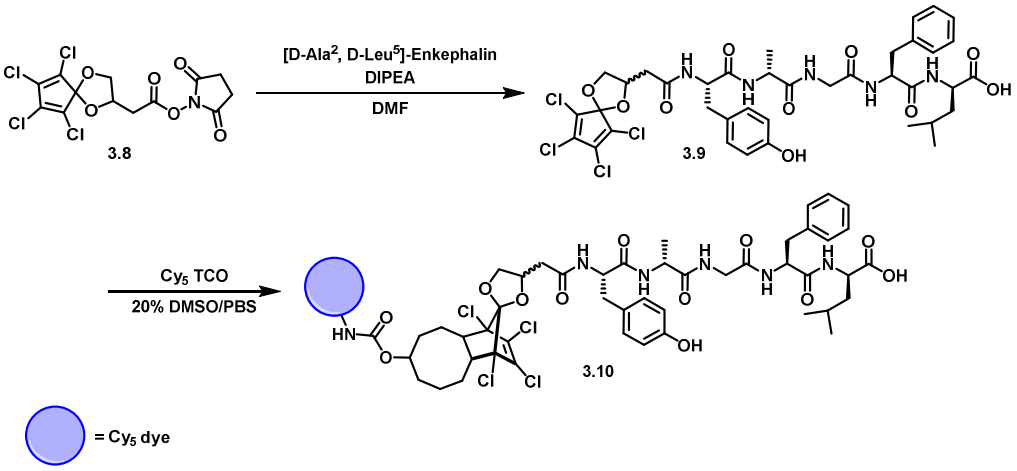

Many bioorthogonal reagents are sensitive to air or light, react with endogenous biological nucleophiles such as thiols, or are unstable as a result of strain, making prolonged labeling studies and storage difficult.[11,28,52] TCK can be stored at room temperature as a white solid with a melting point range of 64.5-65.5 °C. No decomposition or dimerization of TCK was observed by proton NMR after 63 hours of incubation at 37 °C in a 1:1 CD_3CN:D_2O mixture with cysteine. TCK displays high stability under biological conditions and is inert to the nucleophilic thiol cysteine.

3.8 Conclusion

We report TCKs as a new class of bioorthogonal reagents with reaction rates towards *endo*-BCN and TCO-OH that are practical for biological labeling studies. Proof of fluorescence peptide labeling with TCK is demonstrated using a commercial neuropeptide and the near-infrared cyanine dye, Cy5. The enduring stability of TCK is ideal for long-term applications and our computational studies suggest future tandem labeling with azide reactions is plausible. TCK is readily synthesized from inexpensive starting materials and stable at room temperature. The dynamic reactivity, accessibility, and stability found in TCK are essential for adoption as a bioorthogonal reagent.

3.9 Experimental Section

3.9.1 Materials and Methods. NMR spectra were obtained on a Bruker AV300 (300 MHz for ^{1}H; 282 MHz for ^{19}F), a Bruker AV500 (500 MHz for ^{1}H; 125 MHz for ^{13}C), and a Bruker AV600 (600 MHz for ^{1}H; 150 MHz for ^{13}C). ^{1}H and ^{13}C chemical shifts are reported in parts per million (ppm) using the solvent resonance as an internal reference. The coupling constants, *J*, are reported in Hertz (Hz), and the multiplicity are reported as follows: singlet (s), broad single (br s) doublet (d), triplet (t), quartet (q), pentet (p), and multiplet (m). High-resolution mass spectrometry data were collected with a Waters LCT Premier XE time-of-flight instrument controlled by MassLynx 4.1 software or obtained on a Thermo Scientific™ Exactive Mass Spectrometer with DART ID-CUBE. Samples were dissolved in methanol and infused using direct loop injection from a Waters Acquity UPLC into the Multi-Mode Ionization source. HPLC purifications were performed on a Knauer Smartline HPLC system with inline Knauer UV (254 nm) detector. Semi-preprative HPLC was performed using Phenomenex reverse-phase Luna column (10 × 250 mm, 5 μm) with a flow rate of 4 mL/min. Final purity of compounds was determined by analytical HPLC analysis performed with a Phenomenex reverse-phase Luna column (4.6 × 250 mm, 5 μm) with a flow rate of 1 mL/min. Compounds were identified by UV absorbance at 254 nm. All chromatograms were collected by a GinaStar (raytest USA, Inc.; Wilmington, NC, USA) analog to digital converter and GinaStar software (raytest USA, Inc.). ***Small molecule reaction kinetics***: The reaction rates between TCK **2** and dienophiles TCO and BCN were measured under *pseudo*-first order reaction conditions by using 30-100 fold excess dienophile in methanol. The exponential decay in UV absorbance of TCK **2** at 312 nm was measured over time. Spectra were recorded on a Varian Cary 5000 UV-Vis-NIR spectrometer. All the data were recorded at 23 ºC using spectral band-width (SBW) = 1.0 nm, path length = 1.0 cm with increment in data point collection at 6 seconds for 30

minutes. The observed rate constants k′ were determined by fitting each data set to a single-exponential equation. The k′ values were then plotted against the concentration of dienophile and subjected to a linear fit to yield a plot with slope k_2, the second order rate constant. Each kinetic experiment was performed in triplicate and the three k_2 values were averaged. All data was processed on excel software program. All chemicals and reagents were purchased from commercial sources and used without further purification unless noted otherwise. All deuterated solvents were purchased from Cambridge Isotope Laboratories. Anhydrous solvents were obtained by filtration through activated alumina columns unless indicated otherwise. Solvents used for extractions and chromatography were not anhydrous. Reactions and chromatography fractions were analyzed by thin-layer chromatography (TLC) using Merck precoated silica gel 60 F_{254} glass plates (250 μm) and visualized by ultraviolet irradiation, potassium permanganate stain, and phosphomolybdic acid. Flash column chromatography was performed using E. Merck silica gel 60 (230−400 mesh) with compressed air. [D-Ala^2, D-Leu^5]-Enkephalin (cas [60284-47-1]) was purchased from Bachem Americas (product H-1276) and used as received. Cy5-TCO was purchased from Click Chemistry Tools (catalog # 1089-1) and used as received. TCO was synthesized according to literature procedure.[53]

3.9.2 Computational Data

Summary of Cartesian Coordinates computed at M06-2X/6-31G(d) level of theory

TCK

C	0.00638600	-1.18447500	0.01926600
C	-1.25268200	-0.74705400	0.00799900
C	0.00719900	1.18435800	-0.01896400
C	-1.25216700	0.74780800	-0.00795000
Cl	0.58438000	-2.78522000	0.02801900
Cl	-2.68234600	-1.67607100	0.00541600
Cl	-2.68122600	1.67774200	-0.00567100

Cl	0.58643100	2.78458900	-0.02752700
C	0.97182000	-0.00041300	0.00014600
C	3.12315300	0.27030500	0.70938100
C	3.12290000	-0.27142500	-0.71002100
H	3.30376400	1.35087200	0.73164400
H	3.80934900	-0.24121500	1.38576800
H	3.80888400	0.24023100	-1.38655700
H	3.30384400	-1.35194200	-0.73231100
O	1.79337200	-0.01877100	1.13358400
O	1.79305700	0.01748900	-1.13380100

TCO

C	-0.53224900	-1.35815500	-0.40081100
C	-1.87022500	-0.90126400	0.08151300
C	-1.88196700	0.63553400	-0.13569700
H	-1.98078300	-1.11334900	1.15197400
H	-2.71623500	-1.35797100	-0.44330800
C	-0.65044300	1.37601600	0.43040100
H	-2.79100800	1.04829500	0.31867100
H	-1.95633400	0.84166400	-1.21190400
C	0.65044300	1.37600200	-0.43044600
H	-0.42983000	0.98435200	1.43211900
H	-0.95046800	2.41874600	0.58489100
C	1.88196700	0.63553900	0.13567700
H	0.95046800	2.41872700	-0.58497000
H	0.42983000	0.98430500	-1.43215100
C	0.53224900	-1.35814300	0.40085500
C	1.87022500	-0.90126600	-0.08148400
H	1.98078300	-1.11338400	-1.15193900
H	2.71623500	-1.35795700	0.44335100
H	1.95633200	0.84170300	1.21187800
H	2.79100800	1.04828500	-0.31870200
H	-0.37381700	-1.33451800	-1.48130500
H	0.37381700	-1.33447100	1.48134800

TS-TCO

C	-1.36126100	-0.20269500	-0.65335800
C	-1.92427200	-1.58963100	-0.72911000
C	-3.44811400	-1.48303700	-0.96378700
H	-1.74191400	-2.11408000	0.21870300
H	-1.47214100	-2.18482800	-1.53188600
C	-4.19899800	-0.57667400	0.03038600
H	-3.62722300	-1.11736100	-1.98378200

H	-3.87138300	-2.49377100	-0.92148600
C	-4.15930000	0.95384500	-0.24721700
H	-5.24737700	-0.89441400	0.02960600
H	-3.83331600	-0.77970300	1.04591300
C	-3.42315100	1.82874700	0.78486300
H	-3.72885700	1.13880500	-1.24067300
H	-5.19200800	1.31504900	-0.30375600
C	-1.38123200	0.48965700	0.53126500
C	-1.88959100	1.89748200	0.59588700
H	-1.44720300	2.46940000	1.41882200
H	-1.65957100	2.41568100	-0.34051900
H	-3.81718900	2.85126700	0.74004100
H	-3.64649000	1.45737000	1.79390300
C	1.16930200	-0.69675100	1.31762600
C	1.13777900	-1.48251800	0.12005600
H	-1.51701800	-0.09177300	1.44639400
H	-1.38822200	0.38056200	-1.57478200
C	0.98674700	0.62032000	0.99819000
C	0.91771700	-0.65585300	-0.94831600
Cl	1.19224900	1.95364000	2.05417800
Cl	1.22703600	-1.35083700	2.89736600
Cl	1.19109300	-3.19270500	0.08859600
Cl	1.03345600	-1.10122800	-2.60331700
C	1.26510400	0.76818600	-0.49840200
C	2.79590300	1.94109600	-1.72620800
C	1.52366600	2.75979600	-1.59709100
H	3.71421700	2.50477900	-1.55558000
H	2.84542500	1.41828400	-2.68863200
H	1.61790900	3.53856900	-0.83211600
H	1.16582000	3.19048300	-2.53334800
O	0.58399700	1.77329000	-1.17942800
O	2.64594900	1.01584500	-0.65826300

CO

C	0.14776900	-0.58532500	-1.45456400
C	-0.14776900	0.58532500	-1.45456400
C	-0.49811300	1.89720100	-0.90995800
C	-0.08062600	1.87479800	0.57977000
H	-1.57950400	2.06028500	-0.99457000
H	-0.00663000	2.72273000	-1.43483200
C	-0.49811300	0.59888200	1.34493100
H	-0.51489300	2.75455300	1.06906600
H	1.00845800	1.98782100	0.63883700

C	0.49811300	-0.59888200	1.34493100
H	-1.47506900	0.26391400	0.97263500
H	-0.66233300	0.89142400	2.38778700
C	0.08062600	-1.87479800	0.57977000
H	0.66233300	-0.89142400	2.38778700
H	1.47506900	-0.26391400	0.97263500
C	0.49811300	-1.89720100	-0.90995800
H	-1.00845800	-1.98782100	0.63883700
H	0.51489300	-2.75455300	1.06906600
H	0.00663000	-2.72273000	-1.43483200
H	1.57950400	-2.06028500	-0.99457000

TS-CO

C	1.30758000	0.68922500	0.02719700
C	1.31862500	-0.45236100	-0.43957300
C	2.00949900	-1.65307900	-0.94054100
C	3.48029000	-1.63031000	-0.49178500
H	1.52718400	-2.56996100	-0.58263400
H	1.94922800	-1.67463600	-2.03613300
C	4.24929100	-0.34108100	-0.83445100
H	3.97798800	-2.48648900	-0.96198600
H	3.52072000	-1.80103200	0.59075200
C	4.23797200	0.79485800	0.22248100
H	5.29380400	-0.62446700	-1.00277200
H	3.88836700	0.04758800	-1.79624400
C	3.37147100	2.02924000	-0.08822100
H	5.26882900	1.14485300	0.34180600
H	3.94771800	0.38663400	1.20004100
C	1.92662500	1.95731800	0.43512200
H	3.83528600	2.92202600	0.34742000
H	3.34417700	2.18803700	-1.17285700
H	1.90994700	2.03370100	1.53075300
H	1.35211600	2.80967600	0.05625800
C	-1.02307400	-1.25904700	0.86341400
C	-0.89917000	-1.04410100	-0.48504900
C	-1.06500800	0.00387700	1.53030200
C	-0.98170700	1.00527800	0.60076100
Cl	-0.91649300	-2.77093300	1.65743200
Cl	-1.02667500	0.19984100	3.22849600
Cl	-1.25314400	2.67313100	0.89181000
C	-1.32801700	0.40276300	-0.75963800
C	-1.77551100	1.58016400	-2.66950600
C	-2.98792600	0.74696000	-2.29198800

H	-1.90484700	2.63186700	-2.38956800
H	-1.48461700	1.50368600	-3.71836600
H	-3.93840900	1.27887000	-2.35536500
H	-3.03645600	-0.18368500	-2.86937300
Cl	-1.07910400	-2.23606200	-1.70843200
O	-2.72867200	0.47547000	-0.92164200
O	-0.74815300	0.98621600	-1.88224100

***exo*-BCN**

C	-2.41878200	0.60390800	-0.47462200
C	-2.41922000	-0.60400600	-0.47471300
C	-1.85306400	1.93027700	-0.21264900
H	-1.58564600	2.43669000	-1.14759400
H	-2.54520000	2.58635000	0.32564400
C	-1.85317300	-1.93026300	-0.21256800
H	-1.58567300	-2.43669400	-1.14748200
H	-2.54519100	-2.58646000	0.32573300
C	-0.58547700	-1.66616200	0.63919400
H	-0.90236300	-1.22752300	1.59281900
H	-0.09933200	-2.62260700	0.87279500
C	-0.58529400	1.66639800	0.63911300
H	-0.90210700	1.22790500	1.59282800
H	-0.09917200	2.62289900	0.87251500
C	0.42119600	0.76034200	-0.04606900
C	0.42107700	-0.76022000	-0.04604100
C	1.44943600	0.00000000	0.74262200
H	1.30173000	0.00003100	1.82275500
H	0.80137100	-1.16671000	-0.98221400
H	0.80152800	1.16675500	-0.98225800
C	2.90258300	-0.00012400	0.33407400
H	3.40173700	0.88884200	0.75009300
H	3.40157400	-0.88918600	0.75008300
O	2.97228500	-0.00012200	-1.07975000
H	3.90277400	-0.00021500	-1.33776700

TS-*exo*-BCN

C	1.63378400	-0.02929700	-1.18900400
C	2.19479600	-1.09977300	-0.55798100
C	-0.62217900	-0.32366500	0.66540600
C	-0.62601400	-0.51377500	-0.54832800
C	-1.29574900	-0.28370400	1.97177000
H	-0.73738700	-0.84611500	2.72946200
H	-1.36021700	0.75210500	2.32754200

C	-1.30795300	-0.85103100	-1.80612300
H	-0.75784700	-1.61268200	-2.37100900
H	-1.36650700	0.03841300	-2.44590300
C	-2.72453400	-1.35160500	-1.45106700
H	-3.24472600	-1.63127800	-2.37629900
H	-2.63096600	-2.26616000	-0.85339000
C	-3.55384900	-0.32080700	-0.71254600
C	-2.70958900	-0.87474700	1.78490200
H	-3.22295400	-0.88213500	2.75517300
H	-2.61115200	-1.92080900	1.47133200
C	-3.54826800	-0.10074200	0.78859000
H	-3.70261100	0.60323800	-1.26898000
H	-3.69466400	0.94424300	1.05749100
C	-4.73641100	-0.72973000	0.11875000
H	-4.85062200	-1.80242100	0.27609000
C	-6.05004200	0.00643000	0.01698900
H	-6.63827200	-0.40379300	-0.81850600
H	-6.62923500	-0.14624200	0.94090200
O	-5.78141200	1.38179000	-0.18567700
H	-6.62428500	1.84867700	-0.24777800
C	1.62543400	0.35036500	1.10768200
C	2.19028500	-0.86553800	0.85975600
C	1.62136900	1.14235300	-0.20512600
C	1.14961900	3.31993700	-0.72379400
C	2.56778200	3.22317700	-0.18869800
H	1.13478900	3.40898300	-1.81603700
H	0.55157300	4.11436100	-0.27454400
H	3.30591800	3.78465400	-0.76359200
H	2.62298400	3.50261700	0.87010200
O	0.59310500	2.07114500	-0.32542700
O	2.84050400	1.83938100	-0.35906500
Cl	1.59272300	1.16677400	2.61592700
Cl	2.64119900	-2.03014300	2.02970300
Cl	2.65371900	-2.57703100	-1.28767300
Cl	1.60575400	0.26326600	-2.87664900

***endo*-BCN**

C	2.17097200	1.10239200	-0.19156400
C	2.50615600	-0.05606100	-0.26428000
C	1.21280400	2.20188500	-0.03934000
H	1.33779100	2.69995700	0.92948800
H	1.32238200	2.96792500	-0.81379000
C	2.27313400	-1.50351500	-0.28279700

H	2.65690400	-1.97646400	0.62911100
H	2.75483900	-1.99903100	-1.13204600
C	0.73313200	-1.66320300	-0.36836400
H	0.41209000	-1.23368300	-1.32240800
H	0.47695100	-2.73066200	-0.39082700
C	-0.18403600	1.53566600	-0.12903900
H	-0.29702500	1.12731300	-1.13865000
H	-0.97008300	2.28930900	-0.00353100
C	-0.38107500	0.45267700	0.91878600
C	0.01528600	-1.00586300	0.79976900
C	-1.44354100	-0.60849100	0.78198800
H	0.33537900	-1.43275100	1.75003400
H	-0.26976100	0.84294700	1.92976300
H	-2.01958300	-0.82982300	1.67712300
C	-2.27312100	-0.67166100	-0.47129600
H	-2.82659500	-1.62231700	-0.49888000
H	-1.63844000	-0.63904100	-1.36703900
O	-3.16250000	0.43374500	-0.44548000
H	-3.75310400	0.36340300	-1.20769000

TS-*endo*-BCN

C	1.63378400	-0.02929700	-1.18900400
C	2.19479600	-1.09977300	-0.55798100
C	-0.62217900	-0.32366500	0.66540600
C	-0.62601400	-0.51377500	-0.54832800
C	-1.29574900	-0.28370400	1.97177000
H	-0.73738700	-0.84611500	2.72946200
H	-1.36021700	0.75210500	2.32754200
C	-1.30795300	-0.85103100	-1.80612300
H	-0.75784700	-1.61268200	-2.37100900
H	-1.36650700	0.03841300	-2.44590300
C	-2.72453400	-1.35160500	-1.45106700
H	-3.24472600	-1.63127800	-2.37629900
H	-2.63096600	-2.26616000	-0.85339000
C	-3.55384900	-0.32080700	-0.71254600
C	-2.70958900	-0.87474700	1.78490200
H	-3.22295400	-0.88213500	2.75517300
H	-2.61115200	-1.92080900	1.47133200
C	-3.54826800	-0.10074200	0.78859000
H	-3.70261100	0.60323800	-1.26898000
H	-3.69466400	0.94424300	1.05749100
C	-4.73641100	-0.72973000	0.11875000
H	-4.85062200	-1.80242100	0.27609000

C	-6.05004200	0.00643000	0.01698900
H	-6.63827200	-0.40379300	-0.81850600
H	-6.62923500	-0.14624200	0.94090200
O	-5.78141200	1.38179000	-0.18567700
H	-6.62428500	1.84867700	-0.24777800
C	1.62543400	0.35036500	1.10768200
C	2.19028500	-0.86553800	0.85975600
C	1.62136900	1.14235300	-0.20512600
C	1.14961900	3.31993700	-0.72379400
C	2.56778200	3.22317700	-0.18869800
H	1.13478900	3.40898300	-1.81603700
H	0.55157300	4.11436100	-0.27454400
H	3.30591800	3.78465400	-0.76359200
H	2.62298400	3.50261700	0.87010200
O	0.59310500	2.07114500	-0.32542700
O	2.84050400	1.83938100	-0.35906500
Cl	1.59272300	1.16677400	2.61592700
Cl	2.64119900	-2.03014300	2.02970300
Cl	2.65371900	-2.57703100	-1.28767300
Cl	1.60575400	0.26326600	-2.87664900

NB

C	-1.27516700	-0.66838400	-0.50046700
C	-0.08475700	-1.12465100	0.32514200
C	-1.27530100	0.66821800	-0.50043300
H	-1.91564300	-1.32518000	-1.07943800
C	-0.03087800	-0.00005400	1.37633800
C	1.18018900	-0.77734000	-0.52111800
H	-0.11408000	-2.15181500	0.69243300
C	-0.08500000	1.12461600	0.32520000
H	0.89564900	-0.00000300	1.96187900
H	-0.89745500	-0.00019500	2.04245500
H	2.08031700	-1.17261200	-0.03983000
H	1.12344900	-1.20190100	-1.52637900
C	1.18003200	0.77756100	-0.52105600
H	-0.11449600	2.15176900	0.69249900
H	2.08001300	1.17294800	-0.03957200
H	1.12334500	1.20222000	-1.52625000
H	-1.91580200	1.32496900	-1.07943800

TS-NB

C	-0.66267600	0.21097100	-1.13919200
C	-0.15444300	1.40072600	-0.68222100

C	-0.62508600	0.17912900	1.18710400
C	-0.13188400	1.38082400	0.74601400
C	1.05529800	-1.34935200	0.65863000
C	2.42848300	-0.86182600	1.07976400
C	1.02753000	-1.32351600	-0.72142700
H	0.46730100	-2.03222200	1.26219000
C	2.76763100	0.14072100	-0.03635100
C	3.38553600	-2.03042500	0.68611200
H	2.52581100	-0.51742300	2.11129000
C	2.38218700	-0.81567400	-1.17794400
H	3.83272100	0.39517400	-0.05314900
H	2.19600600	1.06580300	-0.00531900
H	4.39319000	-1.83494700	1.06638000
H	3.05272000	-2.98776800	1.09609300
C	3.35482800	-1.99755200	-0.87187400
H	2.43762600	-0.42954900	-2.19777700
H	4.34675100	-1.78413500	-1.28264700
H	3.00714500	-2.93778000	-1.30840600
H	0.42005500	-1.98821400	-1.32610400
Cl	0.58257500	2.59367400	1.71955500
Cl	0.53100600	2.63957100	-1.64372500
C	-1.44642700	-0.40382000	0.03047100
C	-3.66226000	-0.87263200	-0.27781600
C	-2.95034500	-2.12311900	0.20699000
H	-4.61124800	-0.67317800	0.22188700
H	-3.80143500	-0.88156400	-1.36518000
H	-3.11922700	-2.29877100	1.27517300
H	-3.17853200	-3.02376000	-0.36459300
Cl	-1.03946200	-0.19219300	2.81286700
Cl	-1.13008200	-0.10614300	-2.76485400
O	-2.74442700	0.14244900	0.10298900
O	-1.58404300	-1.78893100	-0.02357700

3,3-CP

C	-1.26243200	-0.00006600	0.64750300
C	-1.26247900	-0.00009000	-0.64748000
H	-1.80992200	-0.00008000	1.57833900
H	-1.80997700	-0.00012600	-1.57831000
C	0.09435600	-0.00001700	-0.00003200
C	0.93716500	1.26713700	-0.00001000
H	0.30536500	2.15949300	-0.00002400
H	1.58606600	1.30510700	0.88345900
H	1.58613700	1.30511300	-0.88342400

C	0.93738100	-1.26701100	0.00000300
H	1.58628400	-1.30491600	-0.88345900
H	1.58634700	-1.30481700	0.88342800
H	0.30574800	-2.15949000	0.00008500

TS-3,3-CP

C	-0.32912100	-1.12808600	-0.40411600
C	0.57059500	-0.51486600	-1.23421100
C	-0.38498500	1.17170100	-0.02803300
C	0.53916200	0.89827900	-1.00030200
C	0.62025500	0.36834900	1.92799800
C	0.64365400	-0.94926600	1.71361900
H	0.06295000	1.12858400	2.45814100
H	0.11288500	-1.85493000	1.97340100
C	1.96894300	-0.29042000	1.96190000
Cl	-0.84099300	-2.76259400	-0.50907300
Cl	1.66634600	-1.29251300	-2.29038000
Cl	1.59856700	2.02215900	-1.73209100
Cl	-0.96349200	2.73329000	0.39077700
C	-1.31708200	-0.04627800	0.05325500
C	-3.33352200	-0.44564900	1.05769000
C	-3.55962700	0.27975600	-0.25664300
H	-3.53209500	-1.51939400	0.96759000
H	-3.88137500	-0.02937500	1.90428400
H	-4.36055800	-0.13708400	-0.86887200
H	-3.71826300	1.35402000	-0.10653700
O	-2.32852900	0.04232200	-0.92685500
O	-1.94402300	-0.22284300	1.28131300
C	3.04873200	-0.10176400	0.90619500
H	2.66958500	0.05595200	-0.09902200
H	3.67100700	0.76278000	1.16420900
H	3.69800000	-0.98445500	0.87977000
C	2.59201800	-0.50300700	3.33952300
H	3.23923600	-1.38793200	3.33558100
H	3.21059200	0.35803400	3.61851200
H	1.82704400	-0.64033200	4.10907800

DIBO

C	0.60682100	1.40602300	-0.00921700
C	-0.60704500	1.40624700	0.00957400
C	-0.52887800	-1.27627300	-0.58008000
C	0.52910500	-1.27689600	0.57983600
H	-0.73376300	-2.31043700	-0.87242700
H	-0.08706200	-0.78522200	-1.45465900

H	0.73409000	-2.31139600	0.87093000
H	0.08724500	-0.78695000	1.45500400
C	1.84947800	-0.60116600	0.27083500
C	1.89789700	0.79455600	0.02187900
C	3.11378000	1.43955400	-0.21058000
H	3.12062300	2.50838300	-0.39779500
C	3.04913600	-1.30773600	0.25769800
H	3.03405300	-2.37863200	0.44439900
C	4.26319400	-0.66411400	0.02146600
C	4.29672700	0.70889600	-0.20743900
H	5.24284400	1.20936200	-0.38749700
C	-1.84930200	-0.60106800	-0.27021600
C	-3.04888300	-1.30778100	-0.25768100
H	-3.03360500	-2.37862500	-0.44466100
C	-4.26310100	-0.66436500	-0.02168700
H	-5.18487400	-1.23795600	-0.02213200
C	-1.89804600	0.79464900	-0.02175400
C	-3.11405900	1.43947500	0.21049500
H	-3.12108700	2.50832100	0.39761100
C	-4.29689000	0.70862700	0.20728700
H	-5.24311800	1.20895800	0.38714000
H	5.18504900	-1.23757300	0.02159600

TS-DIBO

C	-0.69046800	0.35061300	-0.91681800
C	0.48628300	0.73747900	-0.79020600
C	-0.42538800	3.40619100	-0.08927800
C	-1.30470200	2.47408000	0.80565200
H	-0.45675300	4.41843600	0.32557000
H	-0.90551200	3.47569500	-1.07387800
H	-1.77965300	3.08154100	1.58141600
H	-0.67190500	1.74707000	1.32512300
C	0.58893300	-0.81445000	1.63827500
C	1.43679400	-0.96935600	0.56505100
C	-0.70660500	-1.27540600	1.28473300
C	-0.68342300	-1.70647600	-0.02598300
Cl	3.14526000	-0.86860900	0.67376000
Cl	0.96608100	-0.02905900	3.10816500
Cl	-2.09930600	-1.12423300	2.26154800
Cl	-1.90667900	-2.65065800	-0.76828900
C	-2.39291300	1.77812300	0.01875100
C	-2.07919700	0.74447600	-0.89672800
C	-3.07431500	0.19316700	-1.70837100

H	-2.80682000	-0.56805800	-2.43234800
C	-3.71873300	2.19420500	0.11185900
H	-3.97342800	2.98633900	0.81164100
C	-4.71447200	1.62355100	-0.67879800
C	-4.38915900	0.63197400	-1.59856000
H	-5.15641100	0.20069500	-2.23373300
C	1.03336100	3.06695500	-0.33444600
C	1.98714500	4.08153500	-0.25843500
H	1.68070200	5.05969600	0.10393400
C	3.30289400	3.88385900	-0.67021600
H	4.01732400	4.69866100	-0.60429700
C	1.45907300	1.79824500	-0.79405000
C	2.76980400	1.61250600	-1.24525700
H	3.04835500	0.64415200	-1.64663300
C	3.68857400	2.65271300	-1.19047000
H	4.70236200	2.49901300	-1.54645900
H	-5.74066100	1.96528100	-0.58442600
C	0.78503800	-1.96991300	-0.38753500
C	1.48123200	-3.10710200	-2.24326200
C	1.94263900	-3.84471000	-0.99848500
H	0.59143900	-3.57093200	-2.68350200
H	2.25255000	-2.97645800	-3.00338500
H	1.77765700	-4.92277900	-1.02508300
H	2.99116400	-3.62727200	-0.76424600
O	1.08505600	-3.29432500	-0.00682000
O	1.15796500	-1.82206900	-1.71972600

Summary of energetic parameters given in hartrees (hf)

ZPE Zero point energy M06-2X/6-31G(d)

H Enthalpy M06-2X/6-31G(d))

SCF Electronic energy (6-311++g(d,p) cpcm=water//M06-2X/6-31G(d))

qG =Free energy with quasiharmonic approximation (6-311++g(d,p) cpcm=water//M06-2X/6-31G(d))

	ZPE	**H**	**E**	**qG**
	-	-	-	-
TCK	2259.928881	2259.915718	2260.281305	2260.21840
TCO	-312.880321	-312.871856	-313.174574	-312.999326
	-		-	-
TS-TCO	2572.804719	-2572.78357	2573.452278	2573.188796
CO	-311.665374	-311.656702	-311.937976	-311.786395
	-	-	-	-
TS-CO	2571.586228	2571.564618	2572.209993	2571.971881

***Endo*-BCN**	-464.166246	-464.154971	-464.201554	-464.53848
	-	-	-	-
TS-*Endo*-BCN	2724.091148	2724.066875	2724.144961	2724.814722
NB	-272.44295	-272.436849	-272.672435	-272.545876
	-	-	-	
TS-NB	2532.358452	2532.339967	2532.942089	-2532.72745
3,3-CP	-195.04065	-195.033857	-195.211371	-195.125829
	-		-	-
TS-3,3-CP	2454.950795	-2454.93165	2455.475261	2455.302477
DIBO	-616.372905	-616.360451	-616.76381	-616.569733
	-	-	-	
TS-DIBO	2876.282572	2876.257134	2877.026878	-2876.74394

3.9.3 Experimental Procedures

A. Diene Synthesis

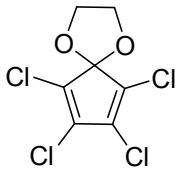

6,7,8,9-Tetrachloro-1,4-dioxaspiro[4.4]nona-6,8-diene (TCK). To a solution of hexachlorocyclopentadiene (11.9 g, 43.63 mmol, 1.0 equiv) in ethylene glycol (18 ml) at 0 °C was added dropwise a solution of KOH (5.4 g, 96 mmol, 2.2 equiv) in ethylene glycol (9 ml) over one hour. The solution was kept at 0 °C until complete addition of KOH and then was allowed to warm to room temperature. The reaction was stirred for 16 hours, diluted with water and extracted with diethyl ether. The organic layer was dried over Na_2SO_4 and concentrated *in vacuo*. The desired product was purified by silica gel column chromatography eluting with hexane ($R_f = 0.2$).[54] ^1H and ^{13}C NMR spectroscopic data were consistent with that previously reported.

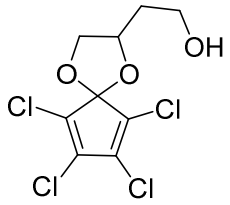

2-(6,7,8,9-Tetrachloro-1,4-dioxaspiro[4.4]nona-6,8-dien-2-yl)ethan-1-ol (3.6). To a solution of hexachlorocyclopentadiene (1 ml, 6.25 mmol, 1.0 equiv) in 1,2,4-butanetriol (1 ml, 11.21 mmol, 1.79 equiv) and *t*-BuOH (6 ml) at 0 °C was added dropwise a solution of KOH (0.876 g, 15.625 mmol, 2.5 equiv) in 1,2,4-butanetriol (1 ml, 11.21 mmol, 1.79 equiv), 2-propanol (16 ml) and *t*-BuOH (9 ml) over 40 minutes. The solution was kept at 0 °C until complete addition of KOH and then was allowed to warm to room temperature. The reaction was stirred for 16 hours, diluted with water and extracted with diethyl ether. The organic layer was dried over Na_2SO_4, filtered, and concentrated *in vacuo*. The desired product was purified by silica gel column chromatography and eluted with 36% diethyl ether in pentane (R_f = 0.3) to give 630 mg as a yellow oil (33% yield). ^{1}H NMR (600 MHz, $CDCl_3$): δ 4.67-4.7 (m, 1H), 4.47-4.45 (dd, *J* = 7.9, 5.8 Hz, 1H), 3.93 (t, *J* = 8.1 Hz, 1H), 3.81-3.85 (m, 2H), 1.93-2.05 (m, 2H), 1.81 (s, 1H); ^{13}C NMR (150 MHz, $CDCl_3$): δ 129.95, 129.34, 128.56, 128.32, 108.51, 77.15, 71.72, 59.32, 35.09.

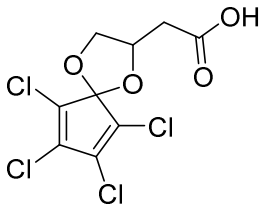

2-(6,7,8,9-Tetrachloro-1,4-dioxaspiro[4.4]nona-6,8-dien-2-yl)acetic acid (3.7). To a solution of diene **3.6** (0.235 g, 0.77 mmol, 1.0 equiv) in DCM (1.5 ml) was added water (1.5 ml) followed by (2,2,6,6-tetramethylpiperidin-1-yl)oxyl (29 mg, 0.20 mmol, 0.25 equiv). The solution was cooled to 0 °C and bis(acetoxy)iodobenzene (0.74 g, 2.31 mmol, 3 equiv) was added. The solution

was stirred for three hours at 0 °C, diluted with DCM (15 ml) and washed with a saturated sodium thiosulfate solution. The organic layer was dried over Na_2SO_4, filtered and concentrated *in vacuo*. The desired product was purified by silica gel column chromatography and eluted with 25% ethyl acetate in hexane (R_f = 0.1) to give 106 mg of the desired product as a white solid (43% yield). ^{1}H NMR (500 MHz, 85% $CDCl_3$, 15% CD_3CN): δ 4.76 (m, 1H), 4.48 (dd, *J* = 8.2, 6.1 Hz, 1H), 3.88 (t, *J* = 7.7 Hz, 1H), 2.79 (dd, *J* = 16.4, 6.4 Hz, 1H), 2.61 (dd, *J* = 16.6, 7.1 Hz, 1H); ^{13}C NMR (133 MHz, 85% $CDCl_3$, 15% CD_3CN): δ 175.99, 135.38, 134.55, 133.98, 133.40, 114.06, 80.14, 76.96, 42.95; HRMS (APCI) (*m/z*) $[M-H]^-$ calcd for $C_9H_6Cl_4O_4$, 316.8937; found 316.8940.

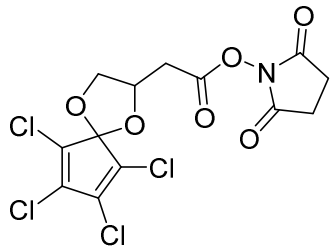

2,5-Dioxopyrrolidin-1-yl-2-(6,7,8,9-tetrachloro-1,4-dioxaspiro[4.4]nona-6,8-dien-2-yl) acetate (3.8). To a solution of diene **3.7** (35 mg, 0.11 mmol, 1.0 equiv) in DCM (1 ml) was added *N*,*N'*-dicyclohexylcarbodiimide(35 mg, 0.16 mmol, 1.5 equiv) followed by *N*-hydroxysuccinimide (14 mg, 0.12 mmol, 1.1 equiv). The solution was shaken for 16 hours at room temperature and the precipitate was removed by centrifugation. The reaction was concentrated and purified by silica gel column chromatography and eluted by a gradient system of 20 – 35% ethyl acetate in hexane to give 40 mg as a white solid (96% yield). ^{1}H NMR (600 MHz, $CDCl_3$): δ 4.92-4.98 (m, 1H), 4.63 (dd, *J* = 8.6, 6.2 Hz, 1H), 4.10 (dd, *J* = 8.8, 6.7 Hz, 1H), 3.26 (dd, *J* = 16.5, 5.7 Hz, 1H), 3.03 (dd, *J* = 16.5, 8.1 Hz, 1H), 2.86 (s, 4H); ^{13}C NMR (125 MHz, $CDCl_3$): δ 168.68, 165.11, 129.61, 129.36, 128.62, 128.56, 109.15, 73.68, 71.33, 35.41, 25.47. HRMS-ESI (*m/z*) $[M+H]^+$ calcd for $C_{13}H_{10}Cl_4NO_6$, 415.9262, found 415.9263.

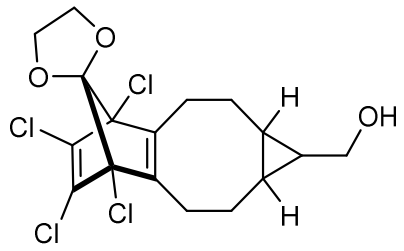

((4'S,7'S)-4',5',6',7'-Tetrachloro-1a',2',3',4',7',8',9',9a'-octahydro-1'H-spiro[[1,3]dioxolane-2,10'-[4,7]methanobenzo[a]cyclopropa[e][8]annulen]-1'-yl)methanol (3.4). To a solution of 6,7,8,9-tetrachloro-1,4-dioxospiro[4,4]nona-6,8-diene (20 mg, 76.4 μmol, 1.9 equiv) in deuterated chloroform (0.5 ml) at room temperature was added BCN (80% endo, 20% exo mixture) (6 mg, 40 μmol, 1 equiv). The solution was stirred for twenty-four hours at room temperature and then concentrated *in vacuo*. The desired product was purified by silica gel column chromatography eluting with 20% EtOAc in hexane (R_f = 0.3) to give 13 mg as an oil containing a mixture of two diastereomers in a 3:2 ratio (stereochemistry undetermined) (79% yield). ^{1}H NMR (600 MHz, $CDCl_3$): δ 4.14-4.25 (m, 8H), 3.65-3.70 (m, 4H), 2.6-2.70 (m, 2.4H), 2.47-2.55 (m, 1.6H), 2.32-2.46 (m, 4H), 2.03-2.10 (m, 1.6H), 1.92-2.01 (m, 2.6H), 1.6-1.71 (m, 2.4H), 1.55-1.6 (m, 1.6H), 1.05-1.18 (m, 2H), 0.96-1.03 (m, 1.6H), 0.7-0.77 (m, 2.4H); ^{13}C NMR (125 MHz, $CDCl_3$): δ 140.14, 138.88, 134.86, 134.71, 132.81, 132.79, 81.75, 81.61, 67.37, 67.31, 67.11, 67.06, 66.92, 60.11, 60.05, 29.71, 27.45, 26.65, 26.44, 26.31, 26.29, 21.88, 21.76, 20.56, 20.56, 20.44, 20.20, 18.30, 17.78. HRMS-ESI (*m/z*) $[M-H]^+$ calcd for $C_{17}H_{17}Cl_4O_3$, 408.9932, found 408.9929.

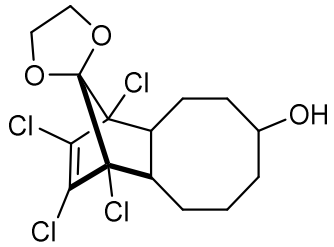

(1'S,4'S,10a'S)-1',2',3',4'-Tetrachloro-1',4',4a',5',6',7',8',9',10',10a'-decahydrospiro[[1,3]dioxolane-2,11'-[1,4]methanobenzo[8]annulen]-7'-ol (3.5). To a solution of 6,7,8,9-tetrachloro-1,4-dioxospiro[4,4]nona-6,8-diene (20 mg, 76.4 µmol, 1.9 equiv) in deuterated chloroform (0.6 ml) at room temperature was added *trans*-cyclooctenol (5 mg, 40 µmol, 1 equiv). The solution was stirred for four hours at room temperature then concentrated *in vacuo*. The desired product was purified by silica gel column chromatography eluting with 15% EtOAc in hexane (R_f = 0.22) to give 12 mg as an oil containing a mixture of two diastereomers in a 1:1 ratio (stereochemistry undetermined) (78% yield). ^{1}H NMR (600 MHz, $CDCl_3$): δ 4.23-4.31 (m, 4H), 4.13-2.21 (m, 4H), 3.96-4.07 (m, 1H), 3.85-3.96 (m, 1H), 2.50-2.60 (dt, *J* = 5.33, 12.83 Hz, 1H), 2.39-2.49 (ddd, *J* = 2.44, 5.42, 12.42 Hz, 1H), 1.74-2.25 (m, 17H), 1.61-1.72 (m, 1H), 1.5 (br s, 2H), 1.37-1.49 (m, 2H), 0.98-1.51 (m, 2H); ^{13}C NMR (125 MHz, $CDCl_3$): δ 131.46, 131.44, 128.32, 128.30, 120.93, 120.85, 78.25, 78.19, 76.95, 72.11, 71.78, 67.74, 65.93, 65.90, 50.57, 50.37, 50.21, 49.76, 36.72, 36.16, 32.80, 29.15, 28.39, 28.20, 28.09, 28.02, 22.71, 21.96, 21.07. HRMS-ESI (*m/z*) $[M-H]^+$ calcd for $C_{15}H_{17}Cl_4O_3$, 384.9932, found 384.9932.

B. Peptide-Diene Conjugate Synthesis

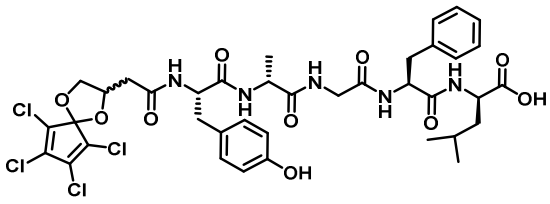

Peptide-Diene Conjugate (3.9). To a solution of peptide (2.6 mg, 3.51 µmol, 1.0 equiv) in DMF (0.2 ml) at room temperature was added diene **3.8** in DMF (62.4 µl, 87.4 mM, 1.2 equiv). After 35 min DIPEA (2.4 µl, 13.7 µmol, 3 equiv) was added. The reaction was shaken for 16 hours and concentrated *in vacuo*. The compound was purified by semi-preparative reverse phase HPLC (20% to 75% CH_3CN in water (both in 0.1% TFA) over 30 minutes, 4mL/min flow rate). HRMS-ESI (*m/z*) $[M+H]^+$ calcd for $C_{38}H_{43}Cl_4N_5O_{10}$, 870.184; found 870.188.

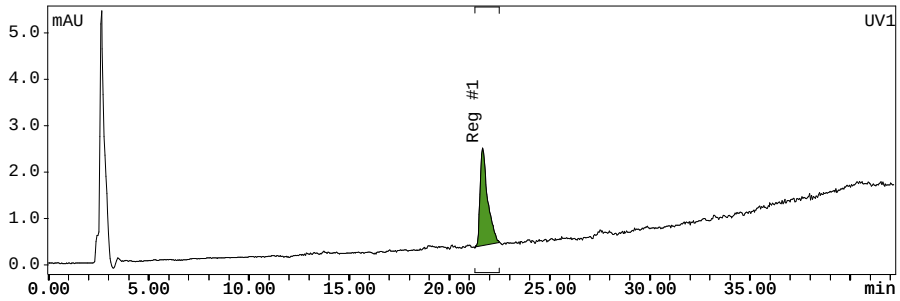

Figure 3.4. HPLC trace of purified peptide-conjugate. HPLC mobile phase: 25% acetonitrile in water (both in 0.1% TFA) to 83% acetonitrile in water over 30 min.

C. Fluorescence Peptide Labeling

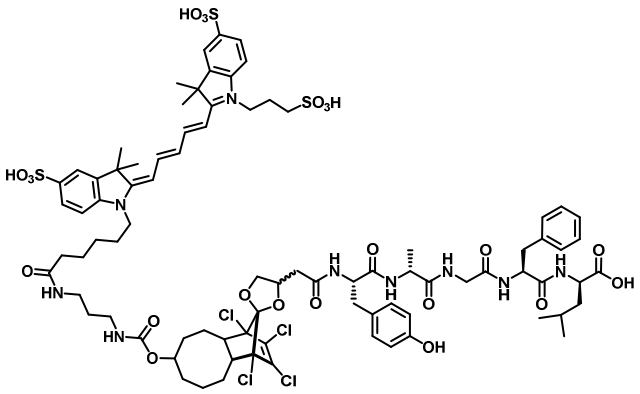

Cy5-labeled peptide (3.10). To a solution of peptide-diene **3.9** (0.147 mg, 0.167 μmol, 1.0 equiv) in 20% DMSO/PBS (0.4 ml) at room temperature was added a solution of Cy5-TCO (0.175 mg, 0.186 μmol, 1.1 equiv) in 20% DMSO/PBS (0.035 ml). HPLC analysis after stirring for 5 h confirmed trace amounts of diene still present and no residual dye. Additional dye (0.1 equiv) was then added and after an additional hour, HPLC showed full consumption of peptide. The solution was then concentrated *in vacuo* and purified by semi-preparative reverse phase HPLC (20% to 75% CH_3CN in water (both in 0.1% TFA) over 30 minutes, 4mL/min flow rate). The identity and purity of the conjugates were confirmed by analytical HPLC and HRMS. Mixture of diastereomers were collected together.

HRMS (MALDI) *m/z* [M+H] calcd for $C_{84}H_{106}N_9O_{22}S_3Cl_4$, 1828.5363; found 1828.5383.

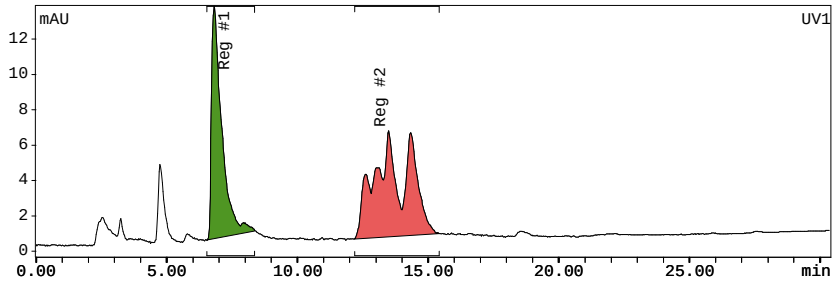

Figure 3.5. HPLC trace of crude reaction, containing unreacted dye (green) and the diastereomeric mixture of products (red). HPLC mobile phase: 25% acetonitrile in water (both in 0.1% TFA) to 83% acetonitrile in water over 30 min.

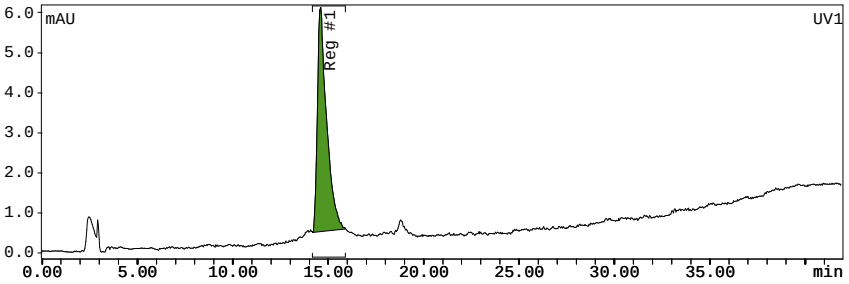

Figure 3.6. HPLC trace of one purified diastereomer. HPLC mobile phase: 25% acetonitrile in water (both in 0.1% TFA) to 83% acetonitrile in water over 30 min.

D. Stability Studies

The stability study for TCK in CD_3CN and D_2O in the presence of cysteine was monitored by ^1H-NMR. The diene (6 mg, 0.023 mmol, 1 equiv) was dissolved in 0.2 ml of CD_3CN. To the diene was added an aliquot of L-cysteine hydrochloride in D_2O (0.164 M, 0.2 mL). The solution was transferred to an NMR tube and diluted with 0.4 ml of a 1:1 CD_3CN:D_2O mixture. The NMR tube was placed in a 37 °C water bath and incubated for 63 h. The proton NMR shows no reaction takes place.

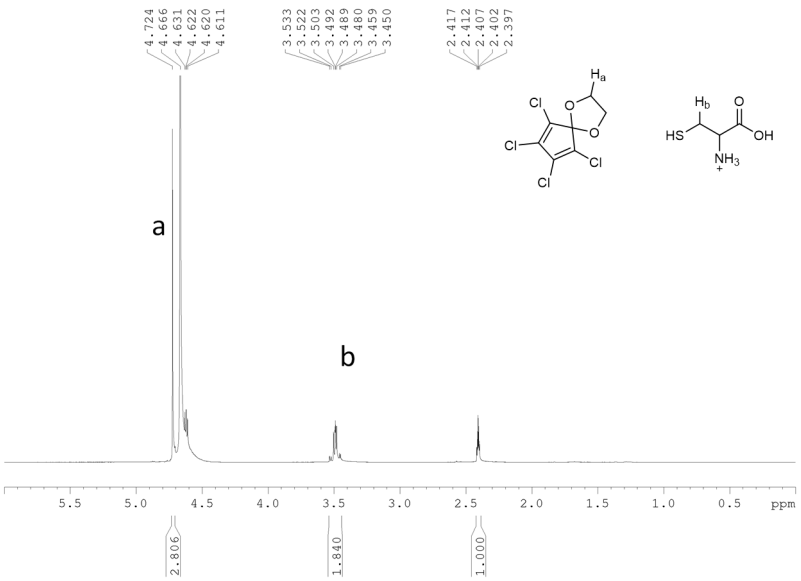

Figure 3.7. Proton NMR of TCK and cysteine mixture after 15-hour incubation at 37 °C.

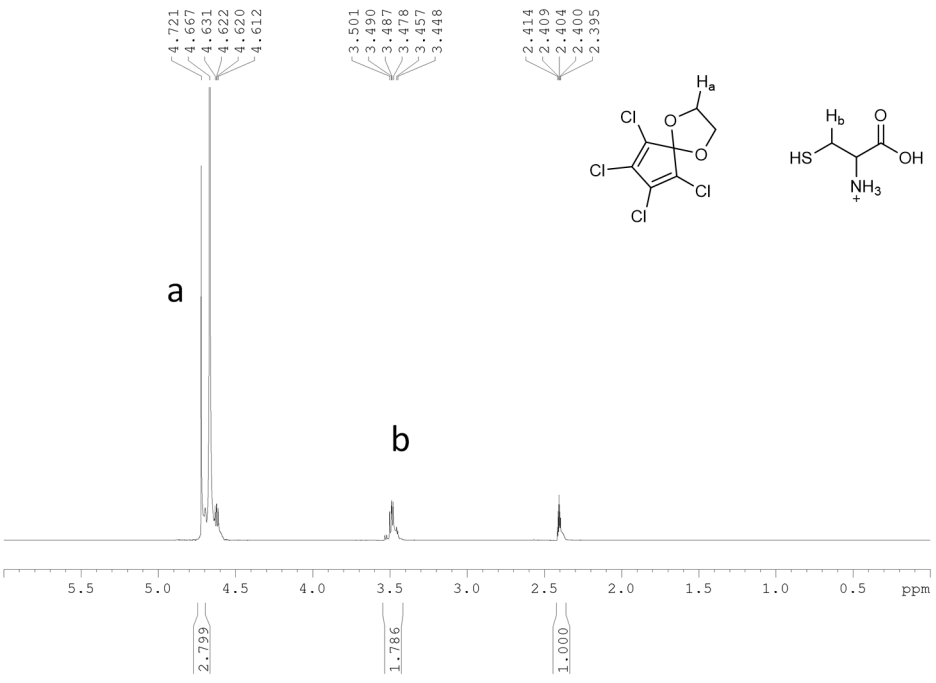

Figure 3.8. Proton NMR of TCK and cysteine mixture after 63-hour incubation at 37 °C.

E. Cross-Over Studies

The cross reactivity of DIBAC with TCK was monitored via NMR spectroscopy at room temperature over a period of 4 h. To a solution of TCK (4.7 mg, 19.5 μmol, 1 equiv) in 0.2 ml of deuterated chloroform, was added a solution of DIBAC (5.1 mg, 19.5 μmol, 1 equiv) in 0.2 ml of deuterated chloroform. No reaction was observed between DIBAC and TCK after 4 h.

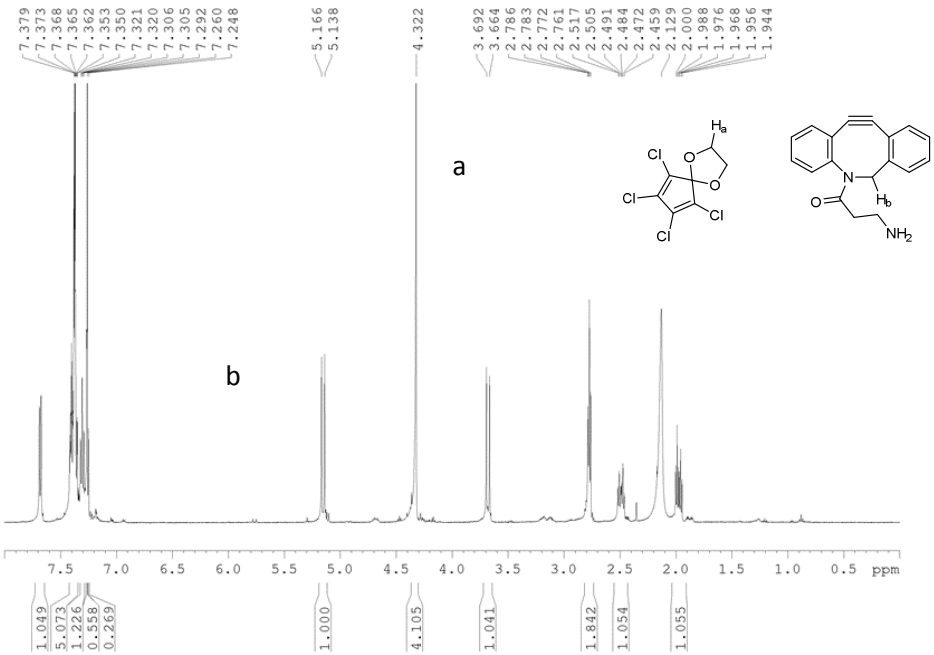

F. Competition Study

To a vial containing a solution of TCK (13.8 mg, 0.0527 mmol, 1.35 equiv) in 0.2 ml of deuterated chloroform was added benzyl azide (4.9 µL, 0.039 mmol, 1 equiv). Immediately after a mixture of TCO (4.92 mg, 0.039 mmol, 1 equiv) in 0.2 ml of deuterated chloroform was then added to the vial. The vial contents were then transferred to a NMR tube and diluted with 0.2 ml of deuterated chloroform. 4 hours after the addition of TCO a proton NMR was taken and showed consumption of the TCO by the diene and no reaction taking place between the azide and TCO.

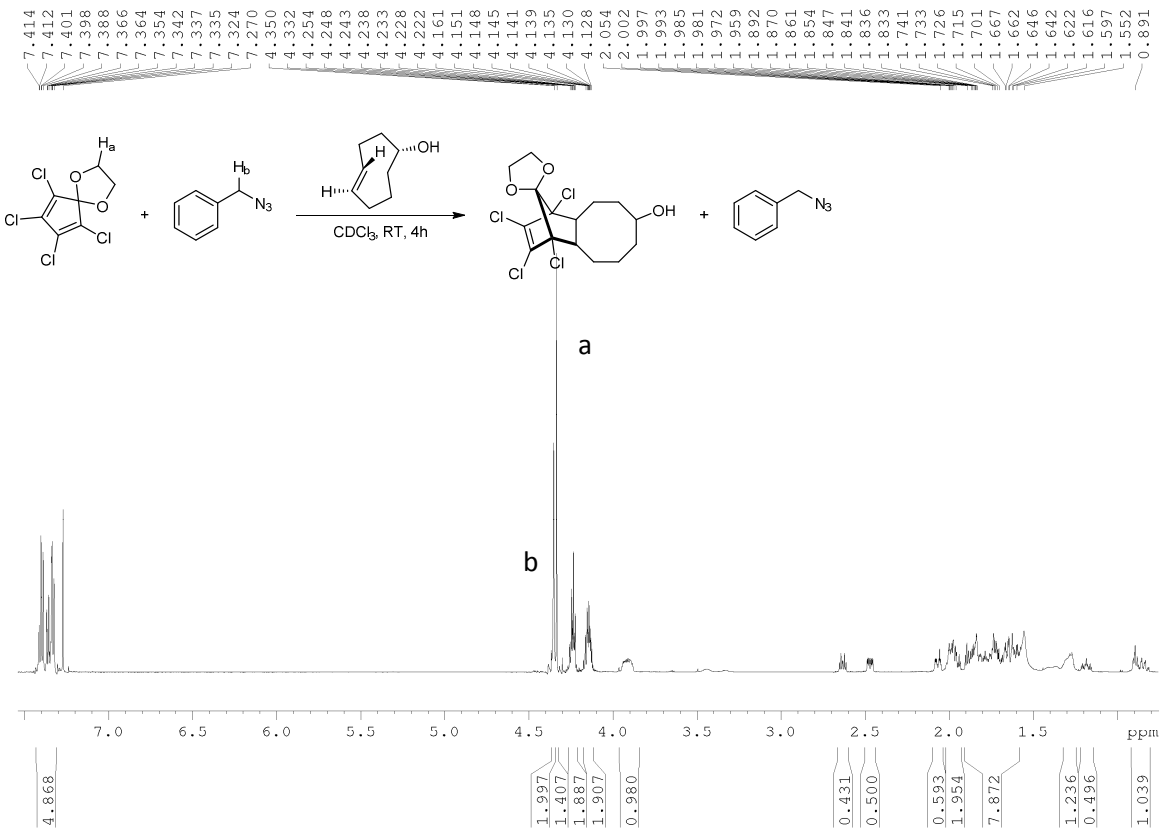

G. UV and Kinetic Studies

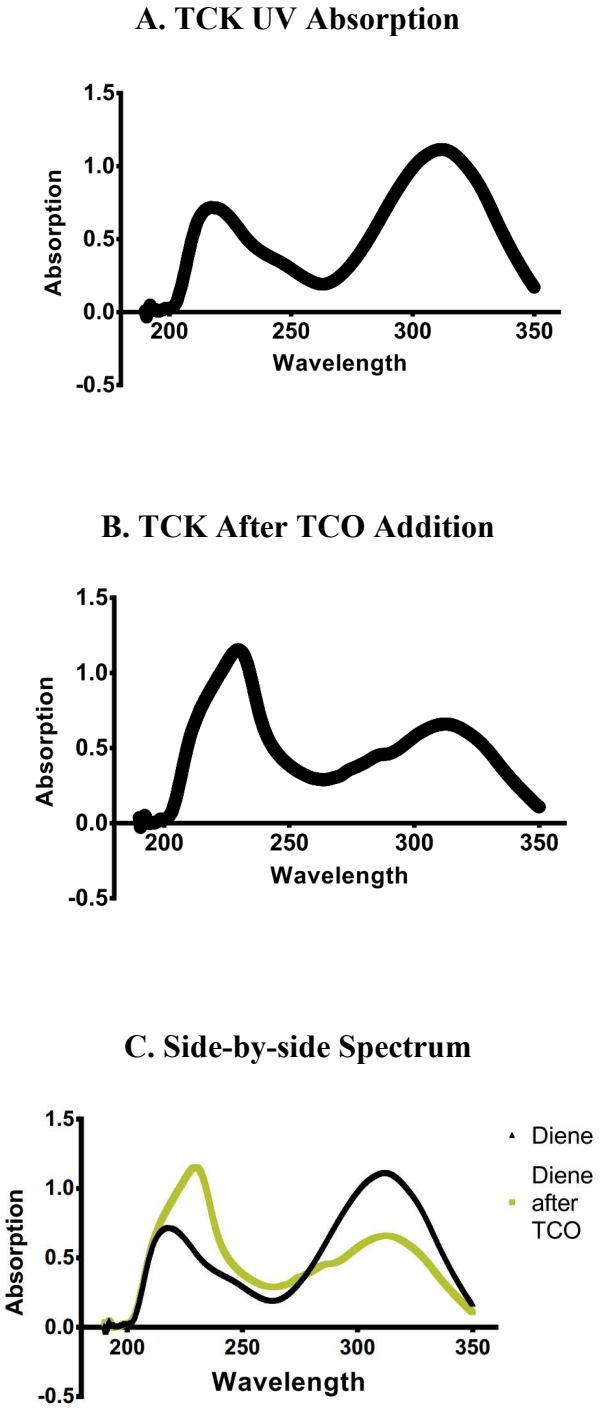

Figure 3.9. UV-vis spectra of TCK (A), the cycloaddition product of TCK and TCO (B). The two spectra overlayed for comparison (C). Measurement at 312 nm was determined as an appropriate wavelength for monitoring consumption of TCK over time.

General Procedure for UV-Vis kinetic analysis between *trans*-cyclooctene and TCK.

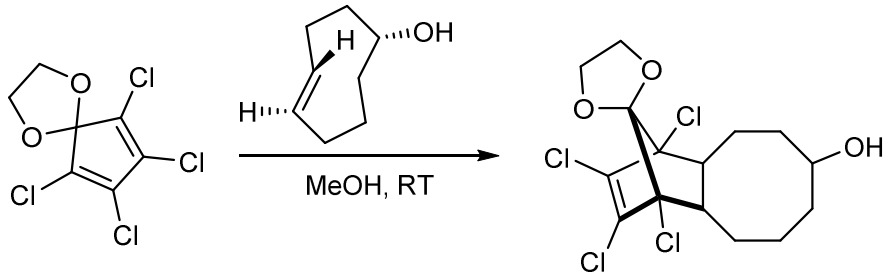

The *pseudo*-first order reaction kinetics for TCK and TCO were measured by following the exponential decay in UV absorbance of TCK at 312 nm upon reaction with 30-100 fold excess TCO in methanol. Stock solutions, 0.444 mM of TCK in methanol and 15, 30, and 45 mM of TCO in methanol were prepared. Equal volumes (0.5 mL each) of stock solutions were mixed, resulting in final concentrations of 0.222 mM TCK and 7.5, 15 and 22.5 mM TCO in methanol. The kinetic experiment was performed in triplicate for each concentration at room temperature. Decay of the wavelength at 312 nm was monitored every 6 seconds for 15-30 minutes.

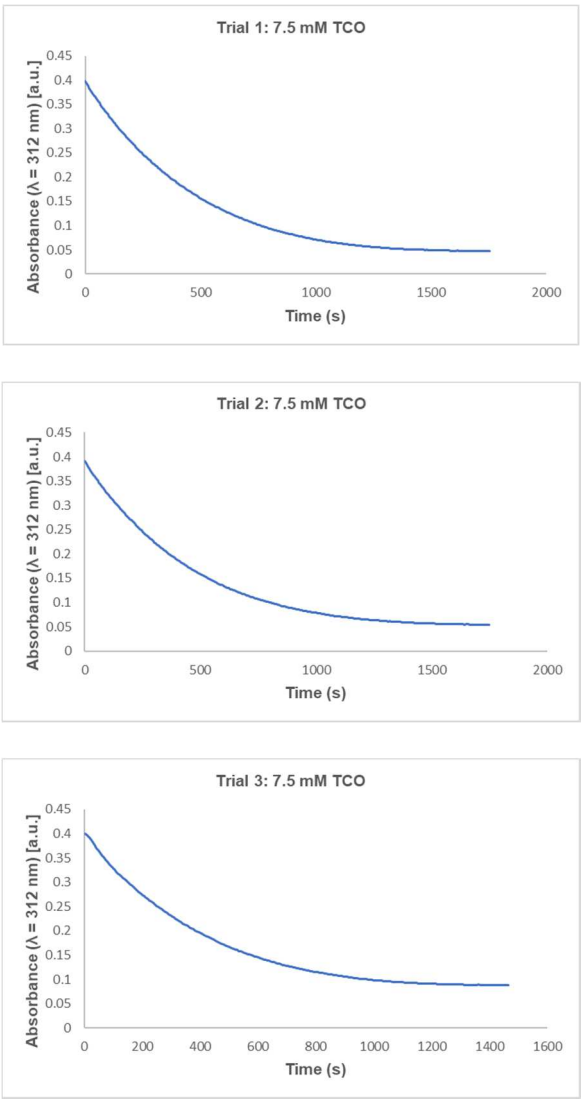

Figure 3.10. **Reaction of TCK and 7.5 mM TCO at room temperature.**

TCK and TCO were mixed in a quartz cuvette and monitored by UV-Vis spectroscopy to monitor the disappearance of the absorbance of the diene peak at 312 nm. The three observed reaction rate constants were averaged: k_{obs} (s^{-1}) = 0.235 $\times 10^{-2} \pm$ 0.00016.

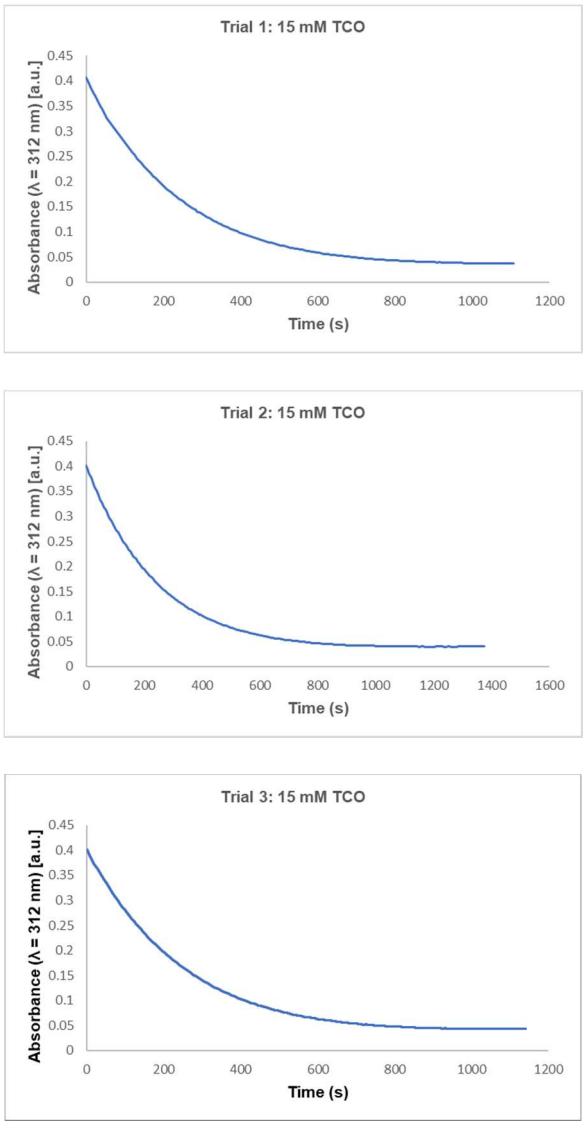

Figure 3.11. **Reaction of TCK and 15 mM TCO at room temperature.**

TCK and TCO were mixed in a quartz cuvette and monitored by UV-Vis spectroscopy to monitor the disappearance of the absorbance of the diene peak at 312 nm. The three observed reaction rate constants were averaged: k_{obs} (s^{-1}) = 0.432 $\times 10^{-2} \pm$ 0.00003.

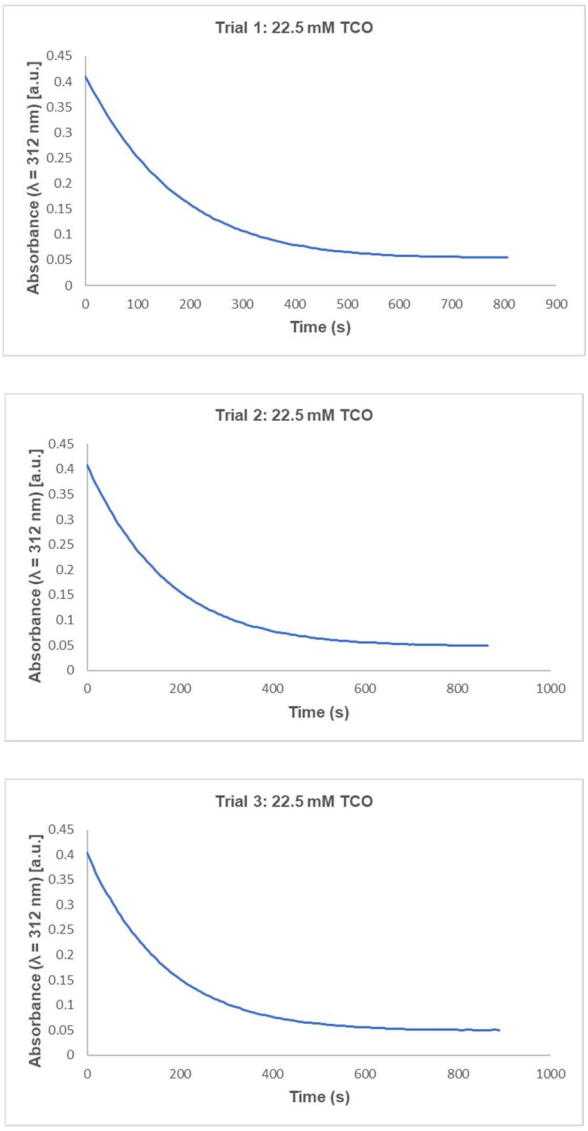

Figure 3.12. **Reaction of TCK and 22.5 mM TCO at room temperature.**

TCK and TCO were mixed in a quartz cuvette and monitored by UV-Vis spectroscopy to monitor the disappearance of the absorbance of the diene peak at 312 nm. The three observed reaction rate constants were averaged: k_{obs} (s^{-1}) = 0.616 $\times 10^{-2} \pm$ 0.00004.

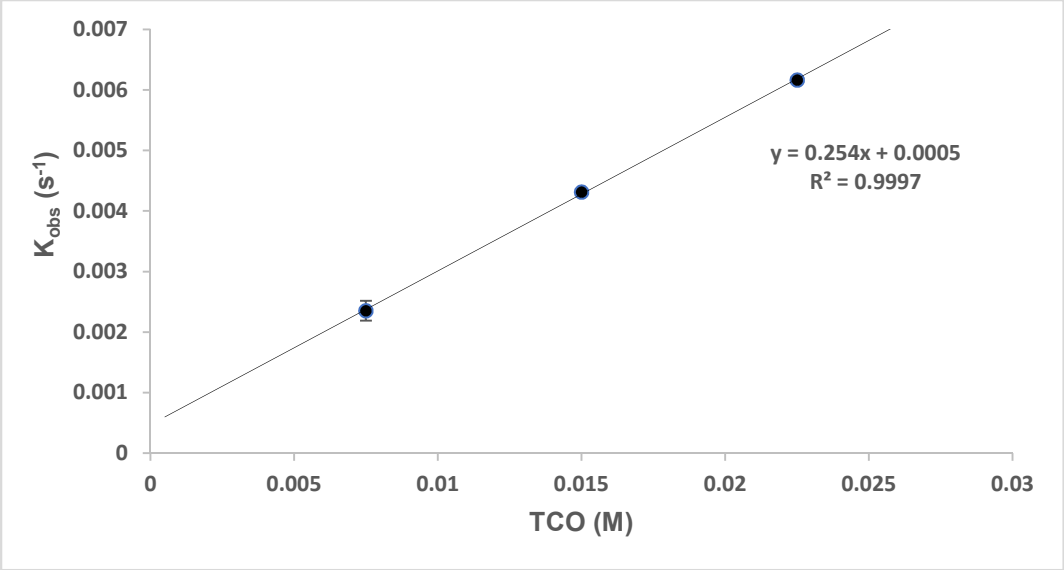

Figure 3.13. **Determination of second-order rate constant, k_2, between TCK and TCO.**

Plot of the average observed rate constants vs. concentration of TCO. The second-order rate constant k_2 is calculated from the slope of the linear regression line. The calculated rate constant for cycloaddition of TCK with TCO in methanol was 0.254 M^{-1} s^{-1}.

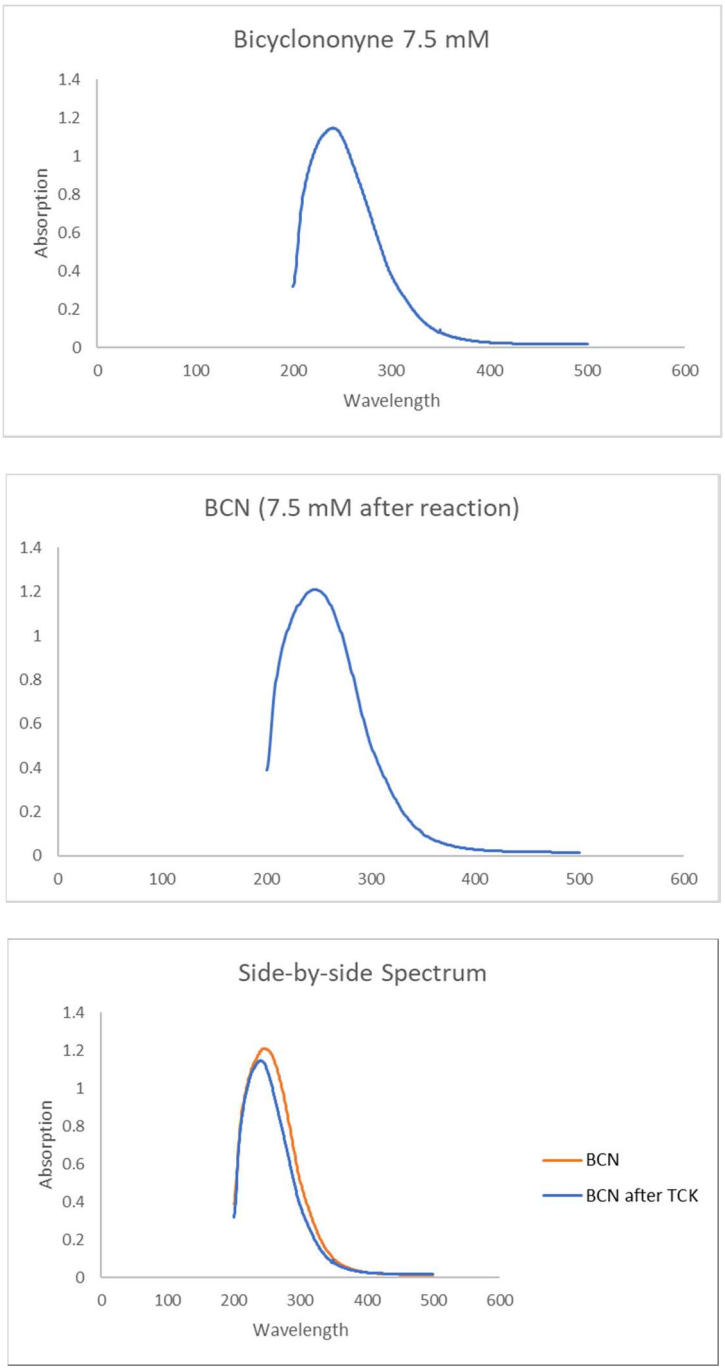

Figure 3.14. **Determination of an appropriate wavelength for decay measurements as means to determine rate.** A) UV-Vis spectrum of BCN. B) UV-Vis spectrum of BCN after reaction with 0.222 mM TCK. Additional loss of absorbance at 312 nm of BCN is negligible.

General Procedure for UV-Vis kinetic analysis between bicyclononyne and TCK.

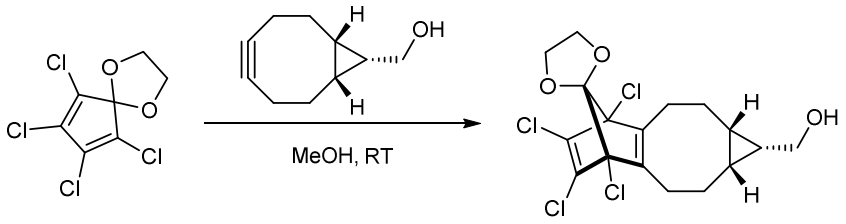

The *pseudo*-first order reaction kinetics for TCK and BCN were measured by following the exponential decay in UV absorbance of TCK at 312 nm upon reaction with 30-60 fold excess BCN in methanol. Stock solutions, 0.444 mM of TCK in methanol and 15, 20, and 30 mM of BCN in methanol were prepared. Equal volumes (0.5 mL each) of stock solutions were mixed, resulting in final concentrations of 0.222 mM TCK and 7.5, 10 and 15 mM BCN in methanol. The kinetic experiment was performed in triplicate for each concentration at room temperature. Decay of the wavelength at 312 nm was monitored every 6 seconds for 15-30 minutes.

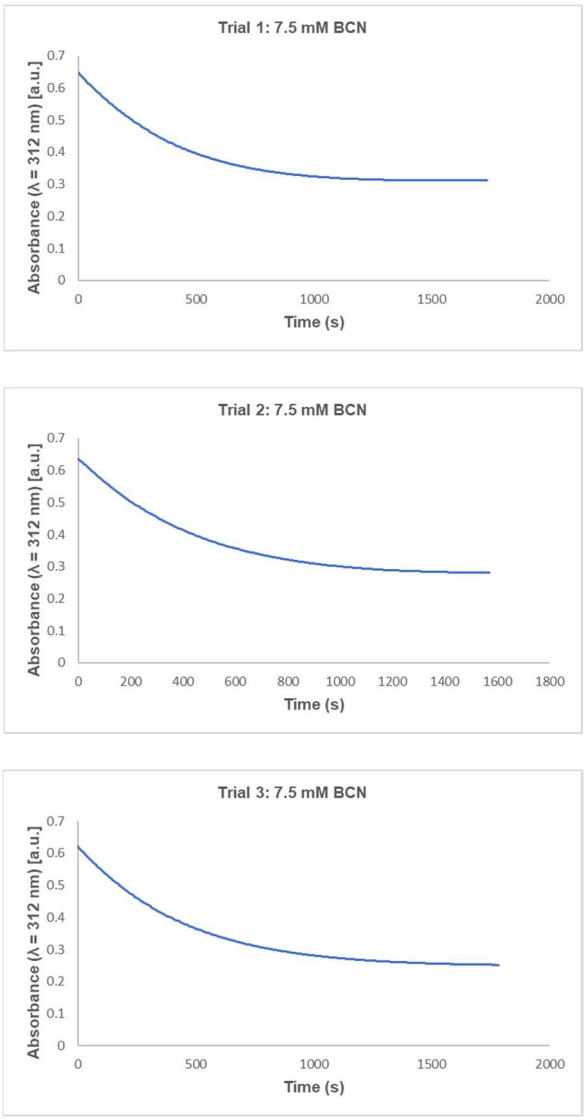

Figure 3.15. **Reaction of TCK and BCN at room temperature and monitored at 312 nm with a BCN concentration of 7.5 mM.**

TCK and BCN were mixed in a quartz cuvette and monitored with UV-Vis spectroscopy following the disappearance of the absorbance of the diene peak at 312 nm. The three observed reaction rate constants were averaged: k_{obs} (s^{-1}) = 0.251 $\times 10^{-2} \pm$ 0.00025.

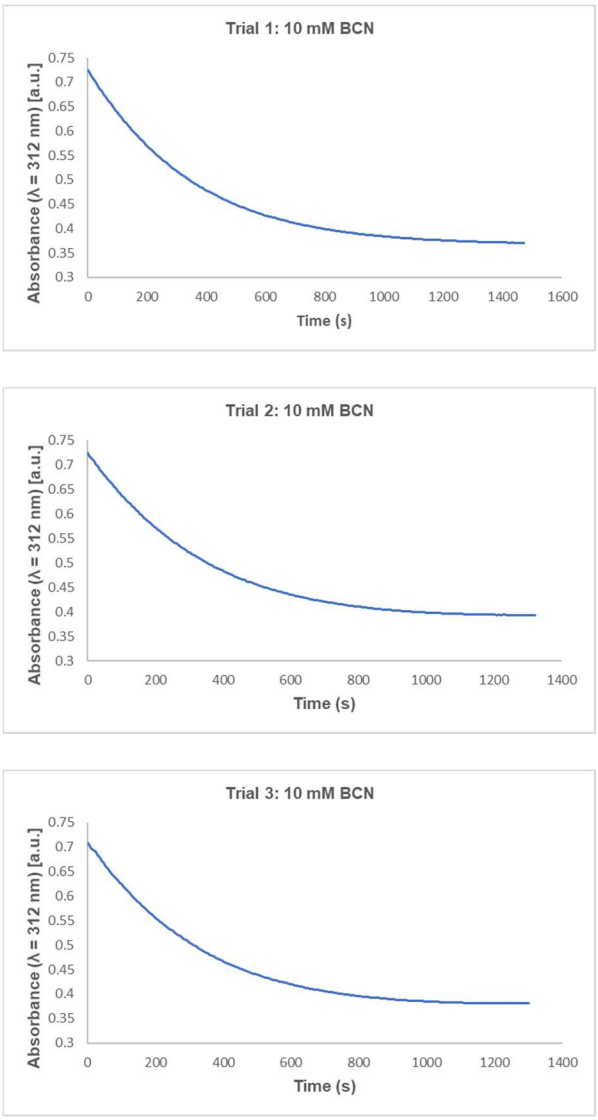

Figure 3.16. **Reaction of TCK and TCO at room temperature and monitored at 312 nm with a BCN concentration of 15 mM.**

TCK and BCN were mixed in a quartz cuvette and monitored with UV-Vis spectroscopy following the disappearance of the absorbance of the diene peak at 312 nm. The three observed reaction rate constants were averaged: k_{obs} (s^{-1}) = 0.315 $\times 10^{-2}$ ± 0.00015.

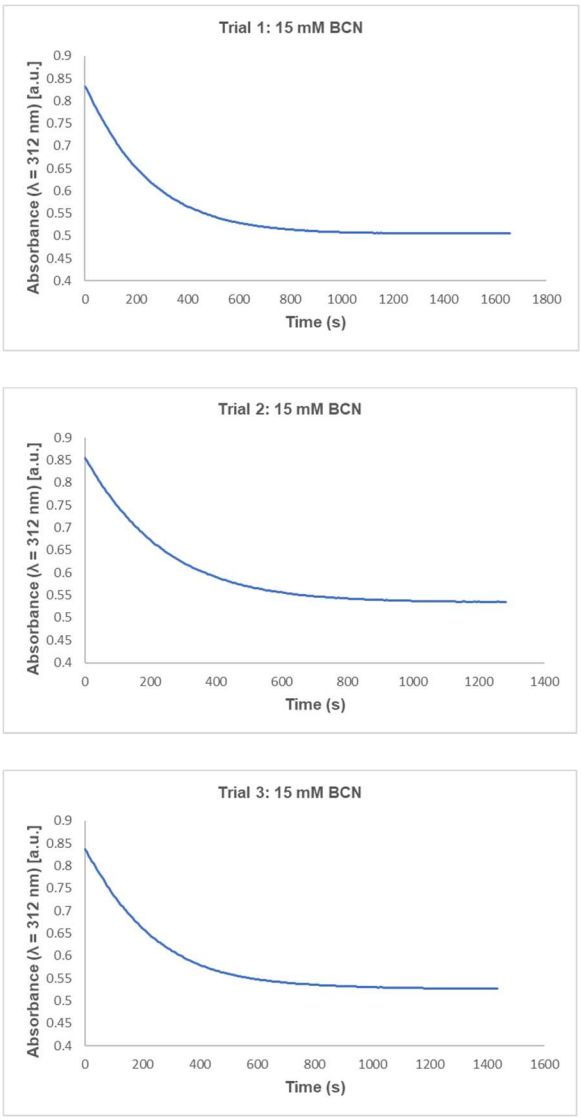

Figure 3.17. **Reaction of TCK and TCO at room temperature and monitored at 312 nm with a BCN concentration of 22.5 mM.**

TCK and BCN were mixed in a quartz cuvette and monitored with UV-Vis spectroscopy following the disappearance of the absorbance of the diene peak at 312 nm. The three observed reaction rate constants were averaged: k_{obs} (s^{-1}) = 0.448 $\times 10^{-2} \pm$ 0.00011.

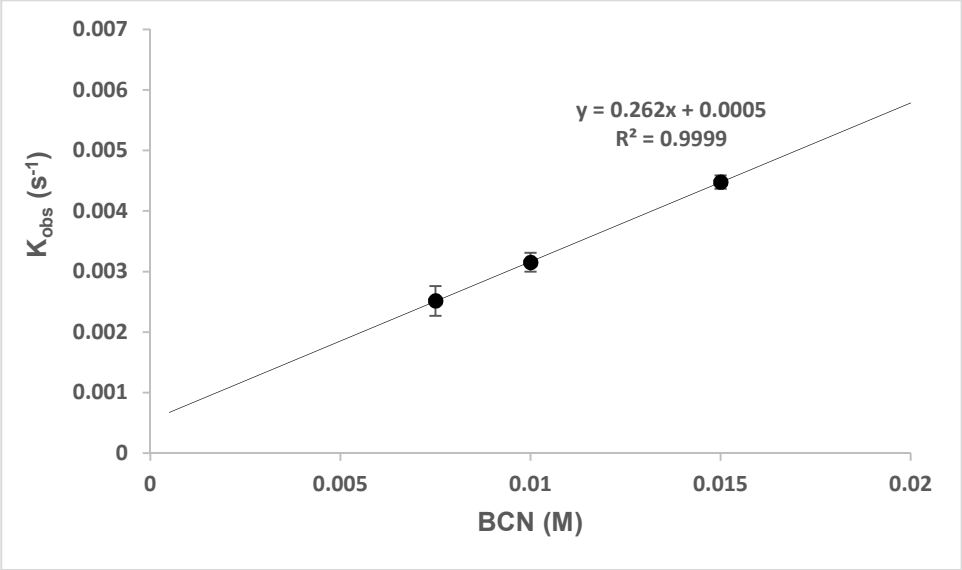

Figure 3.18. **Determination of second-order rate constant, k_2, between TCK and BCN.**

Plot of the average observed rate constants vs. concentration of BCN. The second-order rate constant k_2 is calculated from the slope of the linear regression line. The calculated rate constant for cycloaddition of TCK with BCN in methanol was 0.262 M^{-1} s^{-1}.

3.10 Spectra Relevant to Chapter Three

Readily Accessible Ambiphilic Cyclopentadienes

for Bioorthogonal Labeling

Brian J. Levandowski[†], Raymond F. Gamache[†], Jennifer M. Murphy*, and K. N. Houk*

J. Am. Chem. Soc. **2018***, 140,* 6426 – 6431.

^{1}H NMR

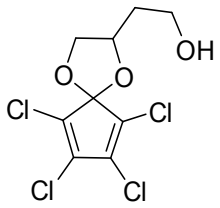
OH
O
O
Cl
Cl
Cl
Cl

3.6

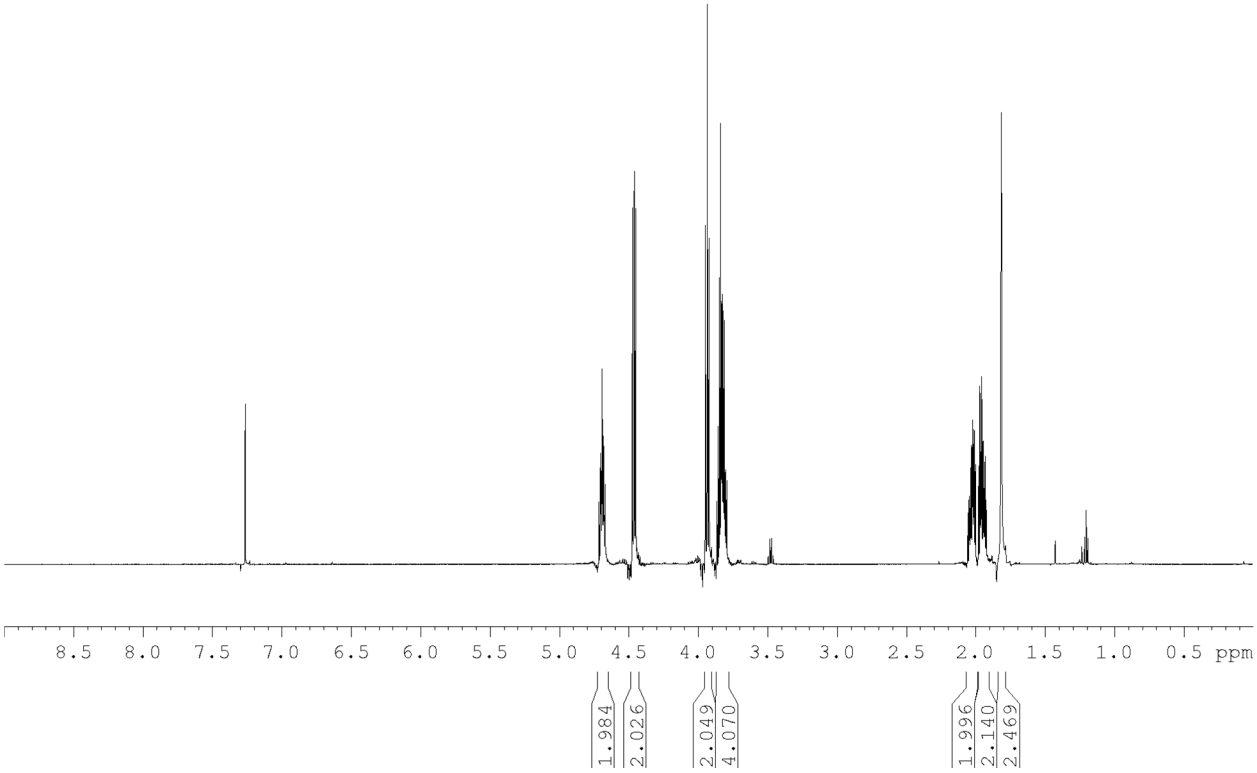
8.5 8.0 7.5 7.0 6.5 6.0 5.5 5.0 4.5 4.0 3.5 3.0 2.5 2.0 1.5 1.0 0.5 ppm
1.984
2.026
2.049
4.070
1.996
2.140
2.469

^{13}C NMR

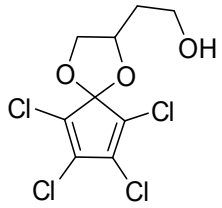
OH
O
O
Cl
Cl
Cl
Cl

3.6

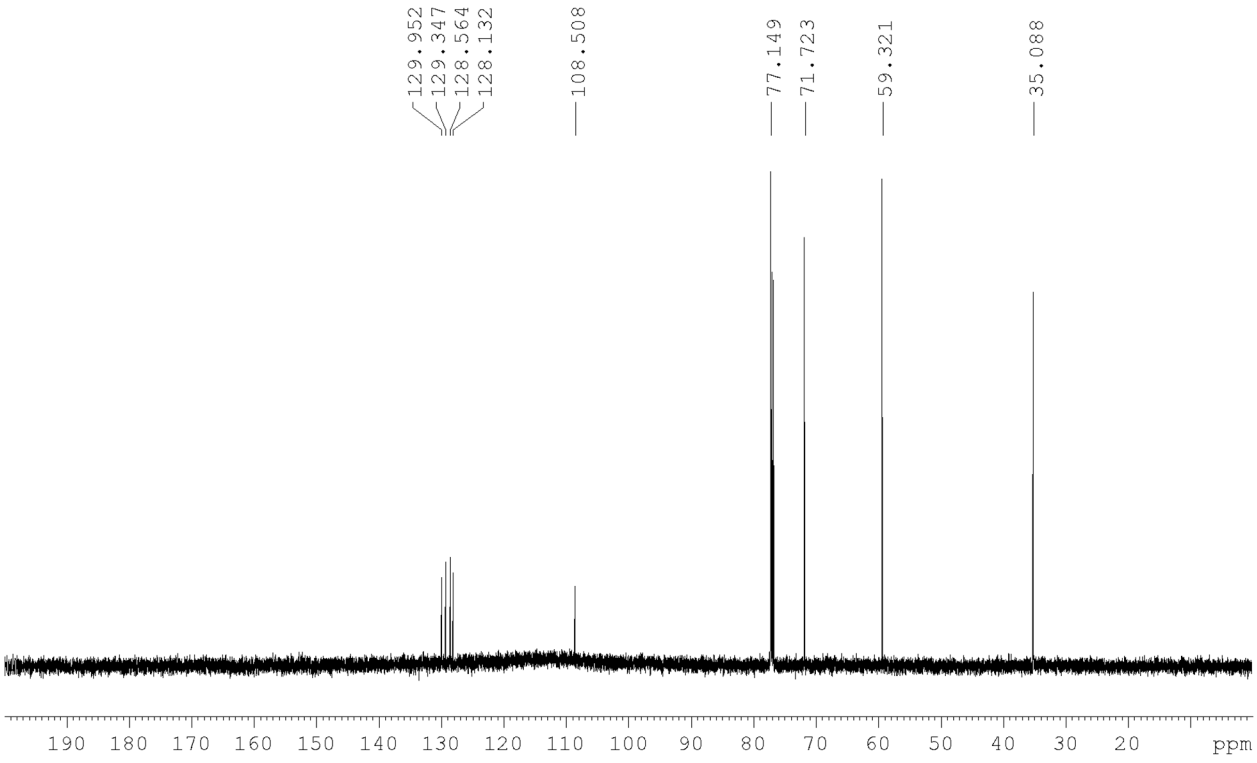
129.952
129.347
128.564
128.132
108.508
77.149
71.723
59.321
35.088
190 180 170 160 150 140 130 120 110 100 90 80 70 60 50 40 30 20 ppm

^{1}H NMR

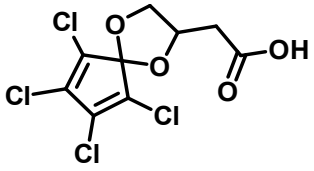
Cl
O
OH
O
Cl
Cl
Cl

3.7

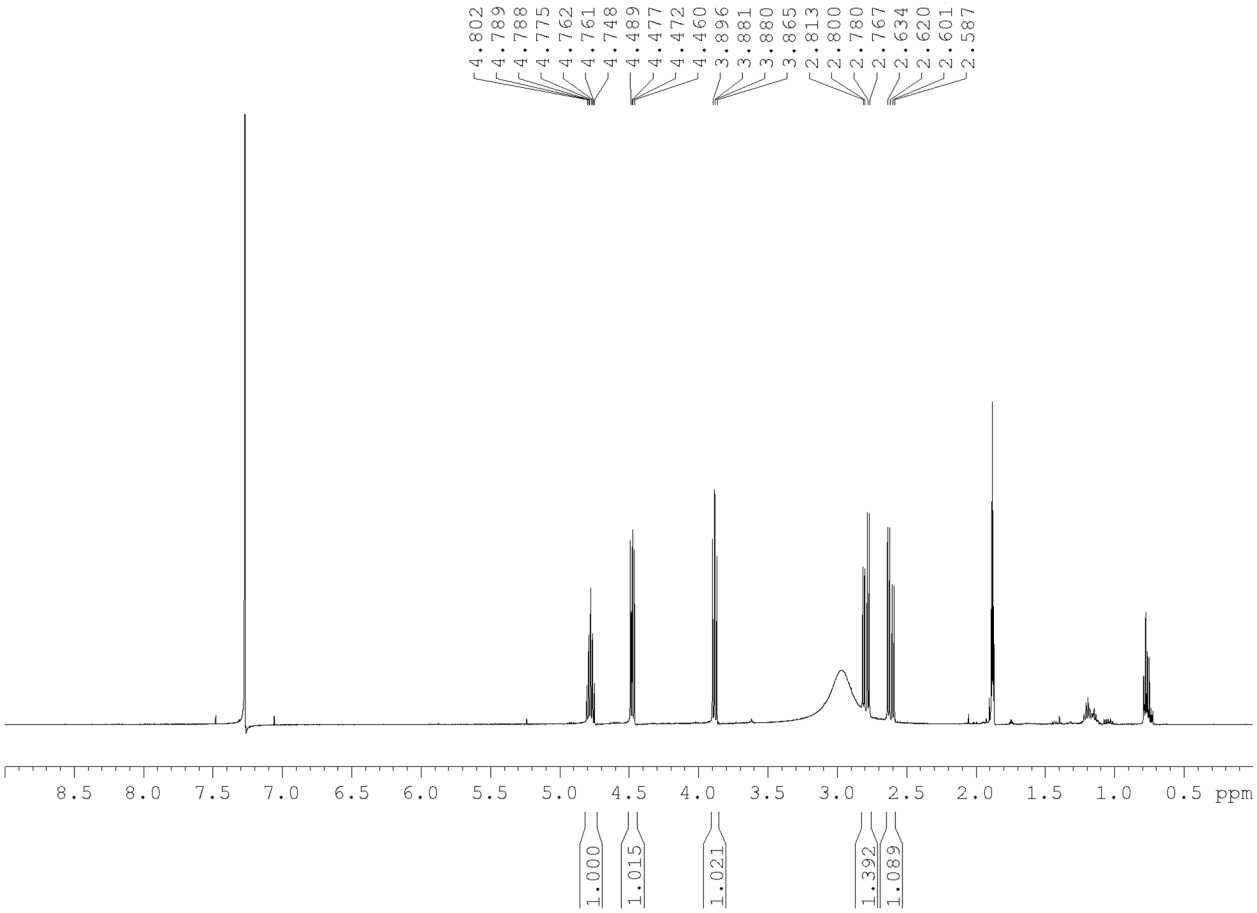
4.802
4.789
4.788
4.775
4.762
4.761
4.748
4.489
4.477
4.472
4.460
3.896
3.881
3.880
3.865
2.813
2.800
2.780
2.767
2.634
2.620
2.601
2.587
8.5 8.0 7.5 7.0 6.5 6.0 5.5 5.0 4.5 4.0 3.5 3.0 2.5 2.0 1.5 1.0 0.5 ppm
1.000
1.015
1.021
1.392
1.089

^{13}C NMR

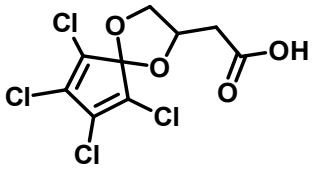
Cl
O
OH
O
Cl
Cl
Cl

3.7

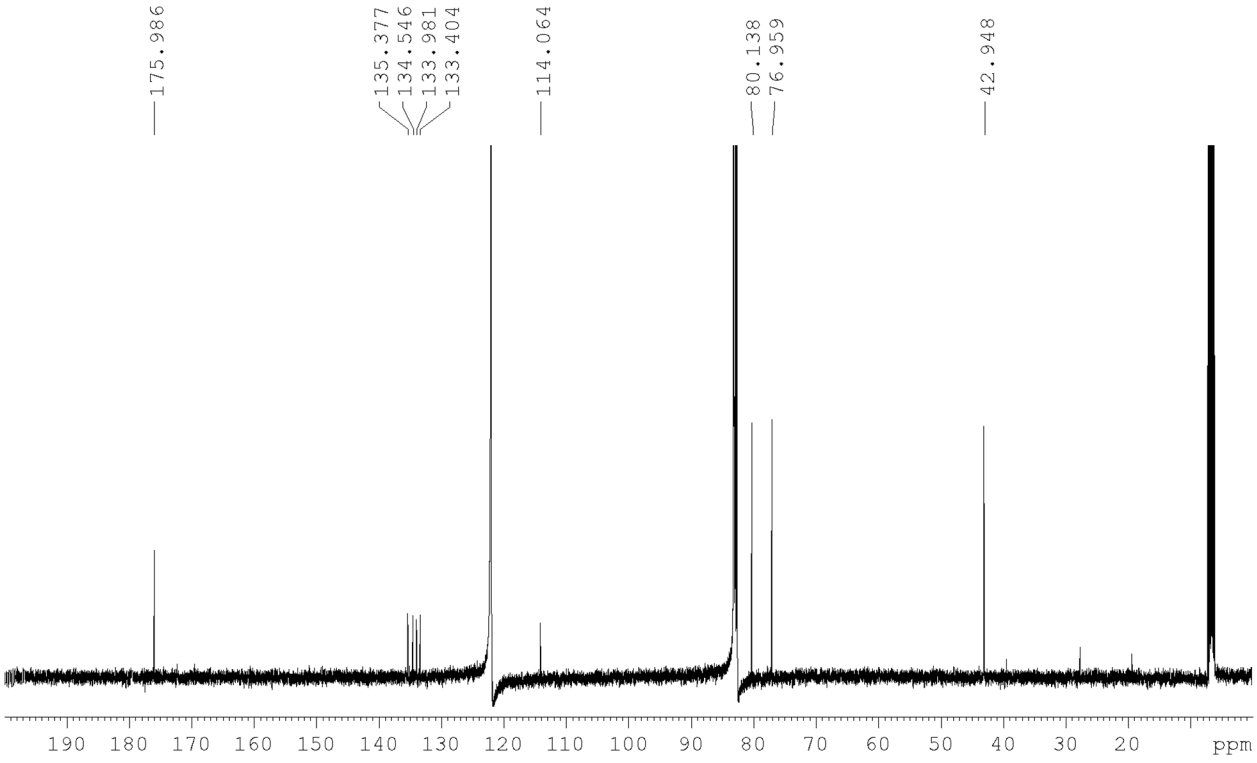
175.986
135.377
134.546
133.981
133.404
114.064
80.138
76.959
42.948
190 180 170 160 150 140 130 120 110 100 90 80 70 60 50 40 30 20 ppm

^{1}H NMR

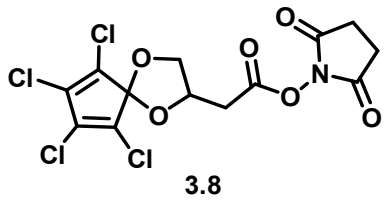
Cl
Cl
Cl
Cl
O
O
O
O
O
N
O

3.8

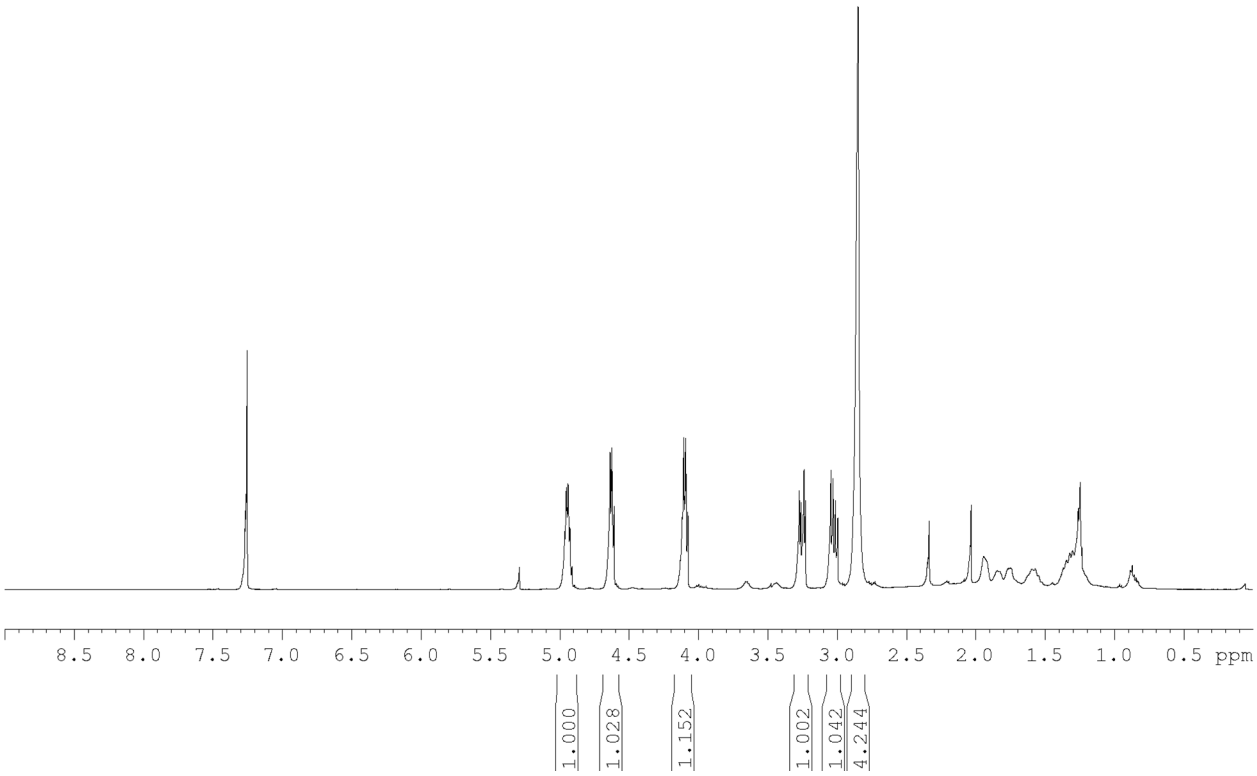
8.5 8.0 7.5 7.0 6.5 6.0 5.5 5.0 4.5 4.0 3.5 3.0 2.5 2.0 1.5 1.0 0.5 ppm
1.000
1.028
1.152
1.002
1.042
4.244

^{13}C NMR

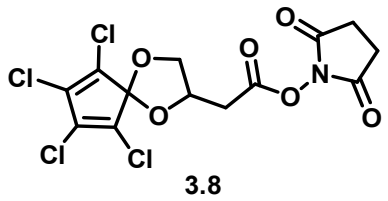
Cl
Cl
Cl
Cl
O
O
O
O
O
N
O

3.8

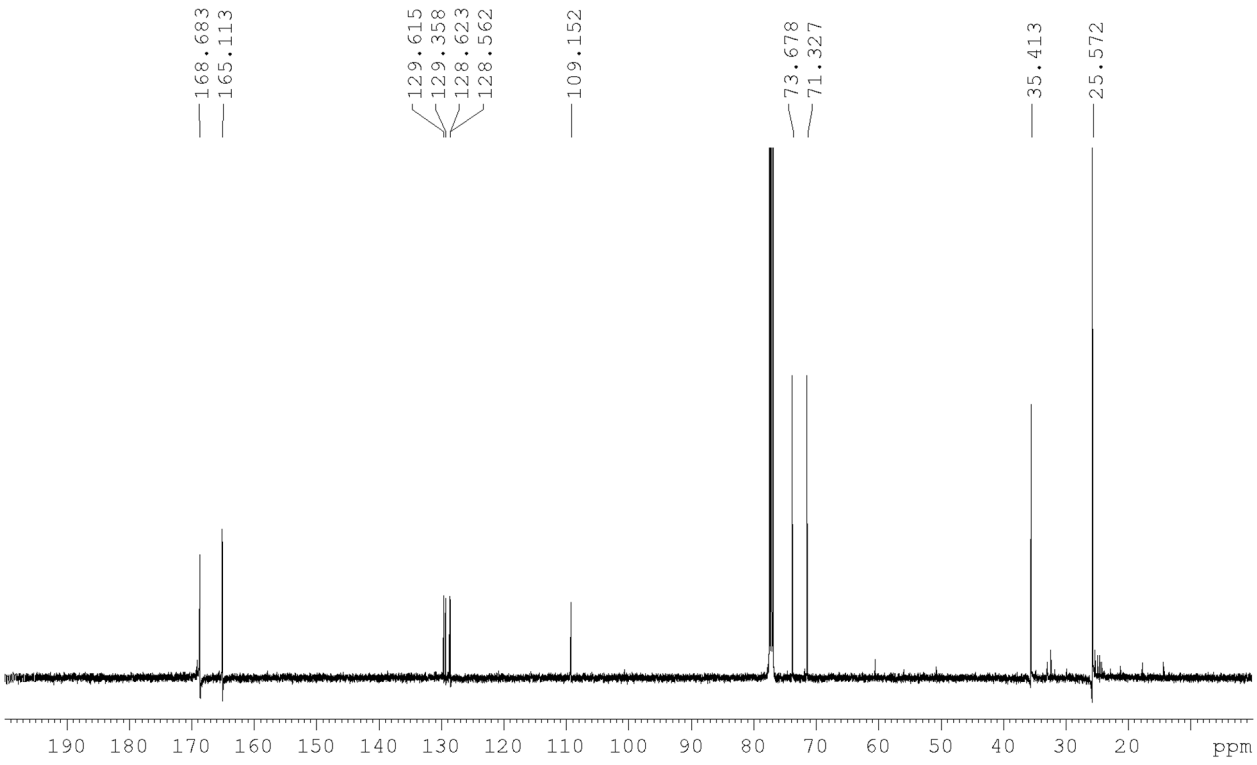
168.683
165.113
129.615
129.358
128.623
128.562
109.152
73.678
71.327
35.413
25.572
190 180 170 160 150 140 130 120 110 100 90 80 70 60 50 40 30 20 ppm

^{1}H NMR

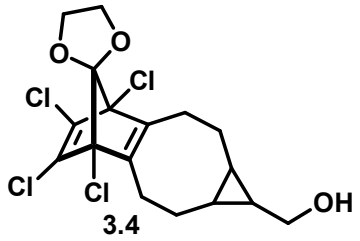
O
O
Cl
Cl
Cl
Cl
OH

3.4

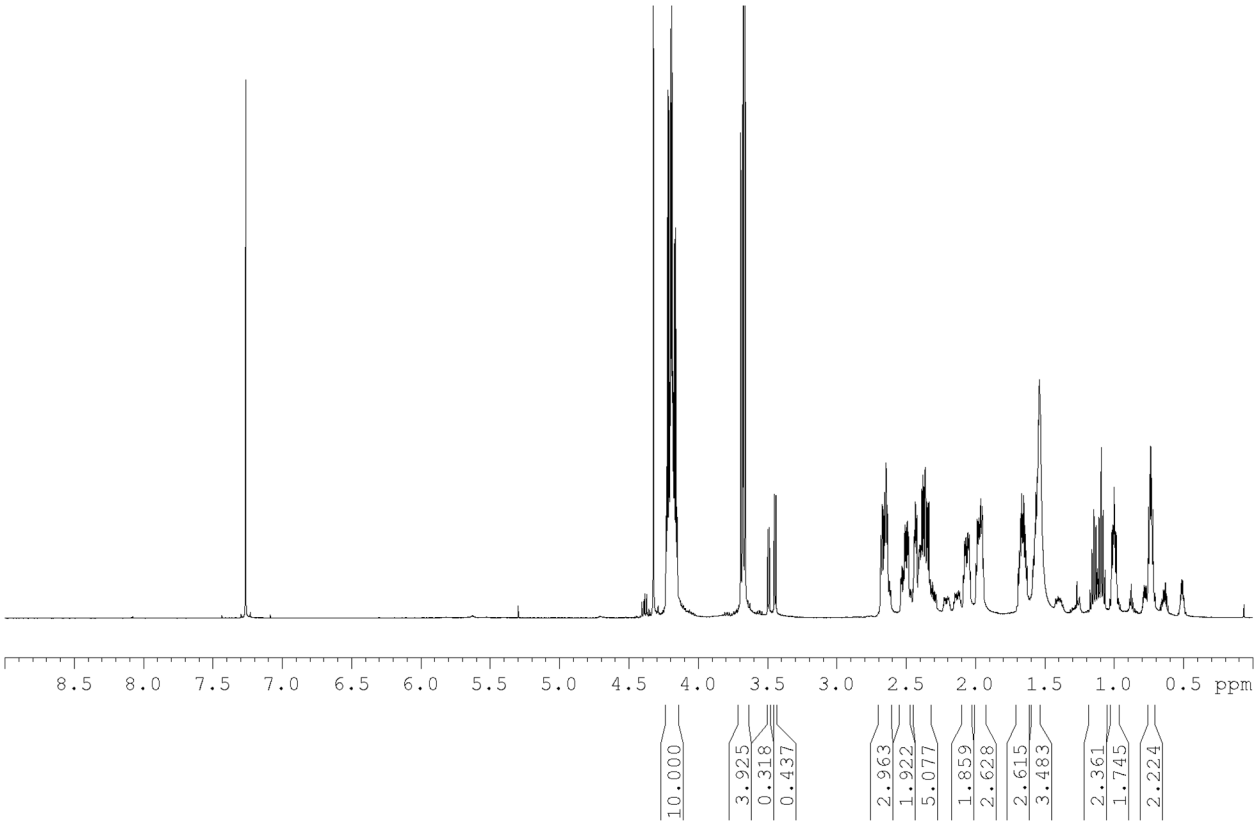
8.5 8.0 7.5 7.0 6.5 6.0 5.5 5.0 4.5 4.0 3.5 3.0 2.5 2.0 1.5 1.0 0.5 ppm
10.000
3.925
0.318
0.437
2.963
1.922
5.077
1.859
2.628
2.615
3.483
2.361
1.745
2.224

^{13}C NMR

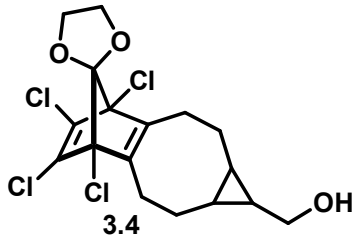
O
O
Cl
Cl
Cl
Cl
OH

3.4

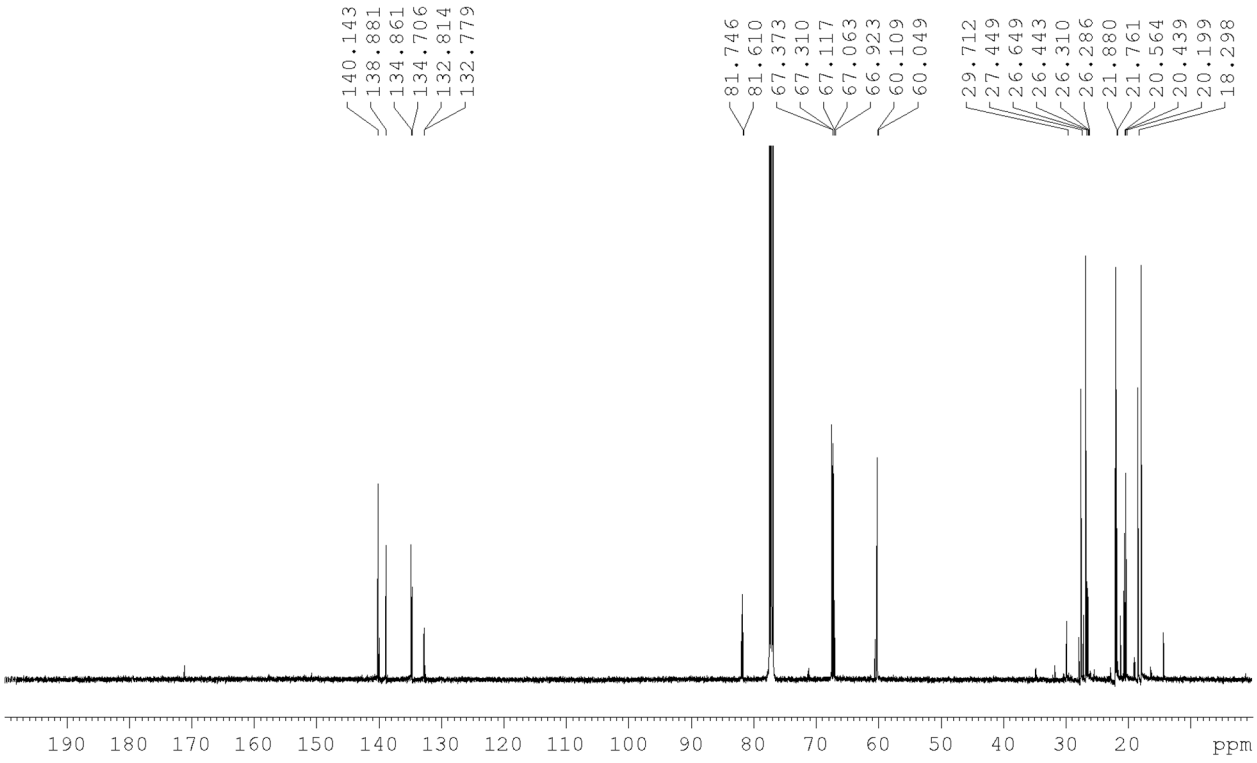
140.143
138.881
134.861
134.706
132.814
132.779
81.746
81.610
67.373
67.310
67.117
67.063
66.923
60.109
60.049
29.712
27.449
26.649
26.443
26.310
26.286
21.880
21.761
20.564
20.439
20.199
18.298
190 180 170 160 150 140 130 120 110 100 90 80 70 60 50 40 30 20 ppm

^{1}H NMR

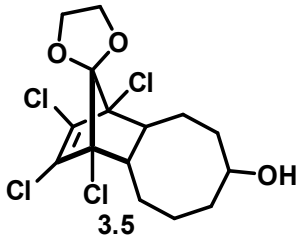
O
O
Cl
Cl
Cl
Cl
OH

3.5

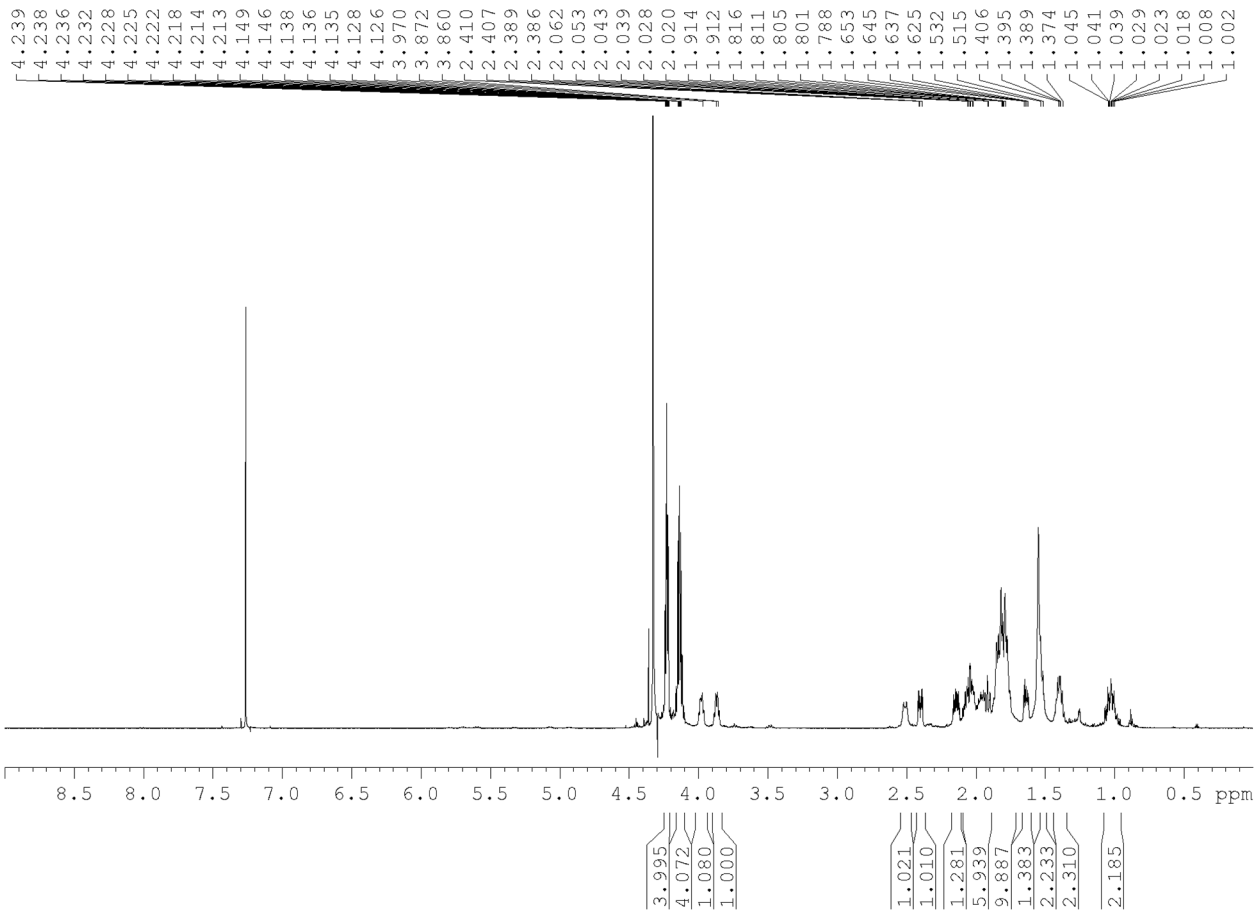
4.239
4.238
4.236
4.232
4.228
4.225
4.222
4.218
4.214
4.213
4.149
4.146
4.138
4.136
4.135
4.128
4.126
3.970
3.872
3.860
2.410
2.407
2.389
2.386
2.062
2.053
2.043
2.039
2.028
2.020
1.914
1.912
1.816
1.811
1.805
1.801
1.788
1.653
1.645
1.637
1.625
1.532
1.515
1.406
1.395
1.389
1.374
1.045
1.041
1.039
1.029
1.023
1.018
1.008
1.002
8.5 8.0 7.5 7.0 6.5 6.0 5.5 5.0 4.5 4.0 3.5 3.0 2.5 2.0 1.5 1.0 0.5 ppm
3.995
4.072
1.080
1.000
1.021
1.010
1.281
5.939
9.887
1.383
2.233
2.310
2.185

^{13}C NMR

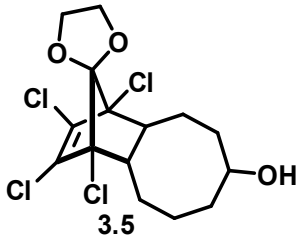
O
O
Cl
Cl
Cl
Cl
OH

3.5

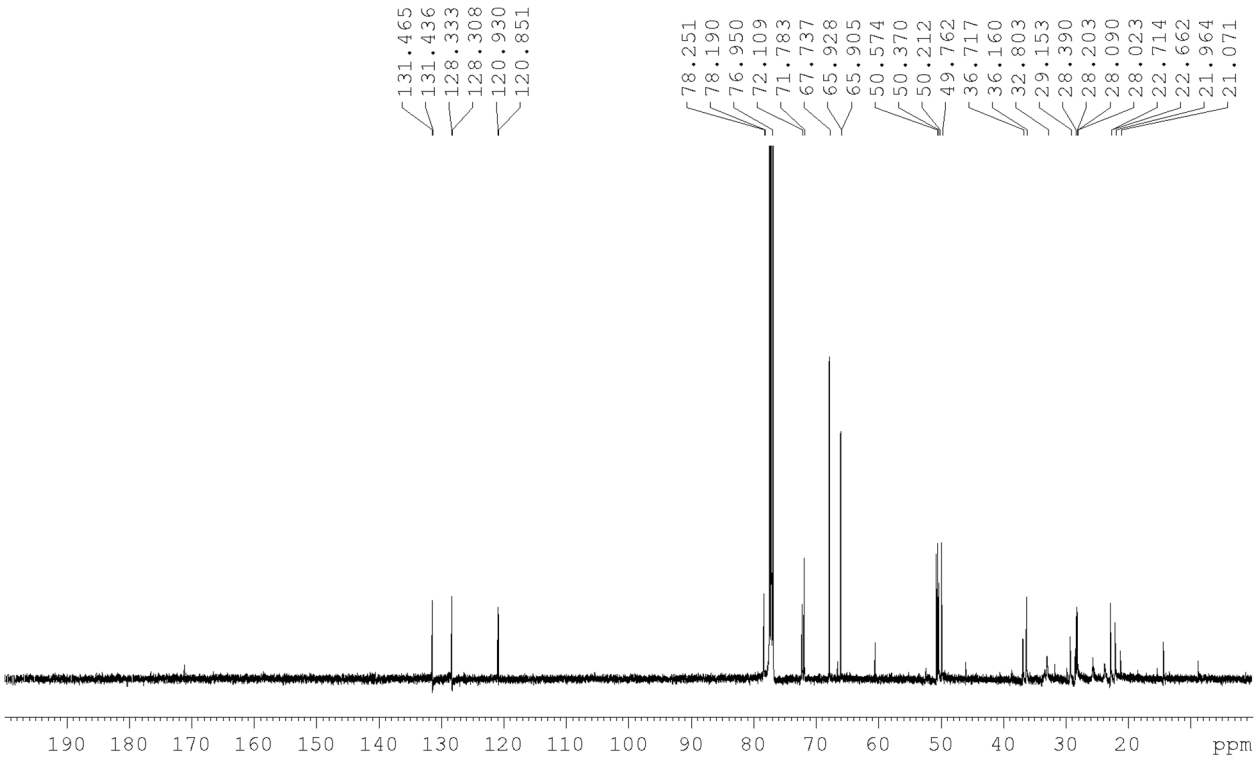
131.465
131.436
128.333
128.308
120.930
120.851
78.251
78.190
76.950
72.109
71.783
67.737
65.928
65.905
50.574
50.370
50.212
49.762
36.717
36.160
32.803
29.153
28.390
28.203
28.090
28.023
22.714
22.662
21.964
21.071
190 180 170 160 150 140 130 120 110 100 90 80 70 60 50 40 30 20 ppm

3.11 Notes and References

(1) Sletten, E. M.; Bertozzi, C. R. *Angew. Chem. Int. Ed.* **2009**, *48*, 6974.

(2) Agard, N. J.; Prescher, J. A.; Bertozzi, C. R. *J. Am. Chem. Soc.* **2004**, *126*, 15046.

(3) Blackman, M. L.; Royzen, M.; Fox, J. M. *J. Am. Chem. Soc.* **2008**, *130*, 13518.

(4) Agard, N. J.; Baskin, J. M.; Prescher, J. A.; Lo, A.; Bertozzi, C. R. *ACS Chem. Biol.* **2006**, *1*, 644.

(5) Baskin, J. M.; Prescher, J. A.; Laughlin, S. T.; Agard, N. J.; Chang, P. V.; Miller, I. A.; Lo, A.; Codelli, J. A.; Bertozzi, C. R. *Proc. Natl. Acad. Sci. U. S. A.* **2007**, *104*, 16793.

(6) Schoenebeck, F.; Ess, D. H.; Jones, G. O.; Houk, K. N. *J. Am. Chem. Soc.* **2009**, *131*, 8121.

(7) Gold, B.; Shevchenko, N. E.; Bonus, N.; Dudley, G. B.; Alabugin, I. V. *J. Org. Chem.* **2012**, *77*, 75.

(8) Ni, R.; Mitsuda, N.; Kashiwagi, T.; Igawa, K.; Tomooka, K. *Angew. Chem. Int. Ed.* **2015**, *54*, 1190.

(9) Burke, E. G.; Gold, B.; Hoang, T. T.; Raines, R. T.; Schomaker, J. M. *J. Am. Chem. Soc.* **2017**, *139*, 8029.

(10) Ning, X.; Guo, J.; Wolfert, M. A.; Boons, G.-J. *Angew. Chem. Int. Ed.* **2008**, *47*, 2253.

(11) Jewett, J. C.; Sletten, E. M.; Bertozzi, C. R. *J. Am. Chem. Soc.* **2010**, *132*, 3688.

(12) Debets, M. F.; van Berkel, S. S.; Schoffelen, S.; Rutjes, F. P. J. T.; van Hest, J. C. M.; van Delft, F. L. *Chem. Commun.* **2010**, *46*, 97.

(13) Dommerholt, J.; Schmidt, S.; Temming, R.; Hendriks, L. J. A.; Rutjes, F. P. J. T.; van Hest, J. C. M.; Lefeber, D. J.; Friedl, P.; van Delft, F. L. *Angew. Chem. Int. Ed.* **2010**, *49*, 9422.

(14) Thalhammer, F.; Wallfahrer, U.; Sauer, J. *Tetrahedron Lett.* **1990**, *31*, 6851.

(15) Sauer, J.; Heldmann, D. K.; Hetzenegger, J.; Krauthan, J.; Sichert, H.; Schuster, J. *Eur. J. Org. Chem.* **1998**, *1998*, 2885.

(16) Chen, W.; Wang, D.; Dai, C.; Hamelberg, D.; Wang, B. *Chem. Commun.* **2012**, *48*, 1736.

(17) Rademacher, P. *Chem. Rev.* **2003**, *103*, 933.

(18) Levandowski, B. J.; Hamlin, T. A.; Bickelhaupt, F. M.; Houk, K. N. *J. Org. Chem.* **2017**, *82*, 8668.

(19) Levandowski, B. J.; Houk, K. N. *J. Am. Chem. Soc.* **2016**, *138*, 16731.

(20) Wang, D.; Chen, W.; Zheng, Y.; Dai, C.; Wang, K.; Ke, B.; Wang, B. *Org. Biomol. Chem.* **2014**, *12*, 3950.

(21) Yang, J.; Šečkutė, J.; Cole, C. M.; Devaraj, N. K. *Angew. Chem. Int. Ed.* **2012**, *51*, 7476.

(22) Patterson, D. M.; Nazarova, L. A.; Xie, B.; Kamber, D. N.; Prescher, J. A. *J. Am. Chem. Soc.* **2012**, *134*, 18638.

(23) Kamber, D. N.; Nazarova, L. A.; Liang, Y.; Lopez, S. A.; Patterson, D. M.; Shih, H.-W.; Houk, K. N.; Prescher, J. A. *J. Am. Chem. Soc.* **2013**, *135*, 13680.

(24) Kamber, D.; Nguyen, S.; Liang, Y.; Liu, F.; Briggs, J.; Shih, H.-. W.; Houk, K. N.; Prescher, J. Isomeric 1,2,4-triazines exhibit distinct profiles of bioorthogonal reactivity. Submitted.

(25) Karver, M. R.; Weissleder, R.; Hilderbrand, S. A. *Angew. Chem. Int. Ed.* **2012**, *51*, 920.

(26) Karver, M. R.; Weissleder, R.; Hilderbrand, S. A. *Bioconjug. Chem.* **2011**, *22*, 2263.

(27) Kamber, D. N.; Liang, Y.; Blizzard, R. J.; Liu, F.; Mehl, R. A.; Houk, K. N.; Prescher, J. A. *J. Am. Chem. Soc.* **2015**, *137*, 8388.

(28) Patterson, D. M.; Nazarova, L. A.; Prescher, J. A. *ACS Chem. Biol.* **2014**, *9*, 592.

(29) McKay, C. S.; Finn, M. G. *Chem. Biol.* **2014**, *21*, 1075.

(30) Diels, O.; Alder, K. *Justus Liebigs Ann. Chem.* **1928**, *460*, 98.

(31) Paquette, L. A.; Wyvratt, M. J. *J. Am. Chem. Soc.* **1974**, *96*, 4671.

(32) Horton, D.; Machinami, T.; Takagi, Y.; Bergmann, C. W.; Christoph, G. C. *J. Chem. Soc. Chem. Commun.* **1983**, No. 20, 1164.

(33) Pang, L. S. K.; Wilson, M. A. *J. Phys. Chem.* **1993**, *97*, 6761.

(34) Bian, S.; Scott, A. M.; Cao, Y.; Liang, Y.; Osuna, S.; Houk, K. N.; Braunschweig, A. B. *J. Am. Chem. Soc.* **2013**, *135*, 9240.

(35) Yousaf, M. N.; Mrksich, M. *J. Am. Chem. Soc.* **1999**, *121*, 4286.

(36) Binger, P.; Wedemann, P.; Goddard, R.; Brinker, U. H. *J. Org. Chem.* **1996**, *61*, 6462.

(37) Wiberg, K. B.; Bartley, W. J. *J. Am. Chem. Soc.* **1960**, *82*, 6375.

(38) Khambata, B. S.; Wassermann, A. *Nature* **1936**, *137*, 496.

(39) Eibler, E.; Burgemeister, T.; Höcht, P.; Prantl, B.; Roßmaier, H.; Schuhbauer, H. M.; Wiest, H.; Sauer, J. *Liebigs Ann./Recl.* **1997**, *1997*, 2451.

(40) Eibler, E.; Höcht, P.; Prantl, B.; Roßmaier, H.; Schuhbauer, H. M.; Wiest, H.; Sauer, J. *Liebigs Ann./Recl.* **1997**, *1997*, 2471.

(41) Nyulászi, L.; Schleyer, P. von R. *J. Am. Chem. Soc.* **1999**, *121*, 6872.

(42) von Ragué Schleyer, P.; Nyulászi, L.; Kárpáti, T. *Eur. J. Org. Chem.* **2003**, *2003*, 1923.

(43) Fernández, I.; Wu, J. I.; Schleyer, P. von R. *Org. Lett.* **2013**, *15*, 2990.

(44) Levandowski, B. J.; Houk, K. N. *J. Org. Chem.* **2015**, *80*, 3530.

(45) Levandowski, B. J.; Zou, L.; Houk, K. N. *J. Comput. Chem.* **2016**, *37*, 117.

(46) Chang, W.-H. *J. Chem. Soc.* **1965**, *0*, 2305.

(47) Zhao, Y.; Truhlar, D. G. *Theor. Chem. Acc.* **2008**, *120*, 215.

(48) Cossi, M.; Rega, N.; Scalmani, G.; Barone, V. *J. Comput. Chem.* **2003**, *24*, 669.

(49) Barone, V.; Cossi, M. *J. Phys. Chem. A* **1998**, *102*, 1995.

(50) Stöckmann, H.; Neves, A. A.; Day, H. A.; Stairs, S.; Brindle, K. M.; Leeper, F. J. *Chem. Commun.* **2011**, *47*, 7203.

(51) Su, T. P. *J. Biomed. Sci.* **2000**, *7*, 195.

(52) Murrey, H. E.; Judkins, J. C.; am Ende, C. W.; Ballard, T. E.; Fang, Y.; Riccardi, K.; Di, L.; Guilmette, E. R.; Schwartz, J. W.; Fox, J. M.; Johnson, D. S. *J. Am. Chem. Soc.* **2015**, *137*, 11461.

(53) Lorenzo, M. M.; Decker, C. G.; Kahveci, M. U.; Paluck, S. J.; Maynard, H. D. *Macromolecules*, **2016**, *49*, 30-37.

(54) Rahul, S.; Mukherjee, S. *Org. Lett.* **2016**, 18, 2305.

CHAPTER FOUR

Development of a Tri-Modal Synthetic Linker Used in the Imaging of PSCA$^+$ Prostate Cancer

Raymond F. Gamache, Kirstin Zettlitz, Wenting Tsai, Anna Wu*, and Jennifer M. Murphy*

4.1 Abstract

Prostate cancer is the most predominant cancer to afflict the male population. Due to the high incidence of this disease, methods to accurately detect, diagnose, and monitor the prostate cancer in its initial stages are of great importance. Immuno-positron emission tomography (ImmunoPET) represents an imaging tool to distinguish tumors from surrounding healthy tissues using a tracer that selectively binds to tumor antigens explicitly expressed on prostate cancer cells. An immunoPET tracer can be joined with a fluorescent probe to provide a dual modality (PET/optical) immunoPET tracer. The PET modality would allow for pre-operative staging while the optical portion would enable intra-operative surgical guidance during tumor resection. The synthesis of a tri-modal linker that is conjugated to a PSCA-targeting cys-diabody which allows for dual PET/NIR imaging of PSCA$^+$ tumors is reported here.

4.2 Introduction

Cancer is the second leading cause of death in the United States.[57] New methods for early detection could drastically lower cancer-related deaths as the highest likelihood of successful treatment is during the initial stages.[58] Not only is early detection difficult, but monitoring disease progression can be challenging as well, especially in the case of solid tumors.[59,60] Of all the cancer

varieties afflicting citizens of the United States, prostate cancer is the leading cancer to affect men.[61]

Molecular imaging is emerging as an essential part of cancer research and clinical care particularly by providing tools for better understanding the biology of disease and its therapeutic modulation. The typical PET tracer used for cancer detection is FDG, which takes advantage of the higher glycolysis rates in cancer cells, which is necessary for their increased replication.[62] Prostate cancer does not fit this mold, however, as it has much lower glycolysis rates. The lower glycolysis rates in prostate cancer prevents the use of FDG as a useful PET tracer for the detection of prostate cancer.[63] Prostate exams and blood tests analyzing prostate-specific antigen (PSA) levels are the typical early tests for this disease. These tests are not the most accurate as there are cases of low PSA count in some prostate cancer patients, typically due to benign prostate hyperplasia.[64] Many groups have looked into new ways of diagnosing this disease particularly by identifying cell surface biomarkers with overexpression in cancerous tissues. For example, prostate specific membrane antigen (PSMA) is a cell surface protein that has several enzymatic functions and is typically up-regulated with androgen deprivation.[65] This antigen is expressed in normal prostate tissue, but is seen in higher quantity with the more aggressive castration resistant prostate cancer.[65] Another biomarker, prostate cancer antigen 3 (PCA3), is a gene produced in much larger quantities in prostate cancer than normal tissue; however, PCR experiments are required to achieve adequate sensitivity for detection.[66,67]

The cancer is typically removed using intraoperative surgery; however, recent evidence shows that surgical excision does not remove all of the tumor when performed in white light. If the surgery is guided by fluorescence, a higher percentage of the cancer is typically removed resulting in a lower risk of reoccurrence due to residual tumor cells being left behind.[68] This

fluorescence-guided surgery approach is made possible by tagging the cancer cells with a NIR fluorescent dye. One method to obtain both the PET imaging and fluorescent imaging of the targeted tumor is through production of a dual-modality tracer, containing a positron emitting isotope and fluorescent dye, that can be attached to a targeted antibody or peptide. ImmunoPET is a powerful tool that can provide non-invasive, quantitative information about specific molecular targets and interactions in living organisms and patients. The high resolution, sensitivity, and quantitative ability of PET in combination with the specificity of tumor-targeting antibodies, make immunoPET an attractive strategy for examining the biology of tumors *in vivo*.

Prostate stem cell antigen (PSCA) is a cell surface antigen overexpressed on prostate cancer tissues as well as a few other cancers but is not typically observed on normal cells.[69] PSCA is known to possess high sensitivity and selectivity, therefore high PSCA expression has become an attractive biomarker to target and exploit for characterization of advance prostate cancer. Prof. Anna Wu's lab at UCLA has engineered cys-diabodies capable of binding with high affinity to PSCA.[70] Their group has previously shown a dual modal cys-diabody capable of targeting PSCA with high specificity;[70] however, the manner at which the proteins were labeled had room for improvement. The fragments were either labeled at two separate sites on the diabody and contained more harmful imaging elements including isotopes such as ^{124}I, which emits more radiation than needed, and can be harmful to the thyroid.[71] Our goal in this project, in collaboration with Prof. Wu's laboratory, was to design and synthesize a universal multifunctional chemical linker which would facilitate labeling of targeting antibody fragments with both a fluorescent dye and a fluorine-18 radioisotope for multimodality imaging. The antibody fragment is conjugated to a chemical linker that contains both a NIR fluorescent dye for optical imaging and a ^{18}F-radioisotope for PET imaging. The combination of PET and optical imaging offers complementary information

beyond what is provided by either method alone. The PET imaging enables a whole-body imaging of localized diseased tissue whereas the fluorescence component may be used for intraoperative staging as a visual guide during surgery. An additional benefit of having both imaging agents on the same linker is that, since its biodistribution is already defined, you could use one tracer for a variety of assays which would simplify regulatory approval of a single agent.

The base of this linker was envisioned to be a lysine residue, which contains three functional handles that could be used in the conjugation of imaging agents and antigen binding compounds. Our group had previously developed a trifunctional chemical linker (Scheme 4.1) to allow rapid imaging of $PSCA^+$ prostate cancer xenografts in nude mice with respectable tumor-to-blood uptake. Linker **4.2** was synthesized through a series of activated ester and acid coupling reactions and contained: a maleimide for site-selective labeling of the diabody through a TCEP reduction of a disulfide, a tetrazine which could react readily with [^{18}F]TCO and a free amine to enable conjugation to a NIR dye for fluorescence guided surgery (Scheme 4.2). While imaging results with the initial linker were promising, a large amount of non-specific retention was present in the gastrointestinal (GI) tract (Figure 4.1). This poses a problem as it would result in a low signal-to noise ratio for targets in the abdominal region. Thus, the synthesis of a multi-modal imaging linker with clearance through the kidneys could make for the easier detection of PSCA expressing cancer.

Scheme 4.1. Retrosynthesis of linker **4.2**, that was used for the dual imaging of PSCA^{+} tumors.

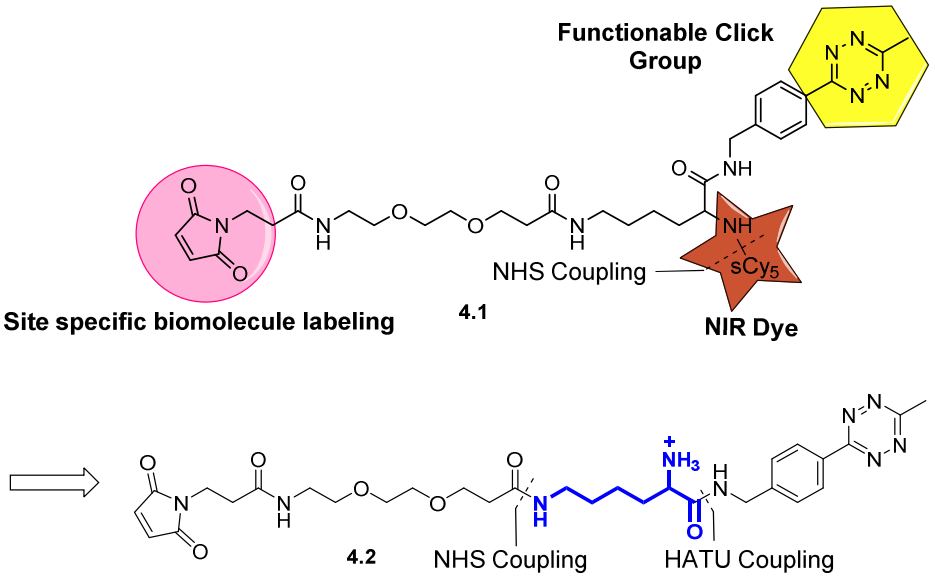

Scheme 4.2. Synthesis and formulation of imaging cys-diabody.

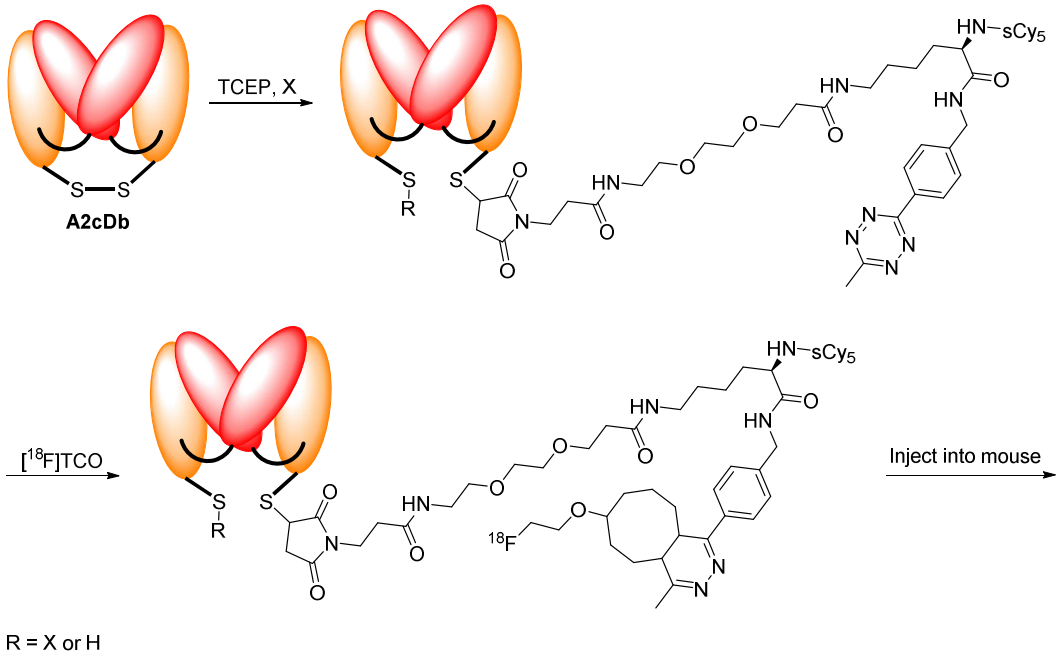

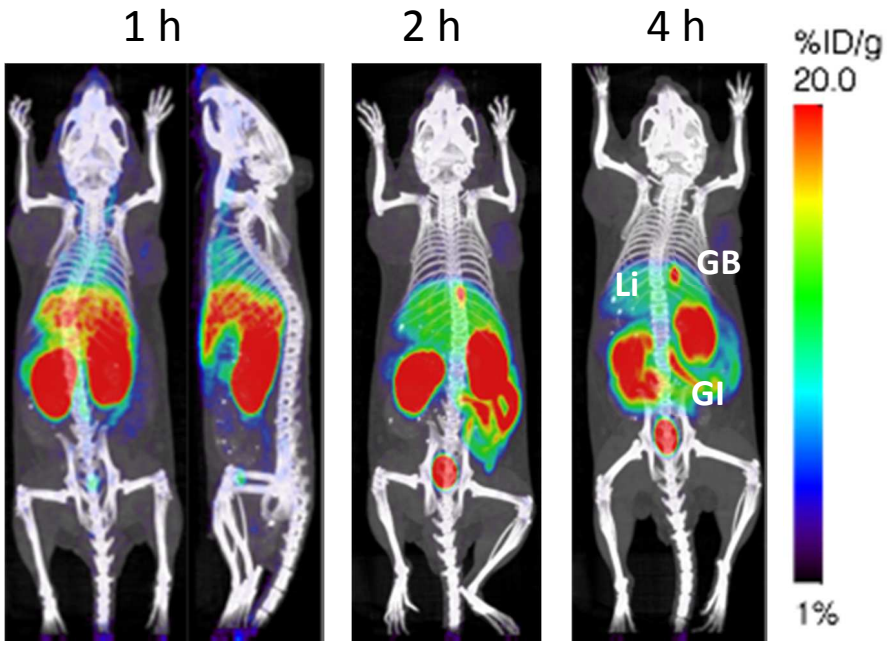

Figure 4.1. Biodistribution of A2cDb conjugated to linker **4.2**. These are male nude mice, with subcutaneous tumors on their left ($PSCA^-$) and right shoulder ($PSCA^+$). (Imaging performed by Dr. Zettlitz)

4.3 Results

The results of the first-generation tracer's biodistribution may have been due to the high lipophilicity. This theory was hypothesized based on the *in vivo* imaging results obtained from antibodies conjugated to DFO and ^{89}Zr. These proteins typically underwent renal clearance and avoided hepatic clearance. The DFO ligand is a highly polar conjugate containing a series of hydroxyl amide functionalities and becomes charged when bound to Zr. Also, of note is the fact that the first-generation tracer initially is cleared through the kidneys during the first hour; however, after two and four hours, larger uptake is seen in the organs associated with the GI tract. The change in uptake is most likely due to the cleavage and break-down of the protein causing metabolites containing ^{18}F to undergo different biodistributions than the initial protein. Breakdown

and cleavage of these proteins is a well-known phenomenon and has been observed before in PET studies when the linker is slightly modified.[72]

We reasoned that boosting the linker's polarity would cause a change in the metabolite clearance from hepatic to renal and generate a more favorable biodistribution. Linker **4.8** was designed to be a second-generation linker, as the inclusion of the DOTA group would significantly increase the polarity and charge of the compound. The linker was synthesized in a similar manner to the previous linker **4.2** (Scheme 4.3). Activated ester coupling of maleimide **4.3** with boc-protected lysine delivered the carboxylic acid **4.4**. An acid coupling of **4.4** with HATU to known tetrazine **4.5** produced bioorthogonal compatible linker **4.6**. Boc deprotection yielding **4.7** was then performed using 4M HCl/dioxane due to the instability of this reaction in the presence of harsher acids, such as TFA. This reaction was low yielding and the HPLC trace of the crude reaction mixture showed the presence of many UV active side products. The final product was obtained from the activated ester coupling using the DOTA-NHS ester and ammonium **4.7** to give the DOTA containing linker **4.8**.

TCEP reduction of the A2cDb cleaves the single disulfide bond present in the protein, enabling the newly formed thiols to react with the maleimide of the linker after overnight incubation. Given that there was a single disulfide in the protein initially; a range of 0-2 linkers per diabody is possible. This small range makes site-selective approaches more amenable as they are less likely to alter the parent protein's binding ability. SDS-PAGE analysis of the conjugation under non-reducing conditions with fluorescent light or Coomassie staining can confirm whether the diabody has any linker attached. The conjugate was acquired with a labeling efficiency of 46.28 and had an immunoreactivity on 22Rv1-PSCA cells of 29%. The [^{18}F]TCO labeled conjugate was purified with a radiochemical purity of 85% and a specific activity of 5.9 μCi/μg.

Scheme 4.3. Synthesis of the DOTA containing PEG linker (**4.8**).

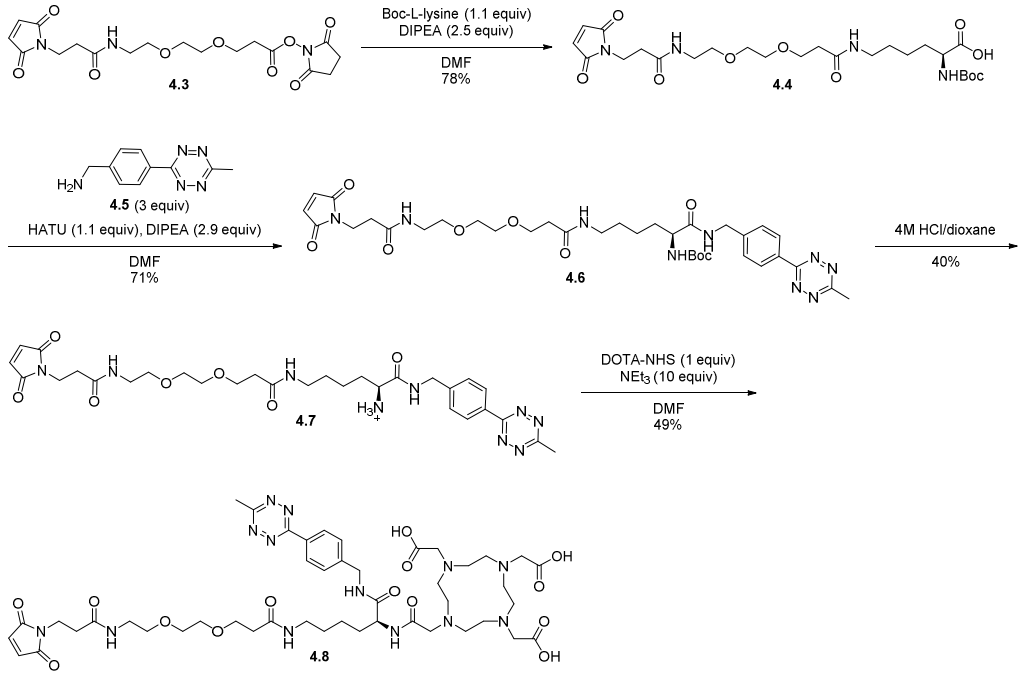

Before pursuing the biodistribution data in the tumor containing mice, we performed microPET/CT studies of the A2cDb DOTA conjugate linker with normal male nude mice. After conjugating the linker **4.8** to the A2cDb and clicking on [^{18}F]TCO, the protein conjugate was applied to the mice through a tail vein injection. The results of this study can be seen in Figure 4.2, demonstrating the *in vivo* biodistribution, and Figure 4.3, showing the *ex vivo* biodistribution. As shown in Figure 4.3 the tracer uptake is now primarily in the kidneys after four hours, which greatly contrasts the results from the previous linkers. The *ex vivo* biodistribution and PET imaging also shows that the linker is metabolized in the kidneys as opposed to the liver.

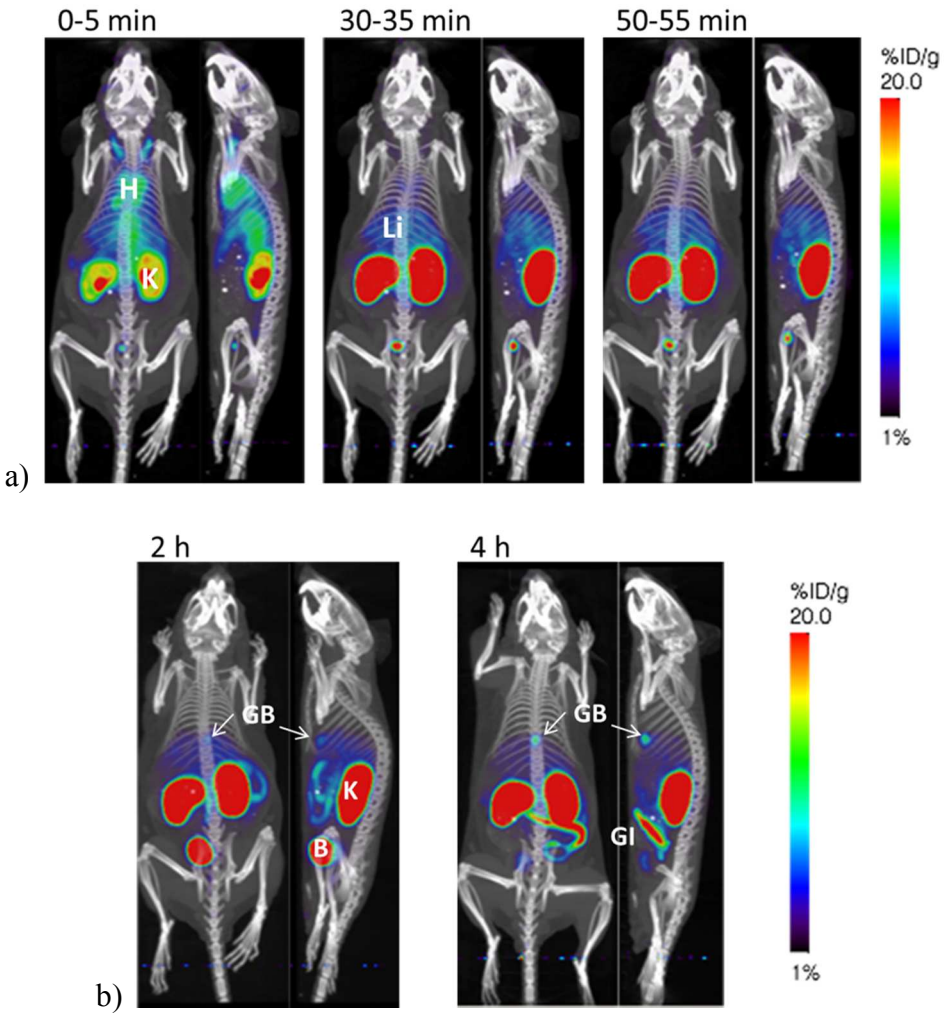

Figure 4.2. A) 1 h dynamic scan, G8 PET/CT, whole body MIP using A2cDb DOTA conjugate linker (**4.8**). B) 10 min static scan, G8 PET/CT, whole body MIP using A2cDb DOTA conjugate linker (**4.8**). (Imaging performed by Dr. Zettlitz)

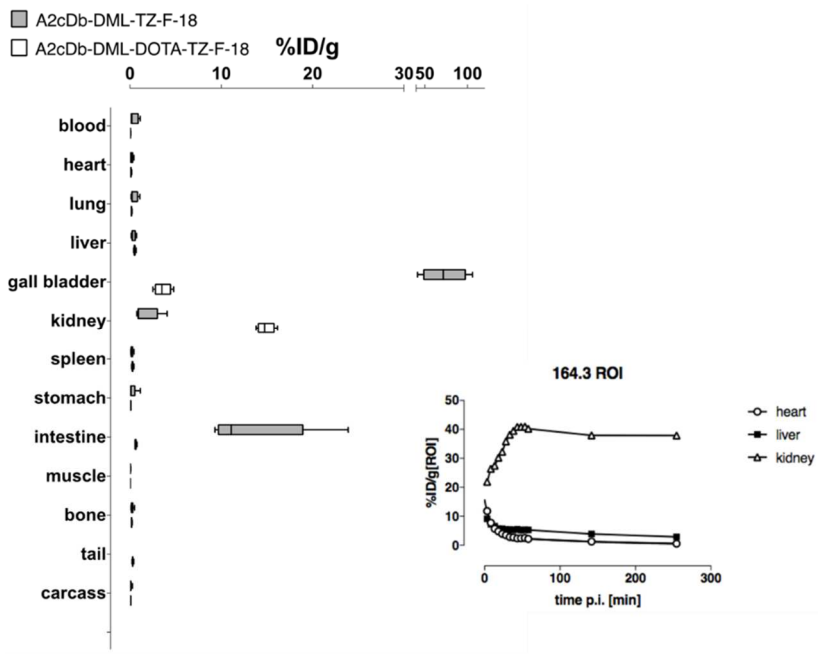

Figure 4.3. *ex vivo* biodistribution of A2cDb DOTA conjugate linker (**4.8**). (Distribution obtained from Prof. Wu's lab)

These promising results led us to pursue imaging studies in male nude mice models containing $PSCA^+$ and $PSCA^-$ tumor xenografts. Our initial study used the tumor model mice and the injection of the A2cDb DOTA linker conjugate after [^{18}F]TCO linkage. The imaging studies as shown in Figures 4.4 and 4.5 demonstrate the valuable change in pharmacokinetics after switching to the new linker. *In vivo* mouse imaging in Figure 4.4 clearly demonstrates the ease of discerning the tumor from background tissue. Figure 4.5 expresses the plotted *ex vivo* biodistribution and makes clear that there is low uptake in the organs associated with the GI tract, and high kidney absorption. The specific numbers of the tracer retention imply that this method could be clinically useful as the positive tumor control to negative tumor control ratio was 7.5 and the positive tumor control to blood uptake was 6.4. Most tracers require ratios over 5.0 for these two studies.

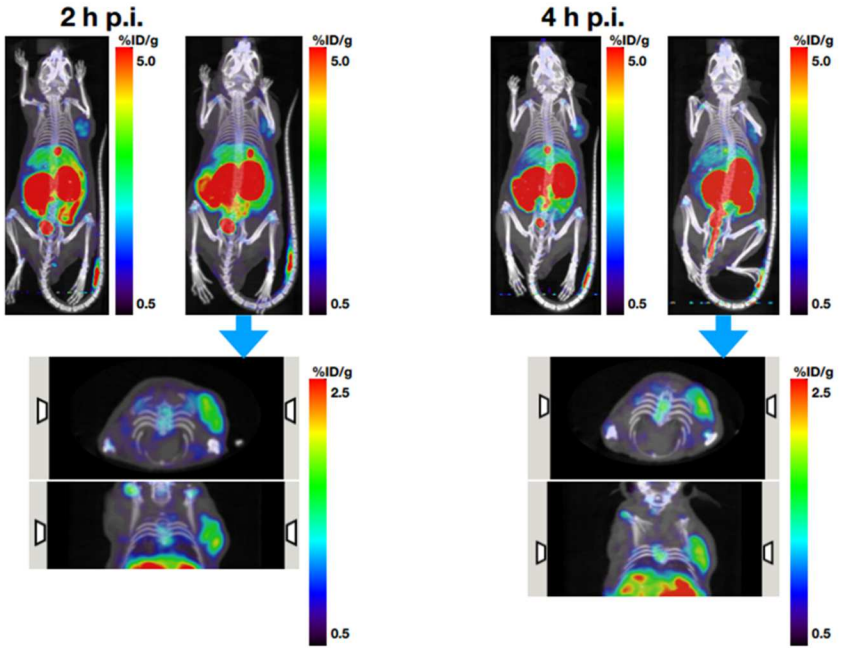

Figure 4.4. A2cDb-DOTA conjugate linkers imaging of male nude mice containing PSCA^{+} and PSCA^{-} tumor xenografts at two and four-hour time points. (Imaging performed by Dr. Zettlitz)

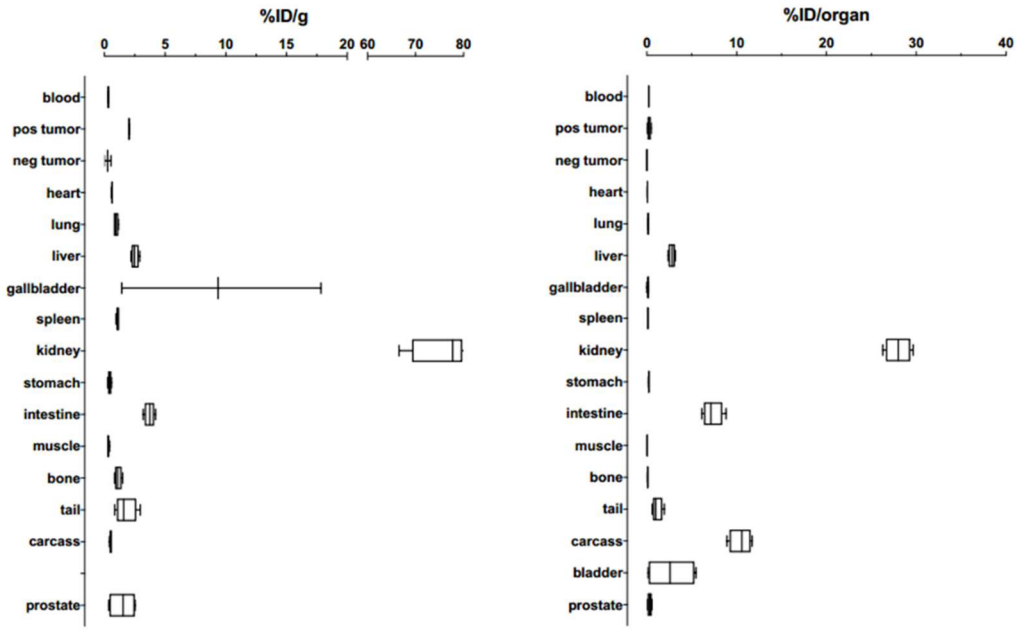

Figure 4.5. *ex vivo* biodistribution of A2cDb DOTA conjugate linker in male nude mice containing PSCA^{+} and PSCA^{-} tumor xenografts. (Distribution obtained from Prof. Wu's lab)

With the initial success of the fluorine-18 studies, we broadened the tracer application by performing different imaging techniques. Investigations of the A2cDb DOTA conjugate linker's potential in intraoperative surgery was evaluated by reacting the conjugate with the TCO-cy5 dye instead of [^{18}F]TCO. Efficient labeling and injection of the fluorescently tagged A2cDb into tumor bearing mice provided evidence that use in surgery is viable (Figure 4.6). 22Rv1-PSCA tumors gave a positive response, except for one tumor, which was smaller and most likely had poor vascularization. The protein linker was then tested with ^{64}Cu, which enabled the antibody fragment to work as both a therapeutic and diagnostic agent due to the ability of this isotope to emit positrons and undergo beta decay. However, this approach gave rise to poor biodistribution and high residual radioactivity in the liver due to ^{64}Cu de-chelation and trapping in the liver (Figure 4.7).

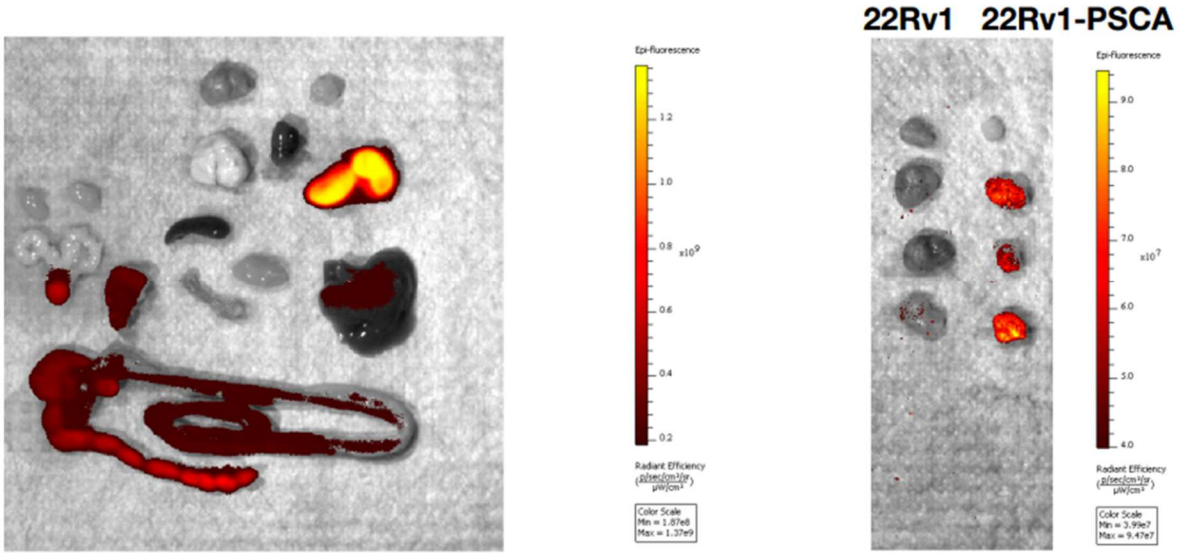

Figure 4.6. *ex vivo* fluorescent imaging using the A2cDb DOTA conjugate linker in male nude mice containing PSCA^{+} and PSCA^{-} tumor xenografts. (Imaging performed by Prof. Wu's lab)

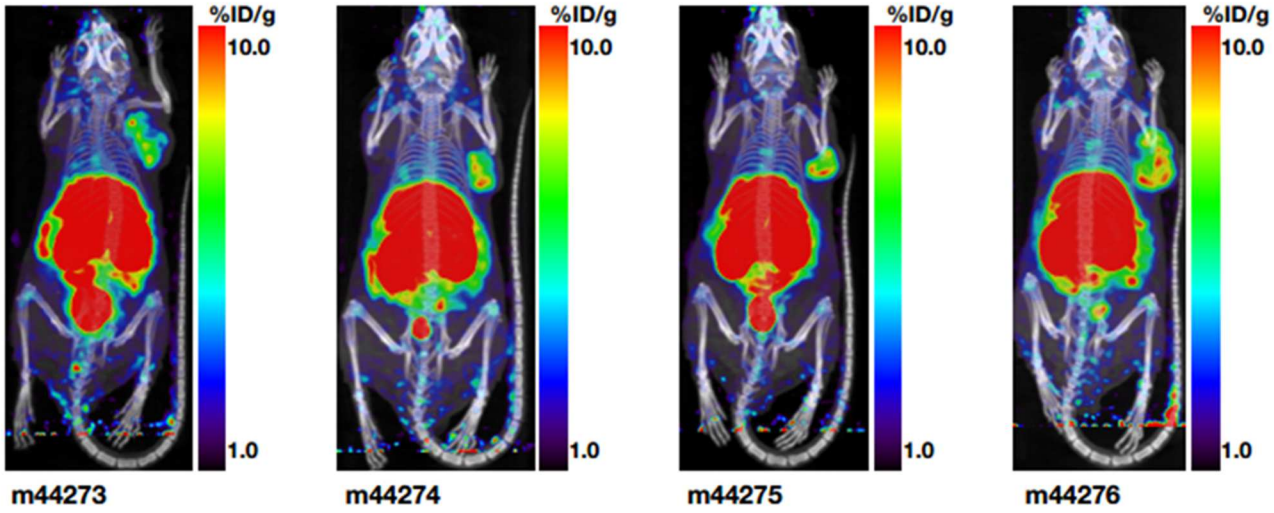

Figure 4.7. PET imaging of male nude mice containing $PSCA^+$ and $PSCA^-$ tumor xenografts using [^{64}Cu]A2cDb DOTA conjugate linker. (Imaging performed by Dr. Zettlitz)

After developing the trifunctional linker and validating that the biodistribution could be significantly optimized via modification of the lipophilicity of the tracer, a new tetra-functional small molecule linker was designed. This linker would incorporate a maleimide, fluorine-18, fluorescent dye and a DOTA functionality. This linker could be conjugated to proteins site selectively through the maleimide group reacting with a cysteine residue. The fluorine-18 would act as a positron emitting isotope for PET imaging, while the fluorescent dye would aid in intraoperative surgery. Therapeutic isotopes such as lutetium-177 and copper-64 could be chelated to the DOTA group enabling therapeutic potential. Synthesis of the envisioned linker **4.13** is shown in Scheme 4.4. Starting from tert-butyl DOTA **4.9,** an activated ester coupling can be performed with N-boc-lysine and base to give carboxylic acid **4.10**. Acid **4.10** can be used in a HATU mediated acid coupling with previous intermediate **4.5** delivering tetrazine **4.11**. Global acid deprotection of **4.11** with TFA will remove the N-boc protecting group and tert-butyl functionalities yielding ammonium salt **4.12**. With the incorporation of maleimide, click group,

and chelator, the last step of NIR dye incorporation was performed through the addition of the activated ester analog of the sCy5 dye producing the tetra functional small molecule **4.13**. Conjugation to the cys-diabody proceeded well with a linker-to-protein ratio of 0.62 with a labeling efficiency of 62.9, specific activity of 16.3 μCi/μg, radiochemical purity of 98.9%, and immunoreactivity of 57.3%. Imaging of the mouse with the tetra-functional linker displays slightly higher uptake in the GI associated organs but retains contrast between the $PSCA^+$ and $PSCA^-$ tumors (Figures 4.8 and 4.9).

Scheme 4.4. Synthesis of tetra functional linker **4.13**.

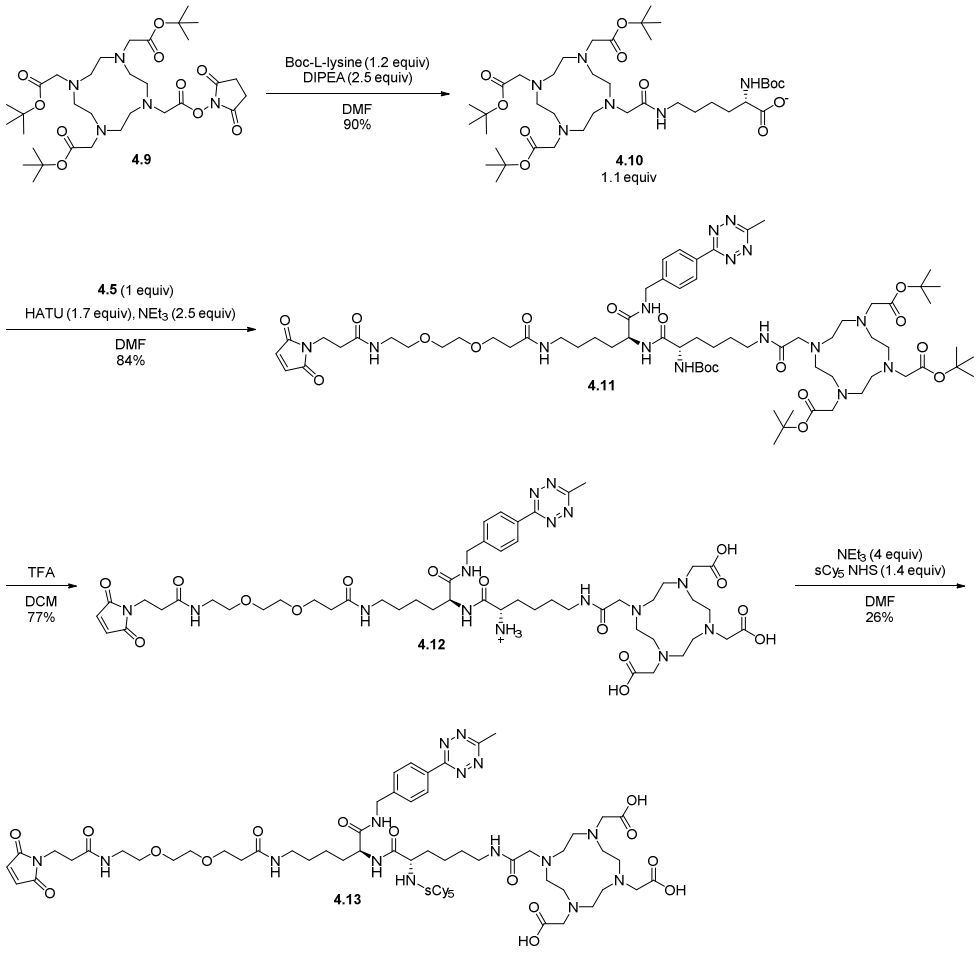

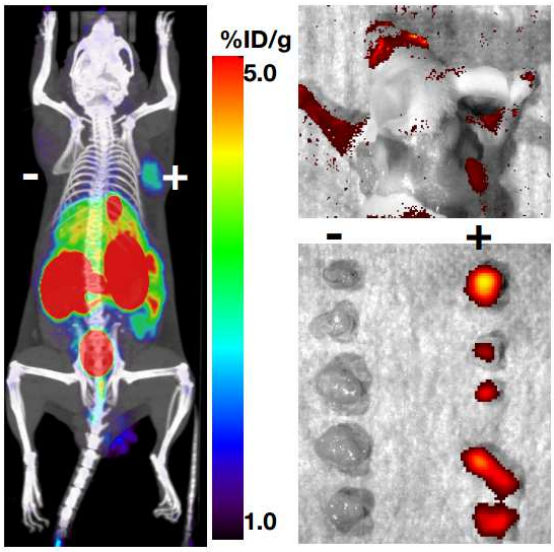

Figure 4.8. Dual-modality immunoPET/NIRF imaging using A2cDb-TFL-sCy5-18F provides both non-invasive whole body imaging to localize PSCA-positive prostate cancer and fluorescent imaging for surgical guidance. (Imaging performed by Dr. Zettlitz)

4.4 Conclusion

In conclusion a new series of multi-functional DOTA containing synthetic linkers have been synthesized for use in biomolecule conjugation. These small molecules contain maleimides for site-selective modifications and have positron emitting isotope incorporation enabling PET imaging as well as fluorescent dyes to aid in intraoperative surgical removal of targeted tissue. Proof of concept was shown through integration of the linker onto an A2cDb that had been engineered to target PSCA. The DOTA containing linkers avoided the GI tract and had most off-site uptake in the kidneys. Success of the tri-functional DOTA conjugates led to the synthesis of a tetra-functional linker that was able to show sharp contrast between the $PSCA^+$ and $PSCA^-$ tumors while still maintaining higher clearance through the kidneys. The tetra-functional linker could

undergo simultaneous fluorine-18 PET and fluorescence imaging, while allowing possible chelation to therapeutic isotopes for cancer treatment.

4.5 Experimental

4.5.1 Materials and Methods

NMR spectra were obtained on a Bruker AV300 (300 MHz for ^{1}H; 282 MHz for ^{19}F), a Bruker AV500 (500 MHz for ^{1}H; 125 MHz for ^{13}C), and a Bruker AV600 (600 MHz for ^{1}H; 150 MHz for ^{13}C). ^{1}H and ^{13}C chemical shifts are reported in parts per million (ppm) using the solvent resonance as an internal reference. The coupling constants, *J*, are reported in Hertz (Hz), and the multiplicity are reported as follows: singlet (s), broad single (br s) doublet (d), triplet (t), quartet (q), pentet (p), and multiplet (m). High-resolution mass spectrometry data were collected with a Waters LCT Premier XE time-of-flight instrument controlled by MassLynx 4.1 software or obtained on a Thermo Scientific™ Exactive Mass Spectrometer with DART ID-CUBE. Samples were dissolved in methanol and infused using direct loop injection from a Waters Acquity UPLC into the Multi-Mode Ionization source. HPLC purifications were performed on a Knauer Smartline HPLC system with inline Knauer UV (254 nm) detector. Semi-preprative HPLC was performed using Phenomenex reverse-phase Luna column (10 × 250 mm, 5 μm) with a flow rate of 4 mL/min. Final purity of compounds was determined by analytical HPLC analysis performed with a Phenomenex reverse-phase Luna column (4.6 × 250 mm, 5 μm) with a flow rate of 1 mL/min. Compounds were identified by UV absorbance at 254 nm. All chromatograms were collected by a GinaStar (raytest USA, Inc.; Wilmington, NC, USA) analog to digital converter and GinaStar software (raytest USA, Inc.). All deuterated solvents were purchased from Cambridge Isotope Laboratories. Anhydrous solvents were obtained by filtration through activated alumina columns unless indicated otherwise. Solvents used for extractions and chromatography were not anhydrous. Reactions and chromatography fractions were analyzed by thin-layer chromatography (TLC) using Merck precoated silica gel 60 F_{254} glass plates (250 μm) and visualized by ultraviolet

irradiation, potassium permanganate stain, and phosphomolybdic acid. Flash column chromatography was performed using E. Merck silica gel 60 (230−400 mesh) with compressed air. DOTA-NHS (catalog # B-280) and DOTA *t*-Bu-NHS (catalog # B-270) were purchased from macrocyclics. Mal-amido-PEG2-NHS (catalog # BP-22156) was purchased from Broadpharm. Cy5-TCO was purchased from Click Chemistry Tools (catalog # 1089-1) and used as received. TCO was synthesized according to literature procedure.[73] Tetrazine **4.5** was synthesized according to a previous literature procedure.[74] [^{18}F]TCO was synthesized and formulated according to a previous literature procedure.[75] Dr. Kirstin Zettlitz performed and optimized all the cys-diabody conjugations to linkers **4.8** and **4.13**, chelated the copper-64 to the **4.8** for imaging, reacted the A2cDb conjugates with [^{18}F]TCO, and performed all the tail vein injections. Dr. Zettlitz also operated the imaging software to format the PET and fluorescence images. Dr. Zettlitz and Wenting Tsai performed the dissections and obtained the *ex vivo* biodistribution.

4.5.2 Experimental Procedures

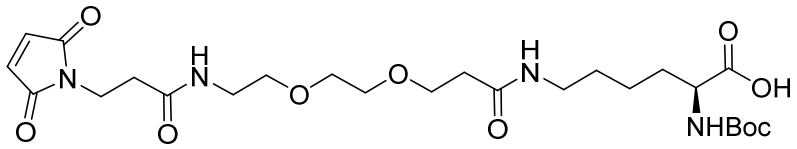

(*S*)-19-((tert-butoxycarbonyl)amino)-1-(2,5-dioxo-2,5-dihydro-1*H*-pyrrol-1-yl)-3,13-dioxo-7,10-dioxa-4,14-diazaicosan-20-oic acid (4.4). A 10 mL round bottom flask equipped with a stir bar and filled with argon was charged with α-Boc-L-lysine (61 mg, 0.248 mmol, 1.1 equiv) and dry DMF (1 mL). To this, *N*,*N*-diisopropylethylamine (86 µL, 0.495 mmol, 2.5 equiv) was added and the mixture was stirred at room temperature for 1 h. Malamido-PEG2-NHS (100 mg, 0.23 mmol, 1.0 equiv) then was then added. The reaction mixture was stirred at room temperature until full consumption of starting materials was indicated by TLC. DMF was removed under reduced

pressure and the crude mixture subjected to flash column chromatography on silica gel (5% MeOH in DCM --> 10% MeOH in DCM) to give 100 mg of the desired product in form of a colorless oil (78%). Stored under argon at -20°C. **^{1}H NMR** (400 MHz, Chloroform-*d*) δ 7.55 (bs, 1H), 6.99 (s, 1H), 6.75 (s, 1H), 6.67 (s, 2H), 5.78 – 5.35 (m, 1H), 4.27 – 3.99 (m, 1H), 3.77 (t, *J* = 7.2 Hz, 2H), 3.70 (t, *J* = 5.8 Hz, 2H), 3.60 – 3.53 (m, 4H), 3.50 (t, *J* = 5.2 Hz, 2H), 3.35 (dd, *J* = 10.4, 5.2 Hz, 2H), 3.19 (dd, *J* = 12.4, 6.3 Hz, 2H), 2.51 (t, *J* = 7.2 Hz, 2H), 2.43 (t, *J* = 5.8 Hz, 2H), 1.86 – 1.72 (m, 1H), 1.71 – 1.59 (m, 1H), 1.56 – 1.43 (m, 2H), 1.41– 1.30 (m, 2H), 1.38 (s, 9H). **^{13}C NMR** (101 MHz, $CDCl_3$) δ 174.71, 172.14, 170.75, 170.64, 155.80, 134.30, 79.85, 70.01, 69.98, 69.58, 67.11, 53.24, 50.38, 39.25, 39.15, 36.80, 34.56, 34.43, 32.00, 28.81, 28.39, 22.44.

ESI(+)-MS: calcd. for $C_{25}H_{40}N_4O_{10} + H^+$, 557.2817; found 557.2847

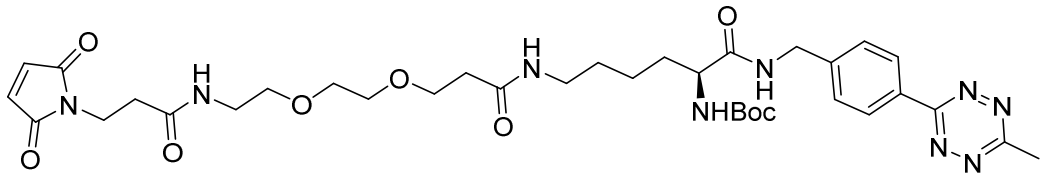

Tert-butyl (*S*)-(22-(2,5-dioxo-2,5-dihydro-1*H*-pyrrol-1-yl)-1-(4-(6-methyl-1,2,4,5-tetrazin-3-yl)phenyl)-3,10,20-trioxo-13,16-dioxa-2,9,19-triazadocosan-4-yl)carbamate (4.6). To a solution of **4.4** (60 mg, 108 µmol, 1.0 equiv) in DMF (1.2 mL) was added HATU (46 mg, 119 µmol, 1.1 equiv) and the mixture was stirred for 10 min at room temperature. To this, a solution (not completely dissolved) of tetrazine **4.5** (76 mg, 319 µmol, 2.96 equiv) in DMF (1.5 mL) was added and the mixture was stirred for another 20 min. After addition of *N*,*N*-diisopropylethylamine (54 µL, 313 µmol, 2.9 equiv), the mixture was stirred at room temperature for 36 hours. DMF was removed under reduced pressure and the crude mixture was subjected to flash column chromatography on silica gel (0% to 10% MeOH in DCM) to give 49 mg (71%) of a deep purple

oil. The compound readily decomposes in $CHCl_3$-d, ACN-d3, and MeOH-d4, and hence we can no clean NMR.

ESI(+)-MS: calcd. for $C_{35}H_{49}N_9O_9 + H^+$, 762.3545; found 762.3546

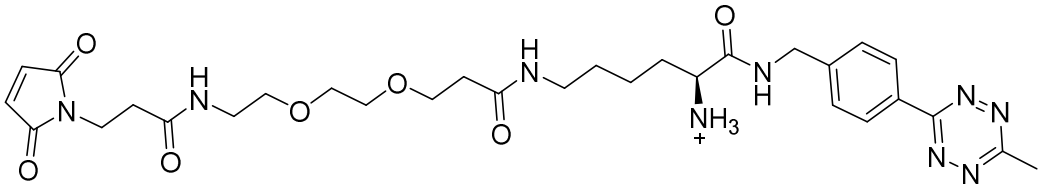

(*S*)-22-(2,5-Dioxo-2,5-dihydro-1*H*-pyrrol-1-yl)-1-(4-(6-methyl-1,2,4,5-tetrazin-3-yl)phenyl)-3,10,20-trioxo-13,16-dioxa-2,9,19-triazadocosan-4-aminium (4.7). To a 4 ml vial containing boc-protected amine X (52.6 mg, 71.1 µmol, 1.0 equiv) in an ice bath was added a solution of HCl/dioxane (4 M, 360 µL). After HCl/dioxane addition, the vial was allowed to warm to room temperature. After 6 h the solvent was removed. The residue was subjected to semi-preparative HPLC purification. The fraction containing the product was lyophilized yielding 19 mg of a purple solid (40 % yield).

ESI(+)-MS: calcd. for $C_{30}H_{41}N_9O_7 + Na^+$, 662.3021; found 662.3022.

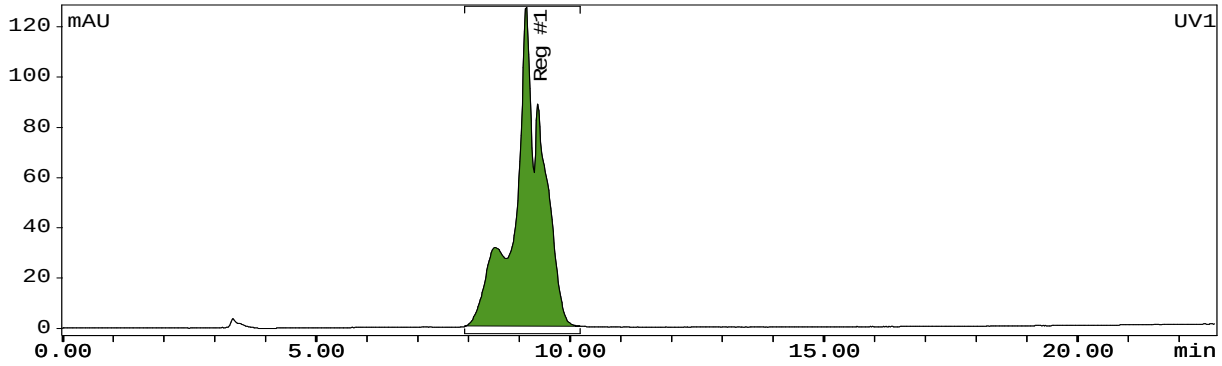

Figure 4.9. HPLC trace of purified **4.7**. HPLC mobile phase: 10% acetonitrile in water (both in 0.1% TFA) is increased to 95% acetonitrile in water over 20 min.

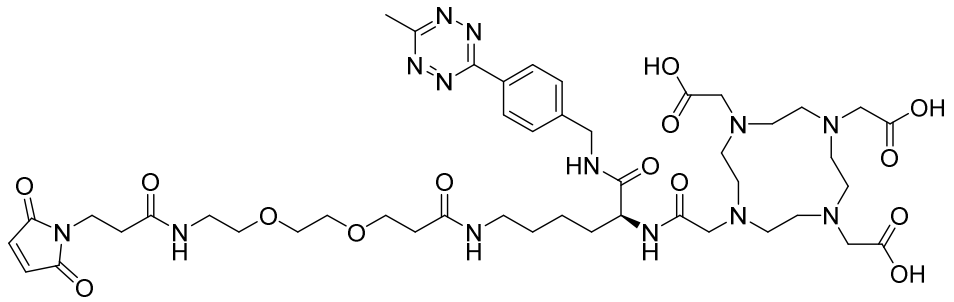

(*S*)-2,2',2''-(10-(22-(2,5-Dioxo-2,5-dihydro-1*H*-pyrrol-1-yl)-4-((4-(6-methyl-1,2,4,5-tetrazin-3-yl)benzyl)carbamoyl)-2,10,20-trioxo-13,16-dioxa-3,9,19-triazadocosyl)-1,4,7,10-tetraazacyclododecane-1,4,7-triyl)triacetic acid (4.8). To a 1.5 mL Eppendorf tube was added **4.7** (3.6 mg, 5.32 μmol, 1 equiv) and dry DMF (0.16 mL). To this, triethylamine (7.4 μL, 53.2 μmol, 10 equiv) was added and the mixture was stirred at room temperature for 15 min. DOTA-NHS (4 mg, 5.32 μmol, 1 equiv) then was then added. The reaction mixture was stirred at room temperature for 16 hours. DMF was then removed under reduced pressure and the residue was subjected to semi-preparative HPLC purification to give 2.7 mg of the desired product as a dark blue solid (49%).

ESI(+)-MS: calcd. for $C_{46}H_{68}N_{13}O_{14}$ $[M+H]^+$, 1026.5009; found 1026.5046.

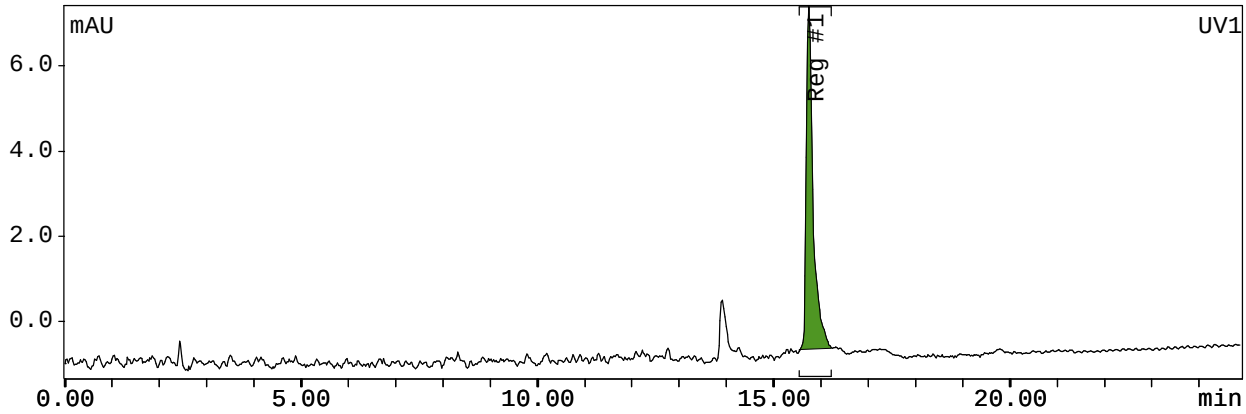

Figure 4.10. HPLC trace of purified **4.8**. HPLC mobile phase: 5% acetonitrile in water (both in 0.1% TFA) is run for 5 min, then acetonitrile is increased to 75% acetonitrile in water over the next 25 min.

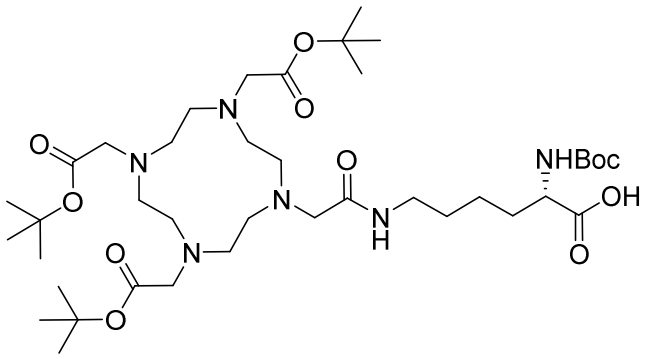

N2-(Tert-butoxycarbonyl)-N6-(2-(4,7,10-tris(2-(tert-butoxy)-2-oxoethyl)-1,4,7,10-tetraazacyclododecan-1-yl)acetyl)-L-lysine (4.10). To a 1.5 ml Eppendorf tube was added α-Boc-L-lysine (13 mg, 54 μmol, 1.2 equiv), DOTA-*t*Bu-NHS **4.9** (30 mg, 45 μmol, 1 equiv), and DMF (0.5 ml). The Eppendorf tube was shaken for 20 min, then *N*,*N*-diisopropylethylamine (24 μL, 0.135 mmol, 2.5 equiv) was added to the vial. The vial was allowed to continue shaking for 16 h, after which the solvent was removed, and the residue was subjected to semi-preparative HPLC for purification. The collected product was lypholized, yielding 36 mg (90% yield).

ESI(+)-MS: calcd. for $C_{52}H_{81}N_{15}O_{15}$ [M-H], 799.5181; found 799.5153.

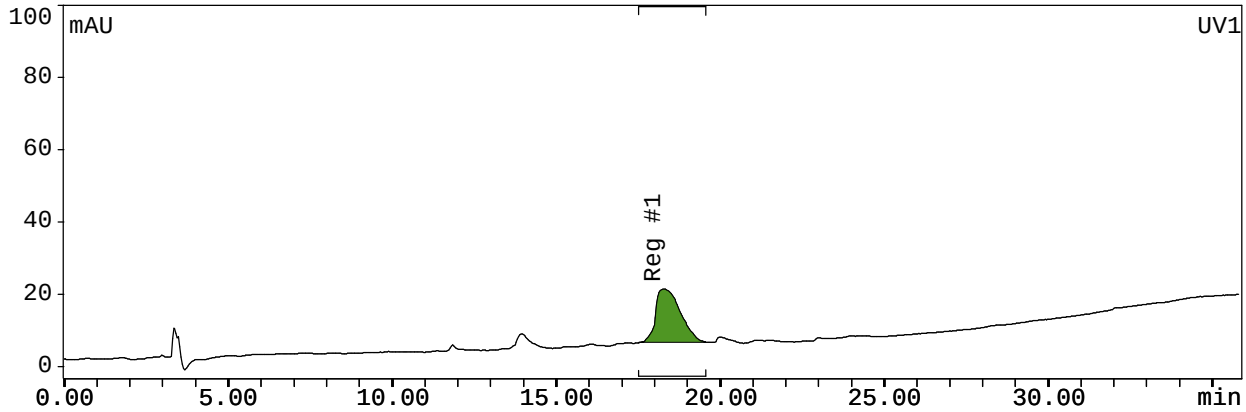

Figure 4.11. HPLC trace of crude **4.10**. HPLC mobile phase: 10% acetonitrile in water (both in 0.1% TFA) is increased to 90% acetonitrile in water over 30 min.

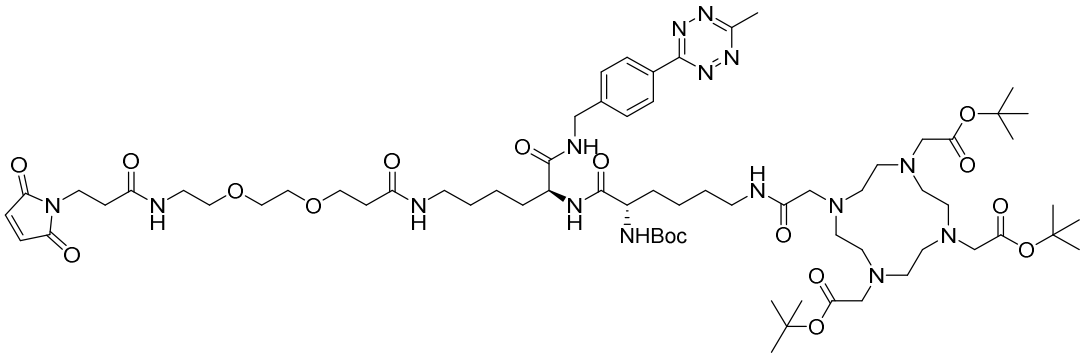

Tri-tert-butyl-2,2',2''-(10-((8*S*,11*S*)-8-((tert-butoxycarbonyl)amino)-29-(2,5-dioxo-2,5-dihydro-1*H*-pyrrol-1-yl)-11-((4-(6-methyl-1,2,4,5-tetrazin-3-yl)benzyl)carbamoyl)-2,9,17,27-tetraoxo-20,23-dioxa-3,10,16,26-tetraazanonacosyl)-1,4,7,10-tetraazacyclododecane-1,4,7-triyl)triacetate (4.11). To a solution of **4.10** (11 mg, 13.7 µmol, 1.1 equiv) in DMF (0.3 mL) was added HATU (8 mg, 21 µmol, 1.7 equiv) and the mixture was stirred for 30 min at room temperature. To this, a solution of **4.5** (8.4 mg, 12.5 µmol, 1 equiv) in DMF (0.2 mL) was added and the mixture was stirred for another 12 min. Triethylamine (4.4 µL, 31.2 µmol, 2.5 equiv) was then added and the mixture was allowed to stir at room temperature for 15 hours. Solvent was removed under reduced pressure and the residue was subjected to semi-preparative HPLC for purification. The desired product was then concentrated to give 15 mg (84% yield) of a purple oil. **ESI(+)-MS**: calcd. for $C_{69}H_{111}N_{15}O_{17}$ $[M+H]^{2+}$, 711.9214; found 711.9209.

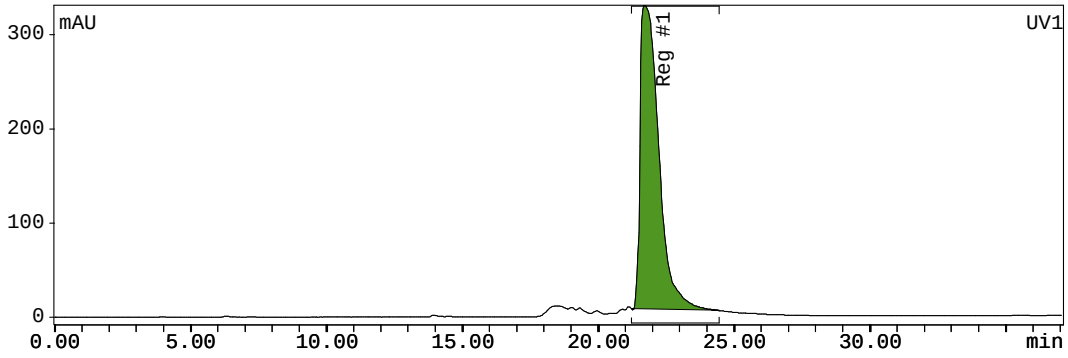

Figure 4.12. HPLC trace of purified **4.11**. HPLC mobile phase: 10% acetonitrile in water (both in 0.1% TFA) is increased to 90% acetonitrile in water over 35 min.

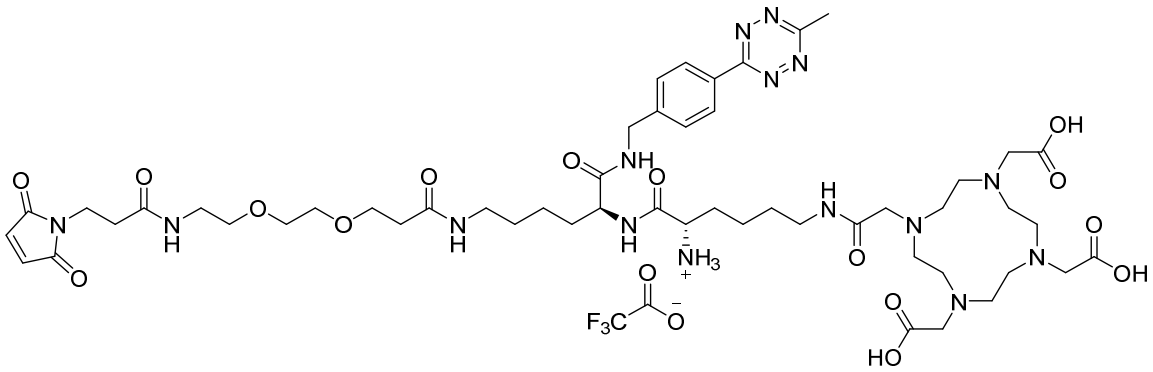

(8*S*,11*S*)-29-(2,5-Dioxo-2,5-dihydro-1*H*-pyrrol-1-yl)-11-((4-(6-methyl-1,2,4,5-tetrazin-3-yl)benzyl)carbamoyl)-2,9,17,27-tetraoxo-1-(4,7,10-tris(carboxymethyl)-1,4,7,10-tetraazacyclododecan-1-yl)-20,23-dioxa-3,10,16,26-tetraazanonacosan-8-aminium 2,2,2-trifluoroacetate (4.12). To a 4 ml vial containing **4.11** (10 mg, 7 μmol, 1.0 equiv) and dichloromethane (0.3 ml) in an ice bath was added concentrated trifluoroacetic acid (0.45 ml) dropwise. The vial was then brought to room temperature and stirred for 3.5 hours. The reaction mixture was then diluted with dichloromethane and concentrated three times, before being subjected to semi-preparative HPLC for purification. The fraction containing the product was lyophilized yielding 6 mg of a purple oil (77 % yield).

ESI(+)-MS: calcd. for $C_{52}H_{81}N_{15}O_{15}$ $[M+H]^{2+}$, 577.8018; found 577.8038.

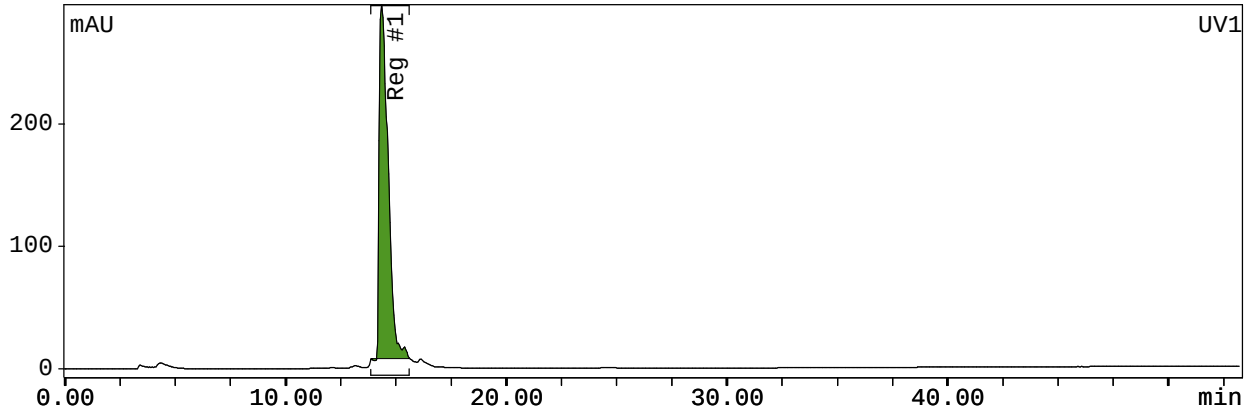

Figure 4.13. HPLC trace of purified **4.12**. HPLC mobile phase: 5% acetonitrile in water (both in 0.1% TFA) is increased to 75% acetonitrile in water over 30 min.

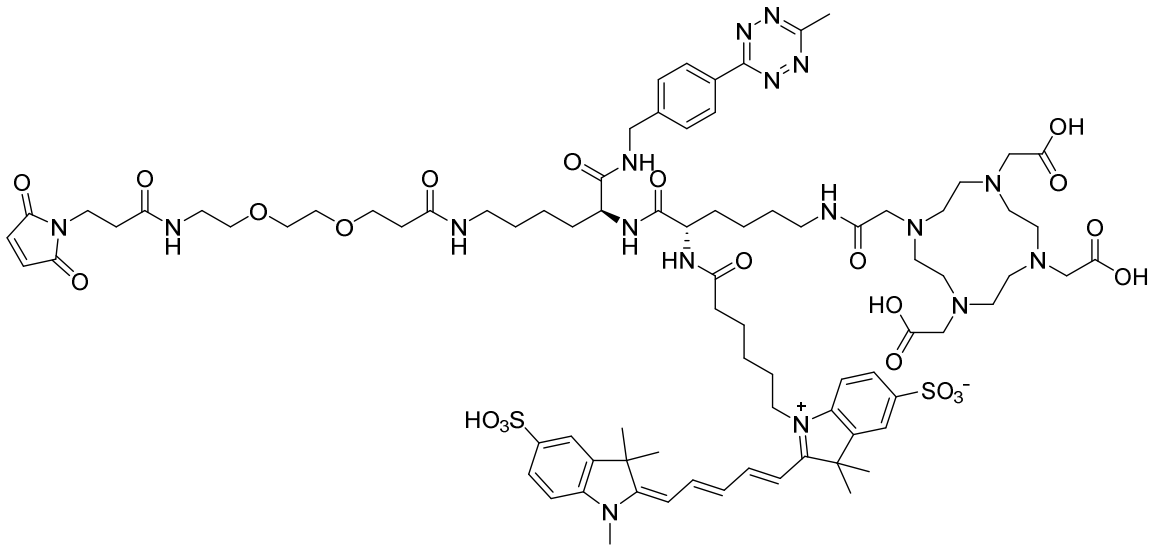

1-((19*S*,22*S*)-1-(2,5-Dioxo-2,5-dihydro-1*H*-pyrrol-1-yl)-19-((4-(6-methyl-1,2,4,5-tetrazin-3-yl)benzyl)carbamoyl)-3,13,21,24-tetraoxo-22-(4-(2-(4,7,10-tris(carboxymethyl)-1,4,7,10-tetraazacyclododecan-1-yl)acetamido)butyl)-7,10-dioxa-4,14,20,23-tetraazanonacosan-29-yl)-3,3-dimethyl-2-((1E,3E)-5-((E)-1,3,3-trimethyl-5-sulfoindolin-2-ylidene)penta-1,3-dien-1-yl)-3H-indol-1-ium-5-sulfonate (4.13). To a 1.5 mL Eppendorf tube was added **4.12** (5 mg, 4.33 μmol, 1 equiv) and dry DMF (0.2 mL). To this, triethylamine (2.4 μL, 17.33 μmol, 4 equiv) was added and the mixture was stirred at room temperature for 15 min. sCy5-NHS (4.6 mg, 6.1 μmol, 1.4 equiv) was then added. The reaction mixture was stirred at room temperature for 16 hours. DMF was then removed under reduced pressure and the residue was subjected to semi-preparative HPLC purification to give 2 mg of the desired product as a dark blue solid (26 % yield). **ESI(+)-MS**: calcd. for $C_{84}H_{117}N_{17}O_{22}S_2$ $[M+H]^{2+}$, 889.9001; found 889.8995.

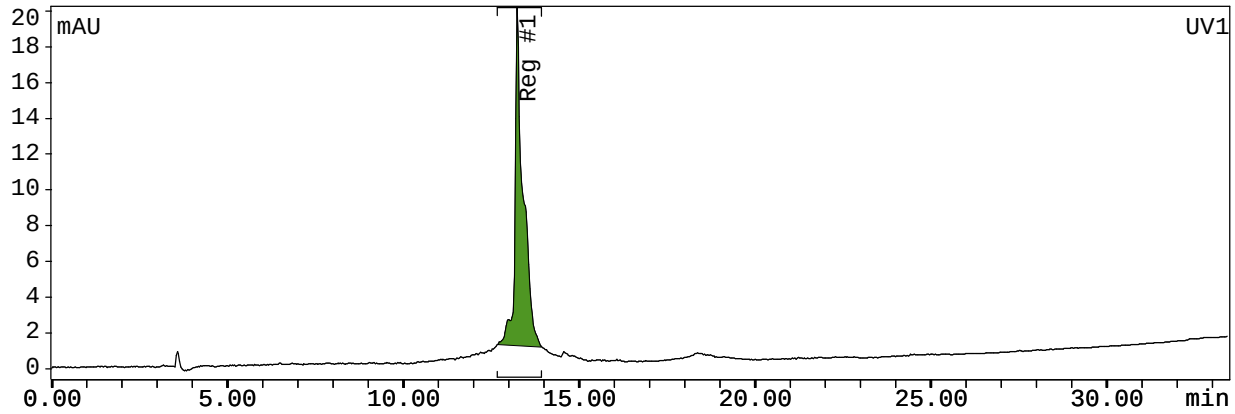

Figure 4.14. HPLC trace of purified **4.13**. HPLC mobile phase: 5% acetonitrile in water (both in 0.1% TFA) is increased to 90% acetonitrile in water over 30 min.

4.6 Spectra Relevant to Chapter Four

Development of a Tri-Modal Synthetic Linker Used in the Imaging of PSCA^{+} Prostate Cancer

^{1}H NMR

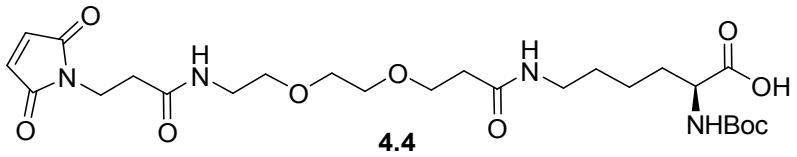

4.4

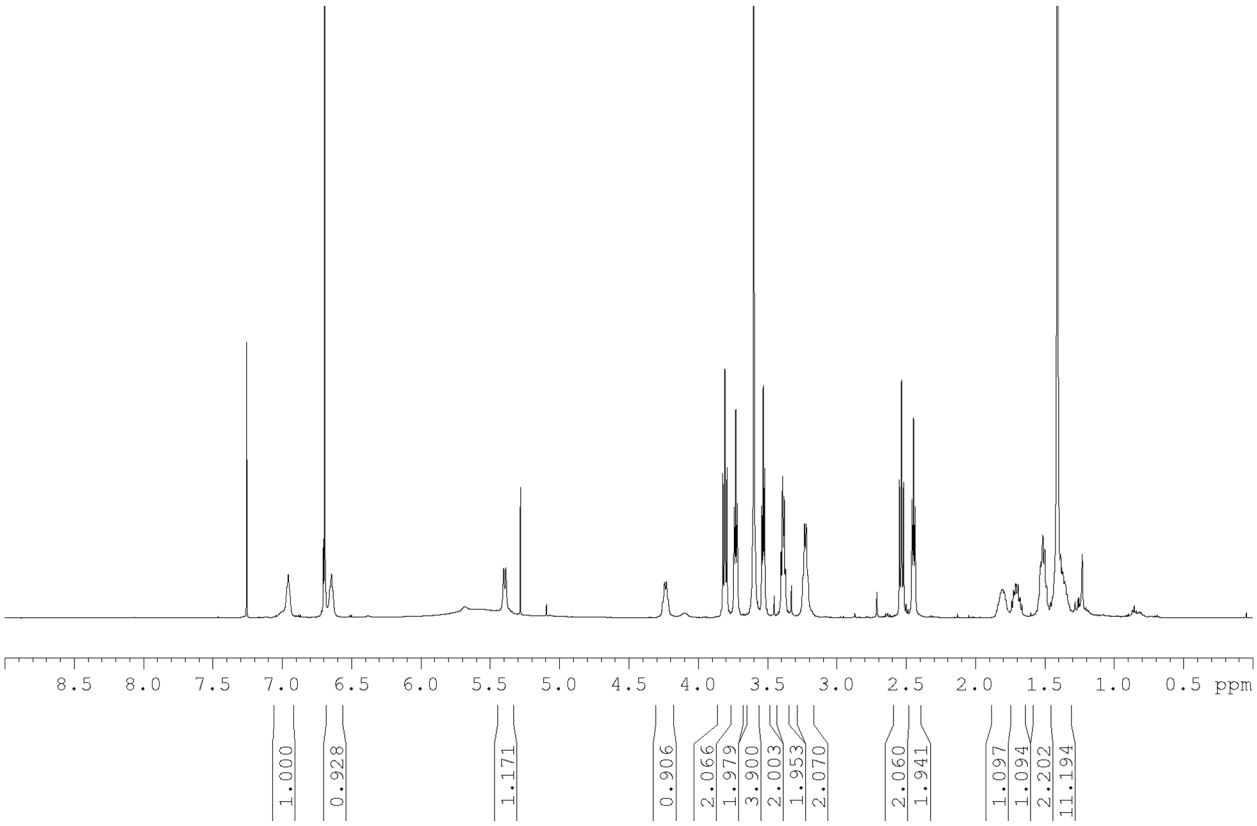
8.5 8.0 7.5 7.0 6.5 6.0 5.5 5.0 4.5 4.0 3.5 3.0 2.5 2.0 1.5 1.0 0.5 ppm
1.000
0.928
1.171
0.906
2.066
1.979
3.900
2.003
1.953
2.070
2.060
1.941
1.097
1.094
2.202
11.194

^{13}C NMR

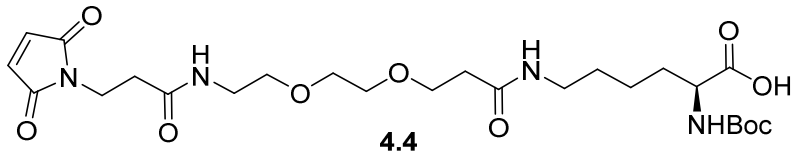

4.4

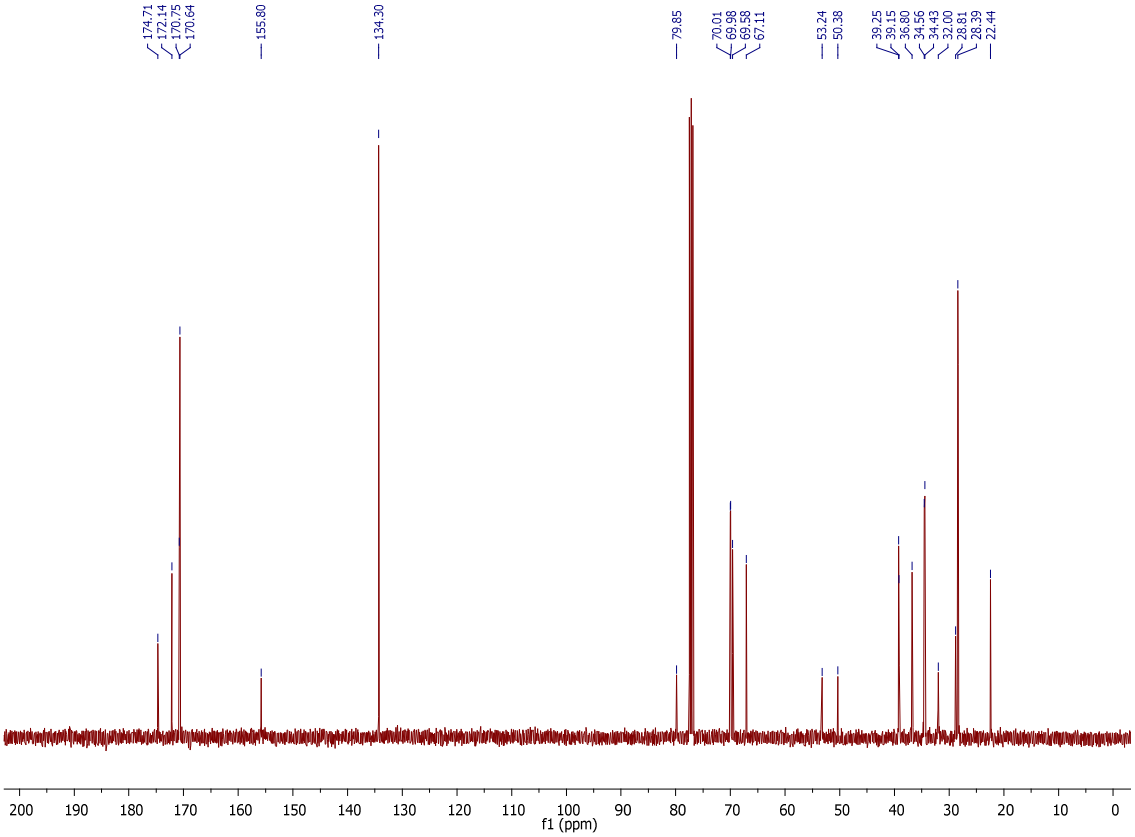
174.71
172.14
170.75
170.64
155.80
134.30
79.85
70.01
69.98
69.58
67.11
53.24
50.38
39.25
39.15
36.80
34.56
34.43
32.00
28.81
28.39
22.44
200 190 180 170 160 150 140 130 120 110 100 90 80 70 60 50 40 30 20 10 0
f1 (ppm)

4.7. Notes and References

(1) Siegel, R. L.; Miller, K. D.; Jemal, A. *CA. Cancer J. Clin.* **2018**, *68*, 7–30.

(2) Wardle, J.; Robb, K.; Vernon, S.; Waller, J. *Am. Psychol.* **2015**, *70*, 119–133.

(3) Husband, J. E.; Schwartz, L. H.; Spencer, J.; Ollivier, L.; King, D. M.; Johnson, R.; Reznek, R. *Br. J. Cancer* **2004**, *90*, 2256–2260.

(4) Weber, W. A. *J. Nucl. Med.* **2009**, *50*, 1S–10S.

(5) Sarkar, S.; Das, S. *Biomed. Eng. Comput. Biol.* **2016**, *7s1*, BECB.S34255.

(6) Almuhaideb, A.; Papathanasiou, N.; Bomanji, J. *Ann. Saudi Med.* **2011**, *31*, 3–13.

(7) Jadvar, H. *J. Nucl. Med.* **2016**, *57*, 25S.

(8) Wilt, T. J.; Scardino, P. T.; Carlsson, S. V; Basch, E. *J. Natl. Cancer Inst.* **2014**, *106*, dju010.

(9) Chang, S. S. *Rev. Urol.* **2004**, *6 Suppl 10*, S13-8.

(10) Neves, A. F.; Araújo, T. G.; Biase, W. K. F. S.; Meola, J.; Alcântara, T. M.; Freitas, D. G.; Goulart, L. R. *Clin. Biochem.* **2008**, *41*, 1191–1198.

(11) Bussemakers, M. J. G.; Van Bokhoven, A.; Verhaegh, G. W.; Smit, F. P.; Karthaus, H. F. M.; Schalken, J. A.; Debruyne, F. M. J.; Ru, N.; Isaacs, W. B.; Buchanan, J. *CANCER Res.* **1999**, *59*, 5975–5979.

(12) Nagaya, T.; Nakamura, Y. A.; Choyke, P. L.; Kobayashi, H. *Front. Oncol.* **2017**, *7*, 314.

(13) Reiter, R. E.; Gu, Z.; Watabe, T.; Thomas, G.; Szigeti, K.; Davis, E.; Wahl, M.; Nisitani, S.; Yamashiro, J.; Le Beau, M. M.; Loda, M.; Witte, O. N. *Proc. Natl. Acad. Sci. U. S. A.* **1998**, *95*, 1735–1740.

(14) Zettlitz, K. A.; Tsai, W.-T. K.; Knowles, S. M.; Kobayashi, N.; Donahue, T. R.; Reiter, R. E.; Wu, A. M. *J. Nucl. Med.* **2018**, jnumed.117.207332.

(15) Kuker, R.; Sztejnberg, M.; Gulec, S. *Mol. Imaging Radionucl. Ther.* **2017**, *26*, 66–73.

(16) Li, L.; Turatti, F.; Crow, D.; Bading, J. R.; Anderson, A.-L.; Poku, E.; Yazaki, P. J.; Williams, L. E.; Tamvakis, D.; Sanders, P.; Leong, D.; Raubitschek, A.; Hudson, P. J.; Colcher, D.; Shively, J. E. *J. Nucl. Med.* **2010**, *51*, 1139–1146.